

**AFRL-VA-WP-TR-2005-3033**

**CONSISTENT STRUCTURAL  
INTEGRITY AND EFFICIENT  
CERTIFICATION WITH ANALYSIS**

**Volume 1: Executive Summary,  
Implemented Solution, and Industry  
Applications**



**Craig Collier**

**Collier Research Corporation  
2 Eaton Street, Suite 504  
Hampton, VA 23669**

**MAY 2005**

**Final Report for 27 June 2002 – 27 June 2004**

**THIS IS A SMALL BUSINESS INNOVATION RESEARCH (SBIR) PHASE II REPORT.**

**Approved for public release; distribution is unlimited.**

**STINFO FINAL REPORT**

**AIR VEHICLES DIRECTORATE  
AIR FORCE RESEARCH LABORATORY  
AIR FORCE MATERIEL COMMAND  
WRIGHT-PATTERSON AIR FORCE BASE, OH 45433-7542**

# NOTICE

Using Government drawings, specifications, or other data included in this document for any purpose other than Government procurement does not in any way obligate the U.S. Government. The fact that the Government formulated or supplied the drawings, specifications, or other data does not license the holder or any other person or corporation; or convey any rights or permission to manufacture, use, or sell any patented invention that may relate to them.

This report was cleared for public release by the Air Force Research Laboratory Wright Site (AFRL/WS) Public Affairs Office (PAO) and is releasable to the National Technical Information Service (NTIS). It will be available to the general public, including foreign nationals.

PAO Case Number: AFRL-WS 05-2762, 12 Dec 2005

THIS TECHNICAL REPORT IS APPROVED FOR PUBLICATION.

//S//

---

DUANE E. VELEY  
Aerospace Engineer  
Structural Design & Development Branch

//S//

---

MICHAEL L. ZEIGLER  
Branch Chief  
Structural Design & Development Branch

//S//

---

MICHAEL D. PILKENTON, Lt Col, USAF  
Deputy Chief  
Structures Division

This report is published in the interest of scientific and technical information exchange and its publication does not constitute the Government's approval or disapproval of its ideas or findings.

REPORT DOCUMENTATION PAGE					Form Approved OMB No. 0704-0188	
<p>The public reporting burden for this collection of information is estimated to average 1 hour per response, including the time for reviewing instructions, searching existing data sources, gathering and maintaining the data needed, and completing and reviewing the collection of information. Send comments regarding this burden estimate or any other aspect of this collection of information, including suggestions for reducing this burden, to Department of Defense, Washington Headquarters Services, Directorate for Information Operations and Reports (0704-0188), 1215 Jefferson Davis Highway, Suite 1204, Arlington, VA 22202-4302. Respondents should be aware that notwithstanding any other provision of law, no person shall be subject to any penalty for failing to comply with a collection of information if it does not display a currently valid OMB control number. <b>PLEASE DO NOT RETURN YOUR FORM TO THE ABOVE ADDRESS.</b></p>						
1. REPORT DATE (DD-MM-YY) May 2005		2. REPORT TYPE Final		3. DATES COVERED (From - To) 06/27/2002 – 06/27/2004		
4. TITLE AND SUBTITLE CONSISTENT STRUCTURAL INTEGRITY AND EFFICIENT CERTIFICATION WITH ANALYSIS Volume 1: Executive Summary, Implemented Solution, and Industry Applications				5a. CONTRACT NUMBER F33615-02-C-3216		
				5b. GRANT NUMBER		
				5c. PROGRAM ELEMENT NUMBER 0605502		
6. AUTHOR(S) Craig Collier				5d. PROJECT NUMBER A01V		
				5e. TASK NUMBER		
				5f. WORK UNIT NUMBER 0A		
7. PERFORMING ORGANIZATION NAME(S) AND ADDRESS(ES) Collier Research Corporation 2 Eaton Street, Suite 504 Hampton, VA 23669				8. PERFORMING ORGANIZATION REPORT NUMBER		
9. SPONSORING/MONITORING AGENCY NAME(S) AND ADDRESS(ES) Air Vehicles Directorate Air Force Research Laboratory Air Force Materiel Command Wright-Patterson AFB, OH 45433-7542				10. SPONSORING/MONITORING AGENCY ACRONYM(S) AFRL/VASD		
				11. SPONSORING/MONITORING AGENCY REPORT NUMBER(S) AFRL-VA-WP-TR-2005-3033		
12. DISTRIBUTION/AVAILABILITY STATEMENT Approved for Public Release: Distribution Unlimited.						
13. SUPPLEMENTARY NOTES This is a Small Business Innovation Research (SBIR) Phase II report. Report contains color. This is Volume 1 of a three-volume work. See also Volume 2 (AFRL-VA-WP-TR-2005-3034) and Volume 3 (AFRL-VA-WP-TR-2005-3035).						
14. ABSTRACT Report developed under SBIR contract for topic AF01-239.  This SBIR report maintains that reliable pretest predictions and efficient certification are suffering from inconsistent structural integrity that is prevalent throughout a project's design maturity. Eight primary inconsistencies practiced in aerospace structural analysis are identified. This SBIR proposes solutions for these inconsistencies and documents software implementation and real world examples. Our primary approach is to couple analytical methods to experimental results to achieve consistent structural integrity by analysis. By establishing repeatable uncertainty from building block test data for unique failure modes, it is possible to identify correlation factors (CFs) that account not only for analysis inaccuracy, but also for observed scatter in test results.  Industry-accepted failure analysis predictions then can be used to design more robustly and to avoid unanticipated design flaws discovered in final design, or, worse yet, those that lead to part failure. The CFs can be used to adjust individual margins of safety to produce more consistent structural integrity in the design and dependability in weight predictions of an aerospace vehicle. Such a capability is most useful during preliminary design where 80 percent of design decisions carry forward to final design, including uninformed ones that bring with them difficulties of meeting weight goals, passing structural testing on the first try, and costly certification.						
15. SUBJECT TERMS SBIR Report, HyperSizer, certification, analysis, structures, aerospace, bonded joints, composite materials						
16. SECURITY CLASSIFICATION OF:			17. LIMITATION OF ABSTRACT: SAR	18. NUMBER OF PAGES 182	19a. NAME OF RESPONSIBLE PERSON (Monitor) Duane E. Veley 19b. TELEPHONE NUMBER (Include Area Code) (937) 255-8286	
a. REPORT Unclassified	b. ABSTRACT Unclassified	c. THIS PAGE Unclassified				

# Table of Contents

<u>Section</u>	<u>Page</u>
<b>PART A: EXECUTIVE SUMMARY</b>	
<b>LIST OF FIGURES.....</b>	<b>VI</b>
<b>LIST OF TABLES.....</b>	<b>X</b>
<b>ACKNOWLEDGMENTS.....</b>	<b>XI</b>
<b>1 EXECUTIVE SUMMARY.....</b>	<b>1</b>
<b>2 INTRODUCTION.....</b>	<b>3</b>
2.1 PROBLEM: MORE TEST FAILURES IN LAST 25 YEARS THAN IN PREVIOUS 50.....	3
2.2 SBIR APPROACH.....	4
2.3 CONNECTION TO HYPERSizer.....	5
2.4 SBIR INNOVATION AND DEVELOPMENT .....	6
2.4.1 Composite laminate and bonded joint strength .....	6
2.4.2 Test data driven reliability analysis and sizing .....	8
2.4.3 SBIR innovation applied to LRS .....	12
2.5 REPORT CONTENTS .....	15
<b>3 SBIR SUCCESS STORY HIGHLIGHTS: LOCKHEED MARTIN AERONAUTICS, ADVANCED DEVELOPMENT PROGRAM (ADP) .....</b>	<b>16</b>
3.1 BUSINESS CONCLUSIONS.....	16
3.1.1 LM Aero ADP, Fort Worth .....	17
3.1.2 LM Aero ADP, Marietta .....	19
3.1.3 Collier Research Corporation .....	20
3.2 LM AERO'S IMPLEMENTATIONS.....	22
3.2.1 F-35 (JSF).....	22
3.2.2 F-22 .....	23
3.2.3 C-130 .....	24
<b>4 COMMERCIALIZATION .....</b>	<b>26</b>
4.1 HYPERSizer® IS A COMMERCIAL PRODUCT .....	26
4.2 NEW SALES DUE TO SBIR.....	29
4.3 NEW TRAINING OF SBIR DEVELOPMENTS .....	29
4.4 TECHNICAL REVIEW AND INTERCHANGE MEETING WITH LM AERO TECHNICAL FELLOWS .....	29
4.5 NEW SBIR PUBLISHED DOCUMENTATION.....	30
4.5.1 Four published papers .....	30
4.6 TRADE SHOWS/CONFERENCE/SYMPOSIUMS ATTENDED WITH EMPHASIS ON SBIR COMMERCIALIZATION.....	30
4.7 COMPANY VISITS .....	31
4.8 PRIMARY SBIR DEVELOPMENTS COMMERCIALY AVAILABLE .....	31
<b>5 SHORTCOMING: INCONSISTENT STRUCTURAL INTEGRITY THROUGHOUT DESIGN MATURITY CAUSES TEST FAILURES .....</b>	<b>32</b>
5.1 EIGHT PRIMARY INCONSISTENCIES OF AEROSPACE STRUCTURAL ANALYSIS .....	32
5.1.1 Inconsistency of deterministic failure analyses.....	33
5.1.2 Inconsistency of the typical one knockdown approach.....	34
5.1.3 Inconsistency of the zero margin-of-safety approach .....	35
5.1.4 Inconsistency of the 1.5 ultimate load approach to safety .....	36
5.1.5 Inconsistency of global-local modeling approaches.....	36
5.1.6 Inconsistency of fidelity during design phases.....	36
5.1.7 Inconsistency of analysis fidelity between test predictions and in-service predictions.....	37

5.1.8	Inconsistency of test data availability.....	37
5.2	EVIDENCE USING THE AFRL VA LONG RANGE STRIKE (LRS) .....	37
<b>6</b>	<b>SOLUTION: PERFORM CONSISTENT STRUCTURAL ANALYSIS IN PRELIMINARY DESIGN TO ACHIEVE EFFICIENT CERTIFICATION.....</b>	<b>38</b>
6.1	CURRENT PRELIMINARY DESIGN PRACTICE .....	39
6.1.1	Manual operation of legacy codes.....	39
6.1.2	Spot checking of anticipated critical failure modes, for a subset of vehicle locations and load cases.....	40
6.1.3	Spreadsheets .....	40
6.2	HYPERSizer SELECTED AS PRELIMINARY DESIGN AUTOMATED ANALYSIS FRAMEWORK .....	40
6.2.1	HyperSizer addresses all eight structural analysis inconsistencies.....	40
6.2.2	HyperSizer Sphere of Influence .....	41
6.3	HYPERSizer TRADITIONAL ANALYSIS OF THE AFRL LONG RANGE STRIKE (LRS) AIRCRAFT.....	43
6.3.1	Load Cases .....	43
6.3.2	FEM.....	43
6.3.3	HyperSizer transformation and display of FEA computed internal loads .....	44
6.3.4	HyperSizer Setup: Components and Groups .....	45
6.3.5	HyperSizer Result: Controlling Failure Analyses.....	46
6.3.6	HyperSizer Result: Controlling Load Case .....	47
6.3.7	HyperSizer Result: Minimum Margins-of-Safety.....	48
6.3.8	HyperSizer Result: Optimum Composite Layup .....	49
6.3.9	HyperSizer Result: Optimum Unit Weights .....	50
<b>7</b>	<b>1<sup>ST</sup> SBIR THRUST: REDUCE ORDER MODELING AND HIGH FIDELITY RAPID ANALYSIS.....</b>	<b>51</b>
7.1	REDUCE ORDER GLOBAL-LOCAL-DETAIL (GLD) MODELING OVERVIEW .....	51
7.2	HYPERSizer AS IT EXISTED.....	53
7.2.1	Efficient and consistent global-local-detail modeling for stiffened and sandwich panels.....	53
7.2.2	Stiffened panels.....	53
7.2.3	Sandwich Panels and Composite Laminates .....	55
7.2.4	Beams.....	55
7.2.5	Joints.....	55
7.3	SBIR INNOVATIONS .....	57
7.3.1	Overview.....	57
7.3.2	Efficient and consistent global-local-detail modeling of composite bonded joints.....	58
7.3.3	Composite bonded joint failure prediction .....	68
7.3.4	HyperSizer Joint analysis comparison to the other methods.....	74
7.3.5	Physically based composite laminate strength failure theories .....	76
7.3.6	Modularity in analytical modeling.....	80
<b>8</b>	<b>2<sup>ND</sup> SBIR THRUST: INTEGRATED TOOLS AND PROCESSES.....</b>	<b>81</b>
8.1	HYPERSizer AS IT EXISTED.....	81
8.1.1	A framework for performing hundreds of traditional analyses.....	81
8.1.2	Traditional closed form and modern numerical failure analyses delivered with HyperSizer.....	82
8.1.3	Plug-ins of customer proprietary and/or legacy specialty analysis codes.....	83
8.1.4	HyperSizer Sizing Optimization Based on Positive Margins for all Failure Modes.....	84
8.1.5	Generating Well Defined Equivalent Stiffness Terms for FEM Update .....	86
8.1.6	Automatic coupling to FEA such as MSC/NASTRAN, for Internal Loads.....	87
8.1.7	Object model for integration into larger software design/analysis systems .....	88
8.2	SBIR INNOVATIONS .....	89
8.2.1	Test data entry into database for all panel, material, and analysis types.....	90
8.2.2	Interactive graphics of test data histogram and correlation factors.....	93
8.2.3	HyperFinder .....	95
8.2.4	Thousands of pages of new analytical methods documents .....	98
8.2.5	HyperFEA.....	99
8.2.6	HyperWeb Services (object model ...) .....	100
<b>9</b>	<b>3<sup>RD</sup> SBIR THRUST: TEST DATA DRIVEN RELIABILITY ANALYSIS .....</b>	<b>103</b>
9.1	HYPERSizer AS IT EXISTED.....	104

9.1.1	Statistically processed design-to FEA computed internal loads .....	104
9.1.2	Separate load factors for limit and ultimate .....	105
9.2	SBIR INNOVATIONS .....	106
9.2.1	PDFs (probability density functions) statistically characterize histograms .....	107
9.2.2	PDF signatures represent test scatter and analysis inaccuracy .....	108
9.2.3	PDF signatures are found to be repeatable and unique for each failure analysis mode .....	110
9.2.4	Two correlation factors are defined for each failure analysis mode .....	112
9.2.5	Two correlation factors for composite material strength demonstrated with HyperSizer .....	114
9.2.6	Two correlation factor values have been established from test data for each failure analysis mode .....	120
9.2.7	HyperSizer implementation of test data driven reliability analysis and sizing optimization .....	124
<b>10</b>	<b>RELIABILITY TRADES DURING PRELIMINARY DESIGN FOR ENTIRE AIRFRAME: AFRL LONG RANGE STRIKE (LRS).....</b>	<b>128</b>
10.1	SPECIFIC AIRFRAME APPLICATION .....	129
10.2	MATERIALS AND PANEL CONCEPTS .....	129
10.3	FAILURE ANALYSES PERFORMED .....	132
10.4	COMPARISON TO 85.1%, 97.7% AND 99.86% RELIABILITY SIZING .....	133
10.5	EFFECT OF FEA STATISTICALLY PROCESSED LOADS .....	133
<b>11</b>	<b>COMPARING ANALYSIS APPROACHES: TRADITIONAL ZERO MARGIN-OF-SAFETY VERSUS NEW TEST DATA DRIVEN RELIABILITY .....</b>	<b>137</b>
11.1	EXAMPLE: ENTIRE AIRFRAME - AFRL LONG RANGE STRIKE (LRS).....	137
11.1.1	Significance of Weight Reduction and Increased Airframe Lifetimes without Failure .....	137
11.1.2	Comparison of load factors and material allowables .....	139
11.1.3	Process for calculating reliability for traditional analysis .....	140
11.1.4	1 <sup>st</sup> step, size airframe to zero margins.....	140
11.1.5	2 <sup>nd</sup> step, pass the traditional optimum variables to the reliability analysis .....	142
11.1.6	3 <sup>rd</sup> step, perform reliability analysis on the traditional design and compute true margins .....	143
11.1.7	4 <sup>th</sup> step, back out reliability for each airframe component .....	144
11.1.8	5 <sup>th</sup> step, compare controlling failure analyses and load cases.....	146
11.2	HOW TO BACK OUT RELIABILITY OF TRADITIONAL ZERO-MARGIN ANALYSIS .....	149
11.3	EXAMPLE: SINGLE AIRFRAME LOCATION - A DETAILED COMPARISON.....	153
11.3.1	Comparing the two analysis methods.....	153
11.3.2	Backing out the traditional sizing reliability.....	157
11.3.3	Calculating an effective knockdown.....	157
11.3.4	Calculating an effective required MS.....	157
<b>12</b>	<b>CONCLUSIONS .....</b>	<b>159</b>
<b>13</b>	<b>REFERENCES.....</b>	<b>162</b>
<b>14</b>	<b>LIST OF ACRONYMS AND ABBREVIATIONS.....</b>	<b>164</b>

## List of Figures

FIGURE		PAGE
1.1	HyperSizer identified failure analysis PDFs before and after applying inaccuracy correlation factors, which feed into the vehicle analysis below	2
1.2	Traditional zero-margin sizing approach cannot produce consistent structural integrity.	2
1.3	Airframe structural weight versus lifetime failures	2
2.1	Aerospace test failures versus analysis predict	3
2.2	HyperSizer used for analysis, sizing trade studies, and weight estimation on the AFRL LRS	6
2.3	New capability to compute interlaminar stress throughout depth of bonded joint.	7
2.4	Airframe structural weight versus lifetime failures	8
2.5	Traditional one knockdown approach to cylindrical panel buckling	9
2.6	Probability density functions (PDF) for seven different failure mode analyses, based on hundreds of test correlations	11
2.7	Application of the PDF for determining desired reliability (allowable load) with the two defined correlation factors (CF).	11
2.8	Traditional zero-margin sizing approach cannot produce consistent structural integrity.	13
2.9	Effect of varying reliability on controlling failure mode.	14
3.1	The STRICT inlet duct program	17
3.2	The Unitized Composite F-16 Horizontal Tail	18
3.3	The NJC Test Box	18
3.4	Top image is verification of HyperSizer buckling to MSC/NASTRAN FEA	22
3.6	Shear Test Panel	25
4.1	HyperSizer Software CD cover	26
4.2	HyperSizer.com website	27
4.3	Success in Recent applications.	28
4.4	Repeat paying customers or significant potential users of HyperSizer provide an immediately reachable target audience	28
5.1	Top half of a composite material failure envelope from the World Wide Failure Exercises (WWFE) Case #2	33
5.2	Traditional one knockdown approach to cylindrical panel buckling	34
5.3	High fidelity analyses provide precision, defined as an ability to hit a bull's eye but not ensuring that all results fall within the target	35
6.1	Cause and effect of better analytical modeling early in design	38
6.2	HyperSizer includes the required core analyses	41
6.3	Three different aircraft types, three different eras, all primarily stiffened structure. Different technology ages, but all similar core principal analyses	42
6.4	Color gradient represents the FEA computed element forces after transformation to the material coordinate system by HyperSizer	44
6.5	Each different color region represents a unique structural component	45
6.6	Controlling failure analyses are shown with different colors and are identified as the failure analyses which produce the lowest margins for any of the 7 load cases	46
6.7	Controlling load cases shown with different colors, are identified as the	47

<b>FIGURE</b>		<b>PAGE</b>
	load cases which produce the lowest margin for any of the many failure analyses performed	
6.8	Minimum margin-of-safety shown for each component where light blue is the highest margin and red is the lowest margin	48
6.9	Optimum layup of traditional design, zero margin sizing approach	49
6.10	Unit weight of traditional design	50
7.1	The implemented Global-Local-Detail process including micromechanics	52
7.2	Four different ways to construct airframe stiffened panel FEMs.	54
7.3	LRS airframe	56
7.4	HyperSizer now includes the ability to predict composite bonded joint failure to help avoid failure such as this.	57
7.5	HyperSizer rapidly and accurately resolves aircraft stiffened structure panel loads	58
7.6	Interlaminar stress calculations throughout depth of bonded joint, including adhesive and laminated adherends	59
7.7	Stress calculations performed by HyperSizer through the depth of the joint show how the interlaminar shear and peel stress vary greatly	60
7.8	HyperSizer computes stress variation through the thickness of each ply.	61
7.9	Example of a non-linear material model used in HyperSizer's bonded joint analysis	62
7.10	Comparisons for the applied moment case between HyperSizer, Ansys 3D solid FEA, Delale and Erdogan's analytical plate theory, and independent 2D shell FEA performed by Delale and Erdogan	64
7.11	Comparisons for the applied tensile force case between HyperSizer, Ansys 3D solid FEA, Delale and Erdogan's analytical plate theory, and independent 2D shell FEA	65
7.12	Adhesive interlaminar shear stresses from membrane tensile force	66
7.13	Adhesive interlaminar peel stresses from membrane tensile force.	67
	Comparisons between HyperSizer, Abaqus 2D plane strain linear and non-linear FEA, and Ansys 3D solid FEA.	
7.14	A common composite failure mode for stiffened aircraft structure occurs at the re-entrant corner of a bonded flange	68
7.15	Failure modes in adhesively bonded joints identified by Heslehurst and Hart-Smith	69
7.16	Failure prediction methods require accurate prediction of out-of-plane interlaminar shear and peel stresses	70
7.17	The full stress state within the bonded joint is calculated by HyperSizer at a user-defined number of y and z locations indicated by the green dots.	71
7.18	Comparison of HyperSizer Bonded Joint analysis with Hart-Smith joint analysis methods	74
7.19	Compressive strength of $[+/-\square]$ s AS4/3502 predicted by different failure theories	77
7.20	LaRC03 failure criteria distinguishes between six different possible physical failures	78
7.21	Composite laminate AS4/3501 test failure data.	80
8.1	The HyperSizer "failure" tab listing MS for a honeycomb sandwich panel	82
8.2	In the illustration, two legacy programs are plugged into the HyperSizer structural analysis and sizing optimization software	83

<b>FIGURE</b>		<b>PAGE</b>
8.3	Illustrated is the process of directly sizing the design by permutation of all continuous and discrete variables	84
8.4	The structural optimization is based on achieving positive margins for every user selected failure mode turned on	85
8.5	HyperSizer's approach is to generate FEM properties for shell finite elements using a planar, 2-D coarse mesh	86
8.6	HyperSizer coupling with FEA. The box marked, "Model Data" represents FEA, and the box marked, "Design Data" represents HyperSizer	87
8.7	The HyperSizer structural analysis and sizing framework which includes delivered analysis along with plug-ins	88
8.8	HyperSizer coupling with a Microsoft Excel spreadsheet by use of HyperSizer's COM based object model	89
8.9	The 1st step is to select the Correlation Category	90
8.10	The 2nd step is to select the Project(s) or Workspace(s) where the problem setup and test data are entered	91
8.11	From the selected workspace, the 3rd step is to select the Group(s) and Component(s)	92
8.12	From the Failure Tab of the selected workspace, the 4th step is to select the Failure Analysis Mode	92
8.13	For this component, the 5th step is to select the Analysis Correlation Category	93
8.14	The 6th and last step is to view the interactive test data histogram graphics.	94
8.15	HyperFinder accessed from the Help Menu	95
8.16	Options available on the Failure Tab	96
8.17	HyperFinder Entries for Honeycomb Facesheet Wrinkling	96
8.18	Selecting HyperSizer Failure Methods for Display in HyperFinder	97
8.19	Tree Structure of HyperSizer Methods Documentation	98
9.1	A statistical approach is used for analyzing potential failure	103
9.2	The HyperSizer user can select the K standard deviation factor for determining the "Design-To" applied loading for strength analysis	104
9.3	The frequency of failure from test data, illustrated as a histogram with a statistical normal distribution (dotted curve on top of vertical bars) used to quantify load carrying confidence.	107
9.4	PDF of test data before normalizing about the test mean of 903	108
9.5	PDF four point composite beam that failed in strength, before normalizing	109
9.6	PDFs of test data after normalizing about test mean	109
9.7	Repeatability and Uniqueness of PDFs	110
9.8	Four PDFs superimposed, this time including results from composite cylindrical buckling	111
9.9	The histogram is normalized to the mean test result, which by definition equals the analysis prediction of expected failure load.	112
9.10	Application of the two correlation factors on a probability density function (PDF) for determining desired reliability (allowable load)	112
9.11	HyperSizer generated failure envelopes for WWFE Case 1	114
9.12	For WWFE Case 1 biaxial $\sigma_y$ - $\tau_{xy}$ failure envelopes of 0o E-glass/LY556 lamina	117
9.13	For WWFE Case 1, biaxial $\sigma_y$ - $\tau_{xy}$ failure envelopes.	117

<b>FIGURE</b>		<b>PAGE</b>
9.14	After applying correlation factors for WWFE Case 1	118
9.15	After applying correlation factors for WWFE Case 1	118
9.16	A HyperSizer representative histogram plot of 130 test data points	119
9.17	Normalizing to theoretical. The relative inaccuracies of the theoretical analysis and their relative scatter from experimental measurements	121
9.18	Normalization to predicted. The PDF signatures of the five different specific failure modes	121
9.19	Application of the (PDF) for determining desired reliability (allowable load)	122
9.18	1st step; HyperSizer failure tab provides the user an option to select which failure analyses to perform reliability analysis	125
9.19	2nd Step. Select reliability %, 1.0 for mechanical load factor, and a consistent FEA Statistical Loading Method	126
9.20	3rd Step. Select 1.0 for a buckling knockdown factor	126
10.1	Airframe structural weight versus lifetime failures	128
10.2	Panel concept for LRSA vehicle analyses.	132
10.3	Effect of varying reliability on controlling failure mode	134
10.4	Effect of varying reliability of the FEA loads processing	135
10.5	Effect of varying reliability on controlling optimum layup	136
11.1	Airframe structural weight versus lifetime failures	138
11.2	Margins-of-safety deltas from the traditional zero-margin sizing	141
11.3	Optimum layup from the traditional zero-margin sizing. This design is sent to the reliability analysis	142
11.4	Predicted margin-of-safety of the traditional design	143
11.5	99.5% Reliability margin-of-safety of the traditional design	144
11.6	The traditional zero-margin sizing approach cannot produce consistent structural integrity	145
11.7	The traditional zero-margin sizing approach cannot produce consistent structural integrity	146
11.8	Compared are the controlling failure modes between the traditional zero-margin approach versus a 99.5% reliability	147
11.9	Compared are the controlling load cases between the traditional zero-margin approach versus a 99.5% reliability approach	148
11.10	The way allowable loads are determined for the two approaches	149
11.11	A graphical representation of how the reliability of the traditional allowable is backed out	150
11.12	A one sided depiction of reliability of a normal distribution	152
11.13	A single airframe location - component 220, used for the detailed example	153
12.1	An example airframe structural weight versus lifetime failures	160
12.2	The overall process for structural certification by analysis	161

## List of Tables

<b>TABLE</b>		<b>PAGE</b>
2.1	Airframe Weight Increases with Increasing Structural Integrity	13
3.1	Panel Concept Trades	23
6.1	Vehicle Load Cases	43
7.1	Summary of theoretical predictions versus test averages of failure loads	73
9.1	Reliability, standard deviations, and lifetime airframe failures for a one sided normal distribution PDF curve	113
9.2	Summary Correlation Factors	120
9.3	All Currently Defined Correlation Factors	123
10.1	Airframe Weight Increases with Increasing Structural Integrity normalized arbitrarily to 1 in 1000 lifetime airframe failures	128
10.2	Vehicle Load Cases	129
10.3	Summary Correlation Factors	132
11.1	The New Test Data Driven Reliability Provides Less Airframe Weight and More Structural Integrity	138
11.2	Contrasting Approaches for the LRS Airframe Analysis	139

## **Acknowledgments**

This material is based upon work supported by the United States Air Force under Contract

1. AFRL VA SBIR Phase I contract # F33615-01-M-3125
2. AFRL VA SBIR Phase II contract # F33615-02-C-3216
3. LM Aero LRSA Contract/PO # 7067581.

# 1 Executive Summary

The accuracy and breadth of analytical modeling has progressed to the point where structural certification is benefiting substantially from analysis. However, the aerospace community's analytical modeling "batting average" needs improvement to more reliably make pretest predictions and avoid expensive full-scale testing failures. This SBIR report maintains that reliable pretest predictions and efficient certification are suffering from inconsistent structural integrity that is prevalent throughout a project's design maturity. Eight primary inconsistencies practiced in aerospace structural analysis are identified. This SBIR proposes solutions for these inconsistencies and documents method development and application on a full airframe. Consistent structural integrity by analysis is achieved by coupling analytical methods to experimental results. By establishing repeatable uncertainty probability density functions (PDF) from building block test data for unique failure modes, it is possible to identify correlation factors (CFs) that account not only for analysis inaccuracy, but also for observed scatter in test results. Industry-accepted failure analysis predictions can then be used to design more robustly and to avoid unanticipated design flaws discovered in final design, or, worse yet, lead to part failure. The CFs can be used to adjust individual margins-of-safety to produce more consistent structural integrity in the design and dependability in weight predictions of an aerospace vehicle. Such a capability is most useful during preliminary design where 80% of design decisions carry forward to final design, including uninformed ones that bring with them difficulties of meeting weight goals, passing structural testing, and costly certification.

This approach, during this SBIR, has been developed and implemented in the HyperSizer® commercial automated analysis and design tool that results in significant design cycle time reduction with the ability to analyze orders of magnitude more designs. Substantial risk reduction in final design is achieved from the integration and use of correlated, higher fidelity failure analyses earlier in the design process. Presented are summary results from a recent Air Force Research Lab (AFRL) Long Range Strike Aircraft preliminary design that compares the traditional, zero margin-of-safety for all failure modes approach, versus the developed approach that achieves higher reliability for all potential failure modes. Based on developed PDFs of several failure analyses from hundreds of collected and entered test data, Fig. 1.1, analysis of the vehicle is more reliable and consistent. Fig 1.2 identifies areas of the vehicle sized using the traditional zero-margin method that results in an unexpected and unacceptable low reliability, even though it is 9% heavier than test-data-driven reliability analysis and design as depicted in Fig. 1.3. Note that the traditional zero-margin analysis currently practiced provides neither acceptable structural integrity nor minimum weight.

To achieve efficient certification through more consistent and reliable analysis, the following primary capabilities were developed with this SBIR funding: a test database integrated with each unique failure mode analysis, hundreds of delivered test data, interactive test data display as histograms, identification of two correlation factors (CF) with each unique analysis, reliability analysis and sizing capability based on test data, rapid bonded composite joint analysis, physically based composite strength analysis, HyperFinder technical documentation and search, and over 500 pages of verification and validation technical documentation.

In summary, this SBIR innovation conclusively provides: 1) substantial weight savings, 2) consistent structural integrity, and 3) more efficient certification along with convincing justification to certification authorities of airframe structural airworthiness.

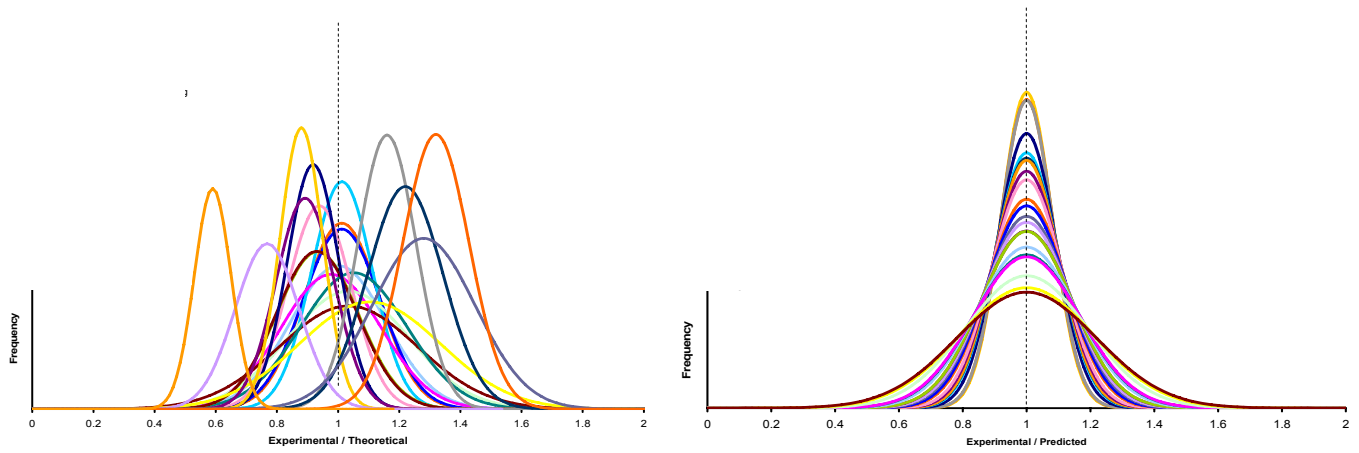


Fig. 1.1, HyperSizer identified failure analysis PDFs before and after applying inaccuracy correlation factors, which feed into the vehicle analysis below.

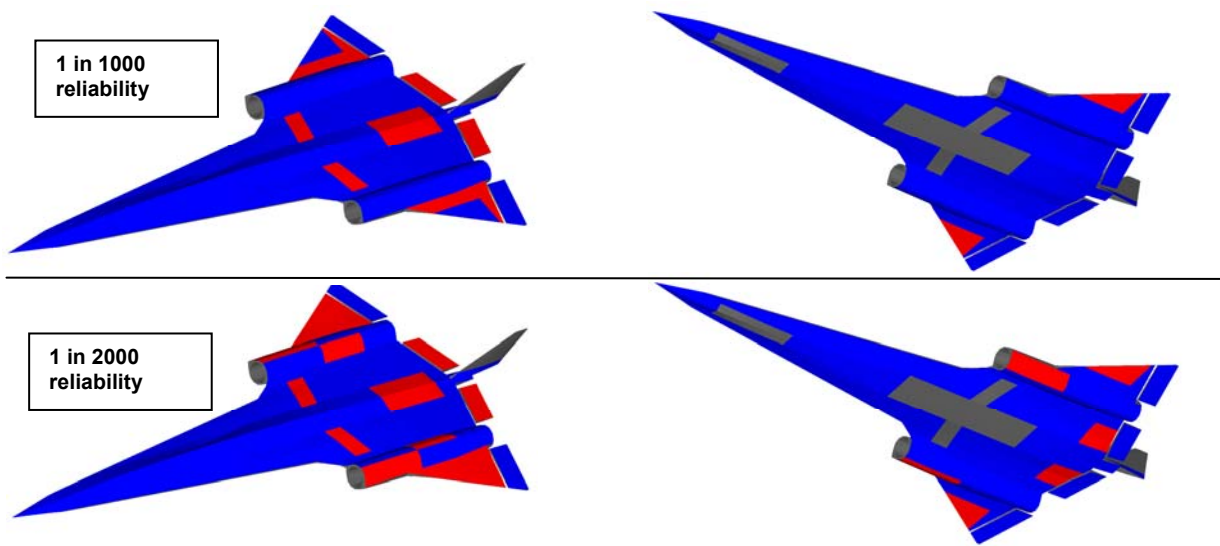


Fig. 1.2, Traditional zero-margin sizing approach cannot produce consistent structural integrity. The major concern is the areas of the vehicle identified in red. These are panel components that have less than 99.5% (1 in 1000) reliability top images and 99.75% (1 in 2000) reliability bottom images.

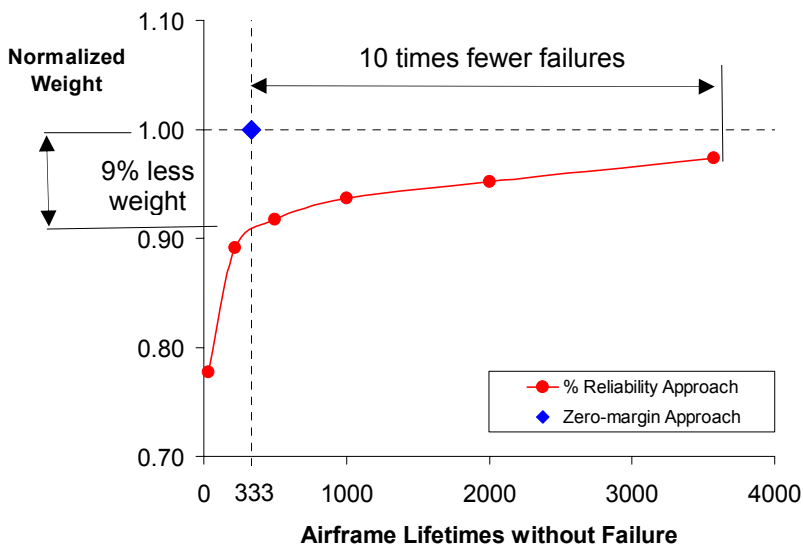


Fig. 1.3, Airframe structural weight versus lifetime failures. Significant reliability can be achieved with moderate weight growth.

## Part A: Introduction

### 2 Introduction

Airframe structural certification continues to require full-scale static testing. Though these tests are major program milestones, they are for the most part, validations of analyses, and not for actual certification of the airframe. Analyses can be used to identify many potential failure modes for all load cases. Physical testing costs and schedule delays prohibit examining all but a few potential failure modes for a limited number of load cases. Physical testing also becomes prohibitively expensive for full scale testing of components with thermal environments. As a result, most structural integrity evidence is provided not by tests, but rather by extensive **strength calculation**, or **stress analysis**, terms that are synonymous with analytical modeling. Analytical modeling of structures means the capability to predict 1) internal load distributions 2) the resulting detail stresses and strains, and 3) failure. Certification of structural integrity requires all three of these predictive capabilities.

#### 2.1 Problem: More test failures in last 25 years than in previous 50

Fig. 2.1 provides a relative score of how well aerospace is doing at predicting structural integrity [1]. The blue curve represents test predictions performed with modern analytical modeling approaches such as Finite Element Analysis (FEA). As compared to the red line, which represents pre-1976 aircraft test failures, this implies more erroneous predictions than in the past. Added to the original plot are green and purple curves. The green vertical line at 150% represents a perceived desired result. But considering statistics, we know this is not obtainable. Therefore, if failures are not to occur before 150%, then the necessary percent failures would follow a statistical distribution similar to that represented with the purple dotted curve.

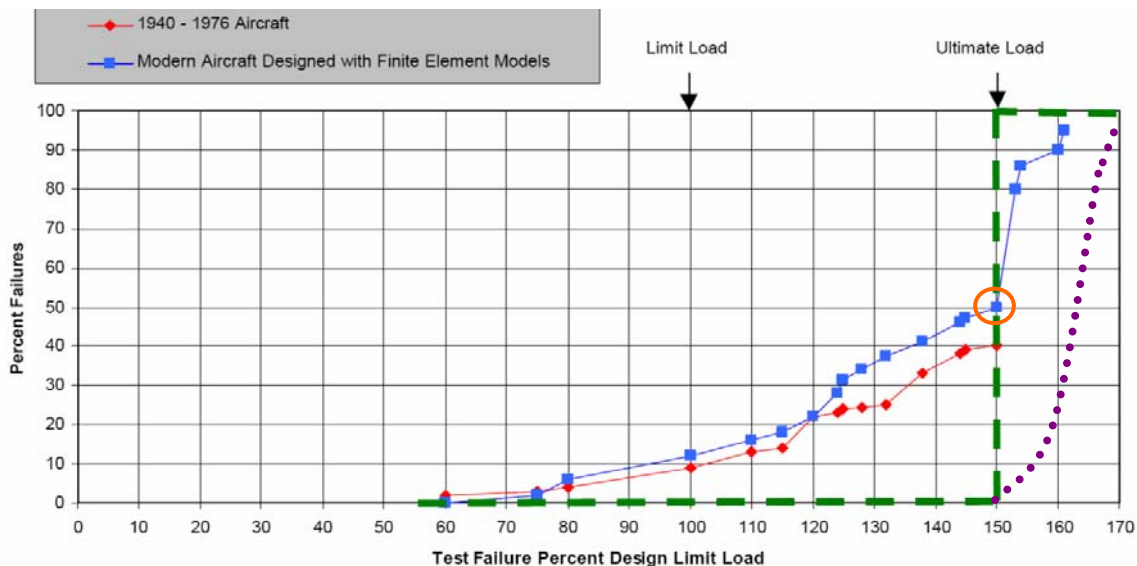


**Fig. 2.1, Aerospace test failures versus analysis predictions**

*Note: Red and Blue curves are percent test failures of wing, fuselage, vertical tail, horizontal tail, and unique major components before reaching required ultimate load of 1.5 Design Limit Load. The green vertical line at 150% represents a perceived desired result, but the purple curve represents the expected statistical distribution.*

The obvious question Fig. 2.1 poses is why structural integrity has not improved in modern times since computing hardware and analytical modeling techniques have improved and are available and applied on a production basis. There are several plausible reasons for this increase in aircraft failure before reaching required ultimate load. The first may appear due to FEA in general in that the Finite Element Model (FEM) is not more accurately capturing structural response of airframe structures. However, though improvements are necessary and will occur over time, it is held that state of the art FEA used in industry is accurately computing running “load paths” throughout the skin panels and internal substructure of airframes. The cause for less accurate pretest predictions may be attributed to three reasons. The first is improperly applied failure analysis predictions. The observed analytical modeling downfall is likely due to over reliance on FEA for detail modeling for detail analysis where specialized analysis tools are more robustly suited for failure prediction. Specialized analysis tools perform better than detailed FEA for failure prediction because they are designed specifically to represent a given phenomena, including its innate boundary conditions, and also because they are correlated to extensive testing to achieve required validation.

A second possible reason more test failures have occurred in the last quarter century is because the FEA-computed internal loads, though far more accurate, are also less conservative in their magnitudes. As a result, there is less room for error in failure predictions in a test environment where the applied load is explicitly known, and, therefore, the internal loads predicted are very accurately quantified without built-in conservatism. It is statistically meaningful to note that with the more accurate internal load predictions of the last quarter century, there are 50% failures at the ultimate design load of 150% limit load, noted with the orange circle in Fig. 2.1. This is expected when industry designs to 150% limit load (DLL), which is analogous to a 50/50 chance of a coin flip. If our goal is to avoid test failure at 150% DLL then we must design considering a statistical distribution as indicated with the purple curve of Fig. 2.1.

The application of validated tools by the aerospace engineering community is based on the traditional zero-margin-of-safety analysis approach, which relies on the use of an historical 1.5 ultimate load factor for necessary conservatism and confidence. In other words, airframe structure is designed to fictitious ultimate loads which are simply the actual worst case expected loads (called limit loads) increased by 50%. The third, and most important reason that test failures occur is that *one constant load factor, applied to all potential failure modes, is not possible to raise all deterministic failure analyses to the same level of safety.* Though providing substantial margin for analysis error, some failures to certain load combinations are not predictable to within 50%. This means that 150% DLL is not sufficient for some failure modes, and too conservative for others.

Described in this report are a design sizing and analysis process, based on building-block test data that brings all applied failure mode analyses to the same reliability. Incorporating this recommended approach, as implemented in HyperSizer, will lead to more consistent structural integrity in airframes and thus, contribute to more successful test programs in the future.

## **2.2 SBIR Approach**

Unlike unique hardware architectures, analysis tools benefit from a history of testing in that all previous test correlations can and should collectively contribute to increased confidence of their use. Analysis tools have and will continue to play an essential role in structural certification. This

report suggests a way to improve reliability of analysis tools so that the aerospace industry will be able to reduce specific architecture testing which accounts for 25 to 30% of product costs.

Though this report includes evaluations of analysis methods, emphasis is on increasing confidence in the predictions made with any given analysis method and the software that implements it. Described is an *analysis building-block* approach for *verification and validation* (V&V), which parallels conventional building-block testing processes. The building-block approach for hardware validation goes from the coupon to the test panel to the subscale article to the full scale test. For analysis methods, a building block process is a systematic way to validate specific analysis method cases, verify implementation in the software tool, calibrate prediction to test data, and establish failure data scatter as probability density functions (PDFs) from tests for probabilistic analyses. The PDFs are then used to define two separate correlation factors for performing test-data-driven reliability described in detail later.

Also described is a process for gaining more benefit from analysis tools by automating their use in conceptual and preliminary design phases. This aspect of minimizing design cycle time is most important since it accounts for 40 to 50% of product development costs. The objective is to deploy analysis tools as soon as reasonable in the design phase to make the biggest impact on the design progression. Referred to as *design by analysis*, this process provides beneficial early identification and avoidance of conceptual and preliminary design problems that could become extremely expensive to remedy in the final design cycle. In this way, *virtual testing* is continuous throughout the design progression, and confidence is maintained in being able to successfully certify structure at time of testing — with no unpleasant surprises.

### **2.3 Connection to HyperSizer**

The SBIR report is not meant to promote the HyperSizer commercial automated analysis and sizing software. However, since the SBIR developments have been incorporated into HyperSizer for the purpose of testing and demonstrating, and for the purpose of readily commercializing the new capabilities, a description of the software is provided. Relevant existing capabilities that provide a partial solution to efficient certification are described. Significant SBIR-developed capabilities were completed that specifically enhance efficient certification, and their descriptions are emphasized. Together, the HyperSizer existing and newly developed SBIR capabilities substantially improve efficient certification by providing three benefits:

- Benefit 1: More successful certification testing
- Benefit 2: Increased reliability (safety)
- Benefit 3: Lowered conservatism (less weight)

HyperSizer provides aerospace industry accepted standard engineering analysis methods, physics-based solutions, empirical data, and plug-in capability for industry and government specialty analysis codes. These analysis methods are automated with their input/output (I/O) seamlessly integrated (thereby reducing human error), linked with leading FEA packages and FEM modelers, and deployed in a modern Microsoft Windows® Operating System (OS) product where data integrity is maintained with an internal database management system. The software is also provided as an object model that can be customized and integrated into customer's proprietary structural analysis process.

HyperSizer was originally developed as a research code at National Aeronautics and Space Administration (NASA) Langley Research Center. Since 1996, it has been commercially

developed and supported by Collier Research. An important aspect toward validation is HyperSizer's data entry safeguard for unforeseen use by a non-developer. That is, a relatively experienced engineer in the subject field, who is not the tool developer, can reliably obtain the correct result with the tool. In addition to analysis, HyperSizer performs automated structural sizing to find the lightest combination of design concept, material, and cross-sectional dimensions for specific vehicle architectures. Referred to as robust sizing, the goal is to identify designs that are more likely to prove successful at time of test certification.

The AFRL Long Range Strike (LRS) shown in Fig. 2.2 is used to identify the innovation, summarize implementation of developments, and highlight the significance of the SBIR developments as implemented in HyperSizer. Sections 6 and 10 provide for more detail.

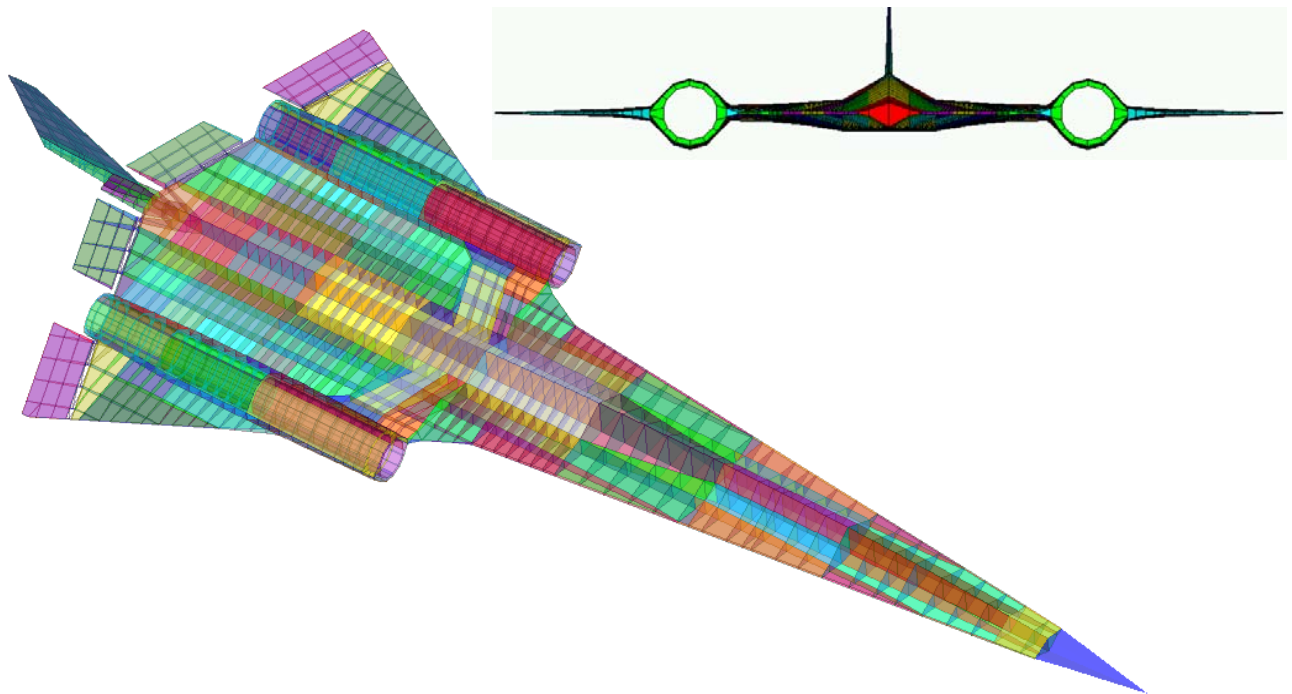


*Fig. 2.2, HyperSizer used for analysis, sizing trade studies, and weight estimation on the AFRL LRS*

*External skin panel structure and internal rib and spar substructure displayed in transparent view.*

## **2.4 SBIR Innovation and Development**

Principal innovation of this SBIR is categorized into two broad areas: test-data-driven reliability analysis and sizing, and new analysis methods and failure prediction for composite laminates and bonded joints.

### **2.4.1 Composite laminate and bonded joint strength**

As a PD tool that specializes in composite stiffened panels, a capability to accurately and rapidly perform non-FEA bonded joint analysis and optimization of the bond between the stiffener flange and skin was required. Developed is a capability to perform accurate and rapid 3D through-the-depth stress/strain predictions for input into 19 specific bonded joint failure criteria. Provided are over 300 pages documenting theoretical development along with verification and validation examples.

For composite bonded joints an extensive development project with six researchers continued for about 16 months on developing powerful and rapid joint stress/strain analysis for both adhesive and ply-by-ply adherends, see Fig. 2.3. In contrast to current industry practices that rely on detailed FEA (slow and susceptible to user error), or 1-D tools like Hart-Smith's A4EI software (limitations) this new method is both accurate for detail analysis and fast for sizing trade studies involving thousands of joint configurations and material combinations. Nineteen (19) different failure criteria are implemented. Comparison to available test data shows good agreement.

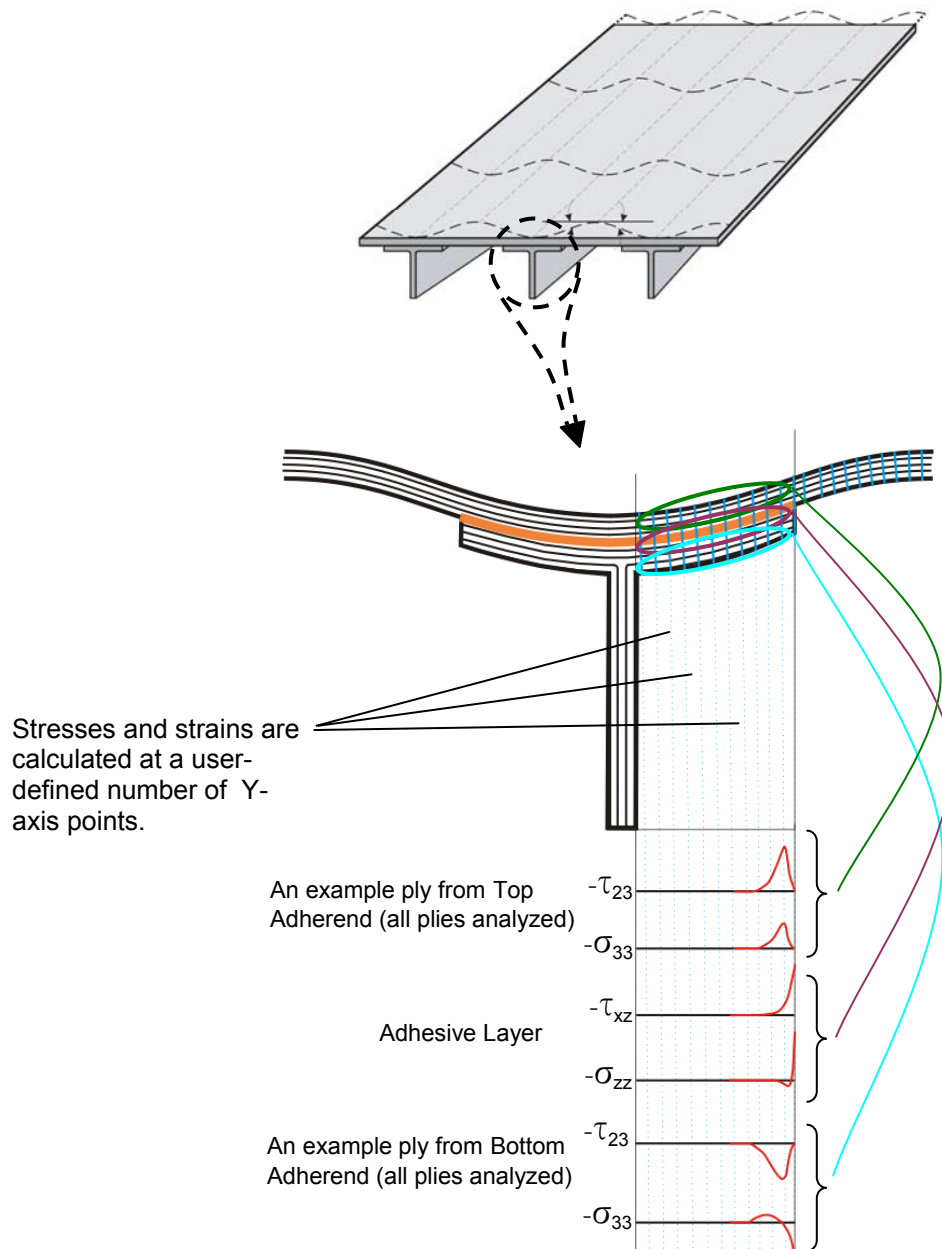


**Fig. 2.3, New capability to compute interlaminar stress throughout depth of bonded joint.**

*Note that adhesive stresses are in the panel coordinate system (x, y, z), adherend stresses are in each ply coordinate (1, 2, 3).*

Another primary analysis method developed is for composite laminate strength. Physics based failure criteria that identify failures between fiber and matrix were implemented and validated. Of particular note is the LaRC03 (2004) failure criterion integrated into HyperSizer which provides similar accuracy to Puck while being far more practical to implement robustly. For all composite failure criteria, CFs have been identified based on 130 different tests data points, including composite laminate failure from the World Wide Failure Exercises (WWFE).

## 2.4.2 Test data driven reliability analysis and sizing

Another primary SBIR development is test data driven reliability analysis and sizing, which we believe highlights this SBIR's innovation of achieving both airframe weight reduction and increased and consistent structural integrity, resulting in fewer lifetime airframe failures. As depicted in Fig. 2.4, the traditional aerospace practice of designing to a zero margin-of-safety and using a 1.5 ultimate load factor does not ensure consistent reliability, thus not providing desired airframe structural integrity. (Table 2.1 contains the data used to generate this plot.) As a comparison, for approximately the same weight as designed with the traditional zero margin approach, the test-data-driven reliability approach provides 10 times more vehicle lifetimes before failure. Holding the zero-margin-provided lifetime failures constant, the reliability approach saves a significant 9% weight (10.3% by linear interpolation).

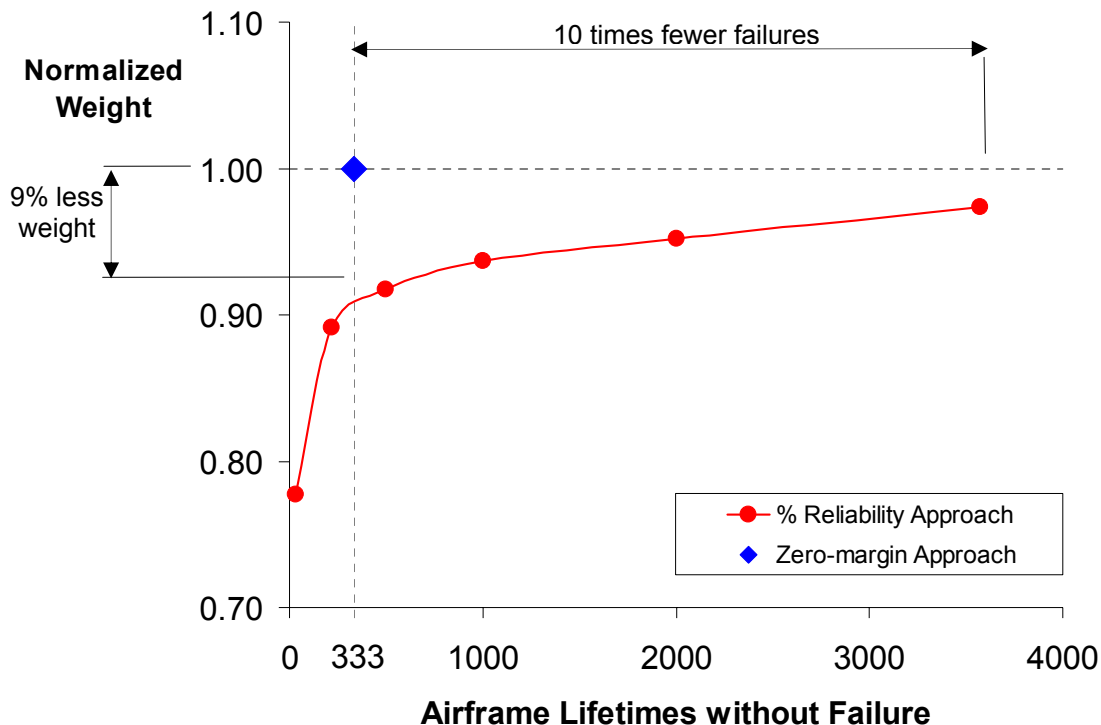


**Fig. 2.4, Airframe structural weight versus lifetime failures**

*Significant reliability can be achieved with moderate weight growth. Note also that the traditional zero-margin analysis currently practiced in aerospace provides neither acceptable structural integrity nor minimum weight.*

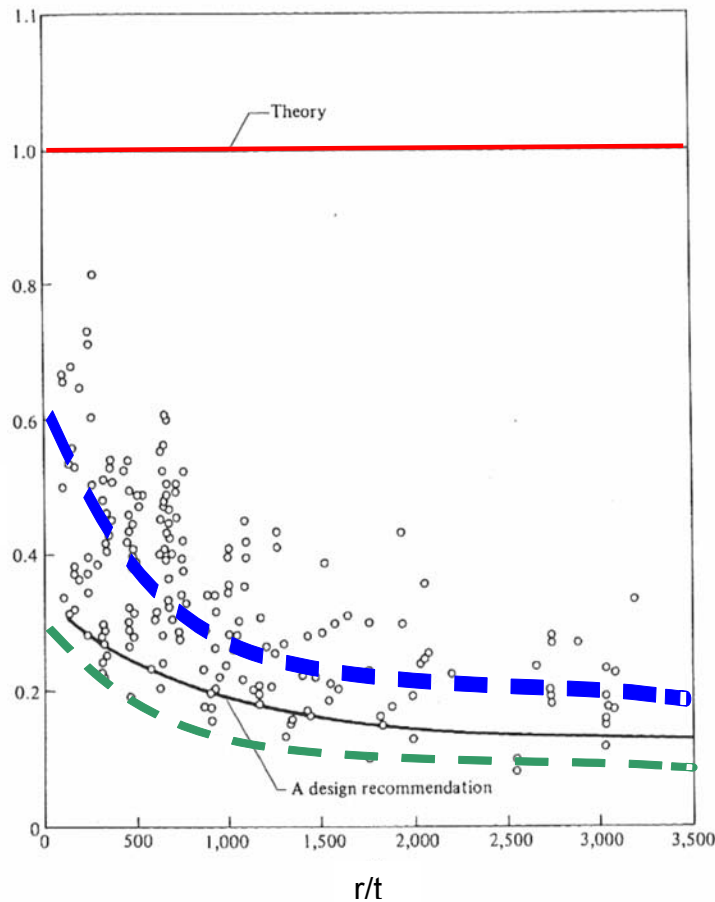


**Fig. 2.5, Traditional one knockdown approach to cylindrical panel buckling**

*Noted as a design recommendation, the black curve is the original NASA SP-8007 knockdown, the green curve, a possible more conservative knockdown, and the blue curve, the average (typical) failure. The original, one constant knockdown equation doesn't give insight into the average test data, nor does it allow the engineer to choose his level of reliability, such as the green curve.*

The classical problem of inaccurate theoretical curved panel buckling is used as an example of how this is achieved, Fig. 2.5 shows cylindrical panel buckling test data as points. Each test data point is normalized against its theoretical value (vertical axis). The horizontal axis represents decreasing theoretical accuracy as the radius/shell thickness ( $r/t$ ) ratio increases. Fig. 2.5 is related to the NASA SP8007 report [2]. Note the large discrepancy between theory (red line) and test results, i.e. inaccuracy of theoretical. The design recommendation is an established knockdown defined as an equation that includes the  $r/t$  ratio. So regardless if the knockdown is expressed as a single value or as a curve fit equation, the NASA one knockdown approach defines a once-and-for-all acceptable limit of risk.

Other curve fit equations, such as the blue and green curves can be defined based on a function of selected parameters. Even though the knockdown (black curve) is somewhat dynamic based on changing variables, in this case the  $r/t$  ratio, the first shortcoming with this traditional

approach is that the acceptable level of risk (black curve) is “cast-in-stone” when first defined, and for the most part unchanging as more test data becomes available. In fact, the actual comparison is rarely known by the practicing engineer.

A second shortcoming is the acceptable level of risk defined originally may not meet the reliability requirement of your particular design (shown as green dashed-curve). A program manager should be able to choose required knockdown/reliability for each design project. Furthermore, insight and flexibility should be provided to bring each analysis failure mode to a consistent value.

The third shortcoming, which also relates directly to the goal of efficient structural certification using analysis, is that with a single knockdown that takes the theoretical value (shown as red line) down to an allowable design-to value, does not provide nor expose any knowledge of an average or expected typical failure load, represented with a blue curve. So unlike being able to use “typical” material properties for test predictions, the user is left to perform test correlations using a “design-to” failure analysis allowable, which should for almost all cases significantly under predict, and be very conservative to test results.

As a note, the NASA knockdown, black curve, is approximately a 90% reliability against failure and is combined with a 1.5 ultimate load factor to achieve considerable conservatism (safety).

Hundreds of test data were collected for seven different failure modes and correlated to theoretical analysis predictions.

- Panel buckling
- Honeycomb wrinkling
- Bonded Joint Delamination
- Bonded Joint Fracture
- Composite Strength Tsai-Hahn
- Composite Strength LaRC03 Matrix Cracking
- Composite Strength LaRC03 Fiber Failure

Shown in Fig. 2.6 are these test results plotted as PDFs, normalized by the ratio of experimental test failure load to theoretical failure load prediction and depicted as a dashed (experimental/theoretical) line. Analysis PDFs that fall left of the dashed line unconservatively predict failure loads higher than experiments. These methods include panel buckling (blue curve) and honeycomb wrinkling (green curve). These theoretical analysis predictions need to be knocked down before using as design allowables. Panel buckling knockdown factors have been historically used to achieve this. However, using a single knockdown must include both analysis inaccuracy and the effects of test data scatter.

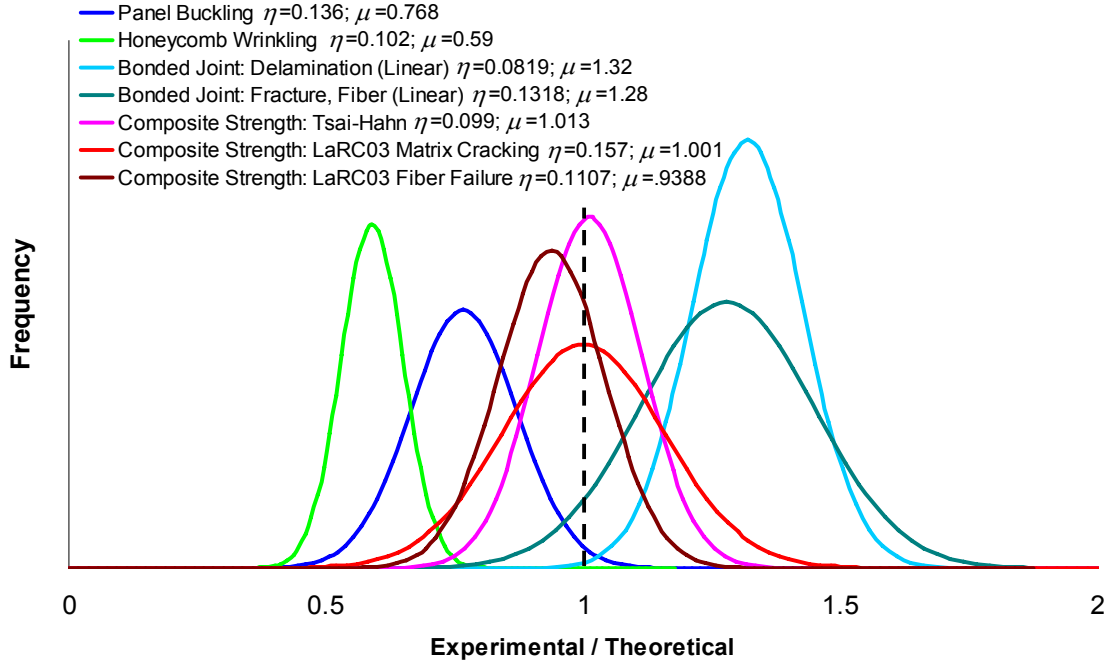


**Fig. 2.6, Probability density functions (PDF) for seven different failure mode analyses, based on hundreds of test correlations.**

The dashed line represents the normalized ratio of (experimental/theoretical). Analysis PDFs that fall left of the dash line unconservatively predict failure loads higher than experiments.

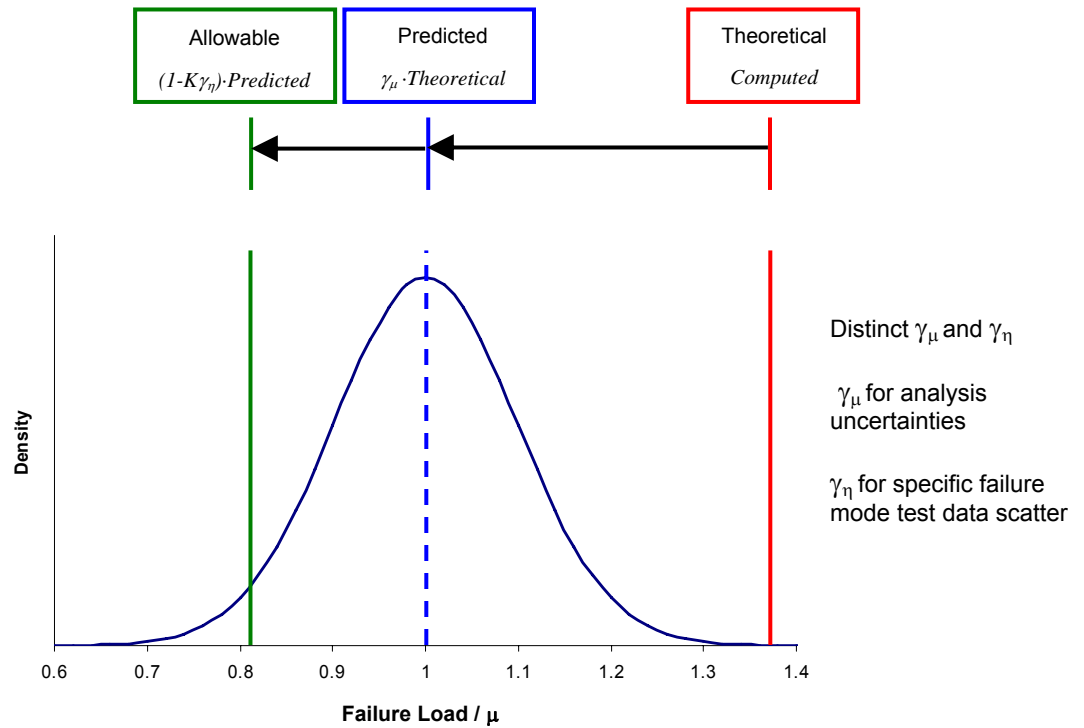


**Fig. 2.7, Application of the PDF for determining desired reliability (allowable load) with the two defined correlation factors (CF).**

The SBIR principal innovation identifies two correlation factors based on experimental data collection:  $\gamma_\mu$  for analysis uncertainties, and  $\gamma_\eta$  for specific failure mode test data scatter repeatability, Fig. 2.7. The approach is to base the calculation of probability of failure (or said in a positive way, reliability against failure) by use of the two newly defined, test data generated CF's. These CFs are generated from normalizing test data PDFs to specific failure analysis methods. In this way fidelity can be selected by the analyst for an airframe structural reliability analysis and sizing. More importantly, consistent structural integrity can be designed in during the preliminary phase of a project. Though this approach is based on probabilistic methods (PM), it is not the traditional and widely reported PM approach in use today. That approach is based on identifying PDFs for input variables (such as variability in material property elastic moduli or manufacturing thickness variations) and computing the effects of their complex interactions on the combined probability of failure. Doing so provides valuable benefits, and though we plan to implement such an approach into HyperSizer in the future, this is completely different from the probabilistic approach developed in this SBIR. Refer to sections 7, 8, 9 of this volume for more detail.

Using HyperSizer's implementation of the test-data-driven reliability developed in Phase II of this SBIR will not cost the end user more money to deploy for production work, nor will it cause a schedule delay to their analysis process. This is a solution that does not cause either to be increased. It is very practical to apply as demonstrated on the AFRL LRS.

### 2.4.3 SBIR innovation applied to LRS

The newly defined CFs for the failure modes of Fig. 2.6, specifically composite laminate strength, panel buckling, and honeycomb sandwich wrinkling were used for a reliability analysis of the AFRL LRS airframe. Shown in Fig. 2.8 are four LRS images where red color identifies weak areas of the airframe that have unacceptable safety based on two different lifetime criteria. As the criteria goes from 1 in 1000 failures to 1 in 2000 failures, as expected, more area shows up red. Table 2.1 lists weight savings of 5.6% and 4.1% respectively while meeting these reliability criteria. More detail and results are provided in Section 10 of this Volume I.

Table 2.1 summarizes the LRS airframe weight increase with increasing structural integrity. The bottom row lists the traditional zero-margin-of-safety results. These results were obtained by using HyperSizer for sizing optimization of each structural component of the external surface assembly. Each sizing variable's bounds were tuned to provide the lightest weight possible, which also means that most components have a near zero margin. Using this as a basis of comparison, this design was 'frozen' and passed to the new reliability analysis.

As described in Section 10, the fidelity of the margins of the frozen design were determined by the developed reliability analysis to be inconsistent. Though most were significantly greater than zero, some were negative. Using the lowest margin of any failure mode, for any component, the airframe reliability was backed out of the HyperSizer analysis to equal 98.5%. This equates to  $(1 / (1 - 0.985)) = 66.6$ , which implies that 1 in 66.6 vehicles will fail due to the design limit loading. However, DLL is statistically predicted to occur once in five (1 in 5) vehicle lifetimes. Therefore, the probability of failure for this approach is 1 in 333,  $(5 * 66.6) = 333$ . Based on the few known actual in-service structural failures, this appears to be low. We postulate that the magnitudes of the limit loads are also likely conservative, meaning airframes likely experience limit loads less than predicted. Therefore, in-service operation loads using the traditional zero-margin approach provides likely more than 1 in 333 lifetime airframe failures.

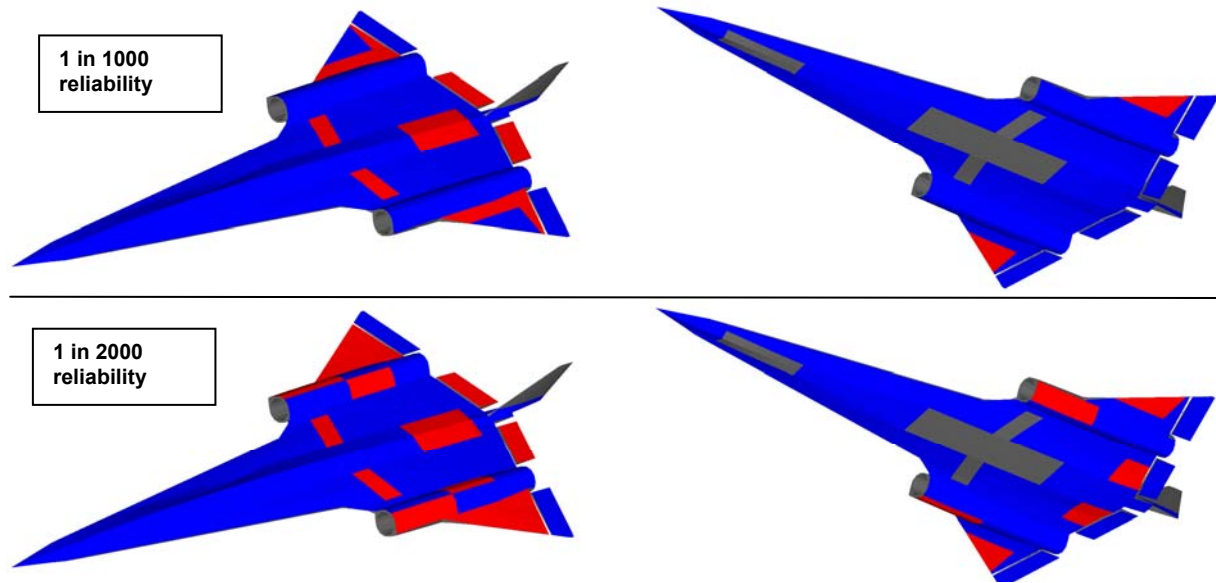


**Fig. 2.8, Traditional zero-margin sizing approach cannot produce consistent structural integrity.** The major concern is the areas of the vehicle identified in red. These are panel components that have less than 99.5% (1 in 1000) reliability top images and 99.75% (1 in 2000) reliability bottom images. The left images are the top of the LRS aircraft and the right images are the bottom. Gray color are unsized areas.

**Table 2.1, Airframe Weight Increases with Increasing Structural Integrity**

PDF Standard Deviation	Reliability	Lifetime Airframe Failures	Normalized Weight	Weight Savings
1 $\sigma$	85.1%	1 in 34	.773	22.7%
2 $\sigma$	97.7%	1 in 217	.887	11.3%
2.33 $\sigma$	99.0%	1 in 500	.912	8.8%
2.58 $\sigma$	99.5%	1 in 1000	.932	6.8%
2.81 $\sigma$	99.75%	1 in 2000	.947	5.3%
3 $\sigma$	99.86%	1 in 3571	.969	3.1%
<b>Traditional</b>	<b>98.5%</b>	<b>1 in 333</b>	<b>1</b>	<b>0%</b>

For traditional zero-margin analysis, the reliability of material strengths (metallic and composite damage initiation) are very high. The use of ‘A’ or ‘B’ Basis allowables from MIL-HDBK- 5 and 17 provide substantial conservatism, especially when combined with the 1.5 ultimate load factor. So a material strength failure is not likely to occur in-service, at least not for pristine (undamaged) material. Other failures, such as instability (panel buckling, local buckling, crippling) or honeycomb wrinkling, are more likely to occur in traditional zero margin designs.

Fig. 2.9 illustrates an interesting result. As the reliability criteria is increased, the controlling failure modes become different. Failure modes which have the highest observed scatter in test results (a higher statistical standard deviation) will control more as reliability is increased. Therefore the relative width of the PDF as shown in Fig. 2.6, and quantified with the CF  $\gamma_\eta$  (also noted simply as  $\eta$ ), affects higher reliabilities. As shown in Fig. 2.6, wrinkling, Tsai-Hahn, and LaRC03 fiber failure criteria all have  $\eta$  values close to 0.1. Panel buckling has a  $\eta = 0.136$  and

LaRC03 matrix cracking composite strength has a  $\eta = 0.157$ . Therefore, as the reliability increases, the controlling failure mode goes toward panel buckling (blue) and LaRC03 matrix cracking (red) which have higher  $\eta$  factors and away from Tsai-Hahn and LaRC03 fiber failures. The  $\gamma_\mu(\mu)$  CF for analysis inaccuracy is constant regardless of % reliability.

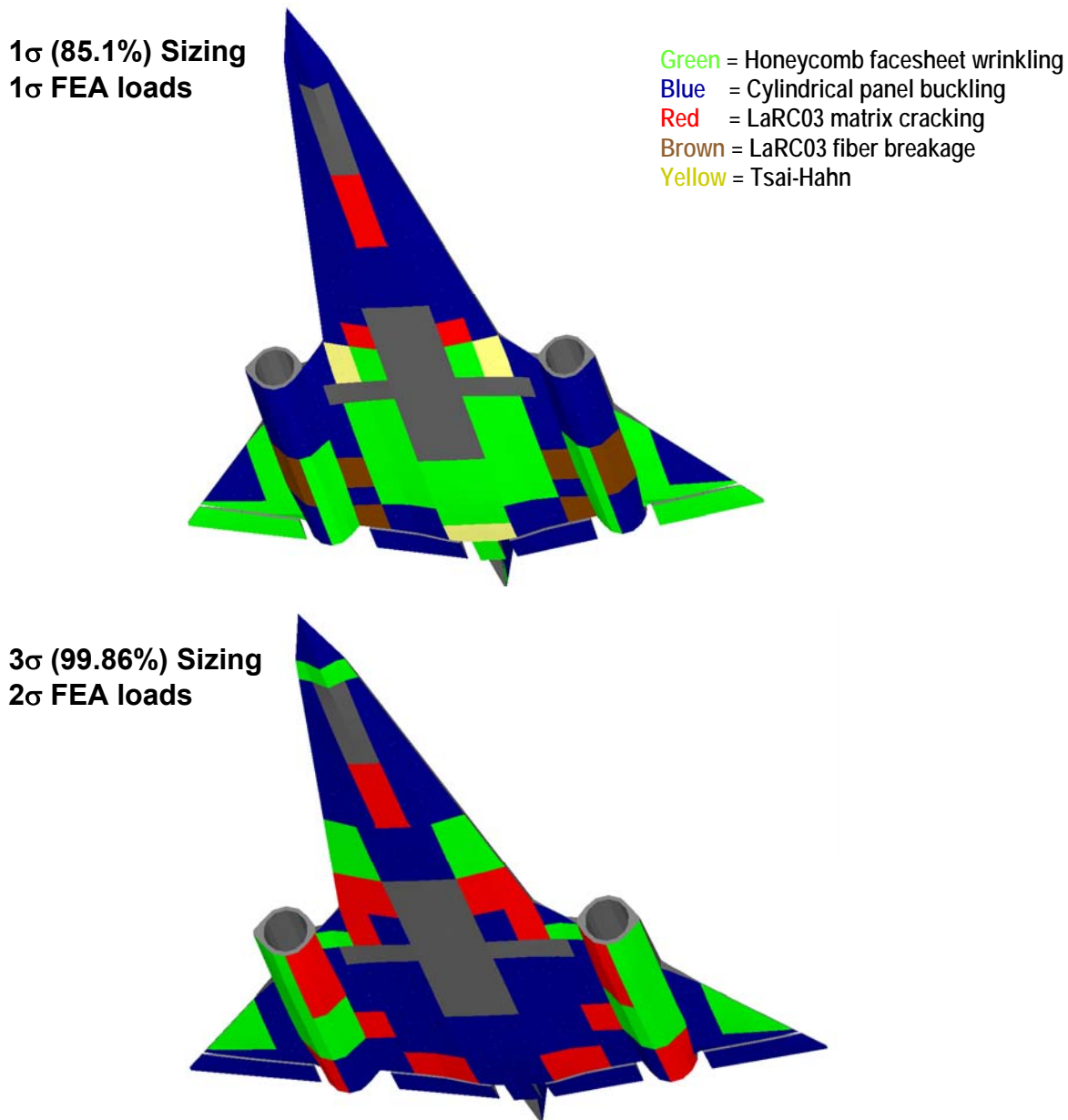


**Fig. 2.9, Effect of varying reliability on controlling failure mode.**

As the specified reliability increases, the controlling failure modes change. At the lowest reliability (1 $\sigma$  or 85.1%), all activated failure modes are controlling some location of the vehicle, with most of the bottom surface controlled by honeycomb wrinkling. Wrinkling, Tsai-Hahn, and LaRC03 fiber failure criteria all have CFs for test scatter,  $\gamma_\eta$ , close to 0.1. As the reliability increases, the controlling failure mode goes toward panel buckling (blue) and LaRC03 matrix cracking (red), which have higher test scatter,  $\gamma_\eta$  factors. The gray areas represent structure not sized in this study such as the doors for the main landing gear and the nose gear.

## **2.5 Report Contents**

The remainder of this Volume I SBIR report is divided into three parts.

### **Part B: SBIR Success Story Highlights and Commercialization (Sections 3 & 4)**

This section covers the subcontractor Lockheed Martin Aeronautics' use of HyperSizer during the SBIR Phase II and their implementation on a small scale on nearly all of their on-going Air Force airframe designs: F-16, F-35, F-22, C-130, and others. Note Lockheed's use of HyperSizer is with both SBIR funding and their own internal funding independent of subcontractor SBIR money. Both a business and technical conclusion is provided. The software sales and training at their facilities are also covered. This section ends with a listing of primary SBIR developments commercially available.

### **Part C: Efficient Certification: An SBIR Implemented Solution (Sections 5 - 9)**

This section starts by describing eight primary inconsistencies of aerospace structural analysis. Three principal SBIR thrusts are put forth as a solution. Description is provided for how the existing HyperSizer and how the new SBIR developments implemented into HyperSizer address each of these thrusts.

1st SBIR thrust: integrate tools and processes

2nd SBIR thrust: reduce order modeling and high fidelity rapid analysis

3rd SBIR thrust: use uncertainty/reliability analysis

### **Part D: SBIR Solution Demonstrated with New HyperSizer Software (Sections 10 & 11)**

This section's purpose is to compare two analysis approaches. The first approach is the traditional zero margin-of-safety currently used in aerospace industry. The second approach is the new SBIR developed approach that uses test data to drive reliability analyses. Two examples are provided. The first is a single vehicle location. The second is an entire airframe preliminary design of the AFRL Long Range Strike (LRS). Though summary results are shown on the previous pages, Section 10 provides more results and trades.

Volume II: Detailed Report on Innovative Research Developed, Applied, and Commercially Available contains approximately 250 pages. The emphasis of Volume 2 is on the theory, implementation and verification & validation of HyperSizer's new and existing failure methods. Limitations, scope, and the purpose of developing a new capability are addressed in detail as well as issues with predicting peak bonded joint interlaminar stresses. Joint failure criteria are also presented in detail. Theoretical implementation of physical based composite laminate stress analysis is described in detail for LaRC03 (NASA Langley 2004) method, Hashin, and Boeing's strain invariant failure theory (SIFT).

Volume III: Appendices of Verification and Validation Examples, Correlation Factors, and Failure Criteria contains approximately 290 pages of extensive verification and validation of composite bonded joint failure, laminate failure, panel buckling failure, and honeycomb sandwich failure. This volume also includes a listing of all correlation categories and their CFs.

## Part B: SBIR Success Story Highlights and Commercialization

### 3 SBIR Success Story Highlights: Lockheed Martin Aeronautics, Advanced Development Program (ADP)

Lockheed Martin Aeronautics Company (LM Aero) Advanced Development Program (ADP) was a major subcontractor to Collier Research Corporation on this SBIR. Work was performed at both LM Aero's Fort Worth and Marietta locations. Both locations report success due to this SBIR.

LM Aero ADP successes on Air Force projects including F-35, F/A-22, C-130, and J-UCAS:

- Vehicle weight reduction
- Design optimizations on future vehicles
- Decreased analysis time (results in a fraction of the time of other methods)
- Design improvements on existing vehicles
- More efficient structural analysis
- More accuracy in quantified analysis and sizing results
- Fast results were achieved in areas where previously capability did not even exist
- Cost savings on analysis and trade studies
- Less costly structural designs
- Higher level of confidence in the LM structures community on selected structural designs
- An architecture for adding LM in-house tools
- A much more robust technique for referencing methods
- More weight-efficient structural designs

#### 3.1 *Business Conclusions*

One of the general benefits of the SBIR was to enable most of the structural engineers within Lockheed Martin to become aware of the unique capabilities of HyperSizer with all of the enhancements achieved through this program. In a specific application under the Advanced Aluminum Aerostructures Initiative CRAD effort, HyperSizer was the tool used to examine alternate material/design configuration options for a redesign of the F/A-22 nose landing gear doors. **The resulting low-manufacturing-cost, virtually weight-neutral design that HyperSizer identified is now being incorporated as the new production design, which will provide a major cost savings benefit to the program.** HyperSizer's availability, made possible through this SBIR, provided the only means possible to conduct the trade studies necessary to examine and derive the most efficient design concept within the limited time and budget constraints of the effort.

As a result of the recognized benefits that HyperSizer has demonstrated, the Lockheed Martin's Advanced Development Programs organization will be using HyperSizer to perform structural trade studies on Air Force CRAD and other internally funded efforts in 2005 and beyond, such as those that will be required on the new advanced mobility platforms. With the increased emphasis being placed on loads-based structural sizings to take place during conceptual design phase of any new aircraft, Lockheed Martin intends to incorporate HyperSizer into its automated structural sizing capabilities for use within a multi-disciplinary optimization type of process.

This will serve to determine realistic optimum material and design concept selections and resulting structural weights for many more design iterations than would have been possible in the past. The result will be a higher level of confidence that the selected structural designs will provide enhanced value to future Air Force products over any designs generated without this technology.

Three distinct reports are presented in this section, each providing a different perspective on the business impact of this SBIR Phase II project. The three reports were provided by:

- 1) *LM Aero ADP, Fort Worth*
- 2) *LM Aero ADP, Marietta*
- 3) *Collier Research Corporation*

### 3.1.1 LM Aero ADP, Fort Worth

Following is the report written by LM Fort Worth:

Through efforts undertaken as a direct result of Lockheed Martin's involvement with this SBIR, real product improvements are being realized on the C-130 and F/A-22 airframes in terms of cost and/or weight reduction. Future design optimizations and existing design improvements are expected on these aircraft as well as on J-UCAS and F-35 through the use of HyperSizer and all of the improvements incorporated during this SBIR. The analysis and sizing results produced were much more accurately quantified and were produced in a small fraction of the time it would have taken to do reduced-quality efforts using other methods – either that or the efforts would not have even been attempted due to lack of capability. The cost savings realized on the analysis and trade study efforts themselves is an additional benefit. The SBIR also allowed these capabilities to become known to, and enabled a confidence to be built in, the Lockheed Martin structures community. It is being shown that the end result is more efficient structural analysis, and more weight-efficient and less costly structural designs, being applied to existing and future Air Force platforms.

The Collier Research SBIR was critical in the completion of several technology development and verification projects within the Advanced Development Programs (ADP) Branch of Lockheed Martin Aeronautics Company. These projects include:

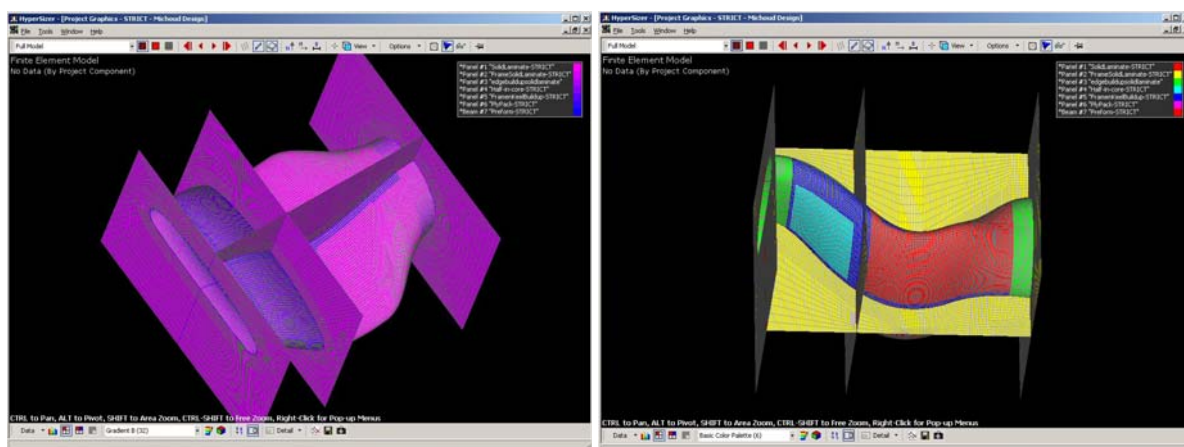


Fig. 3.1, The STRICT inlet duct program (used as analysis correlation tool for 2 phases of this program)

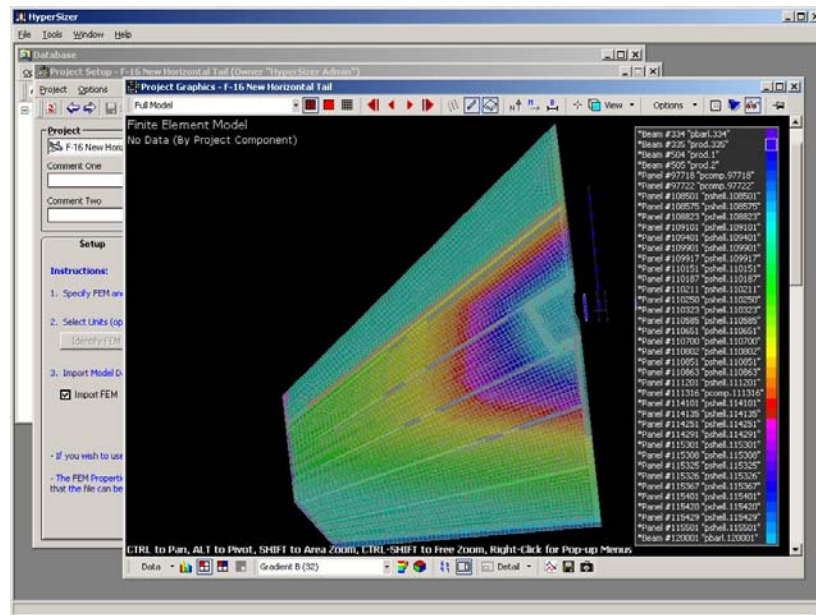


Fig. 3.2, The Unitized Composite F-16 Horizontal Tail (verified skin analysis)

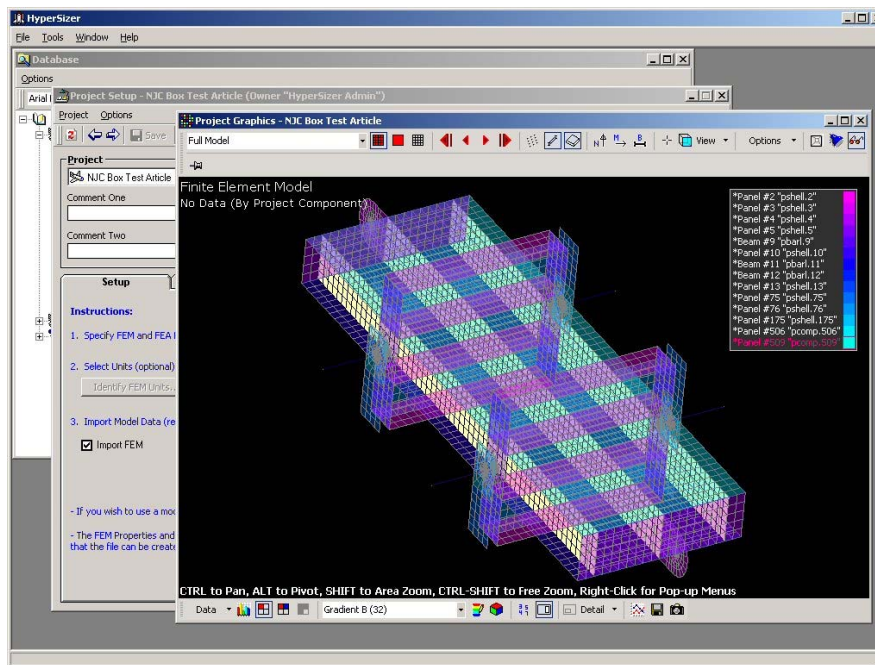


Fig. 3.3, The NJC Test Box (composite box test structure used for evaluating combined loading)

Most of the programs mentioned are technology development and demonstration programs which directly benefit current and future U.S. Air Force projects. In the initial phase of the SBIR, we were trained in the use of HyperSizer and incorporated it as a supplemental analysis tool for several of our projects (some mentioned above). After verifying its usefulness, we provided some useful feedback to Collier Research regarding possible improvements, etc. **Our only**

**regret/drawback was that most of our programs or projects were not fully tested to the point of achieving structural failures. This prevented us from providing data to help Collier Research validate, correlate, and expand the software.**

So, how did HyperSizer help us with our existing programs? It helped us identify critical areas and possible failures that we hadn't considered. It decreased analysis time by providing a "roadmap" for a specific project. This was done with fast and simple manipulations of our existing Finite Element Models that we linked to HyperSizer, or by simply creating standalone HyperSizer models representative of portions of our structure.

At Lockheed Martin Aeronautics Company, we have a vast collection of analysis tools at our disposal. Most of these tools are stand alone codes which help in a step of the analysis process. HyperSizer not only functions as a integrated collection of similar tools, but it also provides the architecture to add some of our tools to its functionality. It clearly augments our ability to design a robust structure while helping make this structure the lightest solution. As structural analysts, we sometimes overlook the overall picture regarding weight. As a result, we typically spend lots of time redesigning the same structure to minimize weight. HyperSizer is the kind of tool to get the analyst on the right track from the start.

Within our group in ADP, we look forward to incorporating HyperSizer into some our current programs, including J-UCAS.

### **3.1.2 LM Aero ADP, Marietta**

Following is the report written by LM Marietta:

One of the purposes of Lockheed Martin's involvement in the SBIR was the collection of historical test data to be used to validate HyperSizer's corresponding analytical solutions. One thing that came to light as test reports were examined was the incomplete nature of the documentation of the test data and the difficulty in locating any correlation of analysis to test results. As a result, the amount of test data deemed useful, at least from the standpoint of usability for the purposes of this effort, was much less than had been expected going into the program. Another issue that required unanticipated resources to try to resolve was that of the proprietary nature of some of the test data and analysis. To be used effectively as in documentation for analysis results, the data had to either be sanitized (which would greatly reduce its usefulness) or be officially determined not to have any detrimental results to Lockheed Martin should it be made available to the general public. An argument was put forth and accepted to change the labeling of the test report data, such that it no longer carried the need to be kept proprietary, and the test data was finally delivered – albeit too late to use within the timeframe of the SBIR.

**As a result of comments received from HyperSizer users in the past regarding a lack of knowledge of the precise methodology used to produce the resulting margins of safety, a much more robust and thorough way of referencing the methods was incorporated into the software, with the development of the HyperFinder search capability and over 1000 pages of technical documentation.**

Along these same lines, it was also decided that a significant benefit could result from having structural methods experts from industry examine and critique the physics behind the answers that HyperSizer generates. As a result, several industry experts in the area of structural analysis

and methods from Lockheed Martin Aeronautics Company agreed to participate in special sessions set up for this purpose. Much of the time was spent going over the applicable methods that HyperSizer uses, to which there was general acceptance for the analyses covered. There was considerable discussion on additional capabilities that should be incorporated.

One subject that came up during the methodology discussions pertained to existing in-house proprietary codes and methods -- especially in the instance where these methods may cross the capability boundaries of HyperSizer. The more philosophical issue of whether or not Lockheed Martin Aeronautics Company should attempt to renew and expand upon some of its own in-house tool development that may contain proprietary, time-tested analytical methods not contained in HyperSizer (but without the efficiency and ease-of-use that HyperSizer has), versus letting an outside entity such as Collier Research use, incorporate, and maintain, and improve upon these capabilities for our internal use. Part of the difficulty of that decision lays in the fact that such an in-house methods development capability would likely never be attained again once it is relinquished.

**There is general agreement, however, that there are capabilities that HyperSizer has that do not exist (either in-house or COTS) that are of tremendous value to the general aerospace structures community – even more so now with the enhancements made during this SBIR and by the industry feedback enabled by this SBIR to be incorporated in future improvements.**

Some effort was devoted to a subject not specifically spelled out in the original SOW. Realizing that the technical accomplishments achieved under the SBIR might never be implemented in future aerospace applications without ensuring that the software product involved got used, steps were taken to reach out to the structures community to inform them of the products capabilities – many of which are either not currently available at all, or if available, are more cumbersome to use. Much of this was accomplished through the publishing and communication of results obtained using HyperSizer on various CRAD activities, as discussed in Section 3.3.

### **3.1.3 Collier Research Corporation**

Our assessment based on exposure to industry methods and practices is that HyperSizer would be a valuable addition to the efficiency and accuracy of aerospace industry methods, especially in preliminary design. HyperSizer performs many different types of failure analyses in a more rapid, automated and less human error manner than currently practiced in the aerospace industry. Though targeted to the preliminary design phases of a program where many rapid trade studies and weight reduction efforts are required, the software incorporates many of the same fidelity analyses currently being used for final design and margin-of-safety reporting. There are several key analyses HyperSizer does not yet perform, but with the substantial methods documentation now available as a result of this SBIR, the end user can determine which analyses HyperSizer is performing and to what level of accuracy. HyperSizer also performs valuable analyses not currently being performed in industry.

Industry in-house legacy codes for certain specific niche applications have extensive verification and validation (V&V). HyperSizer contributes by offering a tightly integrated, controlled, and robust software architecture. HyperSizer also contributes by reducing the possibility of inconsistent boundary conditions assumed between Global-Local-Detail analyses that are inherent with the operation of stand alone codes.

There is a problem getting on an existing or especially old program. The consensus is that a new software tool (regardless if commercial or in-house developed) will only be accepted for use by new programs. A problem as exemplified with existing programs, such as the C-5, is that the project cannot afford to renew efforts in formalizing acceptance of a different method/code for a successful program. If the new code generated the same answer, then there is no compelling reason to adopt the new tool, and if the new tool provides a different answer, then the issue becomes determining whether the new answers or the old ones are correct.

HyperSizer's existing and newly developed SBIR capabilities substantially improve efficient certification by providing three benefits.

- Benefit 1: More successful certification testing
- Benefit 2: Increased reliability (safety)
- Benefit 3: lowered conservatism (less weight)

### **3.1.3.1 Benefit 1: More Successful Certification Testing**

HyperSizer contributes in several ways to the certification by analysis initiative. HyperSizer capabilities are moving beyond the conceptual and preliminary design phases, to mature its usability for final design. Many analyses required for airframe certification are included in its controlled software environment, which in itself is a framework for plugging-in user defined validated analysis codes. It is able to input and maintain analysis building block test data and it is able to use this test data to perform reliability based analysis and design sizing. As an automated sizing tool that achieves consistent structural integrity, it is able to produce robust designs using Probability Density Functions (PDF) signatures as defined with correlation factors.

### **3.1.3.2 Benefit 2: Increased Reliability (Safety)**

Principal innovation of this SBIR is categorized into two broad areas: Test data driven reliability and new analysis failure prediction methods for composite laminates and bonded joints. Both highlight this SBIR's innovation of achieving both airframe weight reduction and increased and consistent structural integrity resulting in fewer lifetime airframe failures. The traditional aerospace practice of designing to a zero margin-of-safety and using a 1.5 ultimate load factor does not ensure consistent reliability, thus not providing desired airframe structural integrity. As a comparison, in the Long Range Strike example described in Section 2, for less weight as designed with the traditional zero margin approach, the **test data driven reliability approach** provide **more vehicle lifetimes before failure**. By holding the zero-margin provided lifetime failures constant, the reliability approach **saves significant weight** (see details in section 2.)

Specifically the developed and demonstrated test data driven reliability includes statistically processed FEA loads, the ability to design for minimum weight using a robust design-by-analysis tool in which the stress analyst, using the same tool, can perform final margin-of-safety reporting. Together a structure may be certified with less testing.

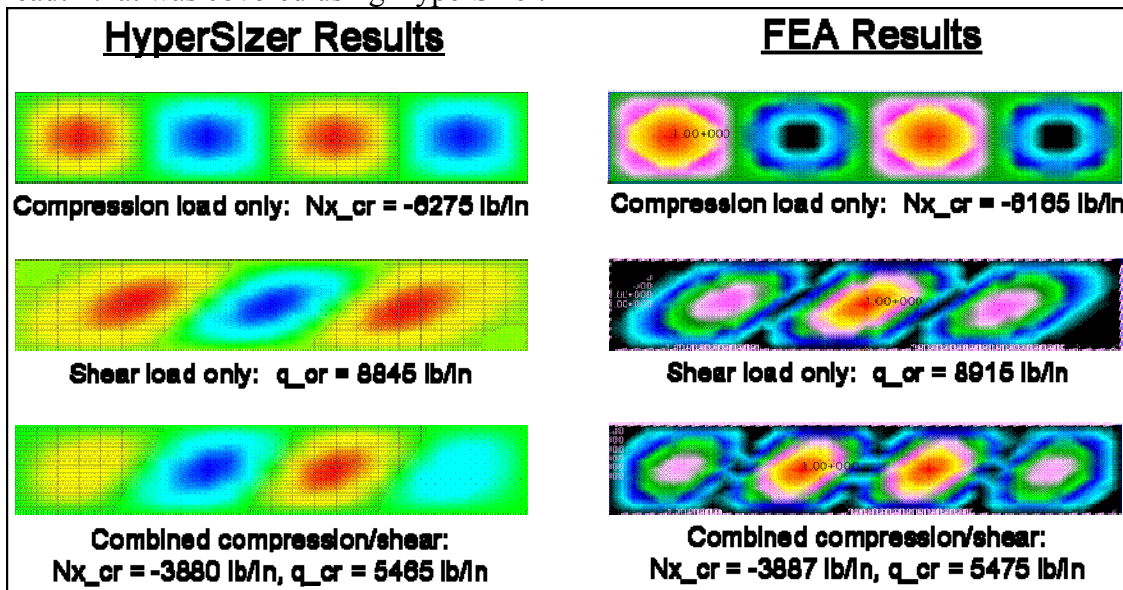
### **3.1.3.3 Benefit 3: Lowered Conservatism (Less Weight)**

Due to the innovative methods developed under this SBIR, ultimate load factors can be set to 1.0 instead of the typical 1.5 because the necessary conservatism is already included in the reliability analysis. This gives the desired benefit of less weight while maintaining increased consistent reliability and safety in the designed product.









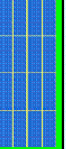
## 3.2 LM Aero's Implementations

### 3.2.1 F-35 (JSF)










During December 2004, the F-35 horizontal tail skin panels were analyzed and optimized with HyperSizer. Many grid-stiffening concepts were evaluated with several loading combinations. The projected HyperSizer weight savings were in the 30-40% range. This trade study took a total of 4 days to complete. No trade study would have taken place that could come close to covering the breadth that was covered using HyperSizer.



### Trade Study Matrix

Load Case	Compr. Ld (lb/in)	Shear Ld (lb/in)	Optimized Stiffening Arrangement for Each Concept and Loading			
			Uniaxial	Isogrid 0° angle	Isogrid angle	Orthogrid
1	-6490	0				
2	-6074	1000				
3	-5628	2000				

Load Case	Compr. Ld (lb/in)	Shear Ld (lb/in)	Optimized Stiffening Arrangement for Each Concept and Loading			
			Uniaxial	Isogrid 0° angle	Isogrid angle	Orthogrid
4	-5143	3000				
5	-4606	4000				
6	-4021	4963				

**Optimum Designs Outlined in Green**

Fig. 3.4, Top image is verification of HyperSizer buckling to MSC/NASTRAN FEA. Note the very close comparisons in buckling load and mode shape. Bottom image is the grid stiffened panel concepts traded and their resulting optimized shapes.

### 3.2.2 F-22

#### F/A-22 nose landing gear door redesign –

Under the Advanced Aluminum Aerostructures Initiative (A<sup>3</sup>I) CRAD effort, several material and design concept combinations for a redesign of the F/A-22 nose landing gear doors were traded using HyperSizer to find the best combination of high stiffness and minimum weight. HyperSizer allowed several trade studies to be run in a very short period of time, and was also used to modify and mature the structural design. An initial validation of the resulting optimum configuration was achieved by the F/A-22 Structures group via FEA. The preliminary projected cost savings for the new NLG doors from Lot 5 on were much more than sufficient to submit a Process Improvement Program (PIP) proposal to perform further design refinement, analysis, and updated cost projections.

It should be noted that the depth, scope, and fidelity of the trade studies performed, resulting in this potentially substantial savings on F/A-22 production costs, would not have been possible within the A<sup>3</sup>I budget and schedule constraints without the use of HyperSizer.

The existing design consists primarily of composite sandwich structure, which uses graphite/epoxy fabric facesheets and a glass/phenolic honeycomb core. Bending and torsional stiffness are the primary design drivers. HyperSizer was used to examine this sandwich portion of the redesign.

**Table 3.1 Panel Concept Trades**

	Design Concept	Weight (lb/ft <sup>2</sup> )	Bending Stiffness (lb-in <sup>2</sup> /in)	Torsional Stiffness (lb-in <sup>2</sup> /in)	Natural Frequency (Hz)	Skin thickness (in)
b/l	Baseline - Gr/Ep Fabric facesheets with glass/phenolic honeycomb core	2.162	424549	117985	2619	
1	Grid-stiffened, non-sandwich - Aluminum skin and grid material	3.358	473774	123144	2218	
2	Grid-stiffened, non-sandwich - SiCp/Al skin and grid material	2.419	457990	121568	2570	
3	Sandwich - Aluminum facesheet with aluminum foam core using <i>full</i> baseline bending and torsional stiffness constraints	2.704	465260	154988	2463	
3a	Sandwich - Aluminum facesheet with aluminum foam core using <i>reduced</i> baseline bending and torsional stiffness constraints	2.173	245043	81629	1993	
4	<b>Sandwich - Aluminum facesheet with aluminum bi-grid core using <i>full</i> baseline bending and torsional stiffness constraints</b>	1.721	487296	151330	3110	0.042
5	Sandwich - Aluminum facesheet with aluminum honeycomb core using <i>full</i> baseline bending and torsional stiffness constraints	1.800	465260	154988	3018	0.038
6	Sandwich - SiCp/Al facesheet with aluminum foam core using <i>full</i> baseline bending and torsional stiffness constraints	2.404	457514	153265	2590	
6a	Sandwich - SiCp/Al facesheet with aluminum foam core using <i>reduced</i> baseline bending and torsional stiffness constraints	2.160	330816	110822	2324	
7	<b>Sandwich - SiCp/Al facesheet with SiCp/Al bi-grid core using <i>full</i> baseline bending and torsional stiffness constraints</b>	1.394	507291	160108	3535	0.032
8	Sandwich - SiCp/Al facesheet with aluminum honeycomb core using <i>full</i> baseline bending and torsional stiffness constraints	1.608	477944	160108	3237	0.032

The baseline composite design was replicated in HyperSizer to establish its unit weight and stiffness properties, taking advantage of the baseline materials' property data already in HyperSizer's standard database and generating the baseline facesheet ply layup definition in the Material Manager. The computed property feature was used to set these minimum D-matrix

properties for the various design concepts considered. Several combinations of concepts and materials were examined. HyperSizer's Material Manager was used to create material properties for particulate-reinforced aluminum material that proved to be a part of the most weight-efficient designs. Table 3.1 summarizes the results of the study.

As a result of this effort, a more detailed design effort will be undertaken within A<sup>3</sup>I that will include a more efficient hinge attachment re-design and detailed features to accommodate the hinge loads and close-out of the sandwich.

### 3.2.3 C-130

#### Center wing bulkhead sizing trades –

Under the Advanced Aluminum Aerostructures Initiative (A<sup>3</sup>I, AFRL/VA CRAD program), trade studies were performed on a C-130 center wing bulkhead web to come up with an integrally-stiffened friction stir welded (FSW) design to replace the structurally efficient (but more costly) fastened hat-stiffened web design. HyperSizer was used to come up with a minimum-weight stiffener cross-section that met the baseline design criteria. Also included in the study were two blade-stiffened designs to quantify the weight penalty that such a cross-section would produce.

Since the section design selected was an elliptical bulb stiffener, Excel was used to convert the I-section rectangular cross-sectional dimensions used in HyperSizer to an equivalent section for the actual design. The ability to generate numerous acceptable cross-sections in quick fashion allowed the design optimization to factor in extrusion manufacturing and cost considerations to determine the overall preferred design. The project stress organization then used these sections as a guide to determining their own final design shown below.

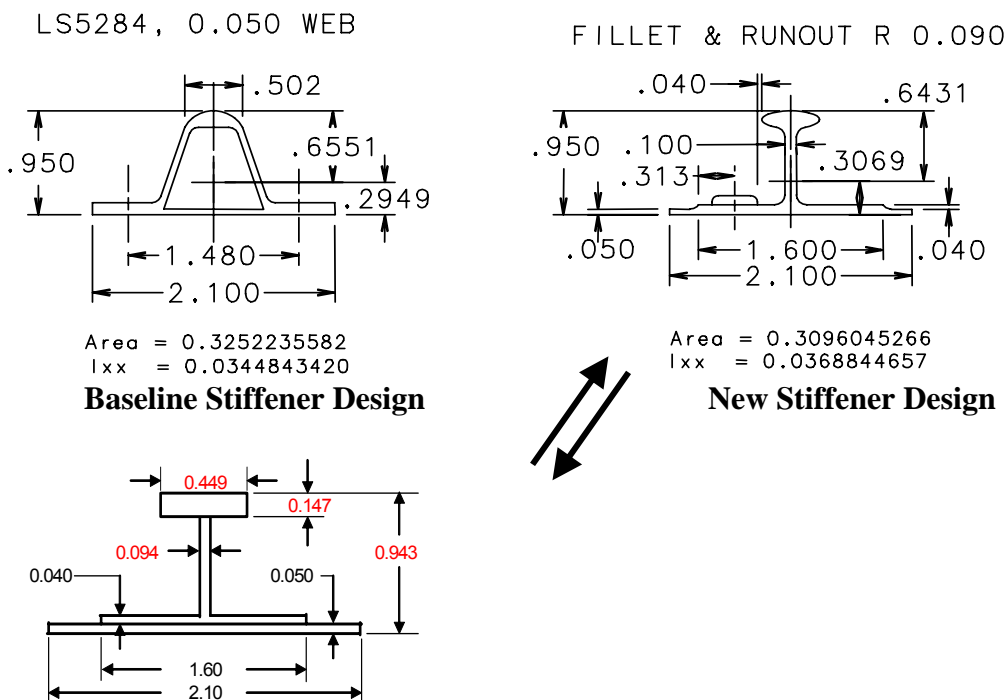


Fig. 3.5, Stiffener Sections

### C-130 center wing bulkhead pre-test buckling predictions –

In order to prove that the new FSW bulkhead panel design could withstand critical applied loading equal to that of the baseline design, side-by-side shear tests of a representative portion of both the baseline and the new panel designs were required. HyperSizer was used to perform an independent analysis of the two panel designs incorporated into the testing arrangement. The articles were square (26.82 inches, rivet-to-rivet) with stiffener spacing of 7.26 inches. Test loading was pure shear accomplished by pulling on two opposite corners of the panel test frame as shown below. This setup allowed for a relatively straightforward analysis.

In order to come up with a buckling factor to include in the HyperSizer input for the baseline analysis, a traditional web buckling analysis was performed. The assumption here was that the baseline stiffener design, whose attach flange thickness was 0.060 inch, when attached to the 0.050-inch web provided a “standard” boundary that would result in the answer that the standard initial buckling loads curve would predict. The buckling factor required in HyperSizer to produce that same critical baseline buckling load was 0.931. A traditional buckling analysis was then performed on the FSW panel configuration, with its slightly different spacing span than the baseline design (5.66 inch versus 5.78 inch for the baseline). When using the 0.931 buckling factor for the integrally stiffened design with its 0.040 land area thickness, an approximately 22% lower buckling load was predicted by HyperSizer versus traditional analysis (167 lb/in versus 213 lb/in). Given that rivet shear on the perimeter attachment was determined to be the critical mode of failure after the panel goes into diagonal tension, it is suspected that the increased loading on the perimeter attachment rivets, resulting from the integrally stiffened panel going into diagonal tension at a lower loading than the baseline design, could result in rivet shear failure at a lower applied load.

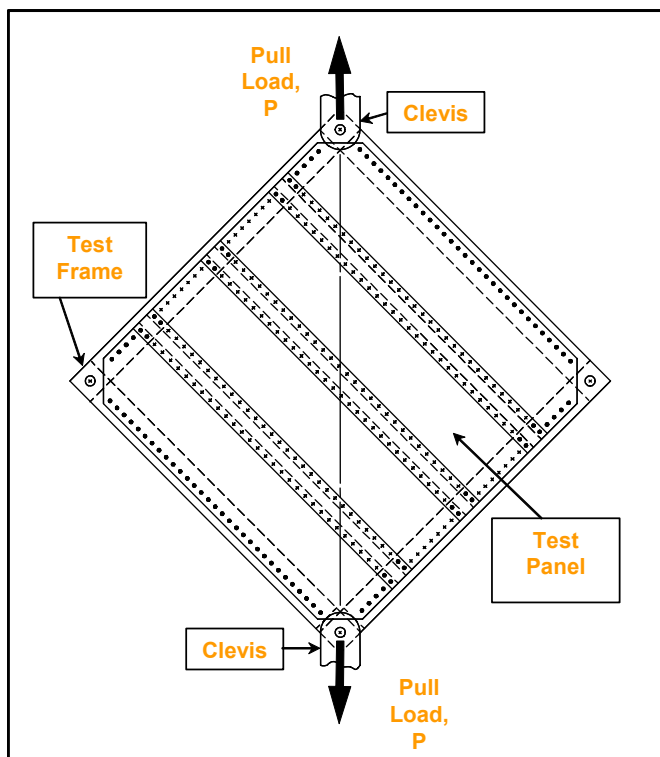


Fig. 3.6. Shear Test Panel

### Panel Shear Test Setup

The thinner-than-recommended 0.040 land thickness was chosen by Project Structures to save additional weight, but its potential negative effect on the design was something that the traditional analysis that was used did not take into account. Unfortunately, the test results were not available at the time of this writing. If the test shows that initial buckling and perimeter attachment rivet failure do occur at a lower applied load for the FSW integrally stiffened panel, then in this instance it is apparent that a design detail was accounted for in HyperSizer that was not taken into account through the traditional means of analysis used to determine the final design.

## 4 Commercialization

### 4.1 HyperSizer® is a Commercial Product

*The SBIR report is not meant to promote the HyperSizer® commercial automated analysis and sizing software. However, since the SBIR developments have been incorporated into HyperSizer for the purpose of testing and demonstrating, and for the purpose of readily commercializing the new capabilities, a description of the software is provided.*

*Relevant existing capabilities that provide a partial solution to efficient certification are described.*

*Significant SBIR developed capabilities were completed that specifically enhance efficient certification and their descriptions are emphasized.*



Fig. 4.1, HyperSizer Software CD cover shown

There is a distinct advantage to this SBIR as we move from Phase II to Phase III. Collier Research already has a commercial product in place that can move the new SBIR innovations into the commercial marketplace. The sole purpose of Phase III of the SBIR Program is commercialization and the existing commercial product, HyperSizer, virtually guarantees this will happen. HyperSizer has a strong user base, existing sales channels, marketing resources, a knowledgeable sales & support team, and a website with a wealth of supporting information.

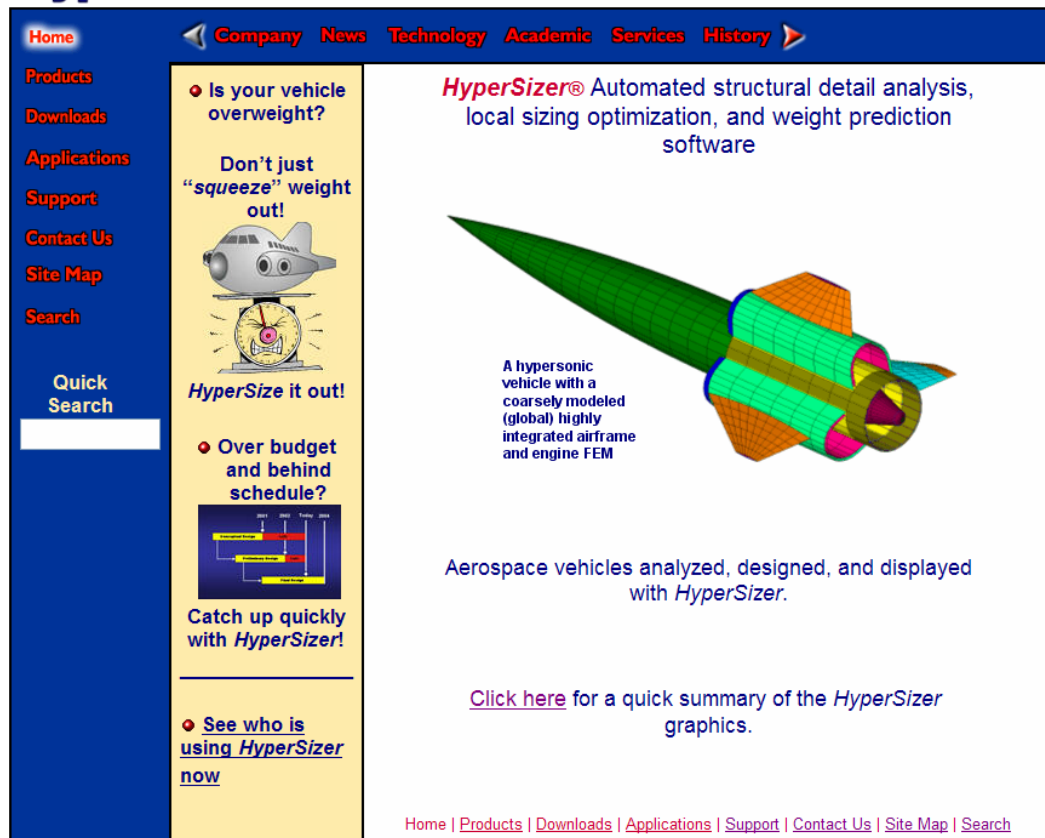


Fig. 4.2, HyperSizer.com website

We have in place marketing and support methods and tools that we use to successfully promote HyperSizer:

- For qualified users/businesses we provide a free evaluation license and provide software download from our commercial web site
- We provide a wealth of marketing and technical materials available through our website
- Support is offered by phone or by email
- Training is available either at our site or at the customer's site
- Documentation such as user's manuals and V&V manuals are available to users
- Continual improvements are made to the software

A successful track record in recent applications, shown in Fig. 4.3, is another marketing tool that can help the aerospace structures community to more readily evaluate and more readily accept newly added innovations, such as the innovations developed under this SBIR.

Lockheed Denver Orbital Space Plane 2004



Sonic Cruiser Boeing 2002



7E7 Boeing 2004



747x Boeing 2001



BWB NASA 2002



JSF Boeing 2001



Long Range Strike Aircraft  
Lockheed/Air Force 2002



**HyperSizer®**  
Structural Sizing Software  
*Designs on the fly*

SLI and 3<sup>rd</sup> Gen Hypersonics NASA 2002



Satellite Launchers,  
OSC/Boeing 2001



3<sup>rd</sup> Gen, GTX/Trailblazer NASA Glenn 2001



Fig. 4.3, Success in Recent applications.

A strong user base of repeat paying customers and/or significant potential users of HyperSizer provide an immediately reachable target audience for the new SBIR innovations. Fig. 4.4 shows customers throughout the United States and internationally as well.

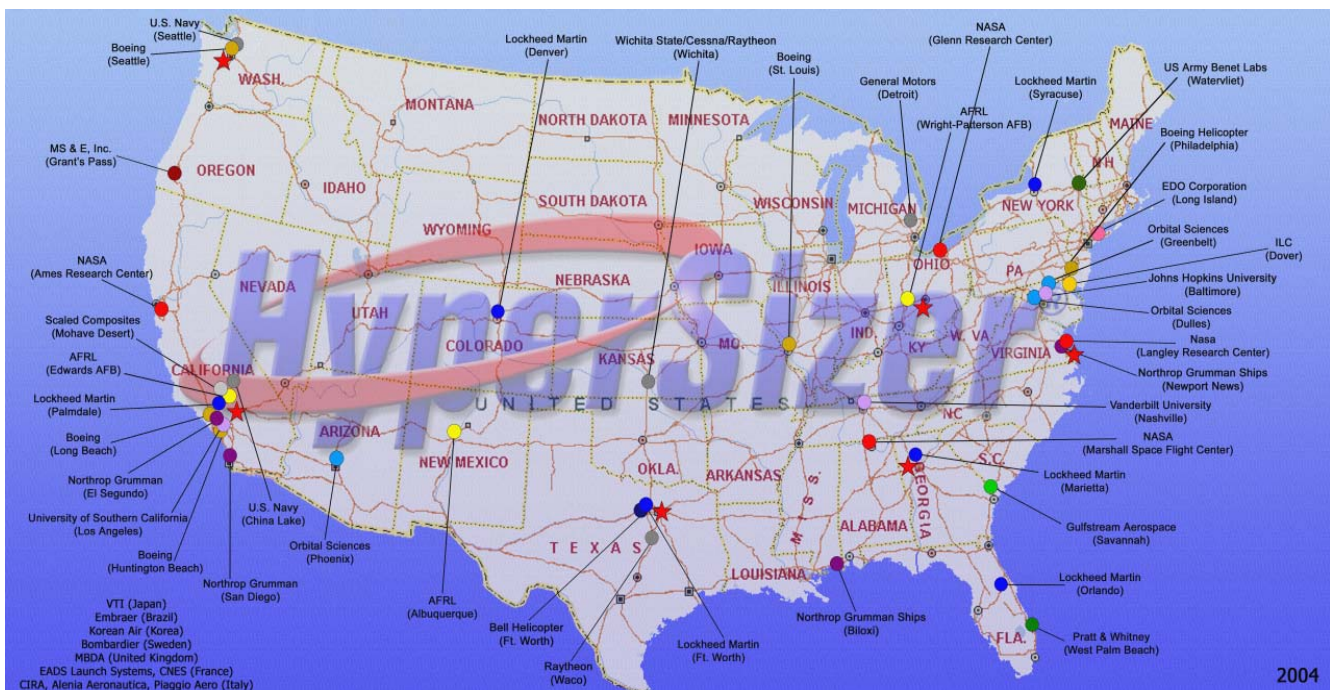


Fig. 4.4, Repeat paying customers or significant potential users of HyperSizer provide an immediately reachable target audience

## **4.2 New sales due to SBIR**

New sales / potential new sales due to the innovations developed under this SBIR include the following organizations:

- Lockheed Martin Palmdale (FALCON and JSF)
- Lockheed Martin Marietta (Existing and future Transports)
- Northrop Grumman, San Diego (J-UCAS)
- Scaled Composites in Mojave Desert
- Northrop Grumman in El Segundo (Air Force Applications J-UCAS and JSF)
- Boeing Huntington Beach (Space Launch)
- USC (The University of Southern California)

All of the above organizations have been introduced to the new innovations developed under this SBIR. These customers have a keen interest in these innovations.

## **4.3 New training of SBIR developments**

### **Marietta, GA; Four days (3-6 May 2004)**

Collier Research provided a four-day HyperSizer training to Lockheed Martin Aeronautics in Marietta, GA. Major training topics included three (3) of the new capabilities developed under this SBIR. During this class, we trained about nine (9) Lockheed Martin engineers: four (4) from their ADP group, two (2) from the C-5 program, and three (3) from the C-130 program.

### **Fort Worth, TX; Four days (12-15 Jan 2004)**

Collier Research provided a four-day HyperSizer training to Lockheed Martin Aeronautics in Ft. Worth, TX. Major training topics included three (3) of the new capabilities developed under this SBIR. During this class, we trained about nine (9) Lockheed Martin engineers and two (2) AFRL VA researchers.

## **4.4 Technical review and interchange meeting with LM Aero Technical Fellows**

Collier Research Corporation principals traveled to Marietta for a three-day meeting with LM Aero on the subject of a HyperSizer methods review. This meeting was setup by **Bob Olliffe**, the SBIR contact at LM Marietta, specifically for this SBIR effort. In attendance were two Lockheed Technical Fellows: **Steve Engelstaad**, **Ed Ingram**, and **Lori Flansburg**, who is on the LM Aero structural analysis methods and tool core team. The purpose of this meeting was to delve in great detail into the methods and verification & validation of HyperSizer so that they can critique our current status, and provide direction for future development. Another purpose was to identify which capabilities of HyperSizer are deemed acceptable for Lockheed's production use. During this meeting our focus centered on the three primary SBIR developments:

- 1) The composite bonded joint between the skin and flange of a stiffened panel
- 2) Test data entry, experimental correlation factors, interactive histogram display, and % reliability sizing as a proposed alternative to the traditional same value margin-of-safety for all failure mode analysis, and

- 3) HyperFinder automated methods documentation maintenance and locator.

## ***4.5 New SBIR published documentation***

### **4.5.1 Four published papers**

As of this writing, four technical papers have been published on the innovations developed under this SBIR.

Three (3) technical papers were directly funded with this SBIR. All three were accepted for the 2005 AIAA SDM conference in Austin, TX April 18-21, 2005, with AFRL acknowledgment. The three papers are titled:

- 1) Consistent Structural Integrity in Preliminary Design Using Experimentally Validated Analysis
- 2) Failure Analysis of Adhesively Bonded Composite Joints
- 3) Stress Analysis of Adhesively Bonded Composite Joints

In addition, a fourth (4<sup>th</sup>) technical paper was published for NATO (North American Treaty Organization) NATO AVT symposium in Paris, France, April 2002, entitled:

- 4) Virtual Testing with Validated Analysis Tools

## ***4.6 Trade Shows/Conference/Symposiums Attended with emphasis on SBIR Commercialization***

- **AIAA (American Institute of Aeronautics and Astronautics)** - Collier attended the 45th AIAA/ASME/ASCE/AHS/ASC Structures, Structural Dynamics and Materials (SDM) Conference April 19-22, 2004 in Palm Springs, CA
- **SAWE (Society of Allied Weight Engineers)** - The week of 17-21 May 2004 Collier presented papers twice at the SAWE conference in Newport Beach, CA. Mostly present were LA aerospace companies since the conference was in Southern CA. The two papers presented were on the subjects of automated preliminary design weight estimating using verified and validated HyperSizer analyses. Later presented HyperSizer at USC by invitation by one of the USC faculty, a professor. This was an open presentation where the aerospace industry also attended so this was another opportunity to promote the AFRL SBIR research. USC has been evaluating HyperSizer and recently submitted a PO for HyperSizer license(s).
- **SAMPE (Society for the Advancement of Material and Process Engineering)** - Also, during same week, 16-20 May 2004, attended some of the SAMPE symposium in Long Beach, CA.
- **AIAA (American Institute of Aeronautics and Astronautics)** - Presenting 3 technical papers at the 46th AIAA/ASME/ASCE/AHS/ASC Structures, Structural Dynamics, and Materials (SDM) Conference Apr 18-21, 2005 Austin, Texas (See section 4.5 above)

## **4.7 Company Visits**

The week after the 2004 AIAA SDM conference in Palm Springs, Collier traveled to, and demonstrated the new SBIR developments to:

1. 23April; **Northrop Grumman in San Diego** (old Teledyne Ryan group), targeted Air Force application: J-UCAS (very well received)
2. 26April; **Scaled Composites in Mojave Desert** (Burt Rutan company), targeted Air Force applications I perceive such as FALCON and others but I cannot confirm since they are either confidential to their prime or secret: (very well received)
3. 27April; **LM Aero in Palmdale** (Skunkworks group), targeted Air Force applications: FALCON, JSF (well received, political hurdles on JSF)
4. 28April; **Northrop Grumman in El Segundo** , targeted Air Force applications: J-UCAS and JSF (well received, political hurdles again on JSF since a LM owned project, It appears that J-UCAS is our best next opportunity, got a way to go though with more follow-up and meetings)
5. 29April; **Boeing in Huntington Beach**, targeted Air Force applications: unknown project names but mention of high speed flight, thermal structures, TPS, bonded joint, methods documentation, test data entry, and object model integration. These HyperSizer capabilities are of PD interest at Boeing (i.e. very well received, but political hurdles to overcome with in-house tool development activities)

We anticipate additional commercial sales with these companies, in due time, that will include these SBIR developments (all of the above have up to date, and current paid licenses of HyperSizer). This is a definite plus for the commercialization objectives of the SBIR.

## **4.8 Primary SBIR Developments Commercially Available**

- Test database integrated with design and analysis data
- Delivered test data
- Interactive test data display as Histograms
- Two correlation factors (CF)
- Test data driven reliability analysis and sizing
- Rapid bonded composite joint analysis
- Physical based composite strength analysis
- HyperFinder technical documentation and search
- Thousand of pages of technical documentation

## Part C: Efficient Certification: An SBIR Implemented Solution

### 5 Shortcoming: Inconsistent Structural Integrity throughout Design Maturity Causes Test Failures

Section 5 identifies eight primary inconsistencies that occur in the analysis of airframe structures which lead to test failures, and hinders structural integrity.

#### ***5.1 Eight primary inconsistencies of aerospace structural analysis***

The inconsistencies are:

1. Deterministic failure analyses
2. The typical one knockdown approach
3. The zero margin-of-safety approach
4. The 1.5 ultimate load approach to safety
5. Global-local modeling approaches
6. Fidelity during design phases
7. Fidelity between test analysis and in-service analysis
8. Test data availability

The first four inconsistencies are related to uncertainty of traditional analyses that are based on sizing structure to a zero margin-of-safety. This SBIR “test data driven reliability” innovation primarily addresses these four. Section 9 focuses on this subject in detail.

The 5<sup>th</sup> inconsistency of global-local modeling approaches is addressed by this SBIR innovation in performing highly integrated stiffened panel composite bonded joint analysis. Section 7, “1<sup>st</sup> SBIR Thrust: Reduce Order Modeling and High Fidelity Rapid Analysis”, focuses on this subject.

The 6<sup>th</sup> inconsistency of fidelity during design phases is addressed by the overall existing and new SBIR HyperSizer developments which allow a very accurate analysis tool suitable for most final analyses to be also practically used in preliminary design. Section 8, “2<sup>nd</sup> SBIR Thrust: Integrated Tools and Processes”, focuses on this subject.

The 7<sup>th</sup> inconsistency of fidelity between test analysis predictions and in-service analysis predictions is caused by the practice of showcasing extremely sophisticated analysis capabilities for test articles to a very few load cases and boundary condition, but which analysis methods are not practically used for production analysis to thousands of load cases.

The 8<sup>th</sup> inconsistency of test data value is caused by the practice of not sharing test data within industry nor within government.

These eight inconsistencies are summarized in this section.

### 5.1.1 Inconsistency of deterministic failure analyses

An aerospace stress analyst spends more time and effort in predicting failure and writing the margin-of-safety stress report than any other activity. This is because failure prediction is the area of most uncertainty and much effort is expended in trying to definitively quantify it. The problem is: failure cannot be deterministically predicted, because failure is not deterministic. The issue is how to handle scatter in experimental testing of observed failure while assigning a deterministic margin to it.

As an example, Fig. 5.1 illustrates scatter for test results from the World Wide Failure Exercises (WWFE) Case #2 [3]. The test is for a composite laminate material subjected to a combination of tension/compression membrane and in-plane shear loads. Only the top half of the composite material failure envelope is shown, meaning tests were assumed not necessary for negative values of shear. This laminate is unidirectional exhibiting no progressive post 1<sup>st</sup> ply failure strength. The computed failure envelopes of seven composite failure theories are superimposed on the test data. All seven failure criteria are calibrated to the three anchor points of pure fiber tension, fiber compression, and ply shear. Even still, for combined bi-axial loads, large variations in predicted strengths are computed with the different theories, with none of them matching all test data. In fact, substantial test scatter is observed at all three anchor points, particularly for pure shear ( $\sigma_{12}$ ), where approximately a 90% difference is reported.

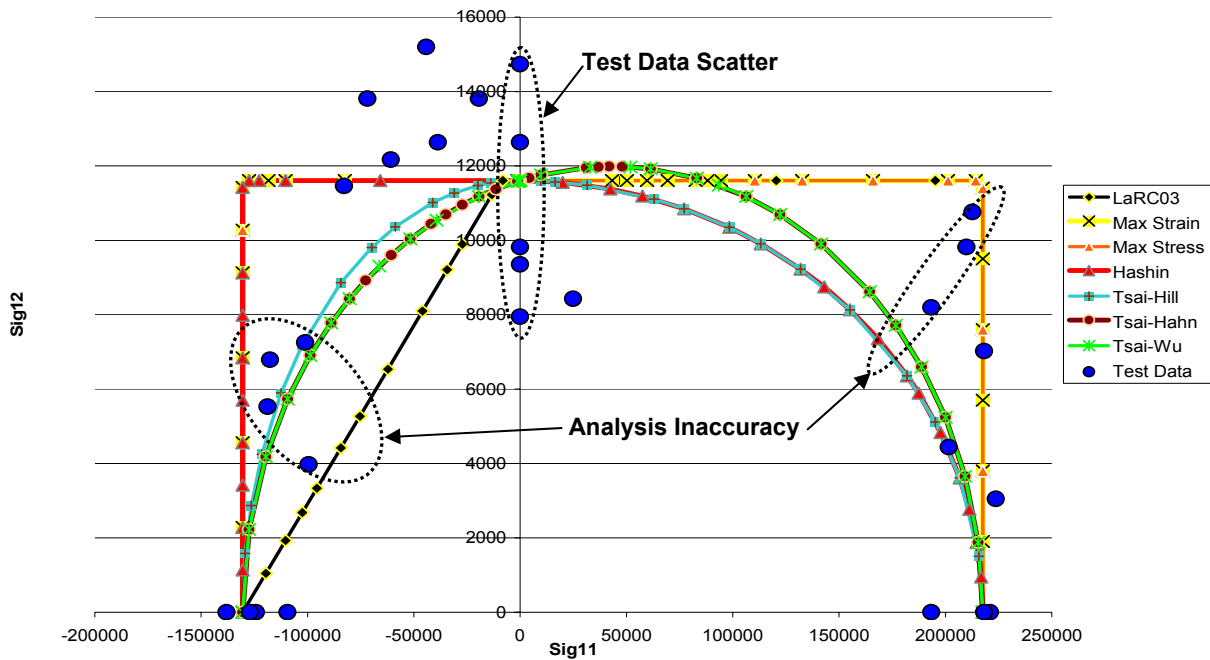
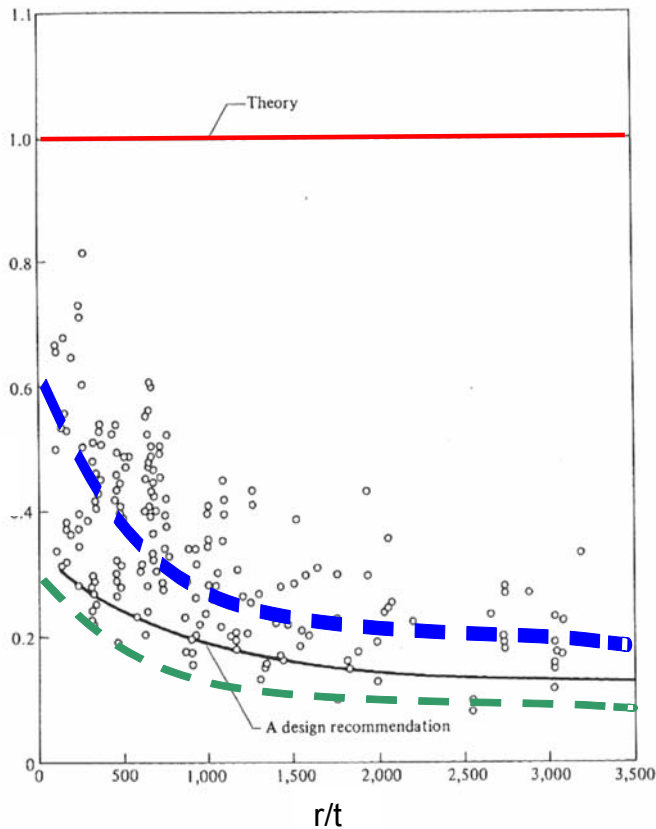


Fig. 5.1, Top half of a composite material failure envelope from the World Wide Failure Exercises (WWFE) Case #2. The vertical axis of pure shear shows approximately a 90% difference in test data scatter for failure stress. Analysis inaccuracy is worst for quadratic failure theory Tsai-Wu for the ply tension quadrant, and worse for max strain, max stress, and LaRC03 for ply compression failure quadrant.

The typical way to address analysis inaccuracy and test failure scatter is to define a **knockdown** to theoretical load. However, the knockdown is a single value that does not provide insight into each failure theories' intrinsic level of uncertainty, as illustrated again for buckling shown next.

### 5.1.2 Inconsistency of the typical one knockdown approach



**Fig. 5.2, Traditional one knockdown approach to cylindrical panel buckling**

*Noted as a design recommendation, the black curve is the original NASA SP-8007 knockdown, the green curve, a possible more conservative knockdown, and the blue curve, the average (typical) failure. The original, one constant knockdown equation doesn't give insight into the average test data, nor does it allow the engineer to choose his level of reliability, such as the green curve.*

practicing engineer.

A second shortcoming is that the acceptable level of risk defined originally may not meet the reliability requirement of your particular design (shown as green dashed-curve). A program manager should be able to choose required knockdown/reliability for each design project. Furthermore, insight and flexibility should be provided to bring each analysis failure mode to a consistent value.

The third shortcoming, which also relates directly to the goal of efficient structural certification using analysis, is that with a single knockdown, which takes the theoretical value (shown as red

Fig. 5.2 shows cylindrical panel buckling test data as points. Each test data point is normalized against its theoretical value (vertical axis). The horizontal axis represents decreasing theoretical accuracy as the radius/shell thickness ( $r/t$ ) ratio increases. Fig. 5.2 is related to the NASA SP8007 report [2]. Note the large discrepancy between theory (red line) and test results, i.e., inaccuracy of theoretical. The design recommendation is an established knockdown defined as an equation that includes the  $r/t$  ratio. So regardless of whether the knockdown is expressed as a single value or as a curve fit equation, the NASA one knockdown approach defines a once-and-for-all acceptable limit of risk.

Other curve fit equations, such as the blue and green curves can be defined based on a function of selected parameters. Even though the knockdown (black curve) is somewhat dynamic based on changing variables, in this case with the  $r/t$  ratio, the first shortcoming with this traditional approach is that the acceptable level of risk (black curve) is cast in stone when first defined, and for the most part is unchanging as more test data becomes available. In fact, the actual comparison is rarely known by the

line) down to an allowable design-to value (represented with a black curve), does not provide nor expose any knowledge of an average or expected typical failure load (represented with a blue curve). So unlike being able to use “typical” material properties for test predictions, the user is left to perform test correlations using a “design-to” failure analysis allowable, which should for almost all cases significantly under predict, and be very conservative to test results.

### 5.1.3 Inconsistency of the zero margin-of-safety approach

It is not possible to achieve consistent structural integrity simply by requiring all failure modes to have a positive (but close to zero) margin-of-safety as in the current industry process of analyzing. This is because there are different levels of inaccuracy for different failure modes. Additionally, different failure modes exhibit different levels of measured scatter in test results. For example, Classical Lamination Theory (CLT) is very reliable in predicting in-plane strains, but less reliable for predicting failure for off axis laminates. Predicting the post-buckled response of a large shear web and the internal strains is a bit less accurate. If one then extracts edge forces to compute bolted joint margins then the reliability is further eroded. Finally, if one desires to predict the post-impact damage response, the confidence in the prediction is almost zero. Clearly if each of these analysis types quantify a zero margin, then there is a veritable safety inconsistency of the structural integrity. For this reason, each failure mode should be targeted to a different required margin based on its unique uncertainty. Such an approach is the first phase of implementing consistency in analysis accuracy. Industry movement in this direction, which has been slow, can be acknowledged with just a few examples. For instance, it is customary for aircraft programs to specify a required  $MS=.25$  for joint strength analysis, especially when the joint is bonded composite [4 and 5].

Fig. 5.3, portrays this concept graphically. If we performed many analyses with high fidelity analysis codes, we would expect some analyses to closely match test results, in terms of this analogy, the analysis predictions fall tightly within the target circle. However, even high fidelity

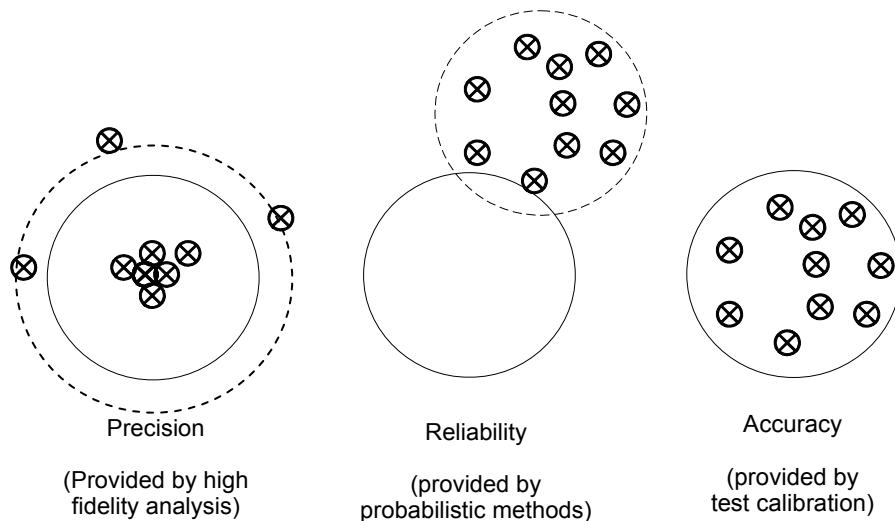


*Fig. 5.3, High fidelity analyses provide precision, defined as an ability to hit a bull's eye but not ensuring that all results fall within the target. Therefore, even with a 1.5 ultimate load factor, which in essence expands the circle to a dashed circle, some analyses for structure designed to a zero margin may still fall outside. Conversely, probabilistic methods reliably bring the scatter into a circle, and physical test calibration then accurately moves the circle onto the target, and a larger diameter target (1.5 load factor) is not necessary.*

analyses are likely to miss the target all together for some cases, and perhaps even outside the larger diameter dashed circle which represents the safety of an additional 1.5 ultimate load factor.

By including probabilistic methods (PM), analysis predictions can reliably be centered close together. By the use of correlation factors (CF) these predictions can then be accurately calibrated to test results. Such an approach would neither target a zero margin-of-safety nor use a 1.5 ultimate load factor.

#### **5.1.4 Inconsistency of the 1.5 ultimate load approach to safety**

It is not possible to achieve consistent structural integrity simply by using a constant load amplification factor to all of the failure mode analyses. The misconception is that all failure analyses are raised to the same level of safety. Each failure mode has its own unique uncertainty, so that by designing to a 50% higher load, 1.5 Design Limit Load (1.5 DLL), many failure predictions are extremely conservative while others don't meet the level of safety required. This line of reasoning suggests that since the design-to load is 1.5 DLL (a 1.5 ultimate load factor), test articles, statistically speaking, should rarely fail at loads close to 1.5 DLL. If they did, then contrary to expectation, it should indicate less confidence in the analysis.

Over the years industry has adopted in a limited way, the use of other load factors for particular strength checks. It has been a long standing requirement that pressure vessels be designed to a burst proof pressure test load of 2.0 times the operating in-service pressure [4].

The solution to the first four inconsistencies is addressed with this SBIR's "test data driven reliability" innovation. Section 9 covers this subject in detail. As depicted in Fig. 5.3, essentially two correlation factors are defined to first bring the analysis predictions within a circle, and second to calibrate them to test values.

#### **5.1.5 Inconsistency of global-local modeling approaches**

The 5th inconsistency is related to the process of making finite element models for different purposes. A global FEM is used to define internal load paths of a structure. Other more detailed models are made to perform localized analysis of a smaller part. Possible additional models are made to focus on particular features of the smaller part. In this process, the loadings and boundary conditions are not consistently applied across the FEMs, such that one FEA solution which is passed as input into a more detailed and localized FEA solution are based on different assumptions, unknowingly to the analyst. Addressed by this SBIR innovation is a consistent method for performing a stiffened panel analysis including its composite bonded joint in a highly integrated analysis. Section 7, "1<sup>st</sup> SBIR Thrust: Reduce Order Modeling and High Fidelity Rapid Analysis", addresses this subject.

#### **5.1.6 Inconsistency of fidelity during design phases**

The 6th inconsistency is related to a set of analysis tools being used for preliminary design (PD) which are different than the analysis tools used for final analysis. This inconsistency is addressed by the overall existing and new SBIR HyperSizer developments which allow a very accurate analysis tool suitable for most final analyses to also be practically used in preliminary design. Section 8, "2<sup>nd</sup> SBIR Thrust: Integrated Tools and Processes", addresses this subject.

### **5.1.7 Inconsistency of analysis fidelity between test predictions and in-service predictions**

The 7th inconsistency is caused by the practice of showcasing extremely sophisticated analysis capabilities for test articles to very few load cases and boundary conditions, giving a false sense of everyday capability to the customer, when in fact, they are not practically used for production analyses that have to be performed to thousands of load cases.

### **5.1.8 Inconsistency of test data availability**

The 8th inconsistency is caused by the practice of not sharing test data within industry nor within government. It is our opinion that there is a wealth of existing applicable test data across airframe programs that would be mutually beneficial. However, in many cases the expensively developed test data is not shared between different programs (F-22 versus F-35 for instance) even when the data is generated inside the same company, much less if a different company. This data could serve as useful and substantial building block knowledge for calibrating failure modes and analysis to the benefit of all.

## ***5.2 Evidence using the AFRL VA Long Range Strike (LRS)***

The first four identified inconsistencies and their proposed solutions are demonstrated by performing before and after analyses on the AFRL VA Long Range Strike (LRS) aircraft. Refer to Section 11, “Comparing Analysis Approaches: Traditional Zero Margin-of-Safety versus New Test Data Driven Reliability” which covers in detail the shortcomings of the conventional approach.

## 6 Solution: Perform Consistent Structural Analysis in Preliminary Design to Achieve Efficient Certification

The first six of the eight inconsistencies identified in Section 5 are best resolved during preliminary design. This SBIR implemented solution is to use more accurate, consistent, and comprehensive analytical modeling during conceptual and preliminary design phases. The purpose of which is to design-in reliability and robustness during sizing optimization, instead of trying to analyze-in reliability (margin) with extremely sophisticated FEA.

Fig. 6.1 is a road map that shows our path to achieving efficient certification by analysis. The map is divided into three parts: red, yellow, and blue. Each part feeds directly into the goal of efficient certification. In each part, several items have been identified that are required and the dashed circles represent those which have been addressed. Maroon circles are items addressed with existing HyperSizer capability, and blue circles highlight items addressed during the SBIR.

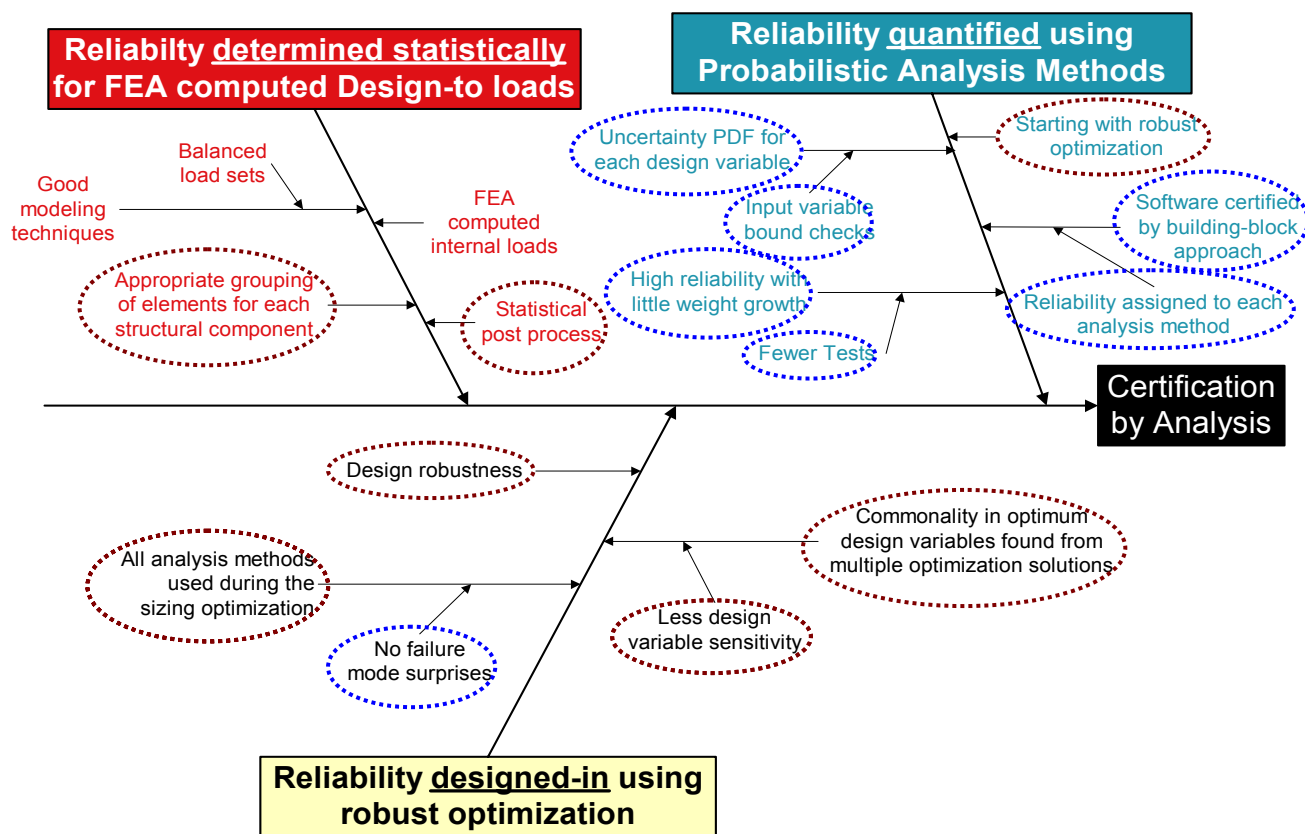


Fig. 6.1, Cause and effect of better analytical modeling early in design. Efficient certification starts with design-by-analysis. Blue circles are SBIR developments. Maroon circles are existing HyperSizer capabilities.

**Reliability Determined Statistically for FEA Computed Design-To Loads.** Red items in Fig. 6.1 address the generation of FEA computed internal loads. The issue is related to what are the “design-to” loads? The answer is to adopt a statistically based approach for determining them from the thousands of load cases.

**Reliability Designed-In Using Robust Optimization.** Yellow items address sizing optimization of the structure. A primary concept is to use nearly all of the available analyses during sizing optimization so that no new failure mode surprises will occur when going to the final analysis design phase. Another primary concept is to minimize design variable sensitivities and find commonality in optimum design variables from multiple optimized solutions.

**Reliability Quantified Using Probabilistic Methods.** Blue items cover the final analysis and margin-of-safety reporting. A key objective is achieving a building block validation and verification (V&V) documented process for analytical modeling. Without such documentation the product customer will not have the basis available for certifying the methods used. To address human error, checks would be applied to each input value that would define an envelope of applicable lower and upper bounds for given analysis methods. Such checks would also catch and filter out inappropriate variable combinations generated by the automated optimization process.

Fig. 6.1 addresses specifically the analysis certification deficiencies identified in [5]:

- Integration/communication of codes
- A building block process
- Higher fidelity methods in early design phases
- Non-deterministic methods

and additionally:

- Modeling errors
- Credibility of analytical results
- Implementation of analysis
- Human errors

In terms of credibility of analytical modeling results, there is a need to rate the level of reliability associated with each failure mode prediction. Thus, there is a need to introduce some sort of statistics or probabilistic evaluation in the building block analysis/test certification process, and this needs to be incorporated into the tool set used in preliminary design to achieve consistent structural analysis.

## ***6.1 Current Preliminary Design Practice***

Since our solution is to design-in consistent structural integrity during preliminary design, the next step is to establish current PD practices. Presented below is a very brief description of that process, which we believe to be problematic.

### **6.1.1 Manual operation of legacy codes**

In the aerospace industry the use of legacy codes for special purpose analyses have been proven to be indispensable. The codes have a wealth of verification and validation (V&V) to support their use based on correlation to test data. However, deficiencies arise in their use.

The first deficiency comes about from manual use. Even though they may be executed from a software menu, their use is not automated. Engineers are required to manually type in required input. The only data usually integrated are material properties. However the design-to loads that are computed with FEA are typed in as well as the boundary conditions and geometric dimensions, etc. The primary concern is manual input allows human mistakes to occur which is the number one cause of analysis error.

### **6.1.2 Spot checking of anticipated critical failure modes, for a subset of vehicle locations and load cases**

The second deficiency again comes about from manual software use. Because of the tedious and labor intensive use of manual input, engineers are not able to perform analysis for all vehicle parts to all load cases. To get the job done in a timely manner, the engineer is left to use his intuition to screen out load cases and less critical parts based on inspection. In essence, a process of spot checking a subset of vehicle locations to a subset of load cases to a subset of failure analyses is the norm.

### **6.1.3 Spreadsheets**

A third deficiency comes about from the use of spreadsheets to automate the analysis process. Unfortunately, the use of spreadsheets has become common place as the chosen software environment for automation. Though spreadsheets are the right tool for financial analysis and general small level administrative tasks, they are not appropriate for highly complex engineering computations that require extensive equations and data management. At the beginning of the automation process, spreadsheets have a compelling ease of use and familiarity. However, as the solution programming matures, the use of spreadsheet cells to enter equations become very difficult to maintain. Furthermore, for an engineering department, the need for verification becomes very challenging if the application is provided in this format.

## ***6.2 HyperSizer Selected as Preliminary Design Automated Analysis Framework***

To overcome these deficiencies in analysis approach, the HyperSizer® commercial structural analysis and sizing optimization software was selected for implementing the SBIR developments. Currently, HyperSizer is used by many companies and government agencies in the aerospace community for product development.

### **6.2.1 HyperSizer addresses all eight structural analysis inconsistencies**

The choice to use HyperSizer for this SBIR is because it addresses all eight of the structural integrity inconsistencies identified in Section 5. As a summary, it is able to perform rapid structural analysis and design sizing that includes many failure analyses for all load conditions for all areas of an airframe. The underlying software architecture is an integrated relational database management system that stores data, prevents accidental data deletion, and handles all I/O automatically between all analysis codes. HyperSizer also automatically couples to FEMs and resulting FEA computed element loads, thus greatly reducing the possibility of human data input errors.

HyperSizer contributes in several ways to the certification by analysis initiative. HyperSizer capabilities are moving beyond the conceptual and preliminary design phases, to mature its usability for final design. Many analyses required for airframe certification are included in its

controlled software environment, which in itself is a framework for plugging-in user defined validated analysis codes. It is able to input and maintain analysis building block test data and to use this test data to perform reliability based analysis and design sizing. As an automated sizing tool that achieves consistent structural integrity, it is able to produce robust designs using Probability Density Functions (PDF) signatures as defined with correlation factors described in following sections.

## 6.2.2 HyperSizer Sphere of Influence

Applications suitable for HyperSizer are most of the common structural features of most of the common air platforms: Fighters, Attack Aircraft, UCAV's, Military Transports, and Space Vehicles. For these airframes, there exists a set of core analyses that are relevant to 80% of the structure. These analyses that are common to nearly all vehicles are identified in Fig. 6.2.

### 6.2.2.1 Commonality in Core Analyses

Through the years, analytical modeling has been quantifying primarily the same structural phenomena, for the same core structural panel and joint types. In addition to metallics, composite materials are prevalent today and are an additional core material type.

Fig. 6.3 illustrates the commonality in airframe construction throughout platform type and era. For all, note the similar built up network of internal substructure frames and bulkheads that support skin panels.

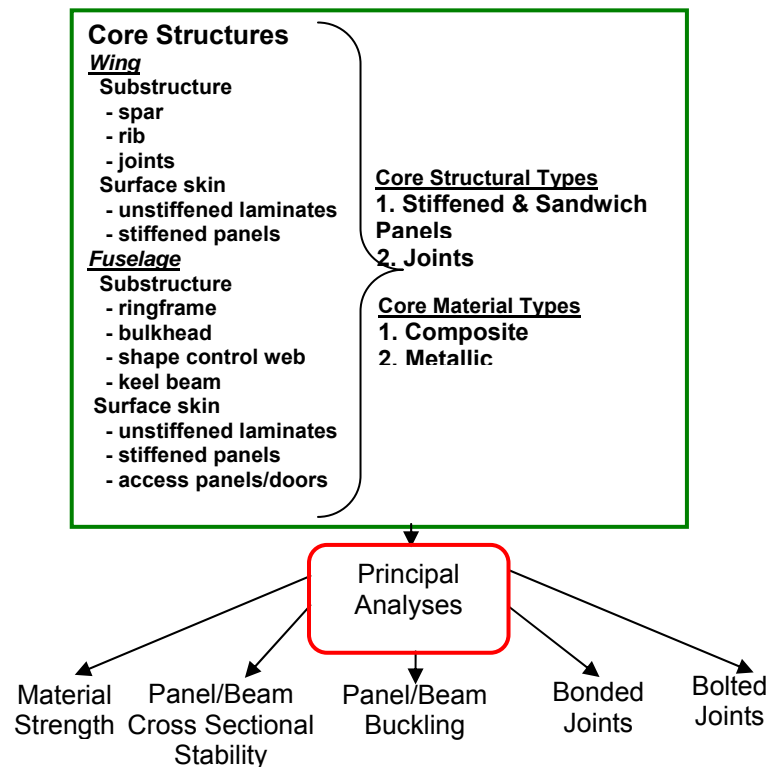
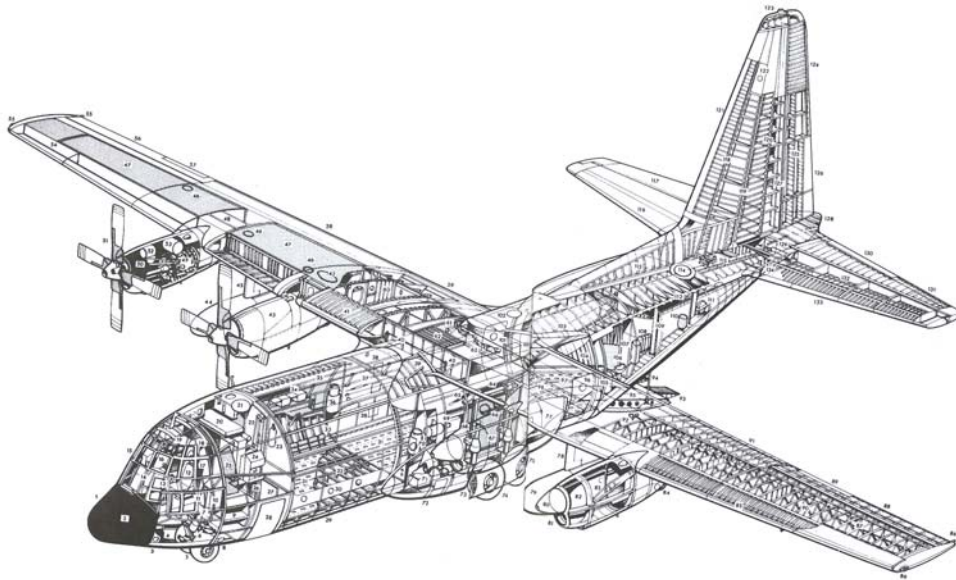
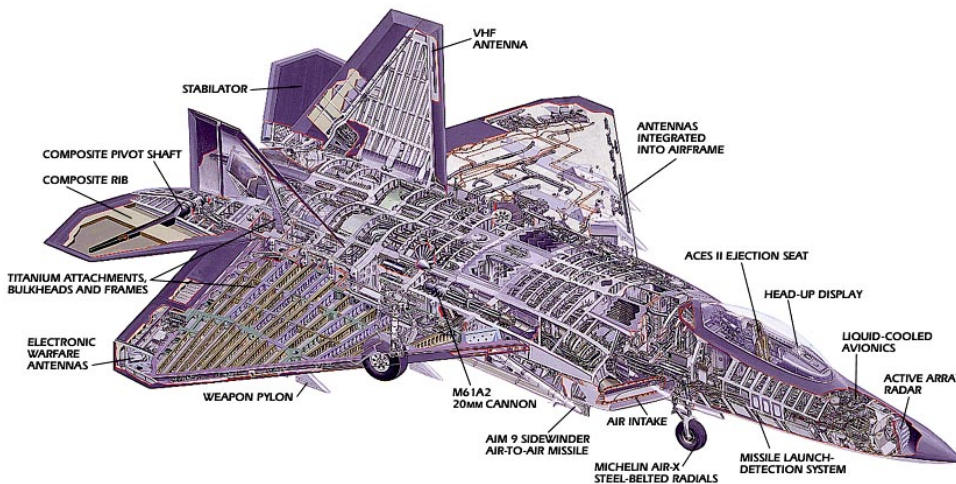


Fig. 6.2, HyperSizer includes the required core analyses.

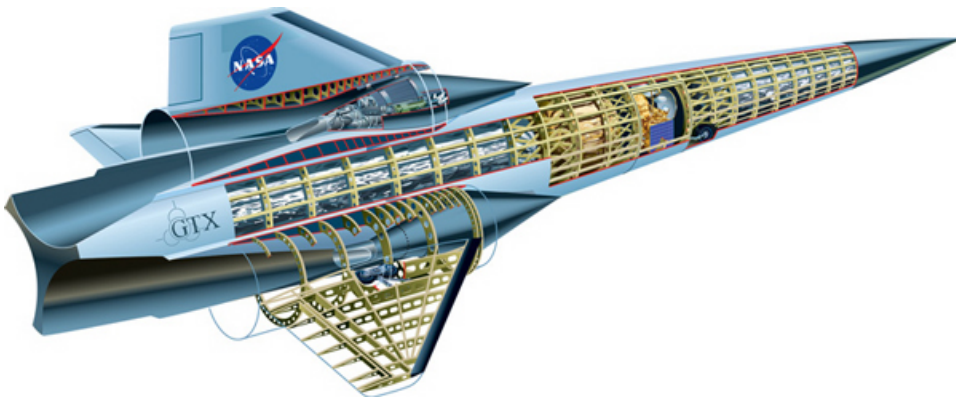
### 6.2.2.2 Commonality in Airframe Construction



*C-130  
Military Transport;  
Metallic  
1950's design*



*F-22  
Military Fighter;  
Metallic and  
Polymer Composite  
1990's design*



*X-planes  
Space Operation  
Vehicle;  
Advanced Polymer,  
Ceramic, and Metal  
Matrix Composite  
Materials  
2020's design*

*Fig. 6.3, Three different aircraft types, three different eras, all primarily stiffened structure. Different technology ages, but all similar core principal analyses.*

### **6.3 HyperSizer Traditional Analysis of the AFRL Long Range Strike (LRS) Aircraft**

To demonstrate the use of HyperSizer as a preliminary design tool, the AFRL Long Range Strike (LRS) aircraft is chosen as the example. It is a high speed and long range strike vehicle designed by LM Aeronautics Company in Fort Worth, TX and sponsored by Air Force Research Lab (AFRL) Air Vehicles Directorate. This vehicle is first presented here with results computed with preexisting HyperSizer capabilities. Sections 10 and 11 provide results for this vehicle that are produced with the new SBIR developments.

#### **6.3.1 Load Cases**

Seven different load cases are defined, as shown in Table 6.1 For each external load case, the airframe loads were balanced. That is the integrated flight pressures are equal to and opposite to the resulting loads from inertial accelerations of its mass. Internal fuel pressures were applied on the relatively flat panels and their resulting secondary panel bending moments computed by HyperSizer offline from FEA. Heating was mapped to the exterior skin with 1D thermal analysis performed to produce structural temperatures resulting in proper temperature dependent material properties and thermally induced stresses.

**Table 6.1, Vehicle Load Cases**

<b>Load Case</b>	<b>Description</b>
#1	3G Begin Cruise
#2	3G Before Weapon Drop
#3	3G End Cruise
#4	2G Begin Cruise
#5	-1G TOGW
#6	Taxi Bump
#7	Vertical Tail Loads

#### **6.3.2 FEM**

A coarse NASTRAN FEM was constructed with primarily shell and beam elements: CQUAD4, CSHEAR, and CBAR. Of particular modeling significance is that only one element spans the internal substructure. Two unique HyperSizer capabilities allow a model with this few elements to get very accurate analysis. The 1<sup>st</sup> is the ability to represent any stiffened panel shape or sandwich construction with a single plane of elements. This capability is described in more detail in Section 7.1 The 2<sup>nd</sup> is the ability to very accurately compute offline from the FEA, panel deflection, moments, and out-of-plane shears caused by normal pressure, such as that caused by fuel. These secondary panel loads are then superimposed with the global FEA computed internal running loads.

The next series of figures (6.4 – 6.10) present some of the typical HyperSizer output. These color plots are generated by HyperSizer and are helpful in quickly understanding the software's scope.

### 6.3.3 HyperSizer transformation and display of FEA computed internal loads

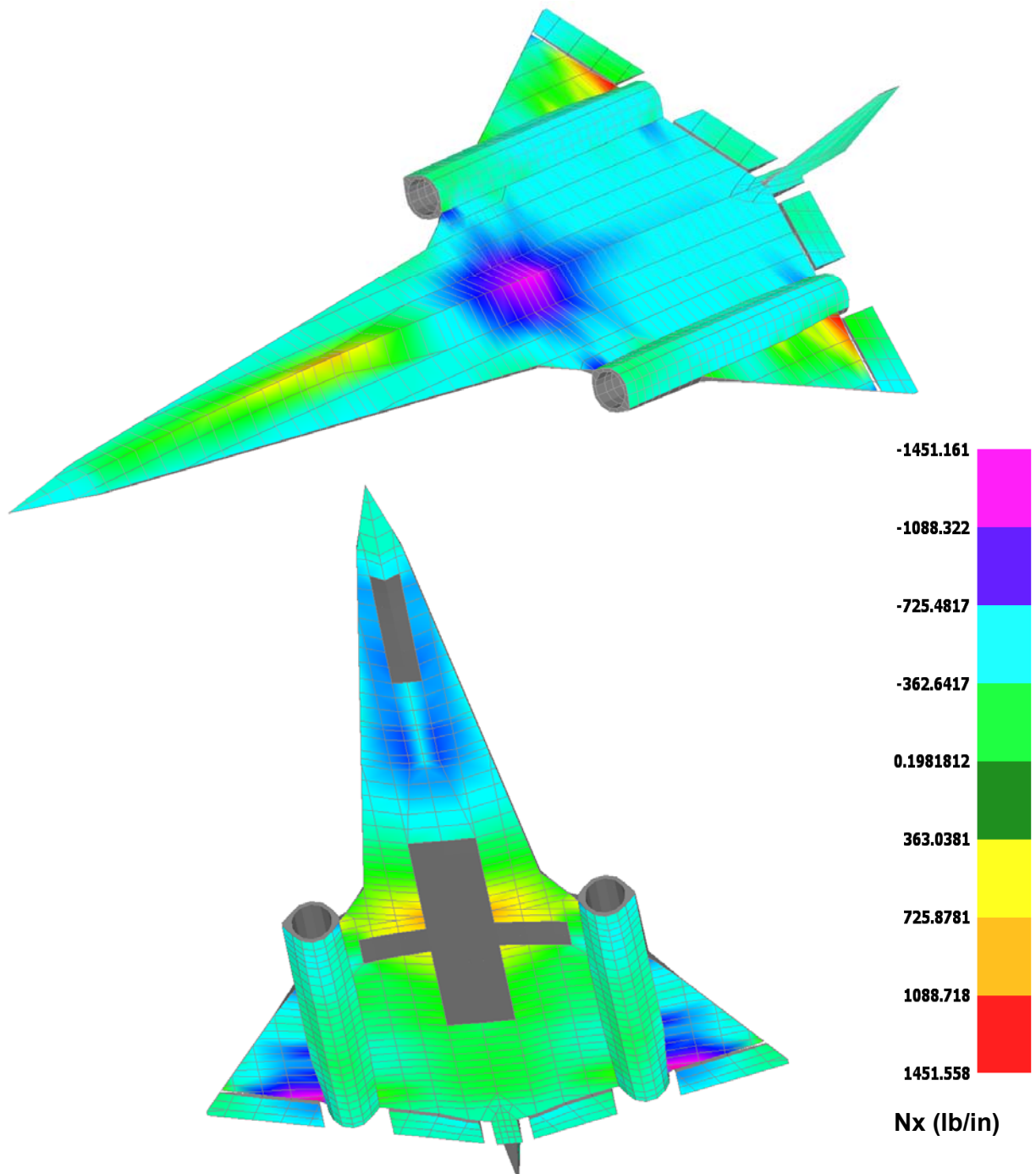
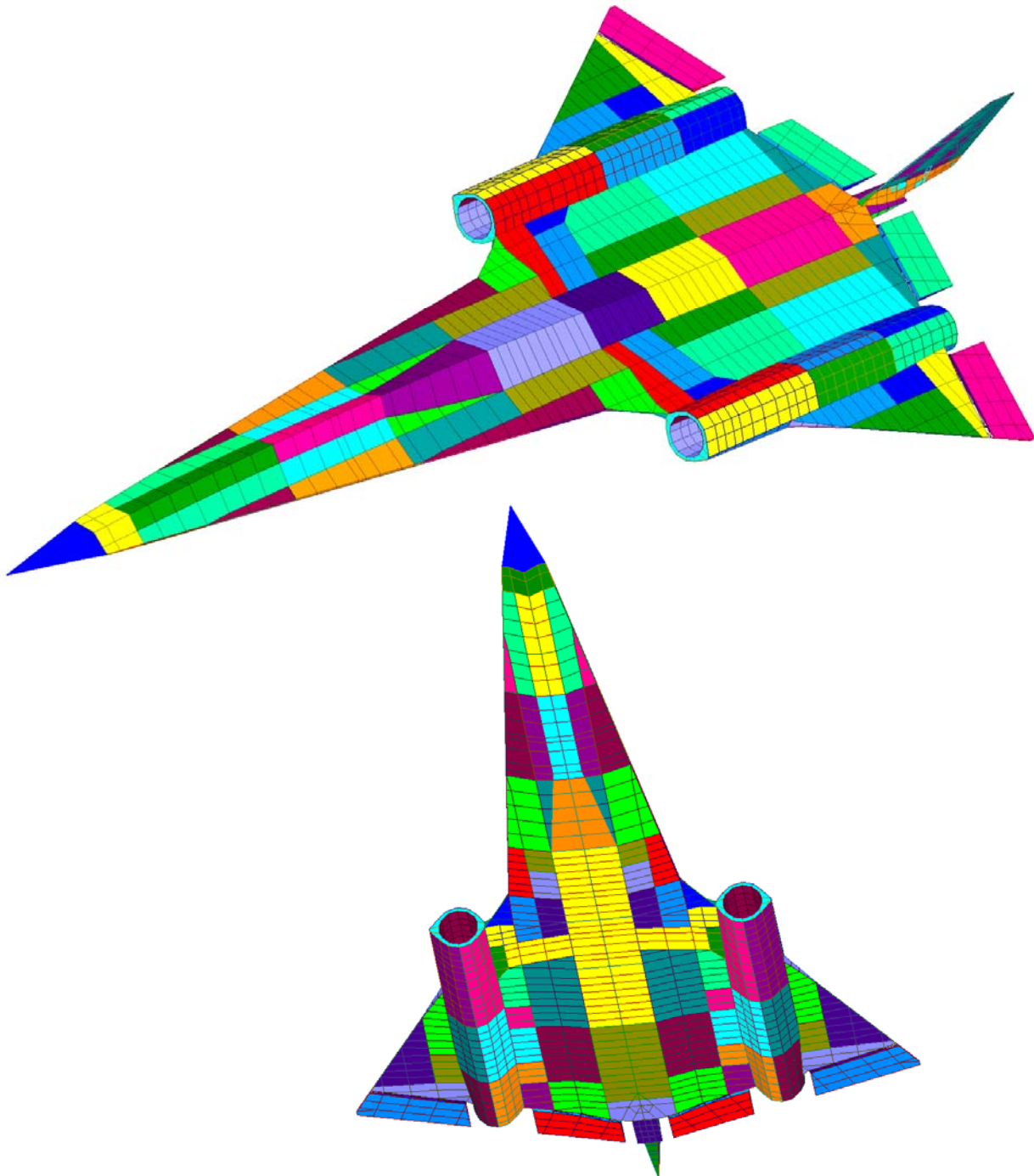


Fig. 6.4, Color gradient represents the FEA computed element forces after transformation to the material coordinate system by HyperSizer. Displayed is load case 5, -1G TOGW, longitudinal membrane force,  $N_x$ .

### 6.3.4 HyperSizer Setup: Components and Groups



*Fig. 6.5, Each different color region represents a unique structural component. Each component is optimized to a different stiffened shape, size, thickness and/or material. The modeler identifies these components by associating a set of shell elements to the same property data. In this case, a group of NASTRAN CQUAD4 elements share the same PSHELL data. This pre-established association is imported by HyperSizer and maintained throughout the FEA iteration process.*

### 6.3.5 HyperSizer Result: Controlling Failure Analyses

Analysis "Composite Strength, LaRC03 Fiber Failure", 1 component	C
Analysis "Composite Strength, LaRC03 Matrix Cracking", 5 components	C
Analysis "Composite Strength, Tsai-Hahn Interaction", 12 components	C
Analysis "Panel Buckling, Curved, Simple, Fixed or Free BC", 46 components	H
[Analysis "Wrinkling, Eqn 2, Honeycomb Core, X, Y & Interaction"], 20 components	C

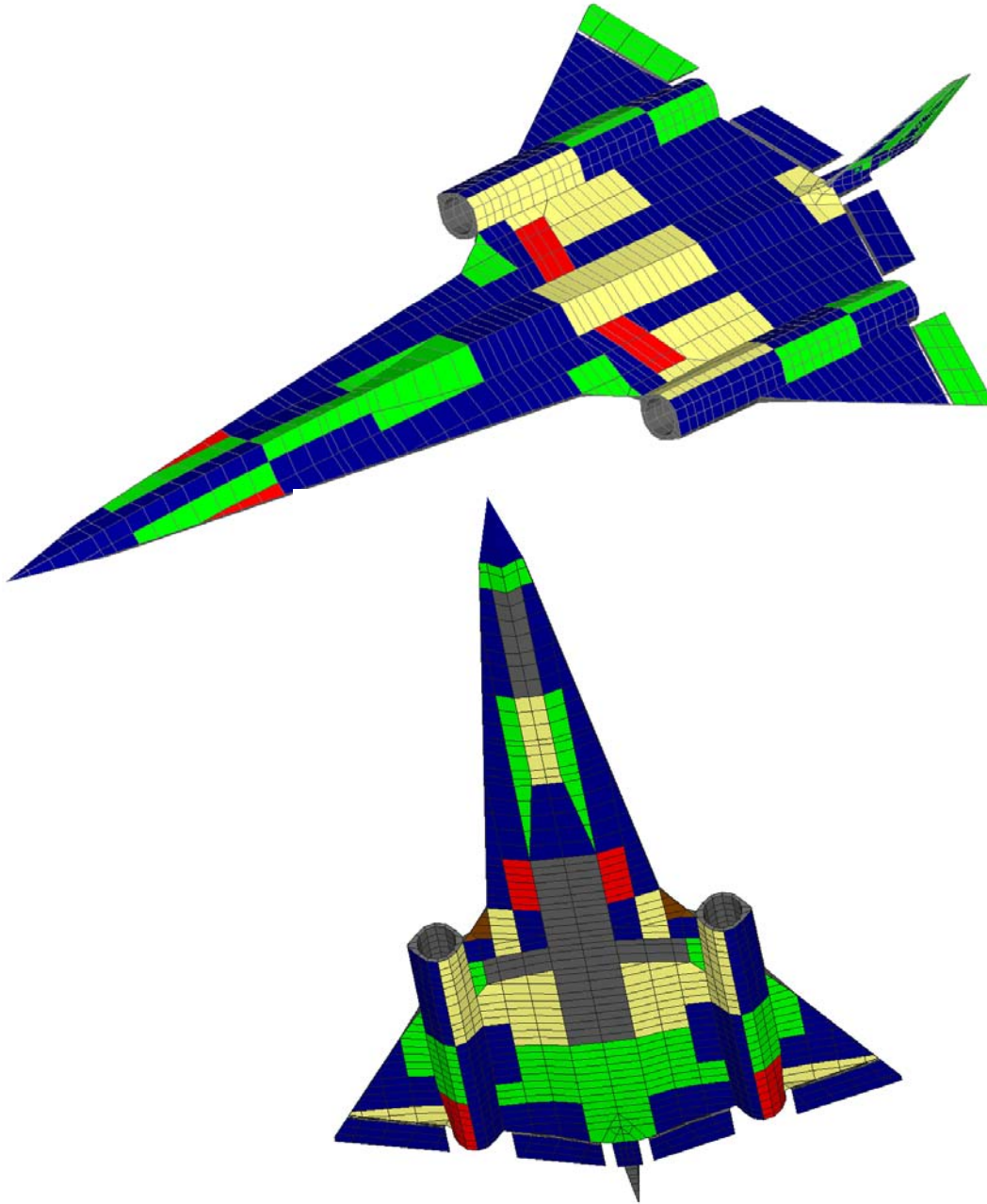


*Fig. 6.6, Controlling failure analyses are shown with different colors and are identified as the failure analyses which produce the lowest margins for any of the 7 load cases. This component based information is useful for understanding how to design the airframe lighter.*

### 6.3.6 HyperSizer Result: Controlling Load Case

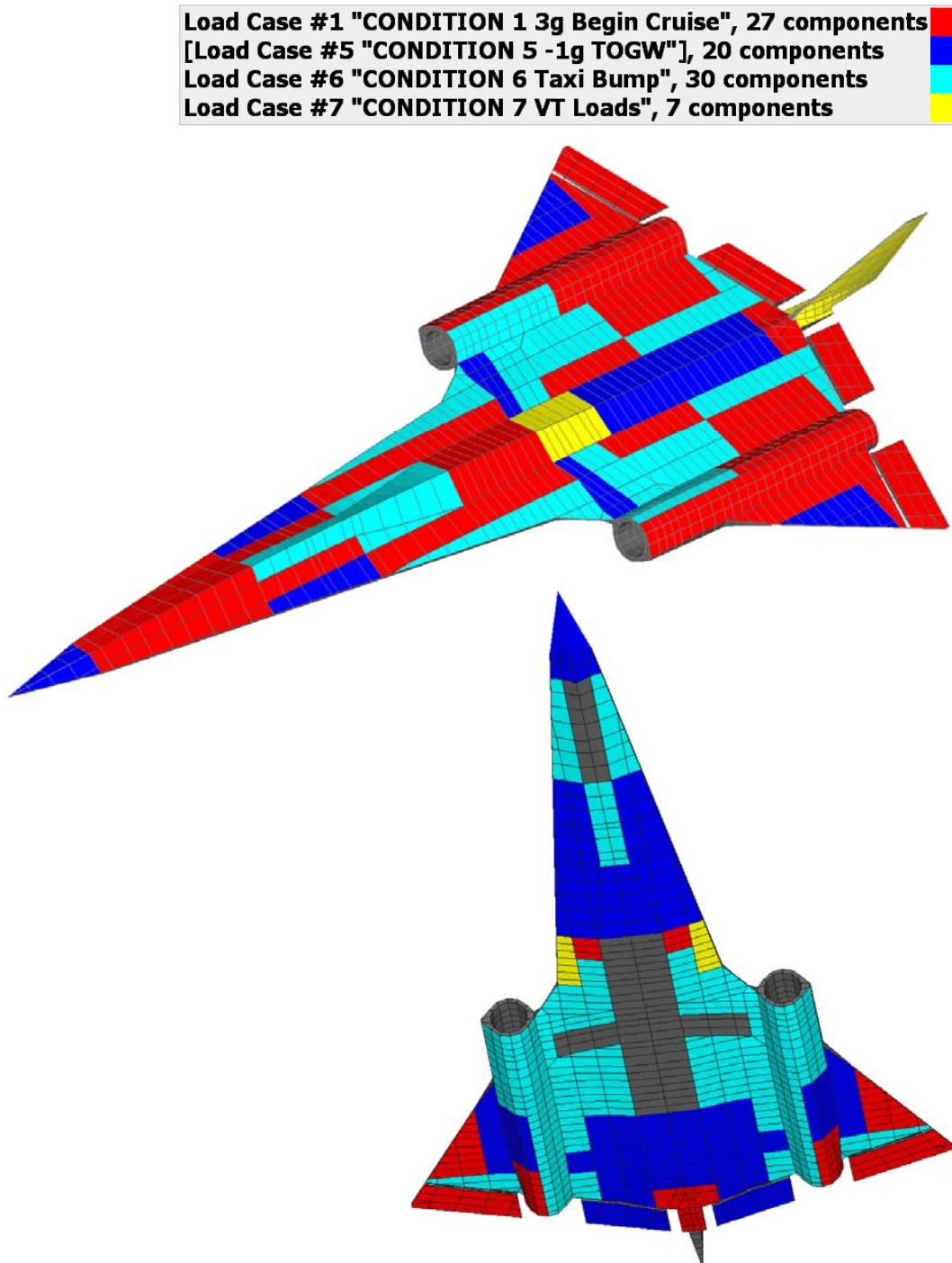


*Fig. 6.7, Controlling load cases shown with different colors, are identified as the load cases which produce the lowest margin for any of the many failure analyses performed. This is component based information.*

### 6.3.7 HyperSizer Result: Minimum Margins-of-Safety

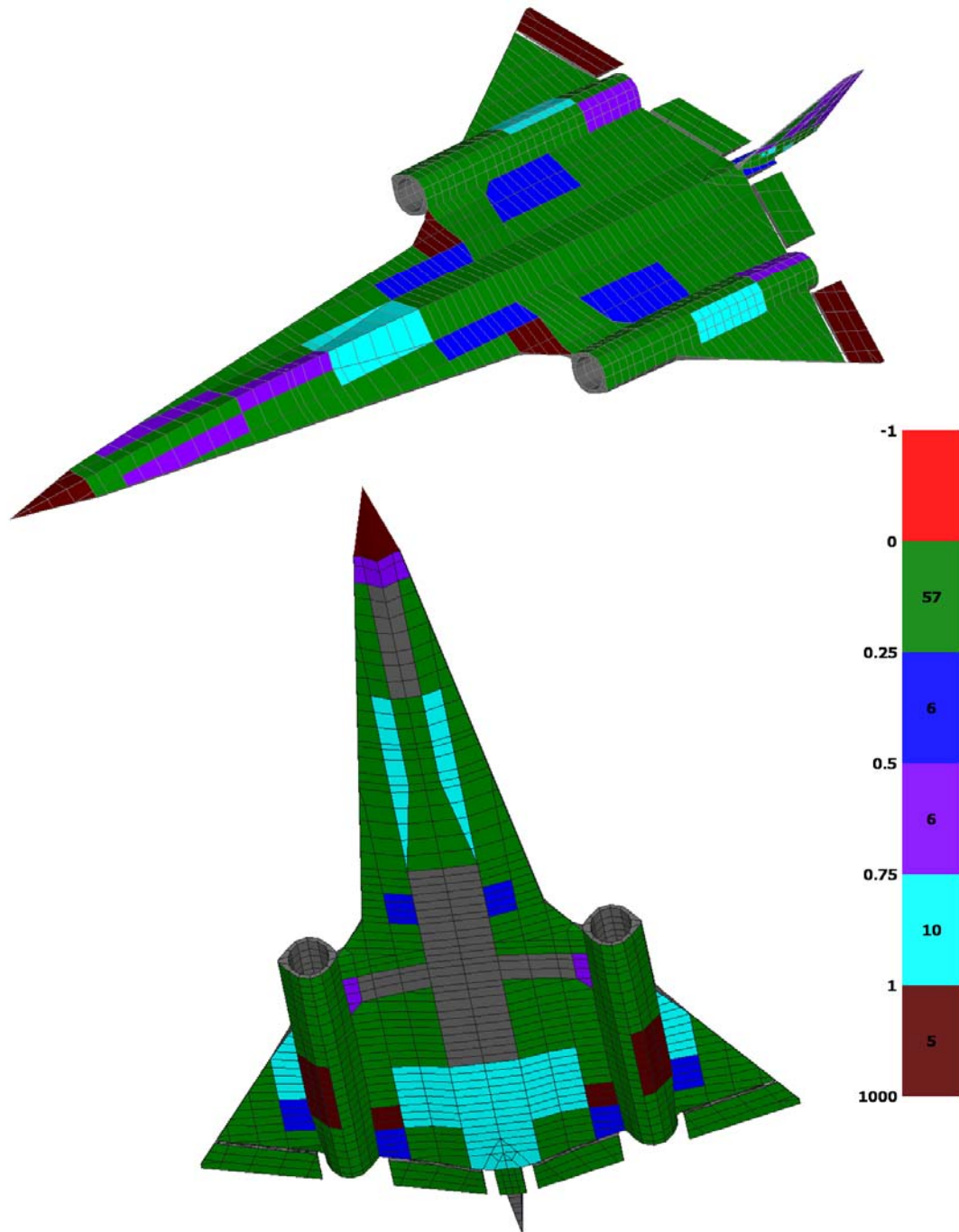


*Fig. 6.8, Minimum margin-of-safety shown for each component where light blue is the highest margin and red is the lowest margin. The brown areas are overly conservative and are also areas that need to be resized. All failure analyses are performed for each of the 7 load cases. Whichever combination of load case and failure analysis that quantifies the lowest margin is tagged as the minimum margin.  $\text{Margin-of-safety} = (\text{allowable load}/\text{applied load}) - 1$*

### 6.3.8 HyperSizer Result: Optimum Composite Layup

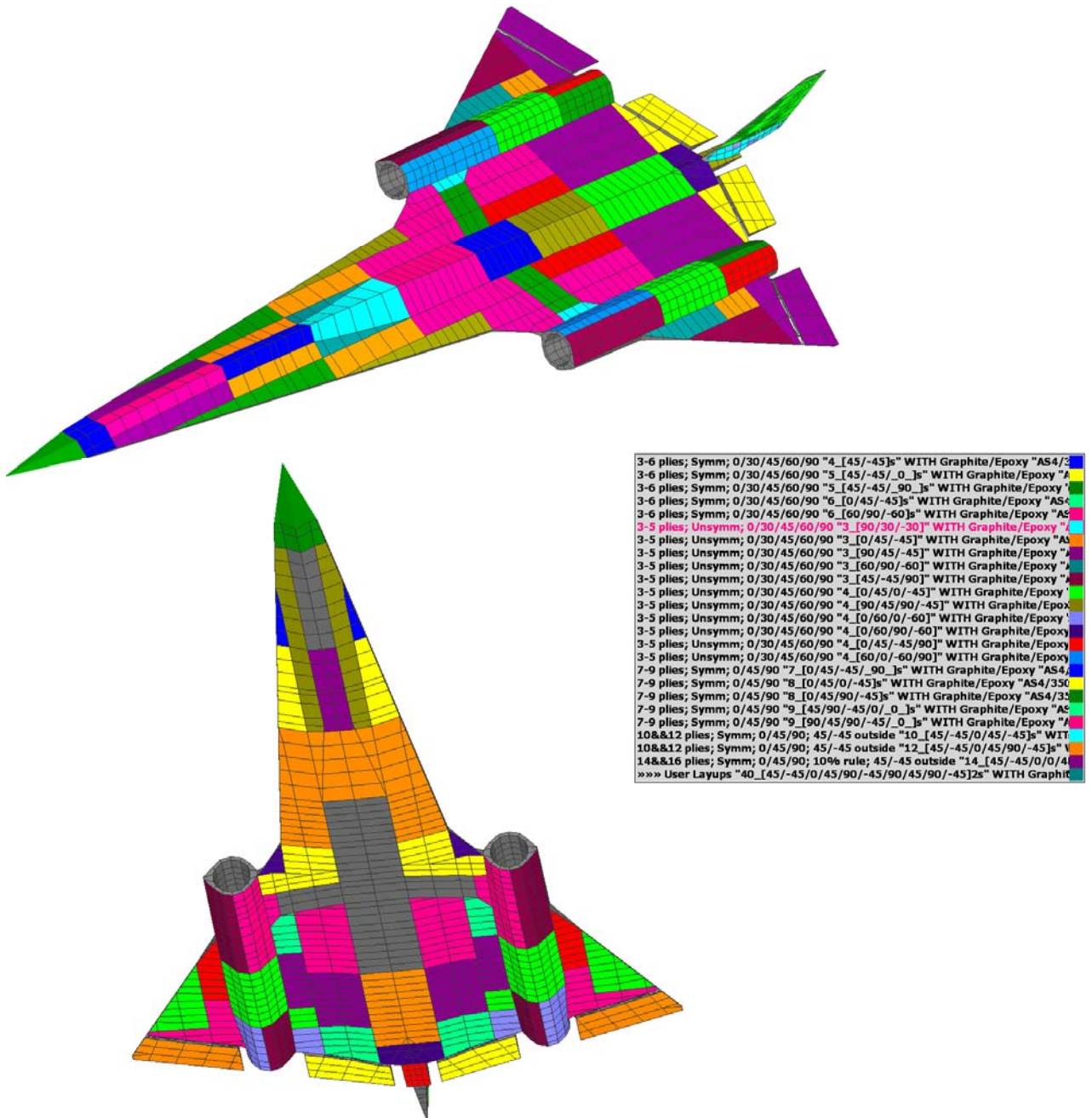


Fig. 6.9, Optimum layup of traditional design, zero margin sizing approach. Each color represents a unique component layup sequence. These layups will later be processed to achieve a manufacturable ply drop off schedule.

### 6.3.9 HyperSizer Result: Optimum Unit Weights

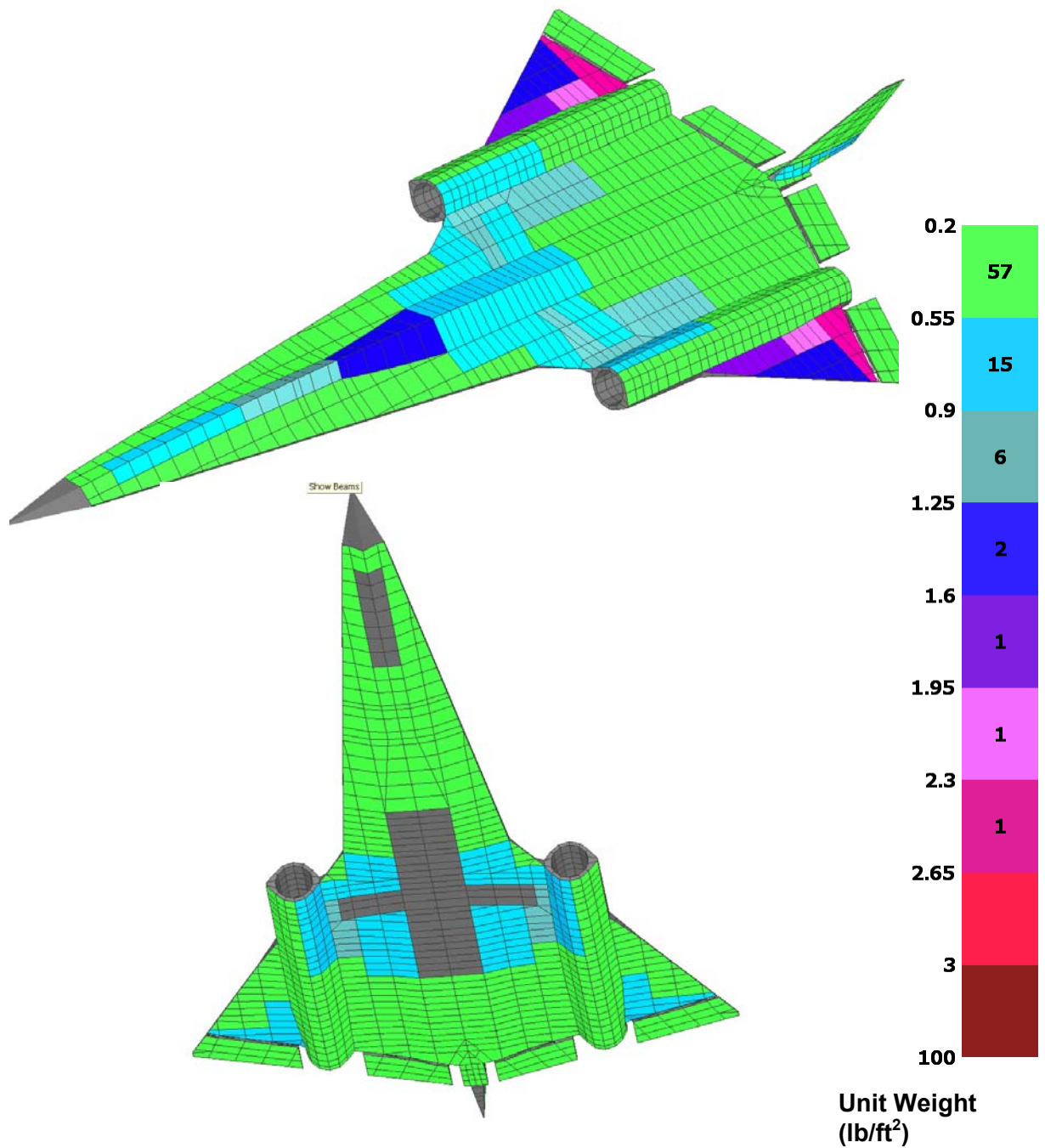


Fig. 6.10, Unit weight of traditional design. Each color represents a different weight. The green color is lighter and red color is heavier.

## 7 1<sup>st</sup> SBIR Thrust: Reduce order modeling and high fidelity rapid analysis

Three major SBIR thrusts are identified to achieve consistent structural integrity and efficient certification with analysis. This first thrust is focused on providing reduced order modeling and high fidelity rapid analysis. The overall approach is to perform the accurate core failure analysis for the fundamental airframe structural constructions as identified in Section 6.2.2.

### 7.1 *Reduce order Global-Local-Detail (GLD) modeling overview*

Shown in Fig. 7.1 is an analytical modeling process that is very rapid and completely consistent. Acreage areas are predominant on vehicles and are being addressed here. FEA is used only at the global level.

Consistent global-local-detail modeling must maintain equilibrium of forces and strain compatibility throughout the process of going from the *global* scale with course-mesh FEA to the *local* and *detail* scale with tools such as HyperSizer, and then possibly to the *micro* scale using micro-mechanics methods such as the Generalized Method of Cells (GMC). The process, as shown here, is best accomplished using *localization* for drilling down, and *homogenization* for coming back up. This efficient process contrasts traditional approaches requiring intensive finite element submodeling. Traditional GLD modeling approaches suffer from the need to choose between applying computed FEA displacement fields or forces from the global FEM to the local FEM. Either choice poses an inconsistency.

In addition to computational and engineering labor efficiency, another primary need for a better GLD process is to reduce human error and to establish consistently used modeling approaches throughout the global, local, detail, and micro analyses. The same treatment of loads and boundary conditions needs to be consistently applied throughout the localization and homogenization modeling process. Aerospace design manuals and analysis methods/tools in use today are still mostly based on simplifying assumptions that decouple important structural behavior. These disconnects in maintaining consistent boundary conditions and loadings throughout the localization and homogenization process are evident even though there is a controlling GUI interface menu system that provides semi-automatic submission of the valuable legacy codes. Most of these codes require manual input of data opening up the possibility for human error. So even if the codes did link I/O from a software coding perspective, they still would not be integrated in a sound and theoretically general manner. This shortcoming is addressed in this section with a more integrated approach. More specifically, Fig. 7.1 represents a modeling and failure prediction process by implementing at the core level a GLD analytical modeling methodology that is physically, mathematically, and computationally consistent and efficient at data transfer as it localizes to the micro level and homogenizes to the global level of the analyses. The emphasis is on minimizing required data transfer and completely automating the process to reduce possible human I/O errors. Such a highly integrated and consistent approach is implemented in HyperSizer.

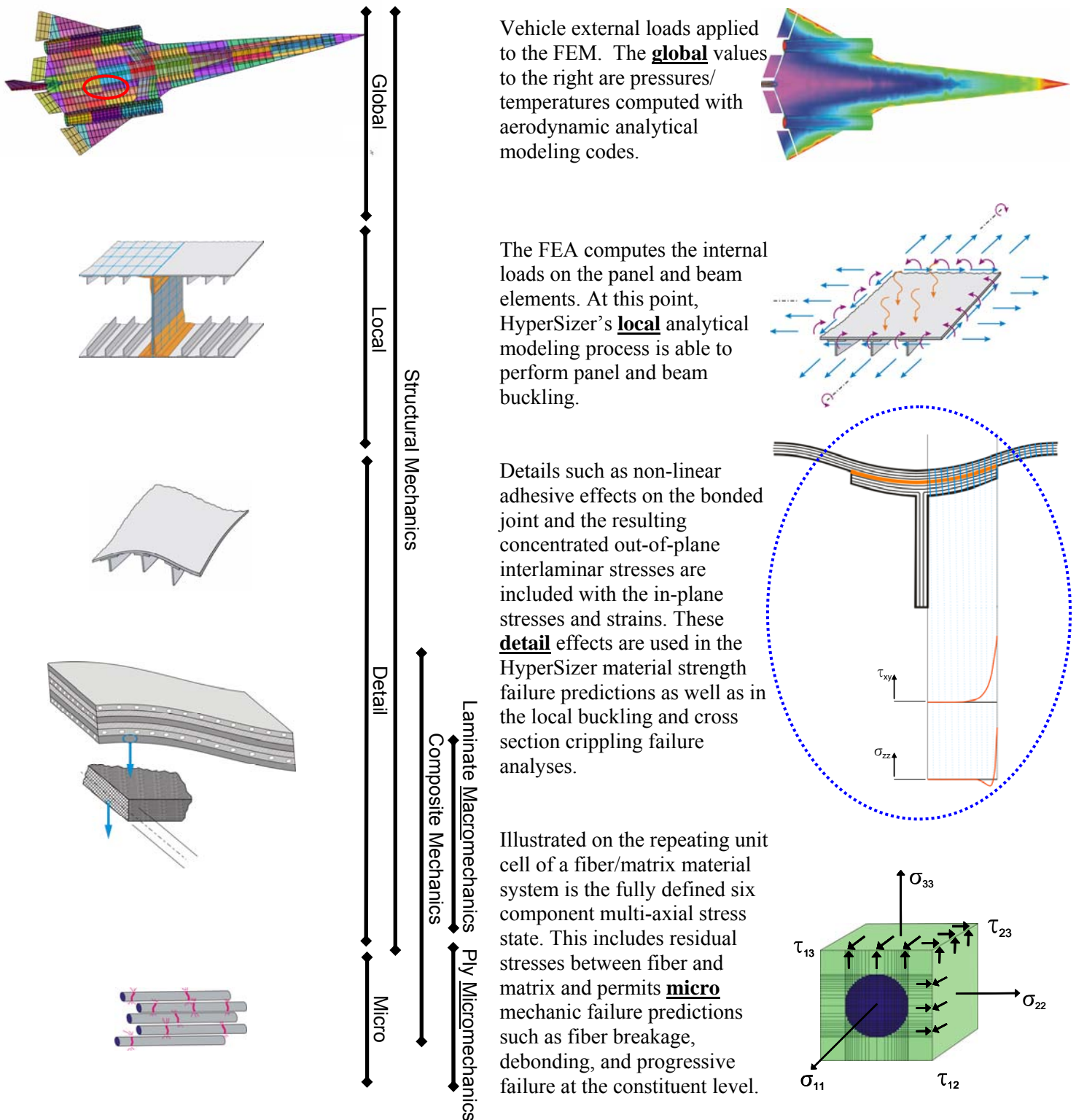


Fig. 7.1, The implemented Global-Local-Detail process including micromechanics. **Localization** is drilling down, and **homogenization** is coming back up in the process.

## 7.2 HyperSizer as it Existed

This 1<sup>st</sup> SBIR thrust was deemed doable within the scope of effort of Phase II due to the extensive existing capabilities of HyperSizer in the technology area of reduce order modeling and high fidelity rapid analysis. Therefore, before describing newly developed capability, preexisting relevant capability is described.

### 7.2.1 Efficient and consistent global-local-detail modeling for stiffened and sandwich panels.

A necessary prerequisite is an understanding of how HyperSizer is able to analytically model stiffened panels without FEA. Doing so greatly reduces finite element count and allows very accurate internal load path predictions with coarsely meshed *global* FEMs. Resulting FEA computed loads are then applied consistently to HyperSizer analytical models of panels and joints which then compute accurate detail ply level stresses and strains.

### 7.2.2 Stiffened panels

Since stiffened panels are a key lightweight design of fuselage and wing surfaces, the ability to model their cross sectional shapes with an equivalent global-local-detail (GLD) modeling approach without having to discretely represent their shapes with finite elements is a fundamental contribution of HyperSizer's thermoelastic formulation.

There are four possible methods to model stiffened shell structures, as shown in Fig. 7.2. The first method is recommended for most of an airframe's "acreage" area. Such modeling in conjunction with a proper GLD approach is recommended if it includes representing, for each shell element, the full compliment of a panel's membrane  $[A]_{3 \times 3}$ , bending  $[D]_{3 \times 3}$ , and membrane-bending coupling  $[B]_{3 \times 3}$ , stiffness matrices as well as their corresponding thermal coefficients  $\{A^\alpha\}_{3 \times 1}$ ,  $\{D^\alpha\}_{3 \times 1}$ ,  $\{B^\alpha\}_{3 \times 1}$ . The primary advantage is a much more efficient and smaller FEM that is most appropriate for a loads model. The second method to model using beam elements to represent the panel stiffeners/longerons has many shortcomings and is never recommended. The third modeling method discretely models each stiffener with shell elements and is suitable for capturing in-plane effects (normal and shear stresses) but not out-of-plane effects (interlaminar shear and peel stresses). This method is not useful for large surface areas due to unmanageable high element count. The fourth modeling approach with solid elements is useful for capturing through-the-thickness interlaminar stresses but suffers from extremely high element count, making modeling of even the smallest detail very time consuming, and difficult in achieving accurate answers for off axis lamina. These types of models are useful for bonded composite joint analysis, but even such small features require over ten thousand solid elements.

HyperSizer models airframe panels with the first approach, in Fig. 7.2, of using a planar 2D FEM mesh, with stiffeners smeared into the thermoelastic formulation. Only the equivalent stiffness and thermal coefficients are necessary to send to the FEM, since HyperSizer defines and uses the discrete cross sectional dimensions in its detailed failure analyses performed offline from the FEA.

Fig. 7.3 describes how the analytical modeling for the LRS aircraft presented in Section 6.3 is carried out. In this depiction, a "Tee" stiffened panel concept is modeled in the loads FEM with a planar 2D mesh.

This allows all panel failure analyses such as panel buckling, crippling, local span buckling, material strength; as well as adhesive joint strength, such as interlaminar delamination, and fiber fracture from the concentrated stress fields near the joint flange re-entrant corner. These types of analyses are properly and consistently performed for in-service boundary conditions to any possible combination of uniform edge loading, normal pressures, and through-the-thickness temperature gradients, as portrayed in Fig. 7.3 (c).

### Four different ways to model stiffened panels

- 1) 2D shells only
- 2) 2D shells with beams for stiffeners
- 3) 2D shells for discrete shape
- 4) 3D solid elements for discrete shape

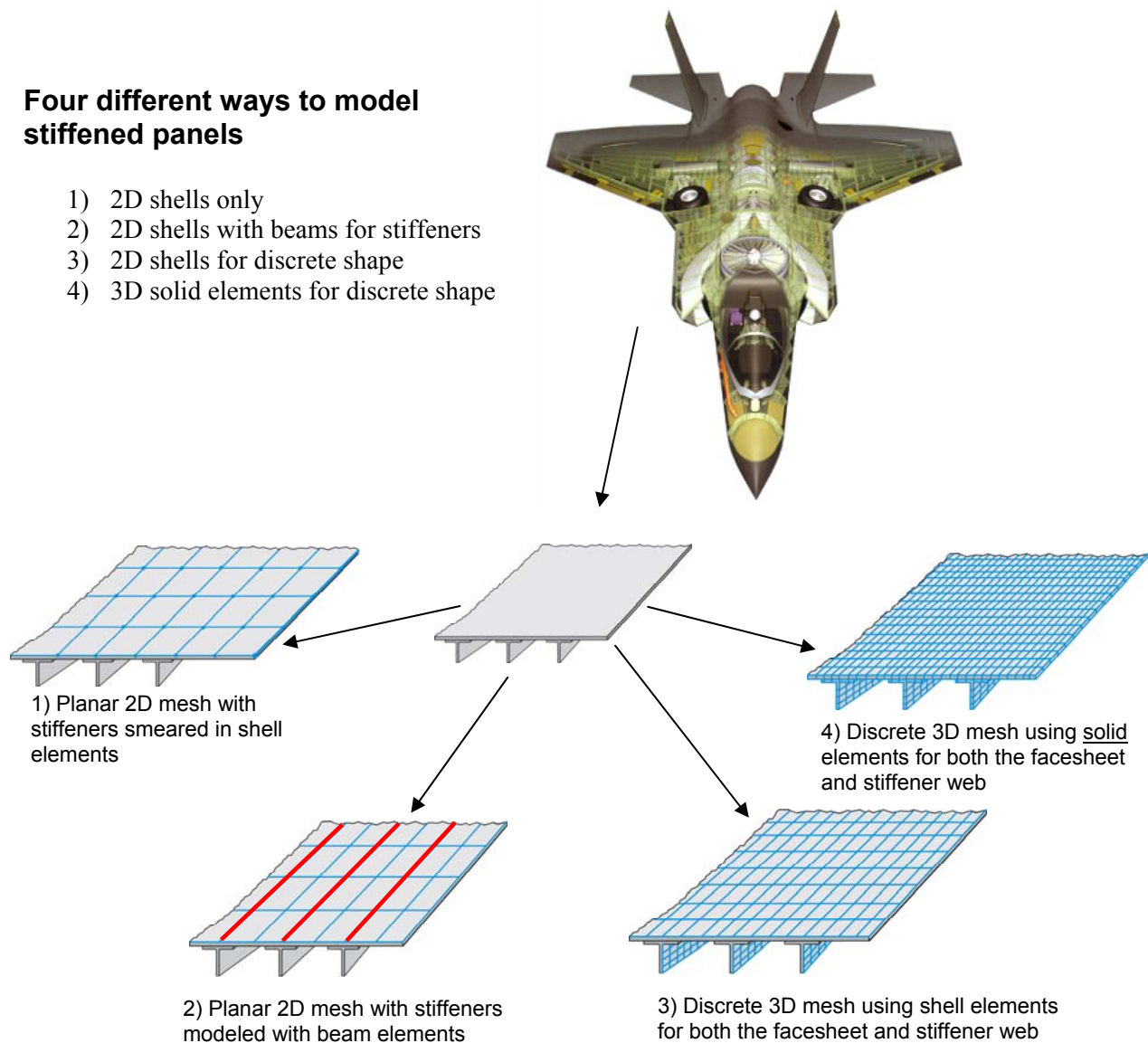


Fig. 7.2, Four different ways to construct airframe stiffened panel FEMs. The preferred modeling approach is number 1) planar 2D mesh with stiffeners smeared in shell elements.

In addition to representing any stiffened panel shape or sandwich construction with a single plane of elements, another important capability is accurately computing offline from FEA, panel deflection, moments, and out-of-plane shears caused by normal pressure, such as those caused by

fuel. This is an important capability because many times the global FEM is not sufficiently refined to accurately capture those secondary bending effects. These secondary panel loads are then superimposed with the global FEA computed internal running loads.

### **7.2.3 Sandwich Panels and Composite Laminates**

Honeycomb or foam core sandwich panels should also be modeled using a 2D planar mesh from the 1<sup>st</sup> listed modeling approach. Rarely should the core be modeled with solid elements, and instead the GLD equivalent smearing modeling approach described for stiffened panels should be used. Transverse shear flexibility (TSF) effects should also be included by defining the shear stiffness  $[G]_{2 \times 2}$ , matrix and sending it to the FEM shell element properties.

Sandwich specific failure modes such as: facesheet wrinkling, intercell dimpling, core shear strength, crushing, and crimping are also best modeled using semi-empirical equations developed from test correlations and not with a detailed FEM that attempts to model the honeycomb core cells.

### **7.2.4 Beams**

1-D bar or beam elements are the recommended element types for modeling ringframes and rib and spar caps. In all cases, a beam's principal (strong) axis needs to be defined using an element orientation vector, and a beam's neutral axis needs to be represented using beam element offsets. For full depth beams, such as wing ribs and spars, the recommended modeling approach is to capture the web with shell elements.

### **7.2.5 Joints**

A discussion of how HyperSizer analyzes a bonded composite (doubler) joint between the panel Tee stiffener and OML skin is presented in the next section of new SBIR developments. The joint between the internal bulkhead and surface panel indicated as a Pi joint, is modeled with a 1D finite element (beam), but at this point is not analyzed with HyperSizer.

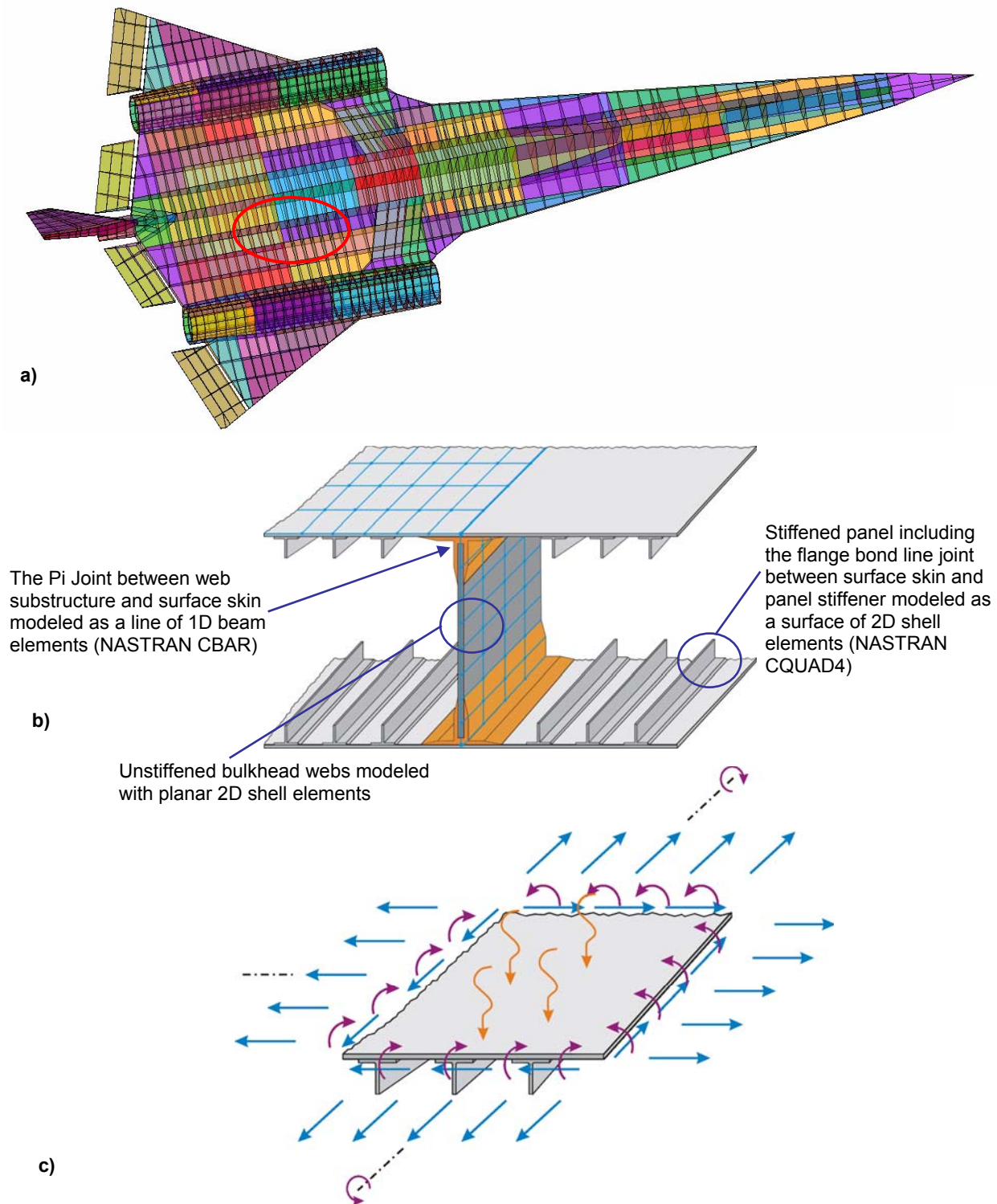


Fig. 7.3, a) LRS airframe coarsely meshed FEM that has one shell element spanning internal bulkheads. The red circle is an arbitrary location on the vehicle as represented with Fig b) that assumes a Tee stiffened panel concept for the OML skin surfaces and an unstiffened plate for the bulkhead web, c) where any combination of FEA computed uniform edge loading, pressure, and through-the-thickness temperature gradient can be applied.

## 7.3 SBIR Innovations

### 7.3.1 Overview

#### 7.3.1.1 Composite Bonded Joints

In the realm of reduced order modeling and high fidelity rapid analysis, a powerful new analysis capability, now available in HyperSizer, extends its thermoelastic and failure analysis formulations for panels and beam to examine the detailed stress fields of composite bonded joints and determine their margins of safety. The goal of this new capability is to provide an efficient analysis that is fast enough to be included in preliminary design, but still accurate enough to achieve near final design solutions. This new capability was a major SBIR effort that included many researchers.

In current practice, the complexity of bonded joint behavior requires generation and analysis of detailed finite element models that are time consuming to develop, run, and post-process. Such detailed finite element analyses, which must include 3D solid elements, are seldom done in preliminary design, where the design dimensions, materials, layups and loads are constantly changing. Therefore, the joint analysis is many times left to final design where changes become much more problematic and costly to implement. More frequently, specialty type codes such as A4EI by Hart-Smith are used in industry as rapid analysis tools. HyperSizer falls within this class of tools but is more accurate and solves more general loadings than A4EI (see section 7.3.4).

HyperSizer captures the primary physics of the bonded joint problem, Fig. 7.4, and does so in a very rapid procedure (on the order of  $1/40^{\text{th}}$  of a second) meaning that bonded joint analysis not only can be performed in preliminary design, but actually becomes a part of the structural optimization procedure.

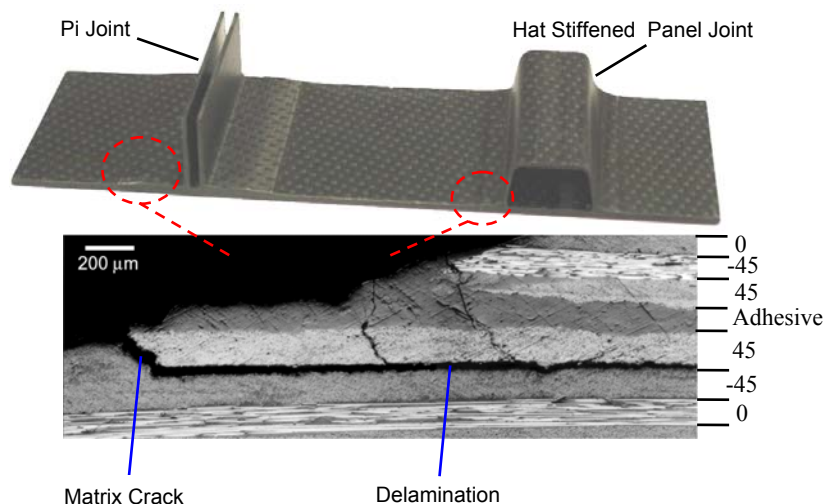


Fig. 7.4, HyperSizer now includes the ability to predict composite bonded joint failure to help avoid failure such as this.

#### 7.3.1.2 Composite Material Strength

Also contributing to high fidelity rapid analysis are new *physically* based composite strength failure criteria now available in HyperSizer:

- Hashin fiber and matrix failure criteria
- LaRC03 fiber and matrix failure criteria, actively developed criteria from NASA Langley
- Strain Invariant Failure Theory (SIFT) on the micromechanics level using the Generalized Method of Cells (GMC), not FEA, actively developed criteria from Boeing

### 7.3.2 Efficient and consistent global-local-detail modeling of composite bonded joints

Much more information is provided in Volume 2, Section 6.

Deriving accurate stress and strain fields in a bonded joint begins with an understanding of the loading and boundary conditions of the assembled structure. In Fig. 7.5 the typical skin-stringer stiffened structure is once again shown, this time with general membrane, bending, out of plane shear and pressure loads. These loads could come from a finite element analysis, fuselage beam theory, or if determinate (such as pressurized tank hoop loads), typed by hand into the HyperSizer interface.

These general airframe loads are reduced by HyperSizer into local “point” loads at the stiffened panel level (b) and resolved to detailed stresses and strains in the joint itself, such as the interlaminar shear and peel stresses shown (c). Note the generality of loads that are passed to the joint analysis including local skin deflections due to pressure, membrane forces, and bending moments in the direction transverse to the stiffener.

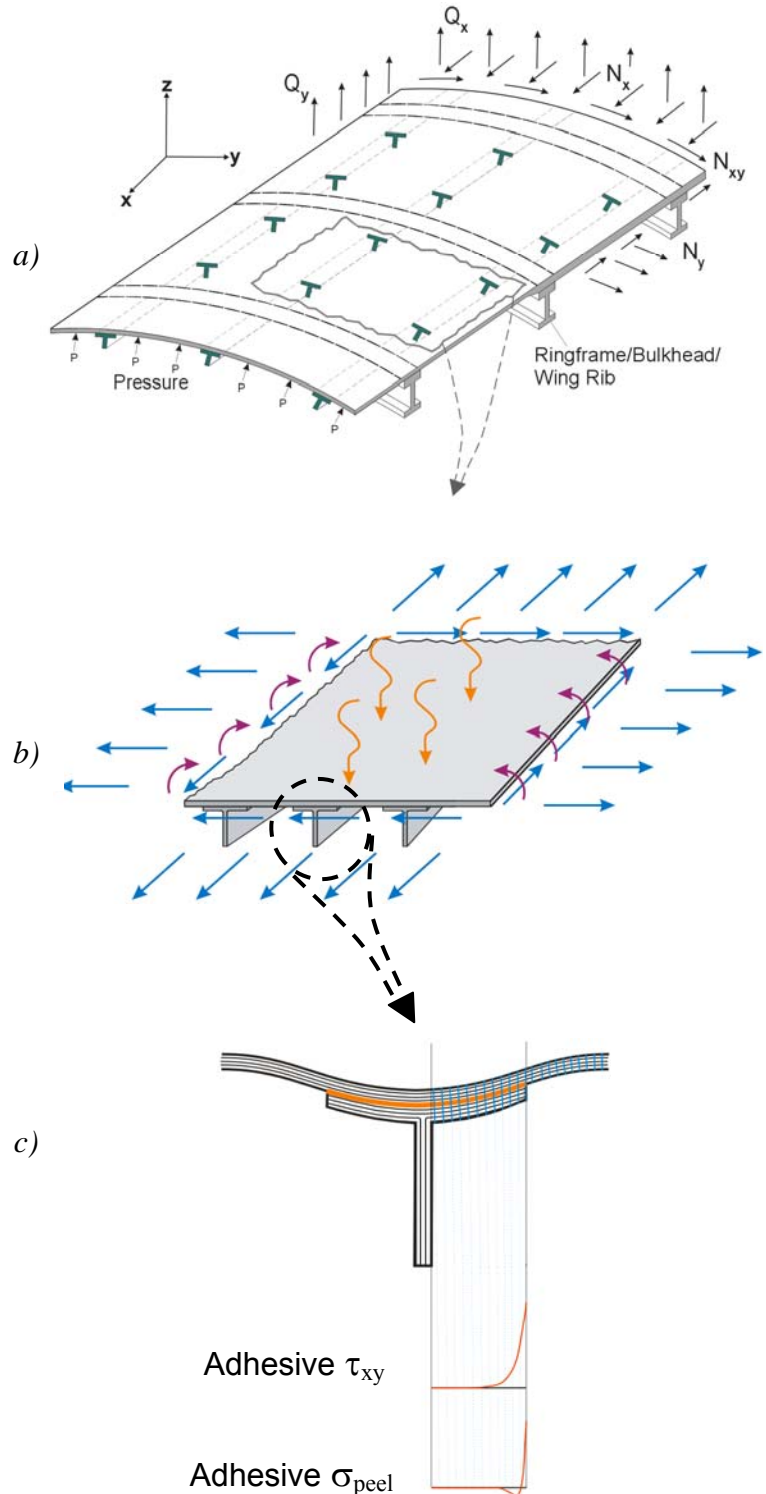
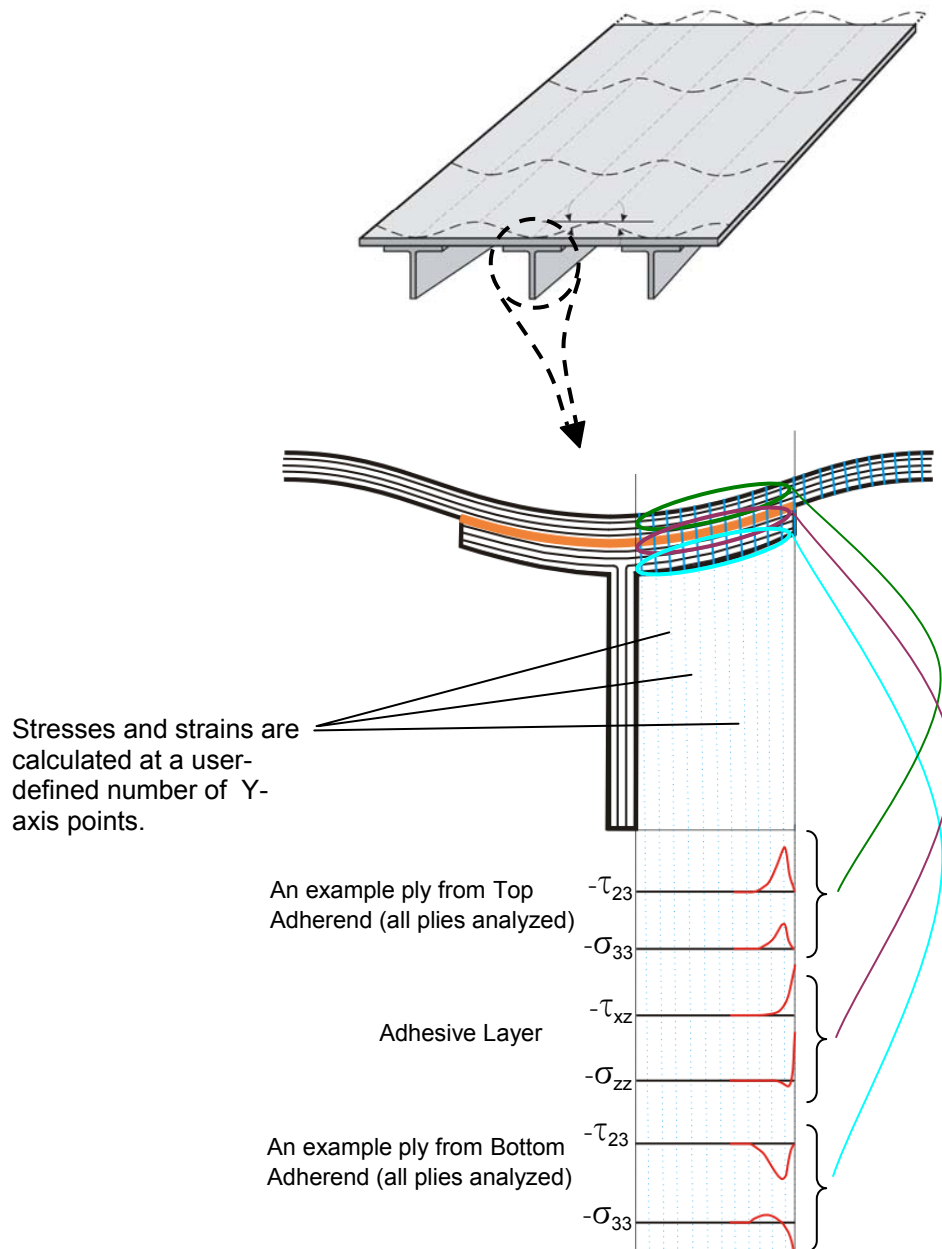


Fig. 7.5, HyperSizer rapidly and accurately resolves aircraft stiffened structure panel loads into interlaminar stresses of the adhesive (as illustrated) and also to the laminate adherends.

HyperSizer's primary results are stress fields throughout the joint and margins of safety. First, plots of stresses and strains are generated in the plane of the joint at any number of user-chosen  $z$  locations as shown by the light blue, purple and green circles of Fig. 7.6. These plots are represented by a user-defined number of points along the joint (panel  $y$  direction) and the failure criteria described in Section 7.3.3 are applied at each of these points.



*Fig. 7.6, Interlaminar stress calculations throughout depth of bonded joint, including adhesive and laminated adherends. Note that adhesive stresses are in the panel coordinate system ( $x, y, z$ ), adherend stresses are in each ply coordinate ( $1, 2, 3$ ).*

In addition to plots in the plane of the joint, HyperSizer also generates through-thickness stress plots, again at user-prescribed  $y$  locations throughout the joint. Fig. 7.7 shows how interlaminar shear (red lines) and peel stresses (black lines) vary greatly as the free edge of the joint is approached. Not only are the magnitudes different, but the character of the curves completely change near the free edge as the peel stress goes from compressive to tensile.

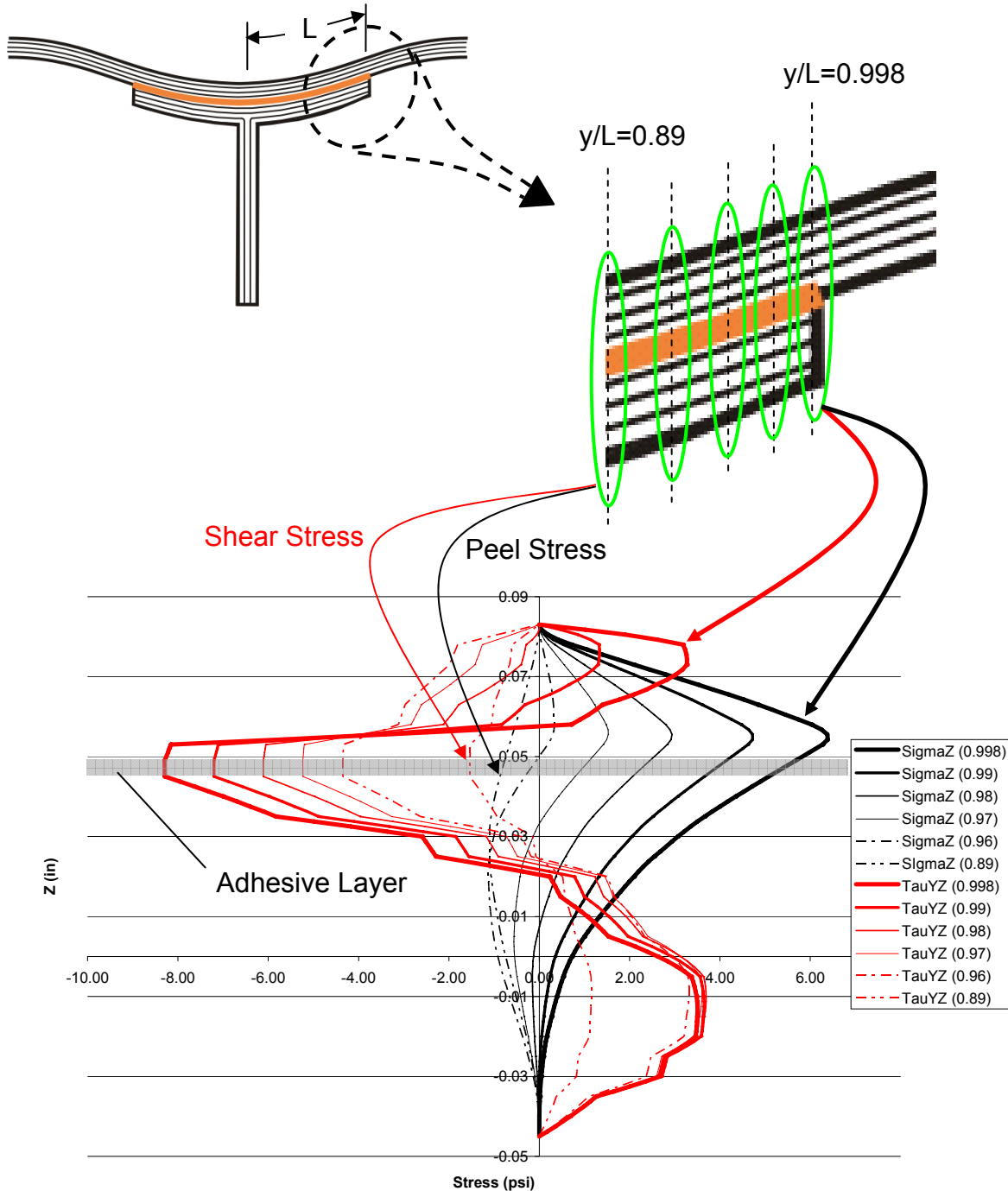
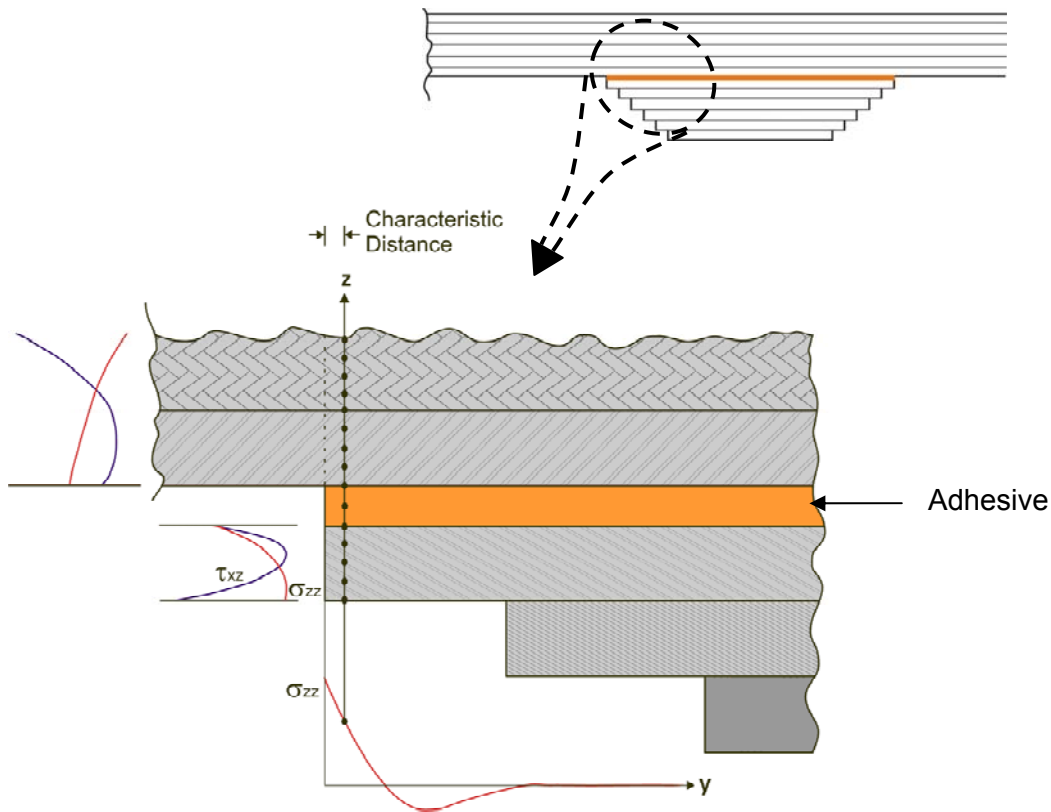


Fig. 7.7, Stress calculations performed by HyperSizer through the depth of the joint show how the interlaminar shear and peel stress vary greatly as the free edge of the joint is approached.

When HyperSizer solves stepped or scarfed joints (just as with the non-stepped joint), the through-thickness, out-of-plane stresses are not constant or even linear through each ply but are actually a cubic function of  $z$ .



*Fig. 7.8, HyperSizer computes stress variation through the thickness of each ply. Note the variation of interlaminar stress in the last ply in contact with the adhesive. Stresses can be established at any user prescribed characteristic distance for use with failure criteria.*

Other important effects are also included in HyperSizer's bonded joint analysis method that will be critical for accurate analysis and sizing. One example is inclusion of non-linear adhesive properties, that can substantially reduce critical stresses, especially in the region of joint free edges. HyperSizer includes these non-linear effects with six different non-linear material models. The non-linear material models have been verified for use in these types of bonded joint by comparing to ABAQUS non-linear FEA.

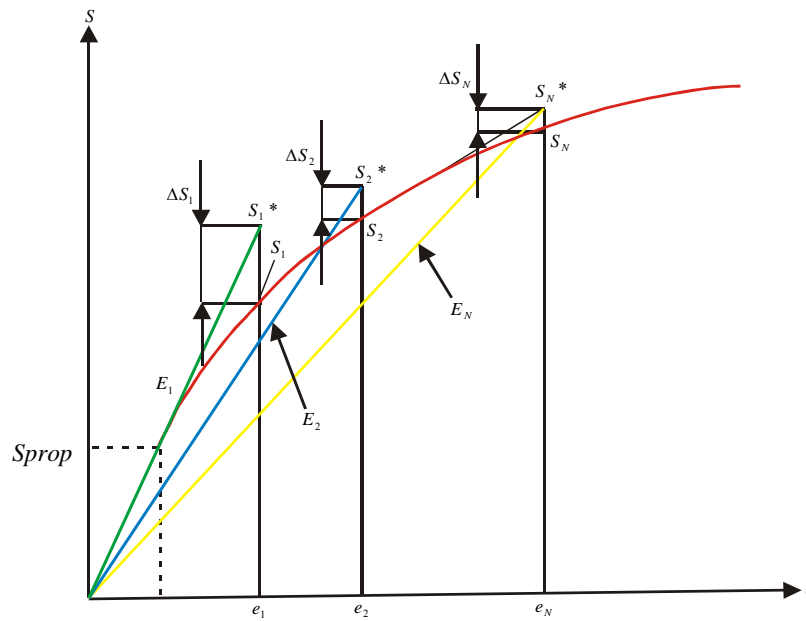


Fig. 7.9, Example of a non-linear material model used in HyperSizer's bonded joint analysis.

### 7.3.2.1 Verification of stress/strain prediction

**Much more information is provided in Volume 3, Sections 6 - 12. Provided are three primary verification example sets, and three primary test data validation cases.**

A sampling of comparison of HyperSizer results to those from a solid model FEA for an aluminum-aluminum joint configuration is shown in the following figures, 7.10 to 7.13. This example is based on a series of results from Delale and Erdogan (Volume 2, Section 6.9.1). A more comprehensive comparison for this problem is provided in Volume 3, Section 6. Volume 3 also presents many more verification and validation problems including those made from composite laminates.

Note that the Erdogan solution is not general (cannot handle composite materials nor general loadings and boundary conditions) as does the implemented approach in HyperSizer. Also note that the method implemented in HyperSizer tends to over predict the dip at  $0.8 < X/L < 0.9$ . Though this appears to be a concern, so far, it has been insignificant in both the prediction of free edge peel and interlaminar stresses that are used in adhesive failure predictions and for failure predictions of delamination and fracture for laminates. It has also been determined that this dip does not effect strain energy release rates calculations using the virtual crack closure technique.

#### ***Case A: Aluminum flange - aluminum plate subjected to applied moment***

Fig. 7.10 shows the HyperSizer solution of adhesive stresses with comparison to Erdogan's plate theory solution [Volume 2, Ref. 6.9.1] and FEA solutions (2D shell Erdogan and 3D solid element ANSYS). The loading for this case is applied moment.

#### ***Case B: Aluminum flange - aluminum plate subjected to applied force***

Fig. 7.11 shows the HyperSizer solution of adhesive stresses with comparison to Erdogan's plate theory solution and FEA solutions (2D shell Erdogan and 3D solid element ANSYS). The loading for this case is applied tensile force.

Figs. 7.12 and 7.13 show in closer detail the HyperSizer solutions compared this time to Abaqus 2D plane strain linear and non-linear FEA, and Ansys 3D solid FEA. At the actual free edge,  $x/L = 1.0$ , substantial oscillations began to occur in the FEA due to the singularity. HyperSizer results are compared to the FEA results in two ways. First, the FEA solutions are projected from the non-oscillating portion of the curve to the free edge and compared to HyperSizer results at the free edge. Second, the solutions are extracted at a characteristic distance from the free edge. This distance is approximately 1/2 of a typical composite ply thickness (0.0055") from the free edge. Using either comparison, results between HyperSizer and FEA match fairly well.

The large oscillating fluctuations in the FEA solutions, particularly for both the linear and non-linear Abaqus FEA for the value of peel and shear stress are problematic and cause difficulty and confusion for the practicing engineer in choosing a proper characteristic distance from the reentrant corner (free edge) in which to select design-to magnitudes. HyperSizer solutions are more stable and robust in this regard and not as sensitive to the arbitrary selection of a characteristic distance.

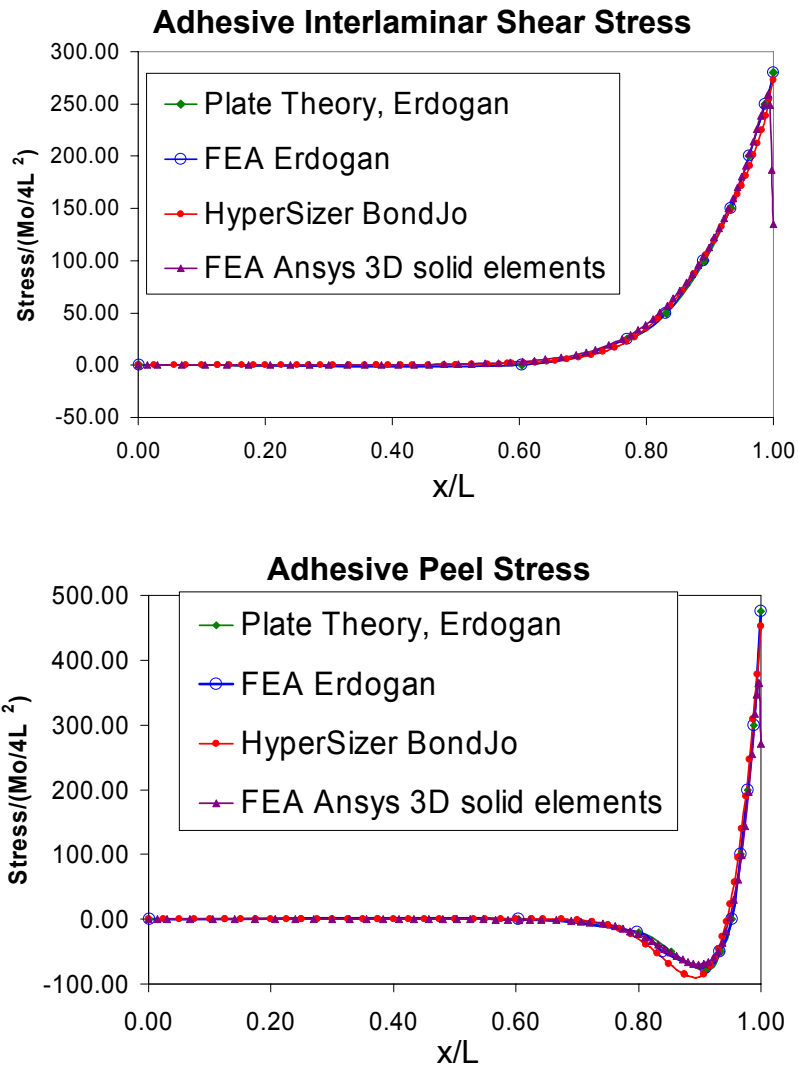
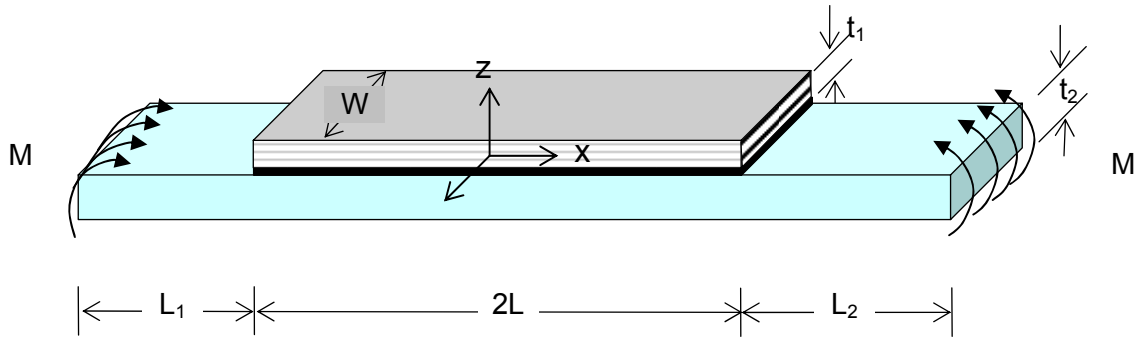


Fig. 7.10, Comparisons for the applied moment case between HyperSizer, Ansys 3D solid FEA, Delale and Erdogan's analytical plate theory, and independent 2D shell FEA performed by Delale and Erdogan.

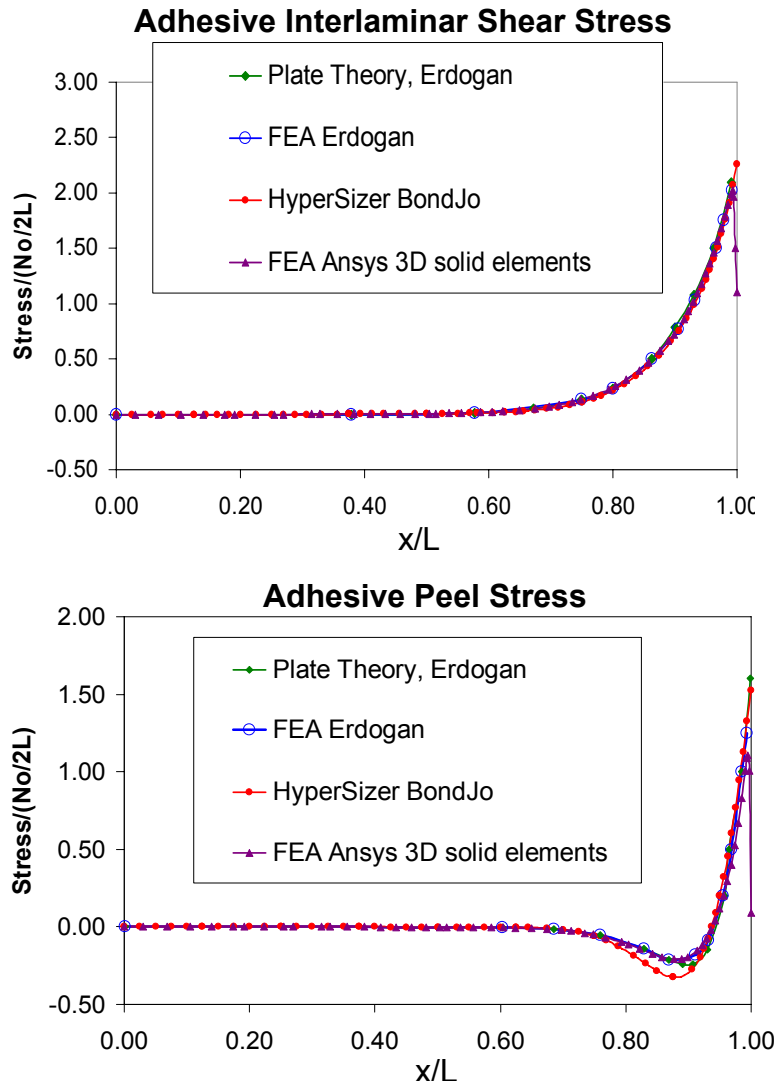
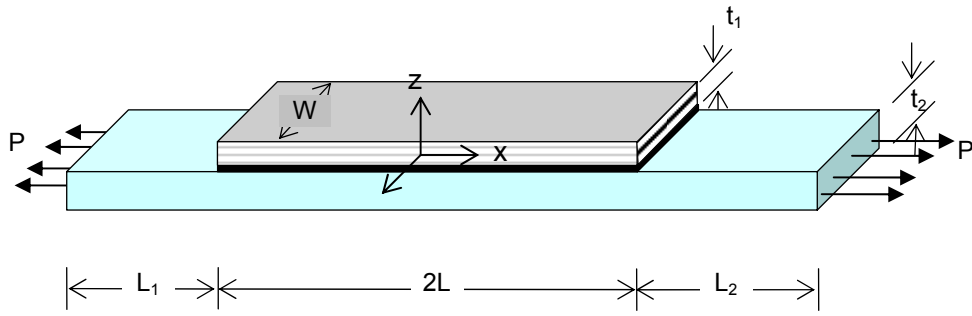


Fig. 7.11, Comparisons for the applied tensile force case between HyperSizer, Ansys 3D solid FEA, Delale and Erdogan's analytical plate theory, and independent 2D shell FEA performed by Delale and Erdogan.

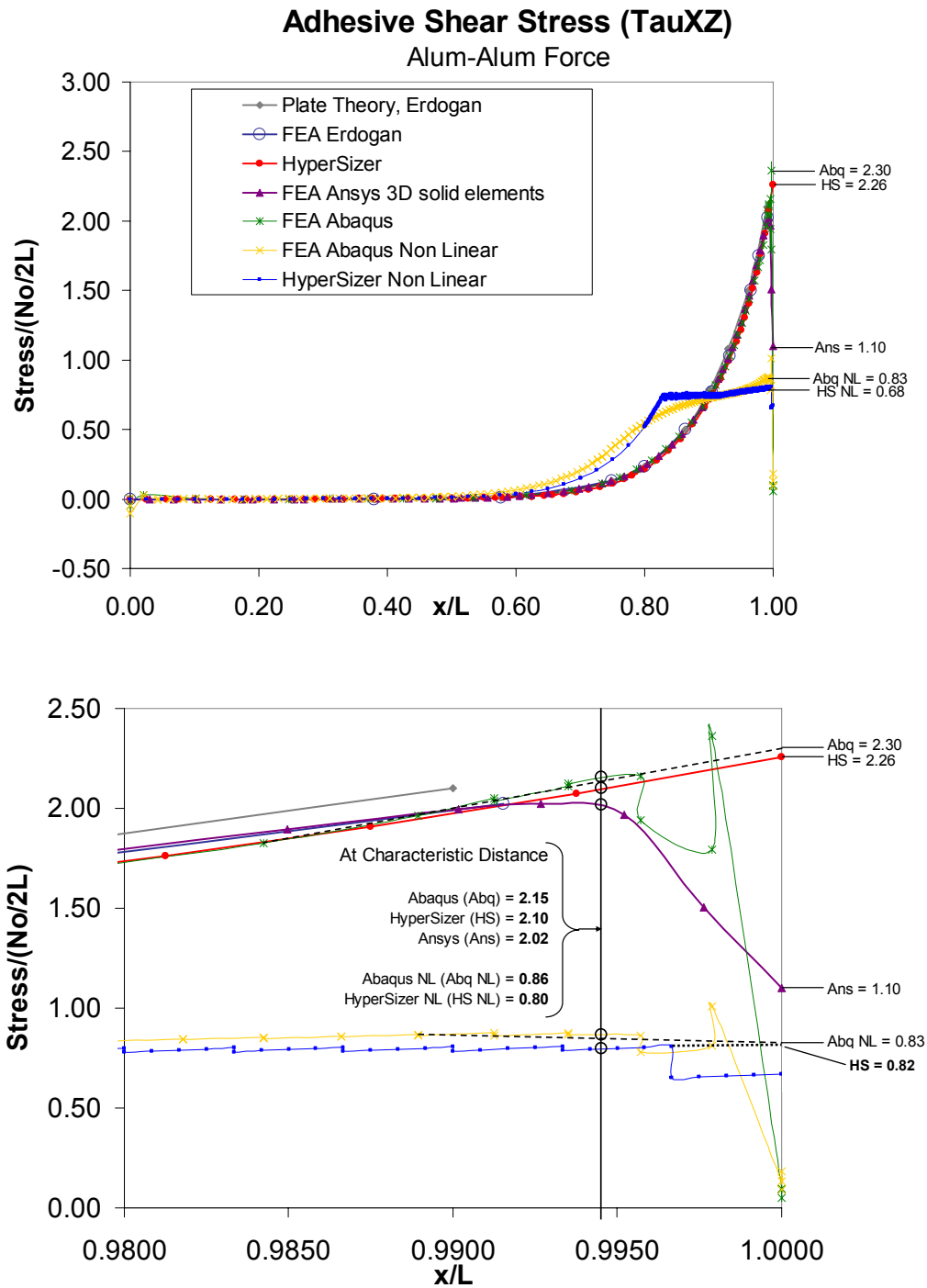


Fig. 7.12, Adhesive interlaminar shear stresses from membrane tensile force. Comparisons between HyperSizer, Abaqus 2D plane strain linear and non-linear FEA, and Ansys 3D solid FEA. Note: HyperSizer = HyperSizer, NL = non-linear.

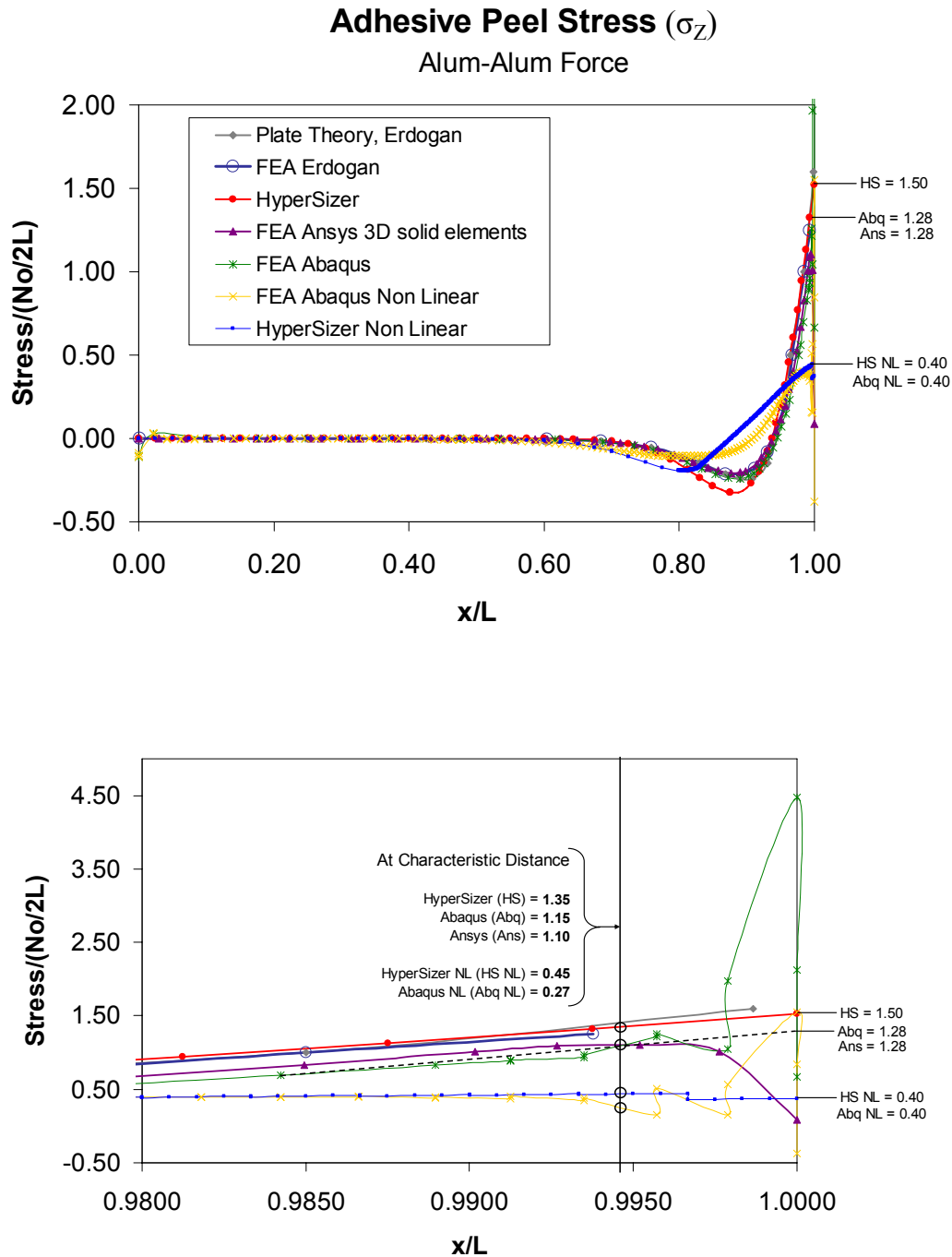


Fig. 7.13, Adhesive interlaminar peel stresses from membrane tensile force. Comparisons between HyperSizer, Abaqus 2D plane strain linear and non-linear FEA, and Ansys 3D solid FEA.

### 7.3.3 Composite bonded joint failure prediction

HyperSizer resolves the full in-plane and interlaminar stress fields in the adherends and the shear and peel stresses in the adhesive layer. Once the numerical issue of stress singularity is resolved, a solution for determining margin-of-safety at areas of stress gradient such as bonded joint reentrant corners is to select a proper characteristic distance to use for comparing computed stress to allowable stress. In most bonded joint failures, damage initiates close to the joint free edge, propagates into the first one or two plies of the adherends and causes either delamination or fracture of laminated adherends. This type of failure is shown in Fig. 7.14. In the failure of adherends, the out-of-plane stresses play an important role, particularly in delamination. HyperSizer's ability to predict these stresses, coupled with its speed, makes it a powerful software tool for preliminary aircraft design.

The purpose for the developing the new HyperSizer joint analysis code is predicting failure for composite bonded doublers. Fig. 7.14 shows a typical skin-stringer type of aircraft structure, which could represent, for example, a wing or fuselage. In previous versions, HyperSizer could isolate a section of this structure (b) for strength and panel stability analysis; however without the bonded joint analysis capability, it would miss failure modes of the type shown at (c). This type of delamination failure is very common in the 1<sup>st</sup> or 2<sup>nd</sup> facesheet ply close to the bonded stiffeners, therefore capturing this failure early in the design process is key.

In addition to delamination failures, several other failure modes have been identified as important for bonded joints. Heslehurst and Hart-Smith [Volume 2, Ref. 6.1.1] identified 6 broad categories of

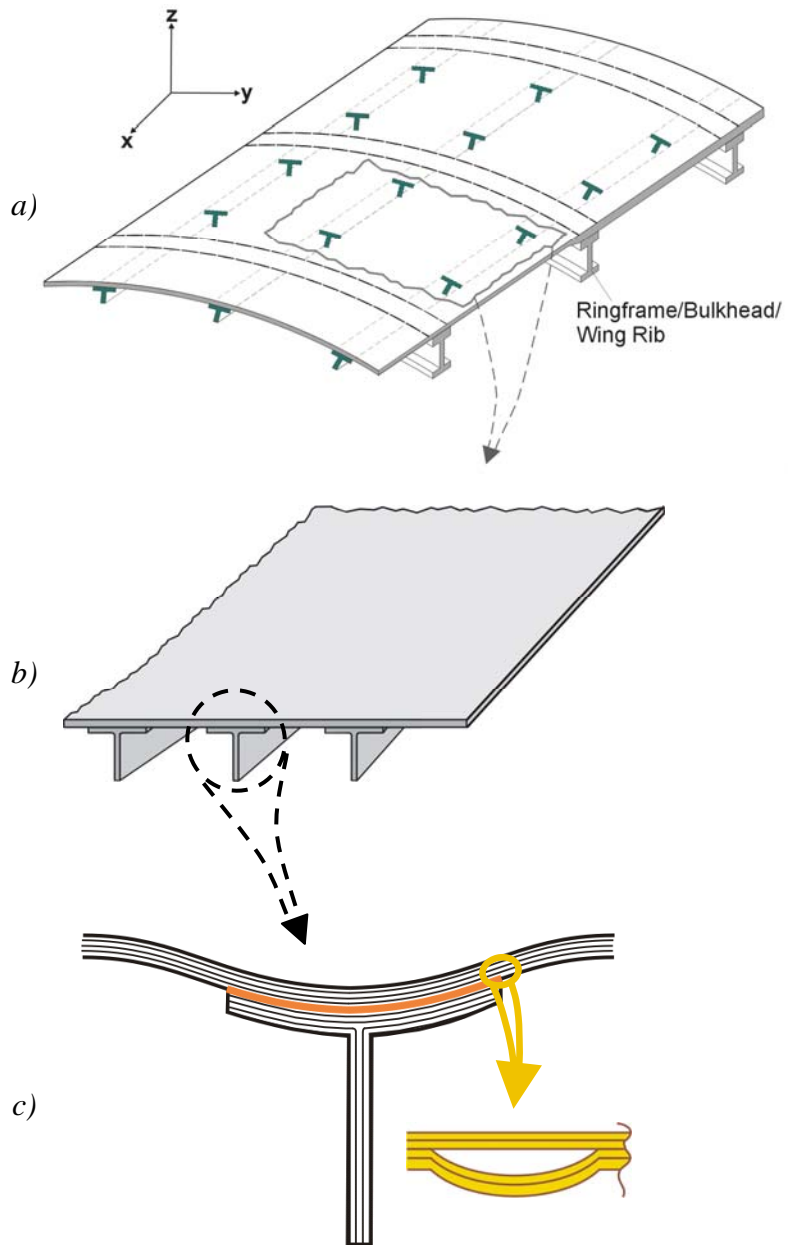


Fig. 7.14, A common composite failure mode for stiffened aircraft structure occurs at the re-entrant corner of a bonded flange.

failure for bonded joints as shown in Fig. 7.15 Categories ‘a’ and ‘b’ include failures that occur in the adherends while ‘c’ through ‘f’ include failures that occur in the adhesive layer.

### 7.3.3.1 Bonded Joint Failure Theory Classifications

The following classifications of bonded joint failure theories were identified by Heslehurst and Hart-Smith [Volume 2, Ref. 6.1.1] and are included in HyperSizer’s failure prediction. Margins-of-safety are computed based on recently published failure criteria. Failure methods are classified into two broad groups, adherend failures (blue) and adhesive failures (orange).

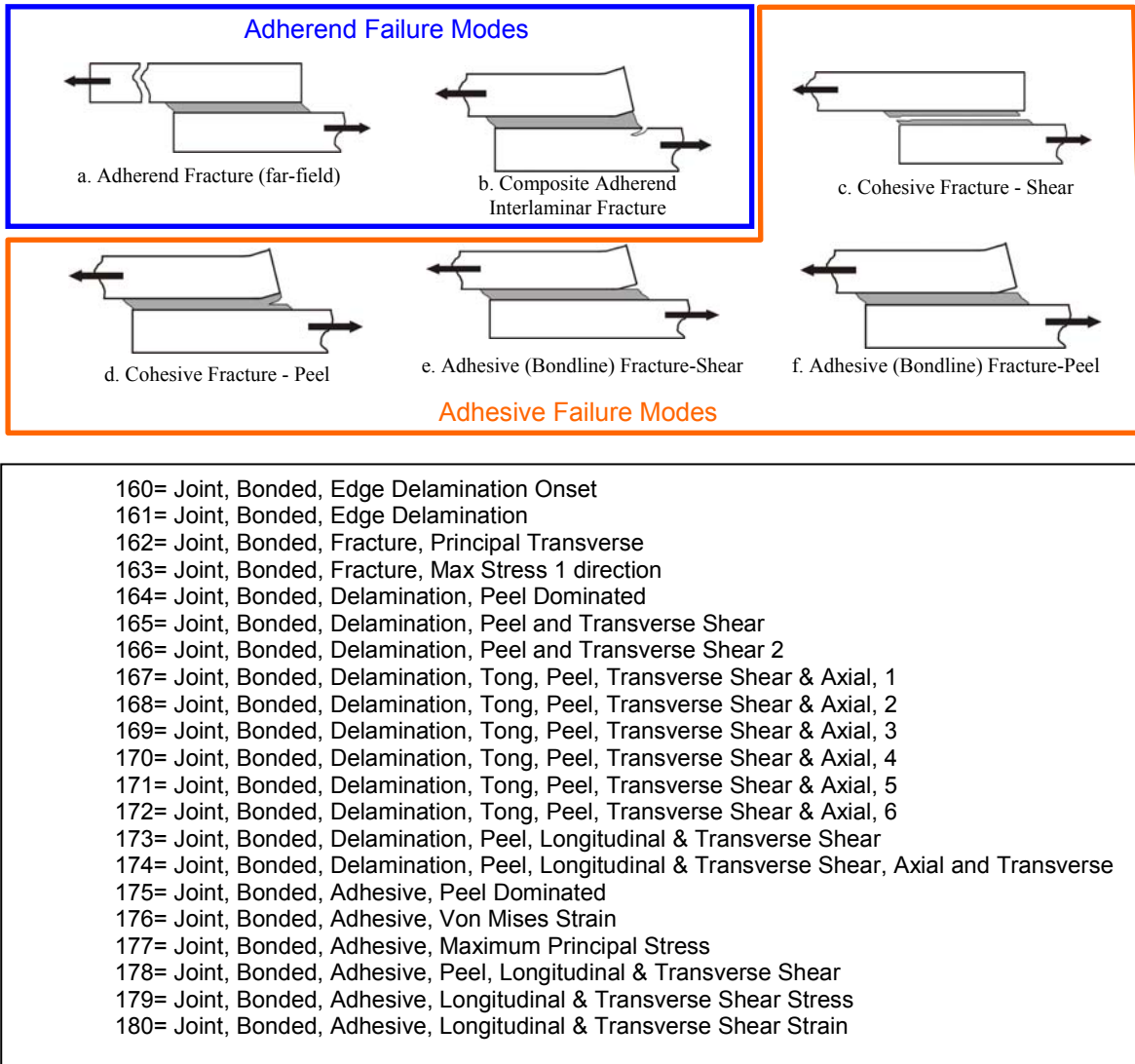
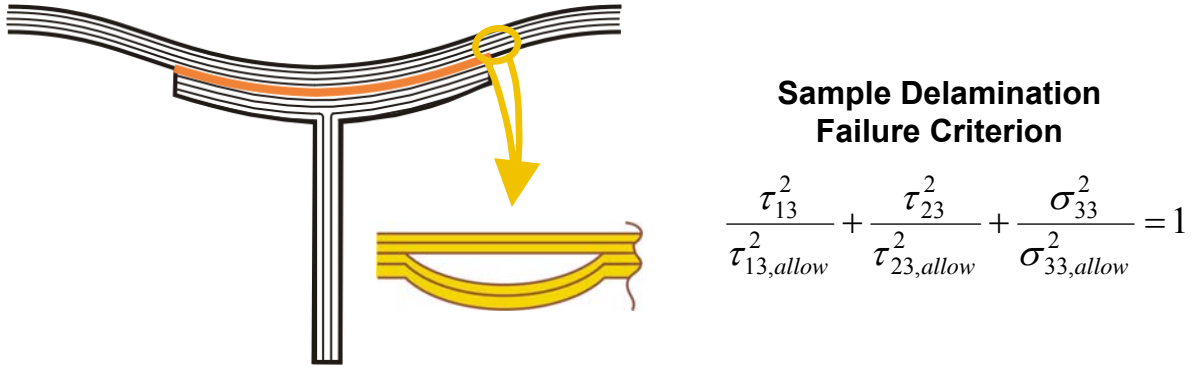


Fig. 7.15, Failure modes in adhesively bonded joints identified by Heslehurst and Hart-Smith, HyperSizer’s bonded joint analysis has built-in 19 failure methods that include all aspects of joint failure including adherend fracture and delamination and adhesive bond-line and strength failures.

While these figures show failure modes for single lap joints, the issues and the failure modes are the same for all types of bonded joints, including bonded doubler joints that we use to represent the facesheet to stiffener joint of a stiffened panel.

Fig. 7.16 again illustrates one of the most common types of failure of bonded joints with a sample failure criterion that attempts to predict that failure. The important thing to note about joint failure criteria (detailed in Volume 2, Section 6.5), is that they rely completely on knowing the stress state in the joint. In this case it depends on the interlaminar shear and peel stresses of the adherends, which in the past have been difficult to obtain without detailed FEA. HyperSizer provides a very rapid method of determining these stresses.



*Fig. 7.16, Failure prediction methods require accurate prediction of out-of-plane interlaminar shear and peel stresses.*

Specifically, 19 different failure criteria have been implemented for joint failure prediction; 2 for adherend fiber or matrix fracture, 11 with interlaminar delamination, and 6 with adhesive strength or bond-line failures. A sample failure criteria is shown here, where  $\sigma_{1,2,3}$  and  $\tau_{12, 23, 13}$  are normal and shear stresses in ply coordinates,  $X_{t,c}$ ,  $Y_{t,c}$  are the tensile and compressive normal stress allowables and  $S$  is the shear stress allowable for the adherends.

$$\left( \frac{\sigma_1^2 - \sigma_1 \sigma_3}{X_t X_c} \right) + \left( \frac{\sigma_2^2 - \sigma_2 \sigma_3}{Y_t Y_c} \right) + \left( \frac{\sigma_3}{Z} \right)^2 + \left( \frac{\tau_{23}}{S_{23}} \right)^2 + \left( \frac{\tau_{13}}{S_{13}} \right)^2 + \left( \frac{\tau_{12}}{S_{12}} \right)^2 = 1$$

The failure criteria and validations of HyperSizer's bonded joint failure method are detailed in [7].

### 7.3.3.2 Joint Failure Location Checks

Bonded Joint failure margins-of-safety are calculated at multiple points in the vicinity of the bonded flange (doubler) for stiffened panels.

The full stress tensor is calculated at multiple stations as shown in Fig. 7.17. Each adherend and each ply are broken into a user-defined number of  $y$  and  $z$  locations, represented by the green dots. The full stress state is evaluated at each of these locations. For a full description of HyperSizer's stress calculation within bonded joints, see Volume 2, Section 6.

Once the stress state is known, margins of safety are calculated using the failure criteria described in Volume 2, Section 6.5.

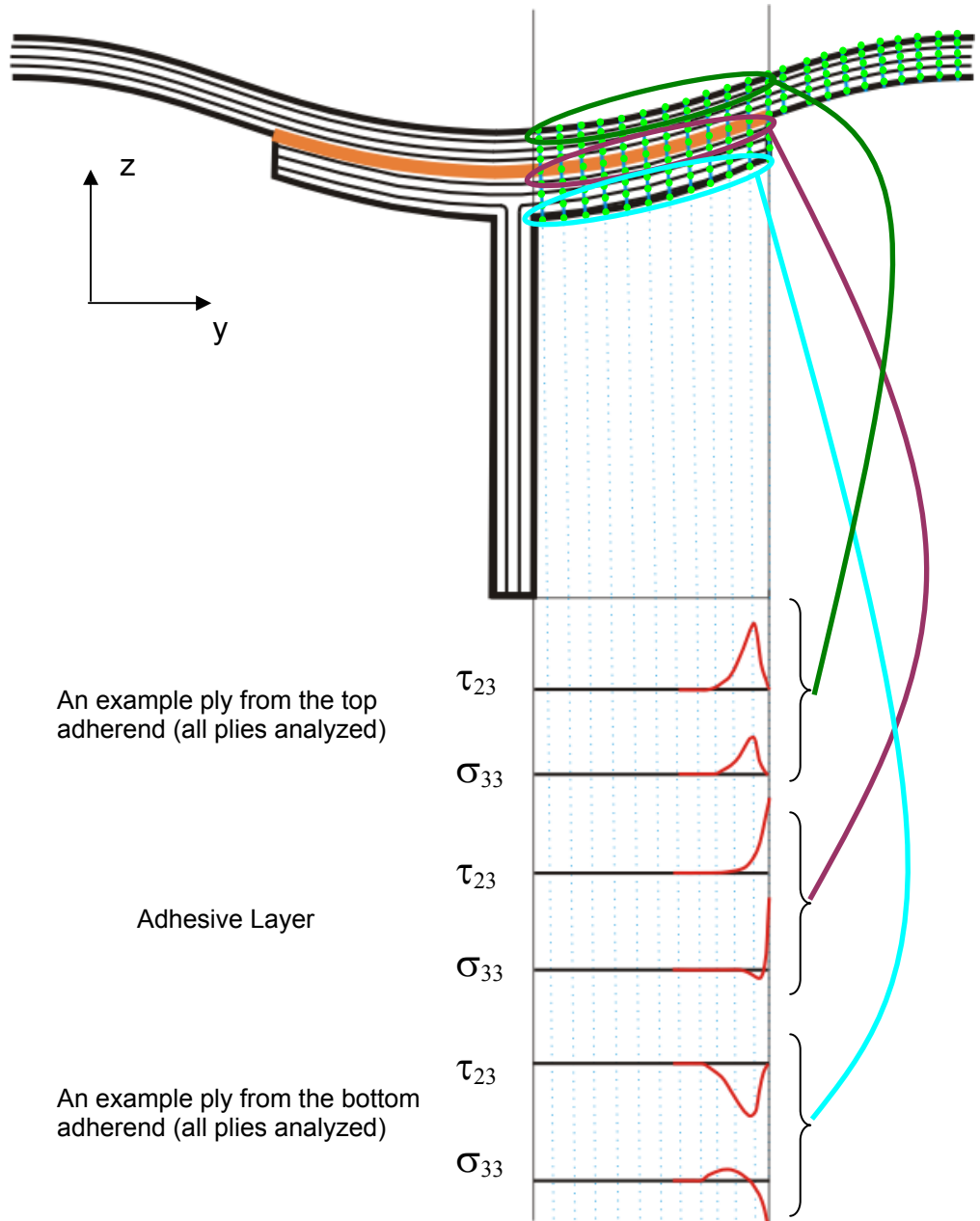


Fig. 7.17, The full stress state within the bonded joint is calculated by HyperSizer at a user-defined number of  $y$  and  $z$  locations indicated by the green dots. A typical bonded joint analysis has approximately 4000 points, where for each of these points, margins-of-safety are calculated using the failure criteria described in detail in Volume 2, Section 6.5.

### 7.3.3.3 Summary of validation test cases

Many leading bonded joint failure theories were implemented and used to make failure predictions for available composite test data. Table 7.1 contains 14 total tests comprised of three different bonded joint designs made of different materials: a bonded doubler, a stepped bonded doubler, and a single-lap joint. The ratio of the 14 linear theoretical to the test results ranges from 0.73 to 0.95, with average equal to 0.84; the ratio of the 14 nonlinear theoretical to the test results ranges from 0.77 to 0.95, with average equal to 0.86. These results show that HyperSizer is as accurate and consistent as highly detailed 3D FEA at predicting initial failure.

The capability of HyperSizer to calculate accurate three-dimensional stresses allows for prediction of failure loads in bonded composite joints with complex 3D stress state. Failure prediction requires not only accurate stress analysis, but also the appropriate failure criteria associated with the specific failure modes. For the bonded joints, the failure occurs either within the adhesive (cohesive failure), or at the adhesive/adherend interface (interface failure), or in the adherends. Metallic adherends generally fail in relatively simple modes compared to composite adherends, which may fail in matrix tension/compression, fiber tension/fiber compression, delamination, etc. In particular, the interfacial failure is rather complex because of formation of chemical bonds, whose strengths are very difficult to measure. In some cases, composite joints fail progressively after damage is initiated at the adherends or in the adhesive. The ultimate failure of joints will not be reached until the progressively accumulated damage exceeds the tolerance. In this paper, a number of failure criteria are presented for damage initiation and implemented in HyperSizer in conjunction with the establishment of experimental database. Included are validation test examples from literature.

The first example is selected from Cheuk and Tong's experiment and analysis for lap shear joints [Volume 2, Ref. 6.10.1]. The original purpose of the study by Cheuk and Tong was to investigate the interlaminar failure of bonded shear lap joints with embedded cracks. In this study, experiments were conducted to identify the failure modes and to measure failure loads of specimens with different length of cracks. In our present study, we select the validation cases from a group of experimental results for the specimens without cracks. It shows that the predicted failure location matches with experimental observation, while the predicted failure load is relatively conservative compared to the measured ultimate failure load in the tests. The discrepancy may be due to the progressive damage involved in the experiment while the predicted failure load is only an account for the damage initiation.

The second validation example is selected from composite bonded skin/stringer specimens tested by NASA [Volume 2, Ref. 6.10.2]. Both linear and nonlinear adhesive properties are considered in this example. The failure criteria of delamination and matrix cracking are used to predict the damage onset and the corresponding margin of safety is checked at each point of the adherends. The predicted location of damage onset by linear analysis is consistent with the experimental observation, while the predicted load for the damage initiation is  $\approx 0.85$  that of the tested average strength. Nonlinear analysis shows that soft adhesive will significantly increase the damage resistance of the adherend.

The last validation example is selected from the bonded single-lap joint specimens studied by Tong [Volume 2, Ref. 6.10.4]. Both linear and nonlinear analyses are performed to predict the failure load of the specimen subjected to longitudinal tension. Maximum stress criterion is used to predict the initial failure of adherends based on the failure mode observed in the tests. Even though only the ultimate failure load is reported in the paper, the load-displacement curves of the joint specimens show very pronounced initial damage and damage evolution prior to the ultimate failure. The predicted failure location matches with the test, and the theoretical failure load correlates well with the measured initial failure load.

Table 7.1 summarizes the theoretical predictions of the failure loads versus test averages for each validation example.

The second line (numbers in parentheses) for Test Set 2 shows a closer comparison to test results when all of the appropriate failure criteria are averaged. The numbers shown in Table 7.1 are actually the lowest failure predictions from any of the applicable failure criteria, and by definition are the lowest theoretical loads.

**Table 7.1, Summary of theoretical predictions versus test averages of failure loads**

Experiment	HyperSizer with Linear Adhesive			HyperSizer with Nonlinear Adhesive	
<i>Test Examples</i> <i>(all the joints are subjected to longitudinal tension)</i>	Failure loads (kN)	Theoretical Failure Load (kN)	Ratio of the Theoretical to the Test	Theoretical Failure Load (kN)	Ratio of the Theoretical to the Test
<u>Test Set 1</u>					
Bonded doubler by Cheuk (Average of 6 tests) Characteristic distance = 0.0	18.6	13.5	<b>0.73</b>	14.4	<b>0.77</b>
<u>Test Set 2</u>					
Stepped bonded doubler by NASA (Average of 5 tests) Characteristic distance = ½ ply thickness	17.8	13.5 (16.8)	<b>0.76</b> <b>(0.94)</b>	15.4 (17.7)	<b>≈ 0.87</b> <b>(0.99)</b>
<u>Test Set 3</u>					
Single-lap joint by Tong (Average of 3 tests) Characteristic distance = 0.0	7.2	6.85	<b>0.95</b>	6.82	<b>0.95</b>

### 7.3.4 HyperSizer Joint analysis comparison to the other methods

Current practices in the aerospace industry related to joints fall into two categories, rapid analysis, semi-closed form methods such as Hart-Smith A4EI, or detailed finite element methods such as ABAQUS, Stresscheck, or B-SAM each of which has strengths and weaknesses. For example, the rapid analysis techniques are generally less accurate, but also less general in that they do not include all of the effects necessary to model all of the problems seen in vehicles. On the other hand, detailed FEAs can take many days to model, execute and pre and post-process, and therefore are impractical to use for design trade studies, and for the thousands of load cases of a final design.

	Bonded Joint Analysis by Hart-Smith	Bonded Joint Analysis by HyperSizer
Solver	1-D closed-form solution using beam theory	A closed-form solution based on Mortensen's unified approach and modification.
Joint types	Conventional joints: Single-, double-lap, scarfed, stepped - joints.	Conventional joints: Single-, double-lap, scarfed, stepped – joints (adherend can be straight or scarfed (ply-drop-off)).
Loads and effects	$N_x, Q_x, M_{xx}$ .	$N_x, Q_x, M_{xx}, N_{xy}, Q_y, M_{yy}$ and $M_{xy}$ are reaction forces). Also can enter strains and curvatures and in any combination with the forces and moments.
	1. Temperature change 2. adherend imbalance 3. defects in <i>bond layer</i> , such as porosity, thickness variation are considered, etc.	1. Temperature change 2. Moisture in laminates 3. Electromagnetic effects
Adherends	Linear elastic homogeneous isotropic beam (not composite), no transverse deformation is accommodated.	Linear elastic classical laminates (could be unsymmetric and unbalanced), no transverse deformation is yet accommodated but will be in a future release.
	Output: 1. Longitudinal normal stress and strain, as well as displacement ( $u, w$ ). 2. Interlaminar stresses are not available	Output: 1. In-plane stresses, strains, and displacement ( $u, v, w$ ). 2. out-of-plane (Interlaminar) stresses are available.
Adhesive	1. Shear spring only. 2. Elasto-plastic material.	1. 2D isotropic linear elastic spring. 2. High order theory (to be developed) 3. nonlinear material 4. Spew fillet effect (to be developed)
	Output: Shear (longitudinal only) stress for most of joint types. A simplified method proposed for solving peel stress does not consider the effect of adhesive shear stress.	Output: Shear (longitudinal & transverse) and peel stresses, which are constants through the thickness by using the spring model, but may vary if using high order theory (HOT).
Convergence of solution	Have stability/convergence problems with stepped_lap joints.	Convergence is more robust. Can manually choose number of segments and points per segment (More automation later)

Fig. 7.18, Comparison of HyperSizer Bonded Joint analysis with Hart-Smith joint analysis methods

The bonded joint capability in HyperSizer falls into the category of rapid analysis techniques. However, in contrast to methods such as Hart-Smith, HyperSizer's analysis methods are much more general in boundary conditions and analysis capabilities. Some of the key differences that distinguish HyperSizer's capability are the ability to analyze unsymmetric and unbalanced

laminates under multi-axial loads. This is especially crucial since nearly all composite joints by definition of bonding two different laminates together are unsymmetric in nature. Fig. 7.18 highlights the differences between HyperSizer and Hart-Smith. HyperSizer in general can analyze most stiffened panel configurations and can readily be extended to other joint types.

Other similar analyses are also available such as Mortensen [8], Smeltzer [9], ESAComp®. These methods have strengths and weaknesses compared with HyperSizer, however, the tight integration of the bonded joint analysis with HyperSizer structural analysis and automation with vehicle-level global FEA makes its bonded joint analysis ideal for reducing manual I/O, and as a consequence reducing human error. Also, the 19 built-in failure methods have been validated against some tests [7]. We have also integrated the joint analysis with probabilistic methods to determine the reliability of structure. As a result, the bonded joint analysis is correlated to available test data. Even if the stress fields are computed with perceived high fidelity such as with a detailed FEA, failure prediction is still not an exact science and the accuracy of the stress/failure prediction in HyperSizer are comparable to those obtained with detailed FEA, but are much more efficient.

### 7.3.5 Physically based composite laminate strength failure theories

This section describes the approach of physically based composite strength failure theories and their practical implementation into HyperSizer for rapid high fidelity analysis.

**Much more information is provided in Volume 2, Section 7. Validation test data cases are contained in Volume 3.**

There exists much research and publications on computational/numerical methods for prediction of stress fields. However, there is substantially less published research on failure prediction. Traditional failure criteria include max strain, max stress, Tsai-Hill, Tsai-Wu, Hoffman, Tsai-Hahn, and Hashin. More recent failure criteria include Puck (performed best on recent World Wide Failure Exercises [3 and 11]) and LARC03 [12] a follow up to Puck. The Puck failure criterion requires special material parameters difficult to attain. In response, to this, the LARC03 failure criterion is similar, but uses more easily obtainable *insitu* material parameters. Another failure criterion of recent popularity is Strain Invariant Failure Theory (SIFT) which requires coupling with a micromechanics method to predict fiber/matrix constituent stress fields. These failure criteria are useful for general laminates but for locations of high stress gradients such as bonded joints, bolt loaded holes, and free edges, other failure criteria that include 3D stress fields as presented in the previous section are appropriate.

Detailed description of three new theories implemented in HyperSizer are in Vol. 2, Section 7:

- Hashin fiber and matrix failure criteria (Section 7.5.3 and 7.8)
- LaRC03 fiber and matrix failure criteria. This is an actively developed criteria from NASA Langley's Carlos Davila (Section 7.5.6 and 7.7)
- Strain Invariant Failure Theory (SIFT) on the micromechanics level using the Generalized Method of Cells (GMC), not FEA. This is an actively developed criteria from Boeing's Jon Gosse. (Section 7.5.7 and 7.9)

We also researched the Puck failure theory and decided not to implement it in HyperSizer because it was not deemed robust nor acceptable by industry. LaRC03 appears to perform comparable to Puck, and requires less specialized parameter correlation. In fact, data types identified by MIL-HDBK- 17 is all that is needed.

Substantial amount of relevant correlation data is provided in Volume 3, Sections 3 & 4. Section 3 contains failure envelopes generated by HyperSizer for failure theories: Max Strain, Max Stress, Tsai-Hill, Tsai-Wu, Tsai-Hahn, Hoffman, Hashin Matrix Cracking, Hashin Fiber Failure, LaRC03 Matrix Cracking, and LaRC03 Fiber Failure. Overlaid on the HyperSizer predicted failure envelopes are test data from WWFE and other published data. Next to the HyperSizer failure envelopes are the published failure envelopes produced by the invited research contributors of the WWFE. This layout provides a convenient visualization comparison. Section 4 provides the CFs and histograms for each failure theory to all of the 130 test data. Important issues related to Material & Processing (M&P) and in-situ strengths are addressed.

#### 7.3.5.1 Background

Practicality, an appropriate engineering cost of applying a theory successfully, is the key to acceptance of any failure theory. Acceptable costs vary with the criticality of a part and the volume of the end product. The cost of applying failure criteria are from the following:

- the programming tool automation
- the verification and validation of the delivered method/tool
- deployment and training cost of the tool

These costs are substantial, especially for more advanced theories that are physically based and challenging to correctly implement and verify. HyperSizer, as a result of this SBIR, provides one means of reducing the implementation cost of deploying many different failure criteria by

- automating their use in a verified tool
- validating all of them with significant test data
- providing a way for the end user to correlate to in-house tests the effects of their specific processing of the material (M&P)
- reducing Information Systems (IS) deployment effort and reducing the amount of engineering end-user training time

### 7.3.5.2 V&V of Failure Criteria

All failure criteria must be backed up with statistically relevant test data before use on a production vehicle. Proper verification and validation for a failure criteria must be given to the industrial end user before its use. To address this need, we have collected 130 test data and have correlated this data to almost all of the currently used failure criteria. Failure theories can be classified as either being physically based (ie. able to distinguish between type of failure: matrix versus fiber) and those that do not distinguish but can still handle general loadings via interaction terms. It will be shown that even though current research and future improvement is likely with the physically based criteria, such as NASA Langley's LaRC03; to date, without specific M&P correlation, the Tsia-Hahn interaction criteria, from our data, is most reliable and accurate. Fig. 7.19 compares tests to failure theory predictions for a specific M&P.

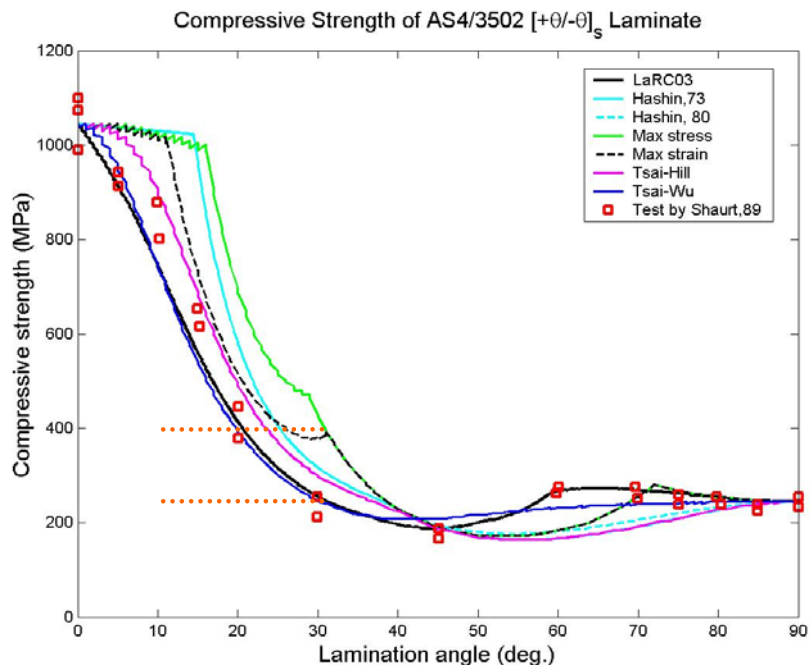


Fig. 7.19, Compressive strength of  $[+/-\theta]_s$  AS4/3502 predicted by different failure theories. For the 0, 90, and 45 angles, the criteria pass through the test data since these angles are test data given anchor points. At different angles the predictions vary. As an example of error, the orange horizontal lines indicate the large difference in test and prediction at  $30^\circ$  for max strain. In this plot LaRC03 matches best. Tsai-Hahn is not included.

HyperSizer implements sophisticated theories such as the promising LaRC03 and the micromechanics based Boeing Strain Invariant Failure Theory (SIFT), but at the same time, is

striking a proper balance between these firmer physical based approaches and the simpler ones that effectively capture behavior on the macroscopic level. The best new research along with traditional methods is investigated to find the right balance of theory and practicality.

### 7.3.5.3 The Physics of Failure

Failure occurs physically at the fiber/matrix constituent level. The fiber, matrix, or the interface that bonds the fiber to the matrix fails. For polymer matrix composites (PMC), failure is brittle even with a ductile matrix material because the material system as a whole is limited by fiber strain. Pure tension fiber failure is straightforward to characterize. Compression fiber failure is likely not limited by the strength of the fiber, but rather by the fiber/matrix interaction during fiber buckling or during kink banding. As such, the fiber waviness and misalignment during processing (M&P) is an important effect and gives rise to the notion of “apparent compression strength.” Less stiff fibers such as fiberglass may actually fail in pure compression strength. Some of the included test data from the World Wide Failure Exercises (WWFE) include both graphite and glass fibers. The failure envelope for a particular glass fiber, Fig. 7.20, depicts six unique physical failures identified by the LaRC03 theory, two of which are for fiber compression. Since observed nonlinear in-plane shear behavior may be due to fiber rotation instead of matrix material nonlinearity, constituent level (micromechanics) based failure prediction may be considered brittle for PMC, though not for Metal Matrix Composites.

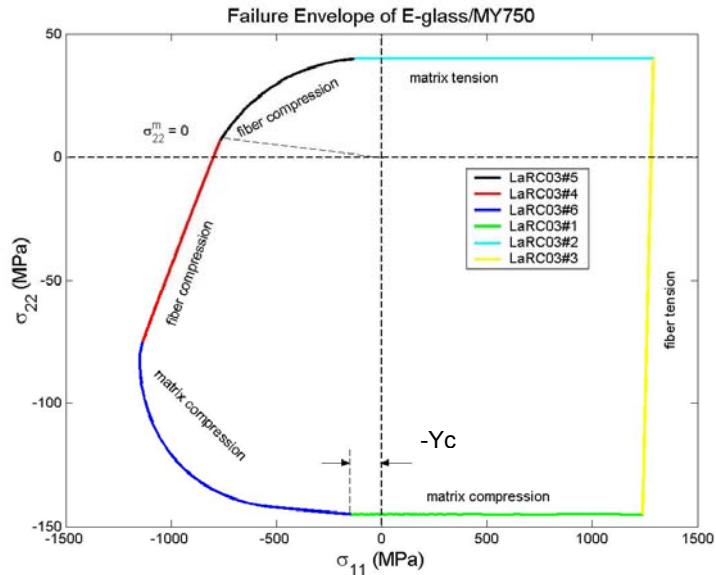


Fig. 7.20, LaRC03 failure criteria distinguishes between six different possible physical failures, and so, unlike interaction criteria such as Tsai-Wu or Tsai-Hahn, is deemed more promising in the long term, especially for progressive failure.

### 7.3.5.4 Uncertainty at the Ply Level

However, even if a failure theory is physically based and able to discern the actual constituent failure, the practical focus is to identify the form and process dependent properties on the macroscopic (ply) level, which by definition includes many of the built-in uncertainties and variability that exist in a laminate. This is particularly true when moisture and temperature play a significant role in the stress/strain when failure occurs. Presented in Vol 2, is a method for including specific M&P effects into all failure criteria correlations, including physically based theories that may not natively capture such macroscopic uncertainties.

Volume 3, Section 3 illustrates significant variation in observed test data. Even the most straightforward strength properties are difficult to measure accurately due to panel processing, specimen machining, test techniques, and intra versus inter lab variability. Combined stress

states are nearly impossible to characterize in a repeatable manner for general use with any failure criteria. Clearly, the need is to view composite strength not in a deterministic fashion, but rather in a probabilistic manner that is founded on establishing these variabilities to derive the required confidence in design.

The traditional manner to include variability in composite materials is to statistically characterize each individual property on the ply level as being either an “A” or “B” Basis design-to value. This design criteria approach is discussed in detail in Volume 2.

#### **7.3.5.5 Failure criteria provided on the micro fiber/matrix constituent level**

A small effort was directed to performing composite strength predictions at the micromechanics level. HyperSizer already had a robust micromechanics core analysis capability based on the Generalized Method of Cells. Several different homogeneous failure criteria were implemented (since constituents are homogeneous on the micro level).

- Max strain
- max stress
- Von Mises
- SIFT

#### **7.3.5.6 Progressive Failure provided on the micro fiber/matrix constituent level**

The above micromechanics based failure criteria were used for damage initiation failure prediction and for progressive failure. A limited number of laminates such unidirectional ply stacks and  $\pm\theta$  ply stacks completely fail when damage initiation begins. However most laminates exhibit post first ply failure strengths. Fig. 7.21 shows some early preliminary results of a prototype test capability as implemented in HyperSizer. Note how a micromechanics based progressive failure approach matches quite well to AS4/3501 test data, at least in the tension-tension loading quadrant.

#### **7.3.5.7 Durability and Damage Tolerance**

It is necessary to analyze composite material in a possible damaged state. There are three primary scenarios of damage: detectable, barely visible, and undetectable. Fracture mechanics energy approaches are used to determine the load at which the delamination crack will not grow. However, damage evolution as reported in reference [13], is not reliably predicted with analysis.

*...progressive damage and residual strength models to accurately predict the fracture of notched laminates, and in fact, most analytical models do not have a complete representation of all failure modes, complex damage states, and combined stress states. For composites, current design and analysis methods are semi-empirical and rely on the building-block approach for design and certification. This approach coupled with analytical modeling can be used to design damage tolerant composite structure.*

In addition, [14] maintains that an issue hindering more reliance on analysis methods is the limited or inappropriate failure criteria for the multitude of damage mechanisms in composites, and the inability to identify dominant damage mode.

### 7.3.6 Modularity in analytical modeling

Implementation of failure prediction is modular and independent from stress field modeling. This allows interchange of stress/strain prediction methods with failure prediction criteria.

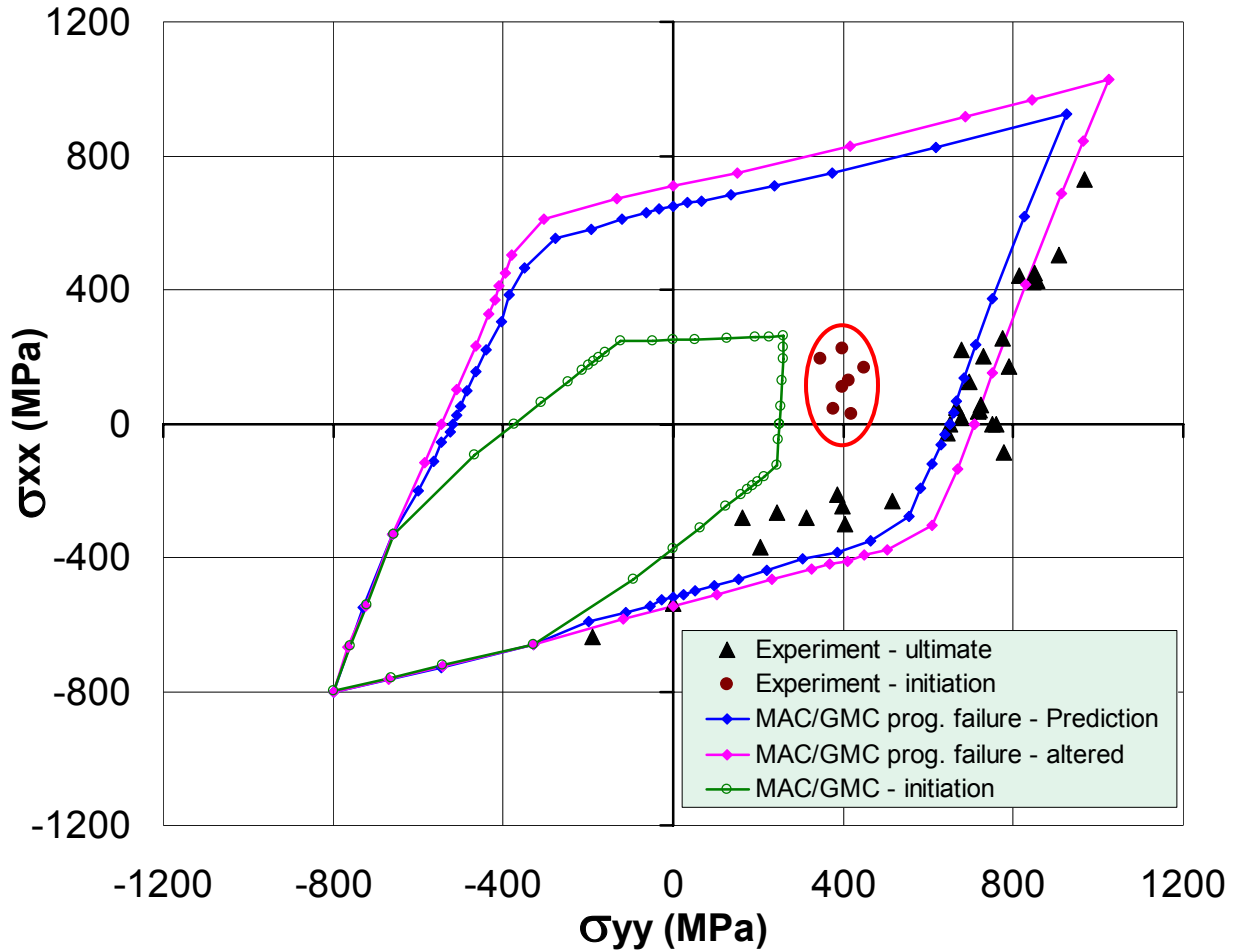


Fig. 7.21, Composite laminate AS4/3501 test failure data. Note how the laminates are capable of carrying additional load after the onset of first ply failure (damage initiation). A prototype micromechanics based progressive failure capability as implemented in HyperSizer matches quite well to AS4/3501 test data, at least in the tension-tension loading quadrant. Considerable more research is required in this area to bring this capability production ready.

## **8 2<sup>nd</sup> SBIR Thrust: Integrated tools and processes**

This 2<sup>nd</sup> SBIR thrust is focused on providing communication of codes in a tightly integrated process. Achieving this will reduce human errors and allow higher fidelity methods in early design phases. The main purpose is to link together legacy codes for special purpose analyses which have proven to be indispensable. These codes have a wealth of verification and validation (V&V) to support their use based on correlation to test data. However, as delineated in Section 6.1, three deficiencies are identified in their current aerospace industry manual use. To overcome these deficiencies in analysis approach, the HyperSizer® commercial structural analysis and sizing optimization software was selected for implementing the SBIR developments. Currently, HyperSizer is used by many companies and government agencies in the aerospace community for product development (PD). The choice to use HyperSizer for this SBIR is because it addresses all eight of the structural integrity inconsistencies identified in Section 5.

### **8.1 *HyperSizer as it Existed***

As a short introduction, HyperSizer is able to perform rapid structural analysis and design sizing that includes many failure analyses for all load conditions for all areas of an airframe. The underlying software architecture is an integrated relational database management system that stores data, prevents accidental data deletion, and handles all I/O automatically between all analysis codes. HyperSizer also automatically couples to FEMs and resulting FEA computed element loads, thus greatly reducing the possibility of human data input errors.

HyperSizer contributes in several ways to the certification by analysis initiative. HyperSizer capabilities are moving beyond the conceptual and preliminary design phases, to mature its usability for final design. Many analyses required for airframe certification are included in its controlled software environment, which in itself is a framework for plugging-in user defined validated analysis codes. It is able to input and maintain analysis building block test data and to use this test data to perform reliability based analysis and design sizing. As an automated sizing tool that achieves consistent structural integrity, it is able to produce robust designs using Probability Density Functions (PDF) signatures as defined with correlation factors described in following sections.

This 2<sup>nd</sup> SBIR thrust was deemed doable within the scope of effort of Phase II due to the extensive existing capabilities of HyperSizer in the technology area of integrated tools and processes. Therefore, before describing newly developed capability, pre-existing relevant capability is described.

#### **8.1.1 A framework for performing hundreds of traditional analyses**

HyperSizer performs hundreds of traditional analyses and assigns margins to each potential failure mode. The next section, 8.1.2, highlights some of the traditional closed form and modern numerical failure analyses delivered with HyperSizer. These analyses are available to all HyperSizer users, and are the best publicly available methods for each unique failure mode. However, HyperSizer in a broader sense is a framework for also incorporating analyses that are developed by others. In this sense, customer legacy and proprietary codes can be tightly integrated or “plugged-in”, as described in section 8.1.3.

### 8.1.2 Traditional closed form and modern numerical failure analyses delivered with HyperSizer

HyperSizer provides many different types of strength and stability analyses, such as beam and panel buckling, cross section local buckling and crippling, local post-buckling, frequency, deformation, stiffness, and material strength based on detailed stresses and strains throughout a built-up shape on a ply-by-ply basis. Some of HyperSizer analysis methods are physics based, and others come from time honored and accepted standard engineering practices and empirical data. HyperSizer's purpose is to automate all of these approved methods for reliable and consistent use by the stress engineer. In short, each unique analysis method incorporated into HyperSizer goes through a check-out process where we 1) validate the method's physics, 2) verify the method's software implementation, 3) calibrate the methods accuracy, and 4) assure the method's correct engineering use with an intuitive GUI and training and technical documentation.

Fig. 8.1 illustrates the "Failure" tab of the primary analysis software form. In this example, a honeycomb panel is being analyzed. The right half of the figure shows two columns. The left most column is a listing of the limit margins-of-safety (MS) and the right column is a listing of the ultimate margins. Next to the margins is a label defining the failure analysis. The failure modes listed at top are generic in that they apply to all panel types, such as buckling. The failure modes listed below are specific to honeycomb sandwich panels such as: facesheet wrinkling and intercell dimpling; and core shear strength, crushing, and crimping. These analyses are best performed using semi-empirical equations developed from test correlations. The user can easily select which analyses to perform by clicking each box on or off. When off, the numerical margin is not computed nor returned back to the "failure" tab interface.

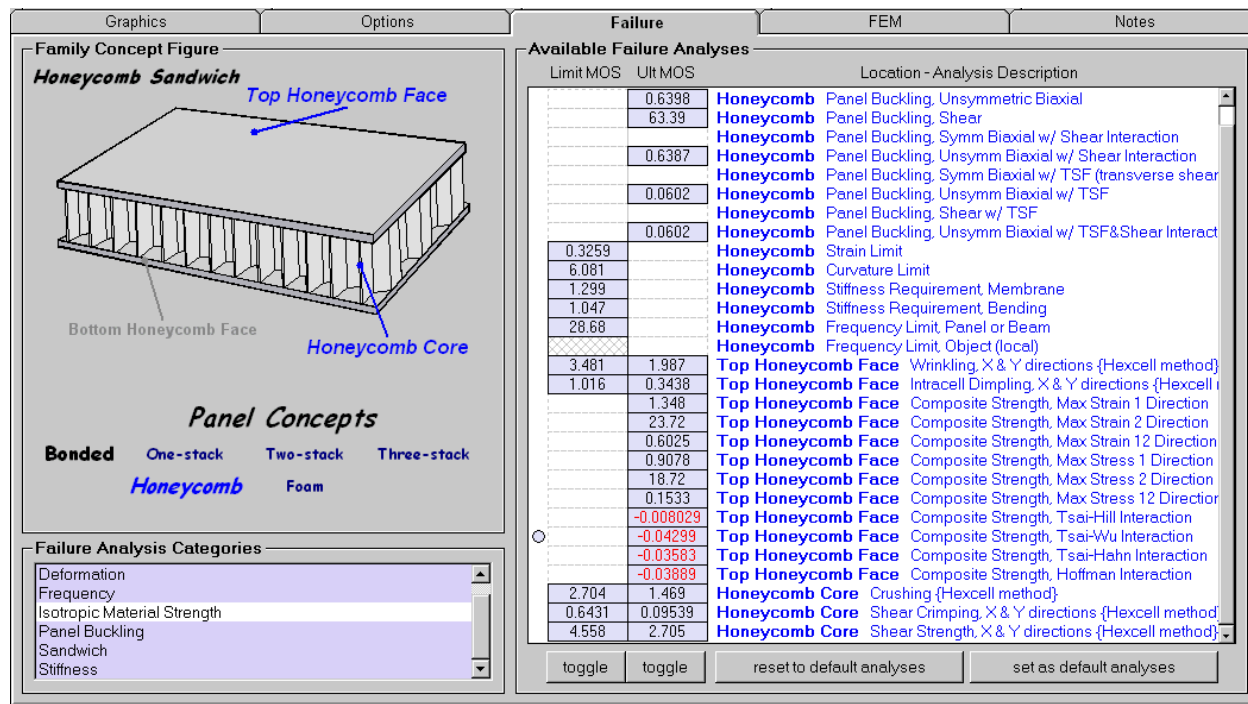


Fig. 8.1, The HyperSizer "failure" tab listing of margins-of-safety (MS) for a honeycomb sandwich panel. Each failure mode analysis is summarized with a MS for limit and ultimate loads.

### 8.1.3 Plug-ins of customer proprietary and/or legacy specialty analysis codes

Each aerospace company usually has analysis methods and associated programs to solve problems in their own unique way. For this reason, there is a capability for the users of these companies to integrate their proprietary and legacy codes into HyperSizer.

HyperSizer provides an engineering environment where user developed or company proprietary analyses codes can be “plugged-in.” This Input/Output integration provides more reliability by reducing possible human error for legacy analysis programs that typically require tedious manual data input. The programs can be written in either Fortran, C, or C++ languages. Legacy codes are invaluable for providing certification-by-analysis because of their validation and verification (V&V) history. Therefore the purpose is to connect in an automated fashion the legacy codes into the data flow stream of other tools and processes, Fig. 8.2.

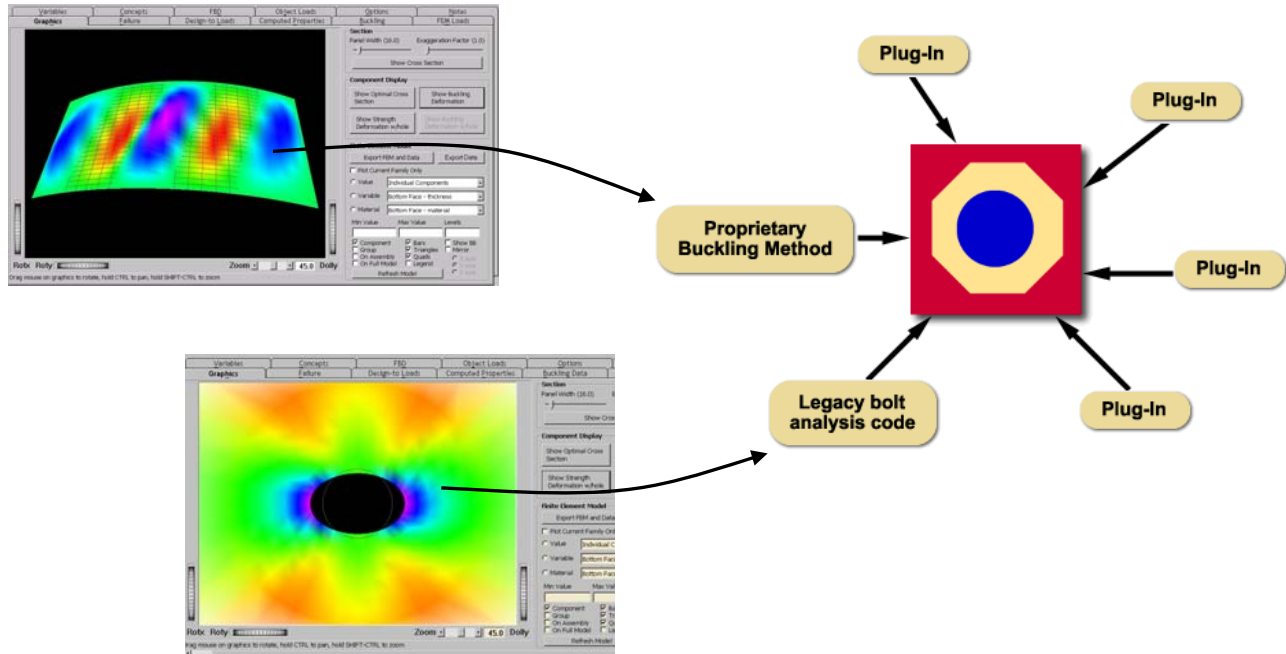


Fig. 8.2, In the illustration, two legacy programs are plugged into the HyperSizer structural analysis and sizing optimization software. The first program is a much used Raleigh Ritz analysis for buckling. The second program is the BJSFM composite unloaded and bolt loaded hole laminate analysis. All of the data associated to these types of programs, including the HyperSizer generated graphical images shown, are completely integrated within the structural analysis and sizing optimization process. This level of tool I/O automation greatly reduces potential human error.

### 8.1.4 HyperSizer Sizing Optimization Based on Positive Margins for all Failure Modes

Making available analysis tools in an automated sizing process to be used during conceptual and preliminary design phases provides a design-by-analysis capability for increased structural reliability. HyperSizer can concurrently optimize panel and beam concepts, material selection, cross sectional dimensions, and layups. In doing so, it can handle complete vehicle systems modeled with many FEM grids and elements and ensure that optimum designs pass all available structural integrity analyses. Its results include accurate weight predictions and multiple equivalent weight designs for manufacturing trades. Fig. 8.3 shows that the design-by-analysis capability is able to find the best combination of all:

- **Panel/beam concepts-** optimum concept found from a library of commonly used designs: Z shape, mechanically fastened panel versus blade shaped, integrally machined stiffened panel
- **Design dimensions and thicknesses-** facesheet, flange, and web sheet thicknesses and widths, heights, stiffener spacings
- **Material selection-** All isotropic metallic, orthotropic composite, foams, and honeycomb cores are available as candidates
- **Layups-** Thousands of pre-defined or user-defined layups are available as candidates for any panel or beam segment

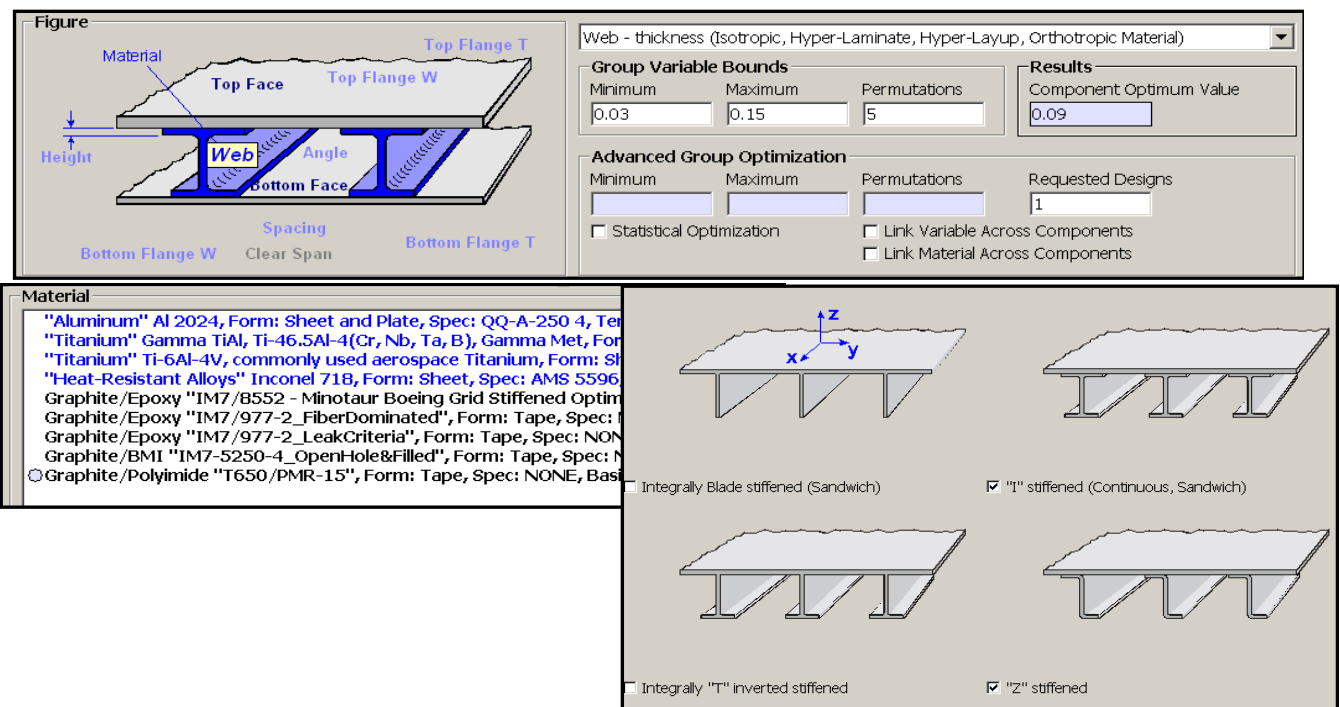


Fig. 8.3, Illustrated is the process of directly sizing the design by permutation of all continuous and discrete variables. This is accomplished by specifying each variable's minimum and maximum bounds, and its number of permutations. Then for variables that have material associated to them, such as the stiffener web, many different composite and metallic materials can be assigned to the variable. In this illustration, HyperSizer determined that the optimum thickness for the web = 0.09" and the optimum material is Gr/Pi as indicated with the blue circle. Different types of concepts can be explored concurrently such as I, T, blade, and Z stiffened shapes. For this optimization, the "I" and "Z" are selected on.

Available Failure Analyses		
Limit MOS	Ult MOS	Location - Analysis Description
	13.82	Honeycomb Panel Buckling, Shear
		Honeycomb Panel Buckling, Symm Biaxial w/ Shear Interaction
	1.383	Honeycomb Panel Buckling, Unsymm Biaxial w/ Shear Interaction
		Honeycomb Panel Buckling, Symm Biaxial w/ TSF (transverse shear
	1.361	Honeycomb Panel Buckling, Unsymm Biaxial w/ TSF
	1000	Honeycomb Panel Buckling, Shear w/ TSF
	1.361	Honeycomb Panel Buckling, Unsymm Biaxial w/ TSF&Shear Interact
		Honeycomb Stiffness Requirement, Membrane
		Honeycomb Stiffness Requirement, Bending
66.2	66.2	Top Honeycomb Face Wrinkling, X & Y directions {Hexcell method}
29.23	29.23	Top Honeycomb Face Intracell Dimpling, X & Y directions {Hexcell method}
	52.48	Top Honeycomb Face Composite Strength, Max Strain 1 Direction
	561.8	Top Honeycomb Face Composite Strength, Max Strain 2 Direction
	1.809	Top Honeycomb Face Composite Strength, Max Strain 12 Direction
	42.16	Top Honeycomb Face Composite Strength, Max Stress 1 Direction
	404.8	Top Honeycomb Face Composite Strength, Max Stress 2 Direction
	1.022	Top Honeycomb Face Composite Strength, Max Stress 12 Direction
	1.02	Top Honeycomb Face Composite Strength, Tsai-Hill Interaction
	1.009	Top Honeycomb Face Composite Strength, Tsai-Wu Interaction
	1.009	Top Honeycomb Face Composite Strength, Tsai-Hahn Interaction
	1.009	Top Honeycomb Face Composite Strength, Hoffman Interaction
1000	1000	Honeycomb Core Crushing {Hexcell method}
1000	1000	Honeycomb Core Shear Crimping, X & Y directions {Hexcell method}
82.37	82.37	Honeycomb Core Shear Strength, X & Y directions {Hexcell method}
66.23	66.23	Bottom Honeycomb Face Wrinkling, X & Y directions {Hexcell method}
29.24	29.24	Bottom Honeycomb Face Intracell Dimpling, X & Y directions {Hexcell method}
	51.06	Bottom Honeycomb Face Composite Strength, Max Strain 1 Direction
	546.9	Bottom Honeycomb Face Composite Strength, Max Strain 2 Direction
	155.9	Bottom Honeycomb Face Composite Strength, Max Strain 12 Direction

Any or all analyses can be selected as optimization criteria

Optimization Requirements		
	Required Value	Computed Value
<b>Symmetric Terms</b>		
A11		5783200
A22		5783200
A33		1969000
D11		15441.62
D22		15441.62
D33		5257.394
<b>Minimum Natural Frequency</b>		
Panel	11	11.0842
Local		0
<b>Deformation</b>		
Strain X		0
Strain Y		0
Curvature X		-2.157177E-03
Curvature Y		-7.57413E-04
Center Deflection	1	0.9984004

Additional optimization criteria includes modal frequency, stiffness, deformation and midspan deflection limits

Fig. 8.4, The structural optimization is based on achieving positive margins for every user selected failure mode turned on. In addition to strength structural integrity, the user can also select requirements for stiffness, frequency, and deformation.

The designer/analyst is not required to derive failure criteria as would be required for formal optimization packages such as those integrated with FEA such as MSC/NASTRAN Solution 200. For any combination of failure analyses turned on by the user, Fig. 8.4, HyperSizer will find the lowest weight panel/beam design from all variable and material combinations that produce positive margins-of-safety. In addition to strength structural integrity, the user can also select additional requirements. For this example, the requirement that the center deflection has to be equal to or less than **1.0** and that the natural frequency has to be greater than **11.0** has been set. As seen in the right column, the optimization produced a design with a frequency of **11.08** and a deflection of **0.998**.

### 8.1.5 Generating Well Defined Equivalent Stiffness Terms for FEM Update

Once the sizing optimization has determined optimum panel and beam concepts, dimensions, thicknesses, materials, and layups; then the next step is to generate FEM property data for update. HyperSizer's uniqueness is a capability to create very accurate thermoelastic stiffness terms that represent any 3D cross sectional panel shape with a 2D planar FEM mesh. This Global/Local/Detail approach is described in Section 7.2. As depicted in Fig. 8.5, this allows a coarsely meshed planar model for the entire airframe. HyperSizer sends back to the FEM for each shell element the full compliment of a panel's membrane  $[A]_{3 \times 3}$ , bending  $[D]_{3 \times 3}$ , and membrane-bending coupling  $[B]_{3 \times 3}$ , stiffness matrices as well as their corresponding thermal coefficients  $\{A^\alpha\}_{3 \times 1}$ ,  $\{D^\alpha\}_{3 \times 1}$ ,  $\{B^\alpha\}_{3 \times 1}$ . For beams, in addition to all of the stiffness terms, the neutral offsets are updated in the FEM.

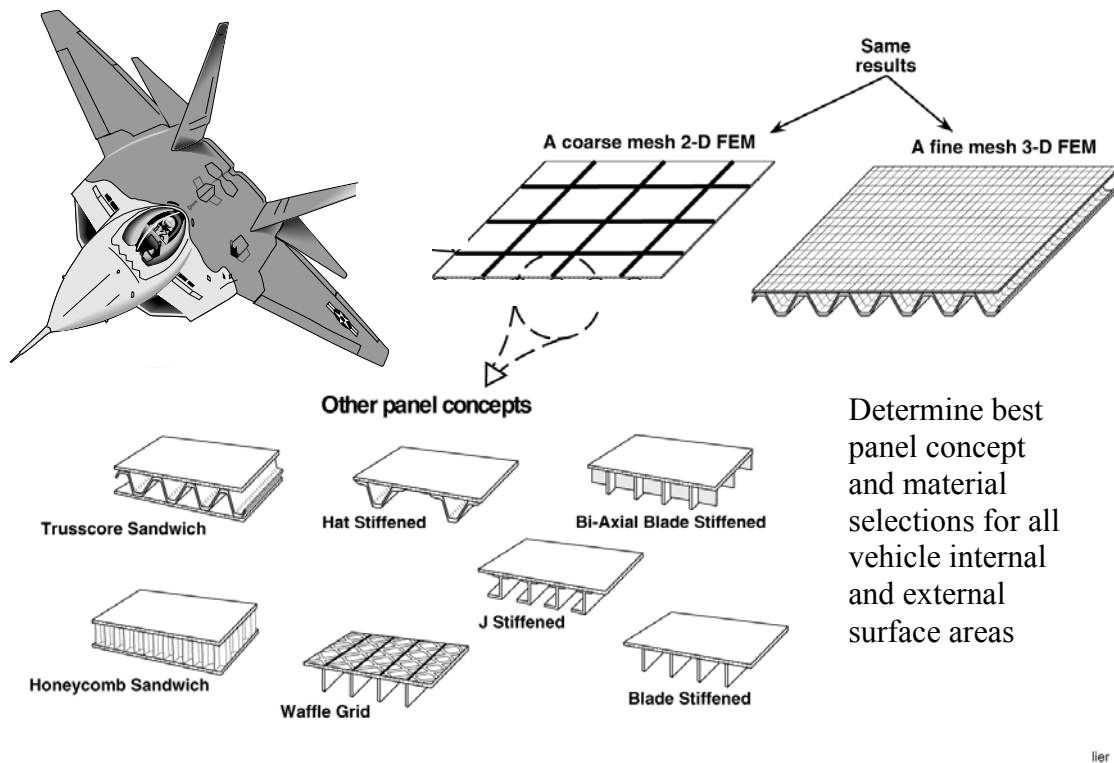


Fig. 8.5, HyperSizer's approach is to generate FEM properties for shell finite elements using a planar, 2-D coarse mesh that permits the FEA solver to compute internal loads as accurately as accomplished with finely meshed 3-D discrete models. This allows the design-by-analysis process to determine the best panel design for all vehicle locations, using the same loads model mesh.

### 8.1.6 Automatic coupling to FEA such as MSC/NASTRAN, for Internal Loads

HyperSizer has two major links in the process of automatic coupling to FEA. The first link as previously described in section 8.1.5 is the updating of the FEM stiffness properties with the current optimized panel and beam designs. The second link, is the reading of the FEA computed **internal** loads (load paths) of the airframe. The second link is represented in Fig. 8.6 as the top arrow going from model data to design data. The first link is represented as the bottom arrow going from the design data to model data. This looping process is continued until convergence is reached.

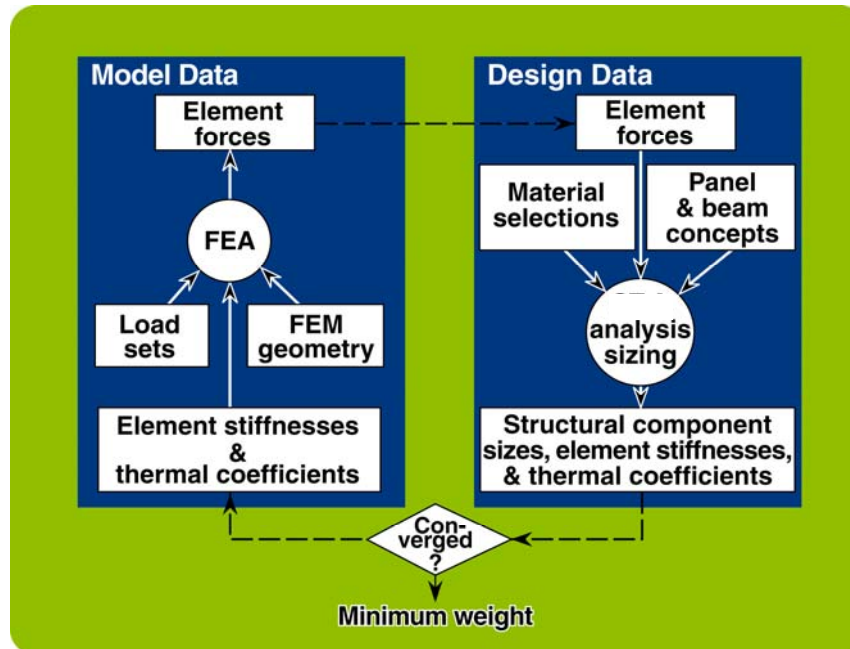


Fig. 8.6, HyperSizer coupling with FEA. The box marked, “Model Data” represents FEA, and the box marked, “Design Data” represents HyperSizer. HyperSizer design data includes temperature dependent material data, a library of panel and beam concepts, and numerous failure mode checks that neither the FEM nor CAD systems contain.

The FEA is used to resolve indeterminate load paths for complex structure and loadings. These load paths are referred to as internal loads or element forces, and are input into the HyperSizer design environment. In order for the FEA to compute these internal loads, the externally applied loads such as pressures and forces are defined on the FEM.

HyperSizer post-processes the computed internal FEA element forces by applying statistical analyses to each individual loading component ( $N_x$ ,  $N_y$ ,  $N_{xy}$ ,  $M_x$ ,  $M_y$ ,  $M_{xy}$ ,  $Q_x$ , and  $Q_y$ ) and to each individual load case. This process has been included to overcome the inconsistency used by industry stress analysts in determining the proper design-to loads. **Section 9.1.1 covers this topic in detail.**

The emphasis in this section is on the value HyperSizer provides in resolving two major challenges in automatic FEA coupling. The first challenge is mastering the mathematics of each individual FEA package supported. That is, the data that HyperSizer generates has to be

manipulated to coincide with the equations and variables of the FEA formulations. Of particular difficulty to resolve are differences in sign conventions, especially for beam orientation vectors and offsets. Other differences that must be accounted are available outputs. For instance, with NASTRAN, element forces are available, but for IDEAS FEA, grid forces must be used.

The second challenge is more related to a computer science level of effort in understanding all of the nuances of each specific electronic FEM and FEA output format. In the case of NASTRAN, it is the bulk data file; for I-DEAS it is their universal file, and for FEMAP; it is their neutral file format. Each of these FEA packages require separate HyperSizer formatting and esoteric file generation techniques.

### 8.1.7 Object model for integration into larger software design/analysis systems

HyperSizer can be included into a larger design process through a built-in object model. Using Microsoft COM and ActiveX technology, HyperSizer's functionality can be called from other processes, such as Excel spreadsheets or Mathcad symbolic equations. COM stands for Component Object Model and is the technology which all native Windows applications, including the operating system itself, are based. ActiveX, formerly known as OLE (or Object Linking and Embedding), enables one process or object to use functions or properties from another process or object. For example, ActiveX enables spreadsheets developed using MS Excel to be embedded into MS Word documents.

Much of the functionality available in the HyperSizer GUI is exposed to outside processes through a HyperSizer ActiveX Automation Server. This means that a client, built using any COM aware application or programming language (such as Visual Basic, Java, Microsoft Excel, MathCAD, etc.) can instantiate objects from the HyperSizer Server and ask these objects to perform functions. For example, a Java applet could be built which would open a HyperSizer database (using a HyperSizer Application object), retrieve a list of

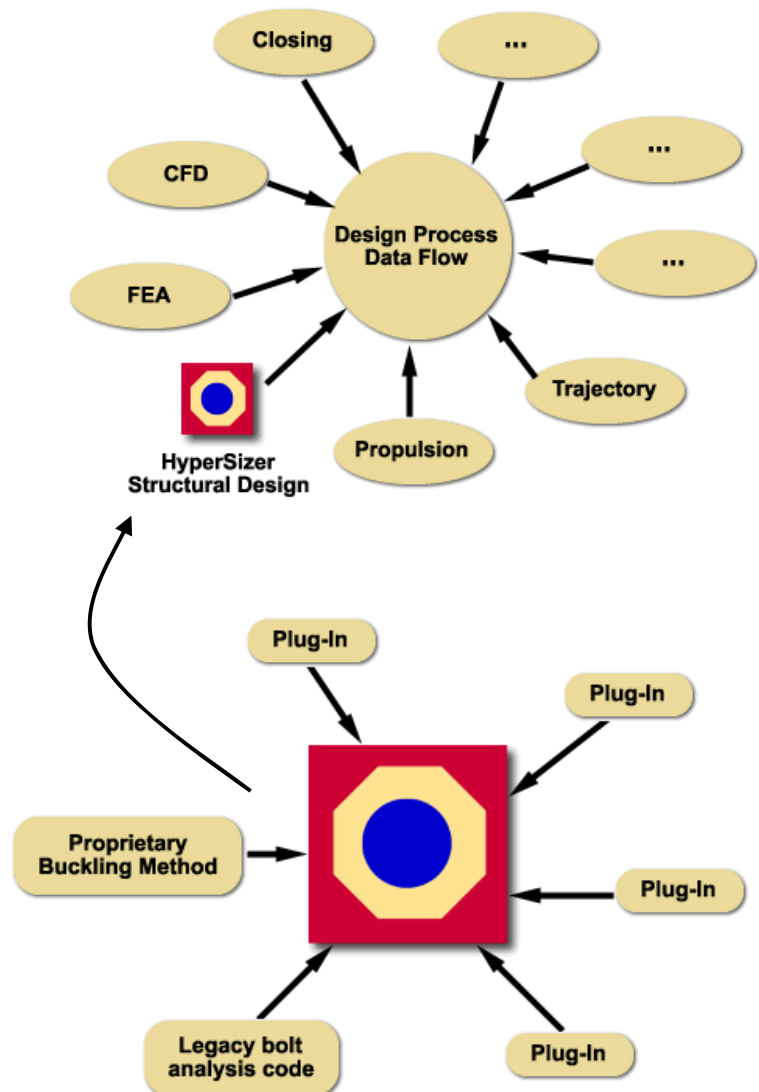
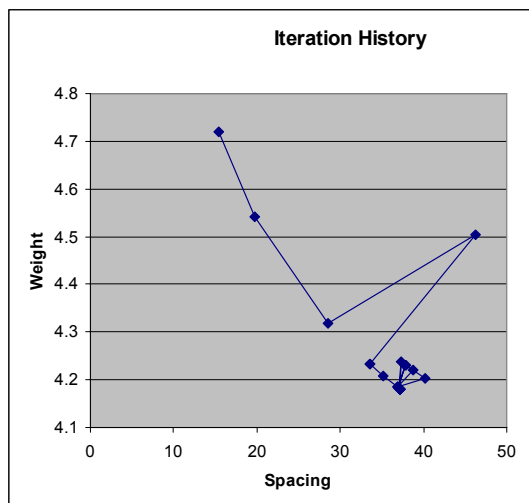


Fig. 8.7, The HyperSizer structural analysis and sizing framework which includes delivered analysis along with plug-ins can then be made part of a larger design system by use of its open and flexible object model. This level of tool I/O automation greatly reduces potential human error.

HyperSizer projects, and then export the materials used by a particular project. Another potential function would be to automatically size a structural component using a Component object.

The HyperSizer server is intended to provide batch functions that can be executed repetitively without user intervention. As an example, the iteration history plot, Fig. 8.8, is from a Microsoft Excel spreadsheet where the Excel non-linear solver was used to optimize the fuselage ringframe spacing of a space launch vehicle. The Excel solver called HyperSizer's panel and beam sizing routines approximately 40 times to determine the optimum spacing. This was all accomplished without ever opening the standalone HyperSizer GUI. (See the HyperSizer Programmer's Manual for more detailed discussions on the Object Model.)



*Fig. 8.8, HyperSizer coupling with a Microsoft Excel spreadsheet by use of HyperSizer's COM based object model. The spreadsheet non-linear solver was coupled with HyperSizer to drive and determine the lowest total weight as a function of ringframe spacing of the panel and beam optimizations performed by HyperSizer.*

## 8.2 SBIR Innovations

Existing HyperSizer capabilities provide code communication in a tightly integrated process for reducing human errors and providing higher fidelity methods in early design phases. Described in this section are new SBIR innovations that address the 2<sup>nd</sup> SBIR Thrust: Integrated tools and processes in three different ways. The first way is by providing a highly integrated system for storing and visualizing test data along with design and analysis data. Two capabilities were developed in this regard:

- Test data entry into database for all panel, material, and analysis types
- Interactive graphics of test data histogram and correlation factors

The second way is by providing a highly integrated system for storing and retrieving detailed technical documentation on implemented analytical methods, and verification and validation examples. Two capabilities were developed in this regard:

- HyperFinder technical document search
- Thousands of pages of new analytical methods documents

The third way is by providing more integration with other engineering software directly, and by more universal web based approaches. Two capabilities were developed in this regard:

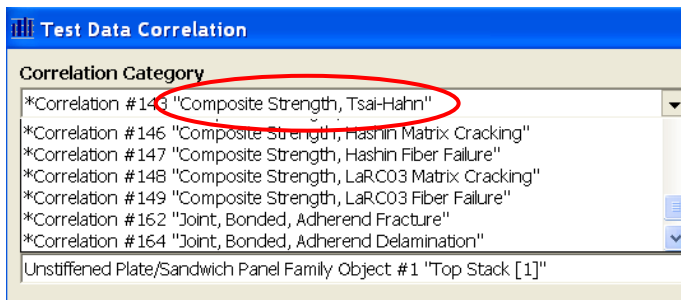
- HyperFEA automated HyperSizer to FEA analysis looping
- HyperWeb Services using HyperSizer object model for execution and data transfer using web based protocols

### 8.2.1 Test data entry into database for all panel, material, and analysis types

A highly integrated system was developed for storing and visualizing test data directly along with corresponding design and analysis data. Test data is very conveniently entered into the database for all panel, material, and analysis types. HyperSizer future production versions will be shipped to customers that include the publicly available test data collected and entered for composite laminate strength, panel buckling, bonded joint strength, and honeycomb sandwich wrinkling. Additionally, users will be able to enter their own test data for over 30 different failure analyses. All test data is preserved and carried forward in future releases of the HyperSizer software.

The next few figures step through the process of entering test data. The summarized steps are:

- 1<sup>st</sup>; select **Correlation Category***
- 2<sup>nd</sup>; select the **Project(s) or Workspace(s)***
- 3<sup>rd</sup>; select the **Group(s) and Component(s)***
- 4<sup>th</sup>; select the **Failure Analysis Mode***
- 5<sup>th</sup>; select the **Analysis Correlation Category** (and enter the data)*
- 6<sup>th</sup>; view the **interactive test data histogram graphics***



*From the Tools/Test Data  
Correlation drop down menu,*

*Fig. 8.9, The 1<sup>st</sup> step is to select the **Correlation Category**. For this example we are choosing the "Composite Strength, Tsai-Hahn" failure criteria.*

**Correlation Test Data - Composite Strength, Tsai-Hahn**

For Project / Workspace:  
 \*Validation - Composite Strength - not progressive - WWFE, 66 tests (Workspace)

Use Test Data from the Following Assemblies:

Assembly #1 "BDJ_mortensen"
*Assembly #2 "AS4/3501-6 [0/-45/+45/90]s laminate, Table 9"
*Assembly #3 "Case 7, AS4/3501-6 Damage initiation matrix cracking components"
*Assembly #4 "All groups/cases except case 7 AS4/3501 laminates"
*Assembly #5 "All Unidirectional Laminate for CF Histogram"

Select All  
Clear All

Use Test Data from the Following Groups:

Group #2 "Mortensen's example, GR/EP+GR/EP, subjected to Ny=100"
*Group #8 "Case 1, E-glass/LY556/HT907/DY063, unidirectional, graph page 1740, Table 1"
*Group #9 "Case 2, T300/BSL914C, unidirectional, graph page 1740, Table 2"
*Group #10 "Case 3, E-glass/MY750 unidirectional, graph page 1741, Table 3"
*Group #11 "Case 4, E-glass/LY556/HT907/DY063 [-30/+30/90]s, graph pp.1742, Table 4, (PF)"
*Group #12 "Case 5, E-glass/LY556/HT907/DY063 [-30/+30/90]s, graph pp. 1743, Table 5, (PF)"
*Group #13 "Case 6, E-glass/MY750 [+55/-55]s laminate, Table 6a,b, (PF)"
*Group #14 "Case 7, AS4/3501-6, [0/-45/+45/90]s laminate, Table 9, (PF)"

Select All  
Clear All

Use Test Data from the Following Components:

Component #1 "AS4/3501-6, [0,45,-45,90]s"
Component #2 "T300/BSL914C, unidirectional"
Component #3 "Component 3"
Component #4 "Component 4"
Component #5 "Component 5"
Component #6 "Component 6"
Component #7 "Component 7"
Component #8 "Component 8"
Component #9 "Component 9"
*Component #10 "Nx=1280"

Select All  
Clear All

\*Note: Item has associated test data values

OK Apply Cancel

Fig. 8.10, The 2<sup>nd</sup> step is to select the **Project(s) or Workspace(s)** where the problem setup and test data are entered. For this example we are choosing the workspace named “Validation – Composite Strength – not progressive – WWFE, 66 tests.” Also, a subset of project data is selected by choosing the assembly “All Unidirectional Laminate for CF Histogram”, which includes groups 8 – 14.

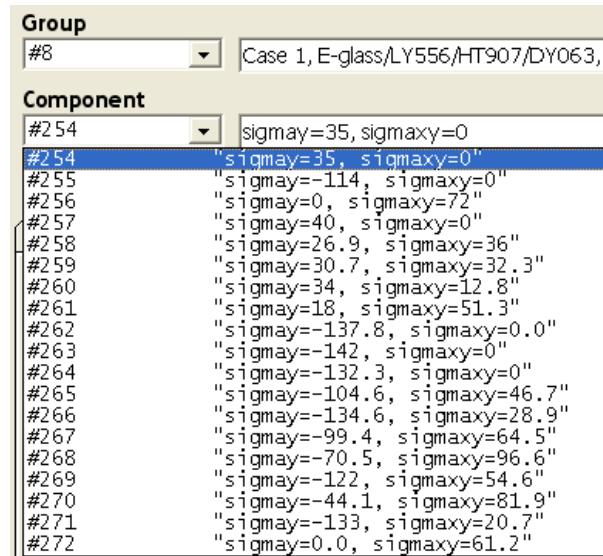


Fig. 8.11, From the selected workspace, the 3<sup>rd</sup> step is to select the **Group(s)** and **Component(s)**. For this example we are choosing Group 8 and the component named “sigmay=35, sigmaxy=0.” This name was chosen by us to indicate the loading.

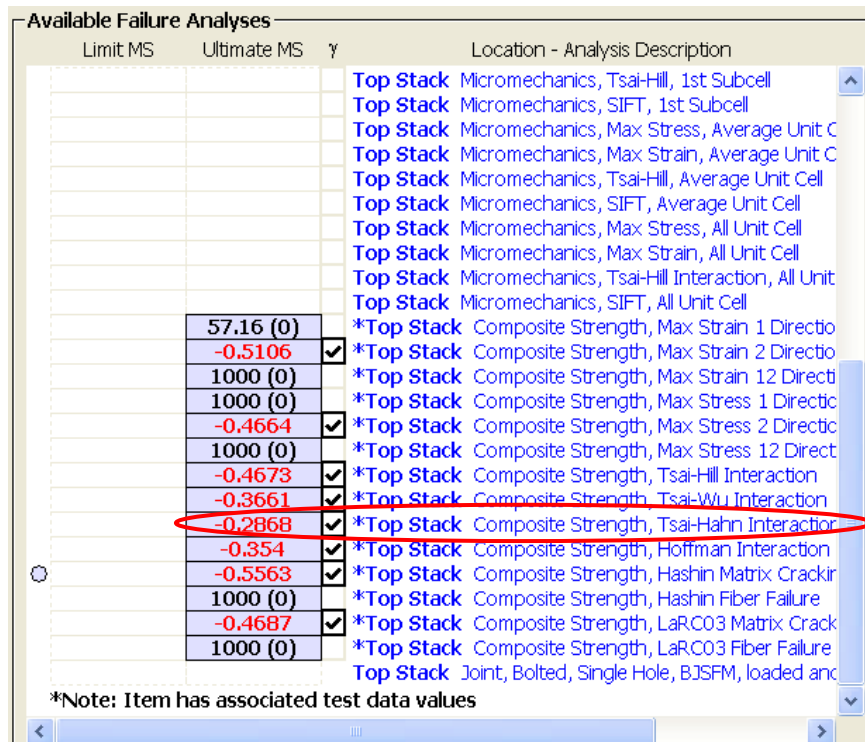


Fig. 8.12, From the **Failure Tab** of the selected workspace, the 4<sup>th</sup> step is to select the **Failure Analysis Mode**. For this example we are choosing the analysis “Composite Strength, Tsai-Hahn” failure criteria. The asterisks indicate the failure modes that have test data entered.

Project Test Data - Project Validation - Composite Strength - not progressiv...

Component (Unstiffened Plate/Sandwich Panel Family)  
 \*Component #254 "sigmay=35, sigmaxy=0"

Analysis  
 \*Analysis #143 "Composite Strength, Tsai-Hahn Interaction"

Concept / Object  
 \*Object #1 "Top Stack [1]"

Test Data Values

0	Add...
	Delete

\*Note: Item has associated test data values

OK Apply Cancel

Fig. 8.13, For this component, the 5<sup>th</sup> step is to select the **Analysis Correlation Category**. For this example we are choosing the analysis “Composite Strength, Tsai-Hahn Interaction.” The object #1, which is the top stack laminate is appropriate for all composite strength correlations. The **Test Data Value** of 0 is entered for the margin-of-safety, meaning the test failure load has been entered into HyperSizer.

## 8.2.2 Interactive graphics of test data histogram and correlation factors

The last step is to visualize the data in the form of a histogram, Fig. 8.14. At this point, one test data point has been entered. In order to make the last step visually meaningful, an example with 130 test data points using the same composite strength Tsai-Hahn failure criteria is illustrated. The user can select the number of bins to display. In this case 15 histogram bars (bins) are shown. The correlation factors and equation also shown on the form are described in Section 9.

The Tsai-Hahn failure theory matches the test data far better than any other failure theory. It is only 1.1% off as indicated by the  $P=T=1.013$  value on the histogram plot. For the same test data, the max strain failure criteria is 8.2% off and Tsai-Hill is 5.1% off.

[Refer to section 9.2.5.2 for more detail about the source of the test data.](#)

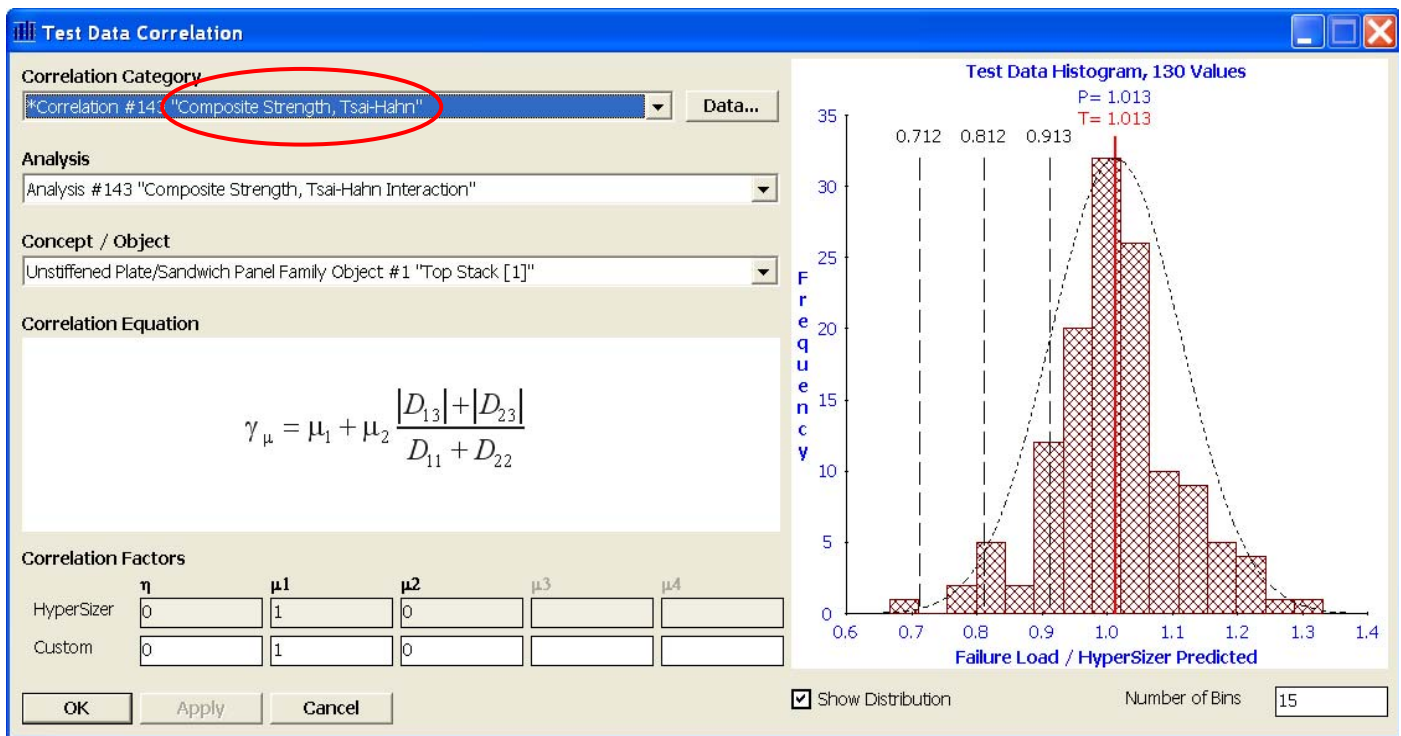


Fig. 8.14, The  $6^{th}$  and last step is to view the interactive test data histogram graphics. 130 test data were entered for the Tsai-Hahn composite strength failure criteria. Frequency on the left axis peaks about 32 for the center vertical bar, representing 32 failures occurred close to the test mean load. Just right, the next bar indicates that 25 tests failed at a load about 5% greater than the test average, etc. The shape made with the histogram bars appears to be a classical shaped bell curve of a normal distribution.

### 8.2.3 HyperFinder

Another new key feature developed for HyperSizer is called “HyperFinder”. HyperFinder represents an innovative new paradigm for creating, managing and locating files related to HyperSizer. HyperFinder does not replace the PDF based user documentation available from the HyperSizer Help menu, but it is intended to greatly enhance this capability by making it easy for users to find documentation on HyperSizer’s methods and equations, verification examples, test data, and other reference documentation.

There are two methods of accessing HyperFinder from within the HyperSizer GUI. First, it is accessed from the main HyperSizer Help Menu.

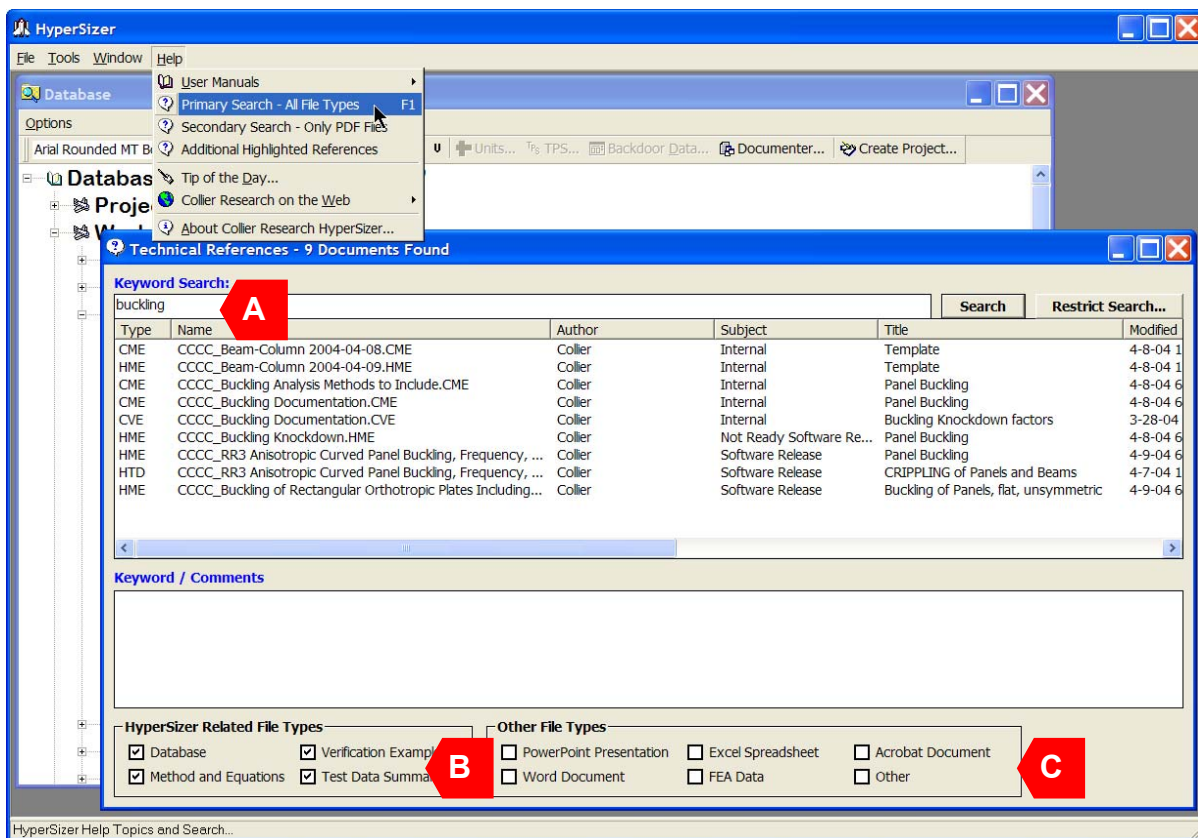


Fig. 8.15, HyperFinder accessed from the Help Menu

When HyperFinder is raised in this way, the “Keyword Search” field (A) will be blank, and by default, all document types will be searched. HyperFinder will search for common file types such as Microsoft PowerPoint, Word, Excel or Adobe PDF documents, but it will also search for documents that are specifically related to HyperSizer. HyperFinder allows the user to filter by document type. In the example shown in Fig. 8.15 (A), the keyword “Buckling” has been entered and the filter has been used to show all files with HyperSizer file types (B), but no other file types (C).

To make it easy to search for HyperSizer specific data, four new document types are provided and identified by file extension. These new file types are:

- .HDB – HyperSizer Database
- .HME – HyperSizer Methods and Equations
- .HVE – HyperSizer Verification Examples
- .HTD – HyperSizer Test Data

The second method for accessing HyperFinder is from the HyperSizer Failure tab. This is where the true power of HyperFinder begins to show. When experienced HyperSizer users click on individual failure methods from the Failure tab of the Sizing form, they will notice several new options for each failure method. Selecting any of the four options for “Methods and Equations...”, “Verification Examples...”, “Test Data Summary...” or “All Technical References...” will cause the HyperFinder form to appear.

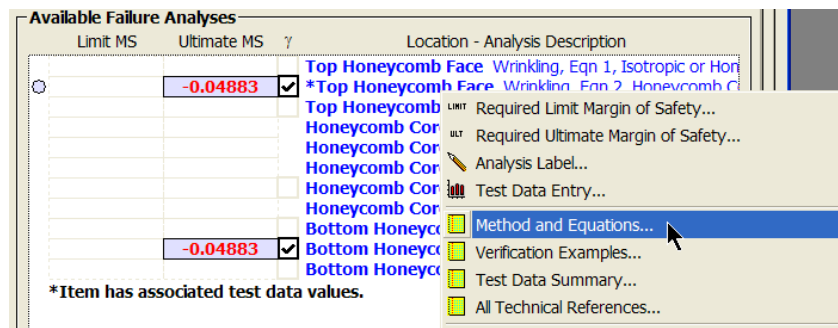


Fig. 8.16, Options available on the Failure Tab

The HyperFinder form will automatically filter documents based on document type. For example, as shown in Figs. 8.16 and 8.17, “Methods and Equations...” was selected for the Honeycomb Wrinkling failure method and the HyperFinder form appeared as shown in Fig. 8.17. By selecting the “Test Data Summary” checkbox (A), an HTD test data document was added to the filter, and appeared in the file list.

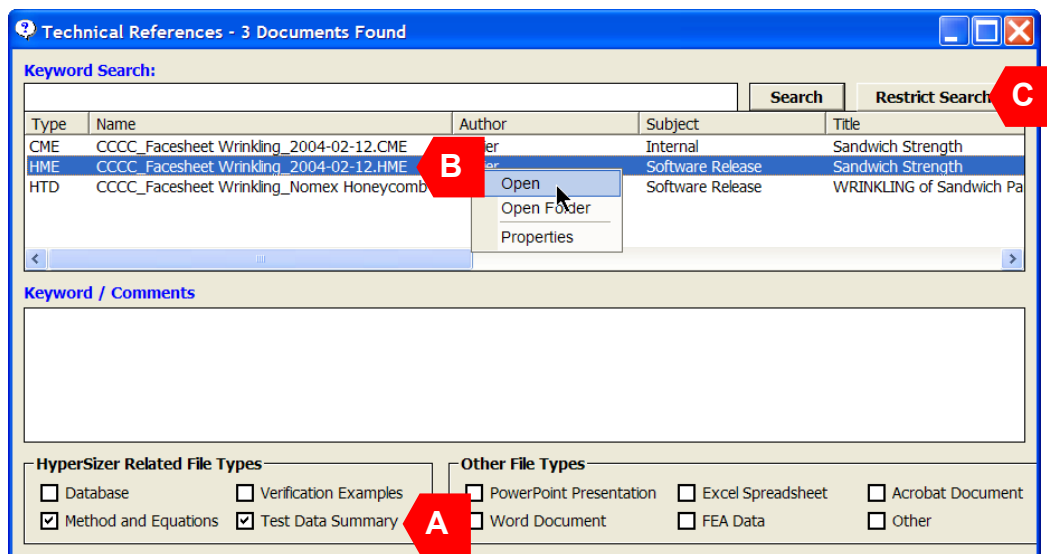


Fig. 8.17, HyperFinder Entries for Honeycomb Facesheet Wrinkling

Right clicking on one of the documents in the file list (B) will raise a pop-up menu that will allow the user to open the file, open the folder containing the file, or view the properties of the file.

Once in the HyperFinder form, the user changes the failure mode of interest by clicking the “Restrict Search...” button (C). This will cause another dialog to appear where any of the HyperSizer analysis methods can be selected. After dismissing this dialog, HyperFinder will display documents related to this newly selected document.

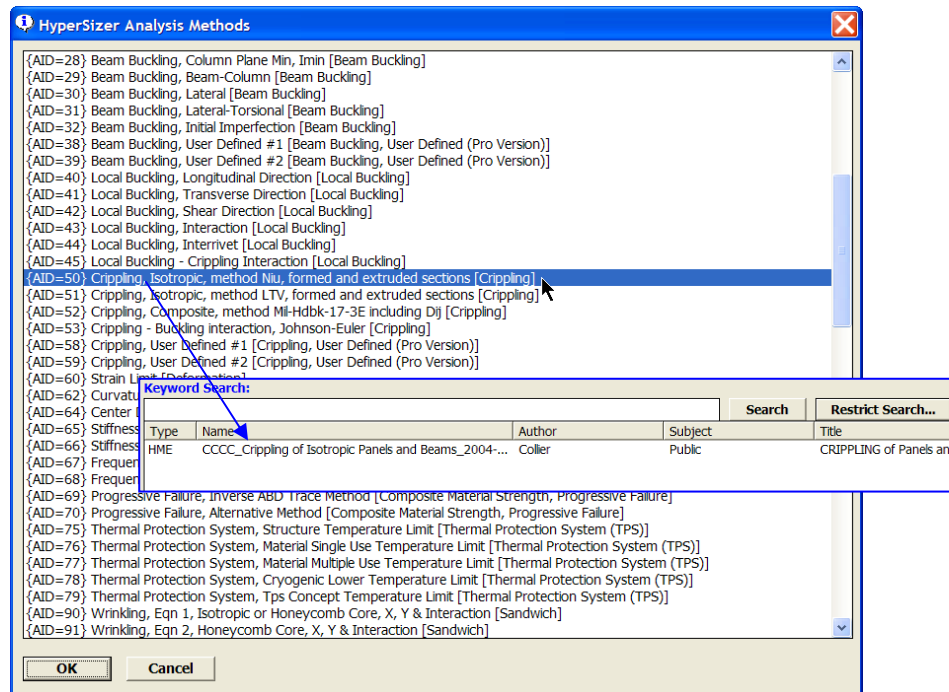


Fig. 8.18, Selecting HyperSizer Failure Methods for Display in HyperFinder

### 8.2.4 Thousands of pages of new analytical methods documents

The documents that are managed and displayed with HyperFinder are to be distributed with the HyperSizer installation onto a user's computer into a specific file folder structure. Alternatively, these documents could be installed to a central location that is accessible to multiple users over a network. While HyperFinder makes the job of finding HyperSizer methods related documentation very easy, a great deal of care went into the hierarchical directory structure design, which makes file folder navigation easy and intuitive. The layout of the tree structure is shown in Fig. 8.19.

The overall methods are broken down into those that deal with failure, loading, optimization, stiffness formulation, etc. Then under the category of Failure for example, each analysis method is broken down from general to specific categories.

For example, as shown in Fig. 8.19, there are two specific methods for sandwich facesheet wrinkling, these are analysis ID 90 and 91, the first of which is for either isotropic or honeycomb cores, and the second of which is specific to honeycomb cores. There is a folder for each of these specific failure methods (A). Documentation for facesheet wrinkling in general (i.e. not related to a specific method) would go in the "Wrinkling" folder (B). Documentation related to all sandwich failure methods would go in the "Sandwich" folder (C), and so on.

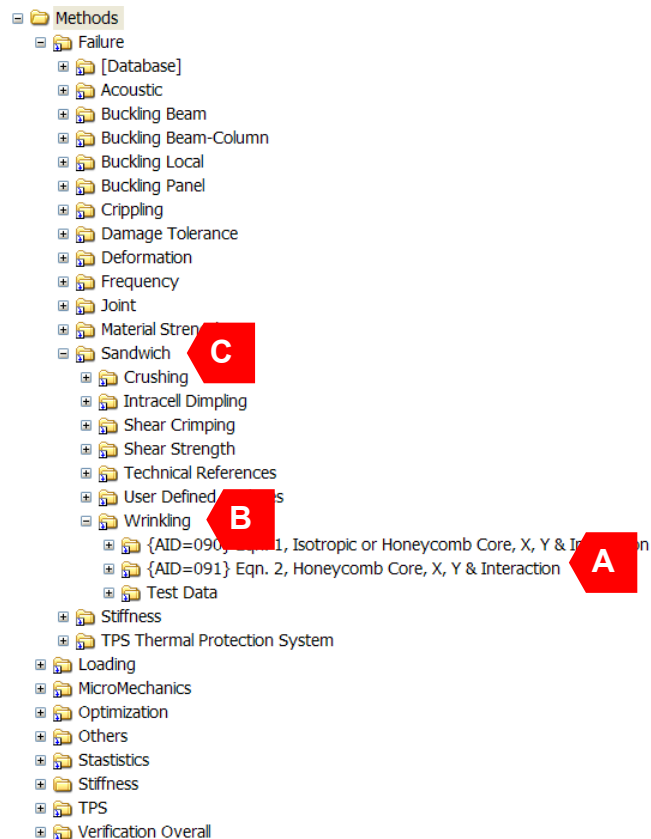


Fig. 8.19, Tree Structure of HyperSizer Methods Documentation

When HyperFinder searches for documentation for a particular failure method, it will begin in the specific folder for that particular method and if no documentation is found for that method in particular, it will continue up the tree from specific to general until a document is found that will be listed in the HyperFinder file list.

## 8.2.5 HyperFEA

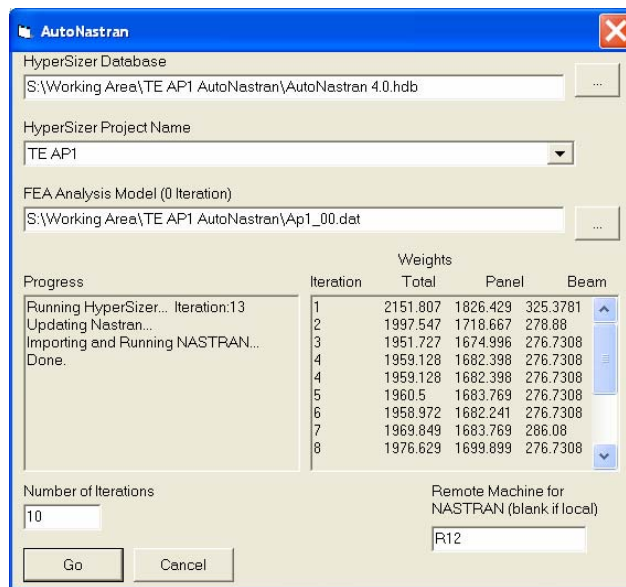
HyperFEA is an automated process to submit and iterate between HyperSizer and FEA solvers.

### 8.2.5.1 Introduction

A procedure has been developed using the COM/ActiveX object models built into HyperSizer and MSC.visualNastran (FEMAP) that automates iterations between HyperSizer, which determines structural masses and stiffnesses, and MSC/NASTRAN FEA, which determines internal loads. The code that implements this procedure is called “HyperFEA”.

### 8.2.5.2 AutoNastran Interface

HyperFEA is a standalone application that controls both the HyperSizer and FEMAP applications given the filenames and project names controlling the process.



**AutoNastran**

HyperSizer Database  
S:\Working Area\TE AP1 AutoNastran\AutoNastran 4.0.hdb

HyperSizer Project Name  
TE AP1

FEA Analysis Model (0 Iteration)  
S:\Working Area\TE AP1 AutoNastran\Ap1\_00.dat

Progress  
Running HyperSizer... Iteration:13  
Updating Nastran...  
Importing and Running NASTRAN...  
Done.

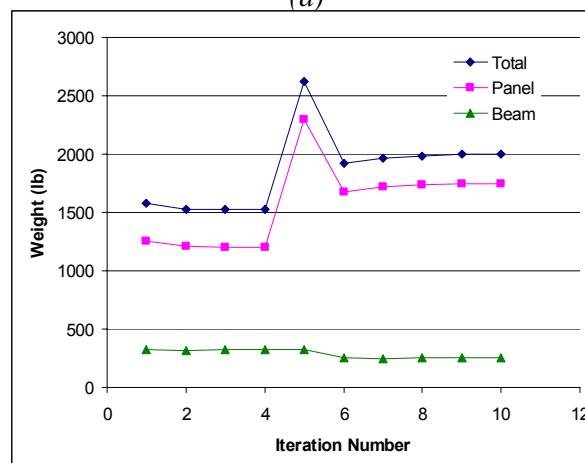
Iteration	Weights		
	Total	Panel	Beam
1	2151.807	1826.429	325.3781
2	1997.547	1718.667	278.88
3	1951.727	1674.996	276.7308
4	1959.128	1682.398	276.7308
4	1959.128	1682.398	276.7308
5	1960.5	1683.769	276.7308
6	1958.972	1682.241	276.7308
7	1969.849	1683.769	286.08
8	1976.629	1699.899	276.7308

Number of Iterations  
10

Remote Machine for NASTRAN (blank if local)  
R12

Go Cancel

(a)



(b)

Fig. 8.20, The HyperFEA interface (a) allows the user to enter a Hypersizer database name and project name as well as the FEM that is to be iterated. A sample HyperSizer-FEA convergence is shown graphically in (b).

[Refer to Volume 3, Section 19 for more detailed information.](#)

## 8.2.6 HyperWeb Services (object model ...)

### Meeting Notes and Design Document for HyperSizer Web Services

A meeting was held at AFRL in October 2003 with Phil Yarrington(CRC), Craig Collier(CRC), Duane Veley (AFRL), and Ray Kolonay (AFRL) to discuss the possibilities of developing a web-services based environment that could either call HyperSizer and/or allow HyperSizer to call other analysis codes. As a result of this Collier Research proposed and partially carried out an activity to investigate .NET and web services and how they can be used with HyperSizer to establish an enterprise-wide engineering environment. This environment should allow industry and government designers and analysts to easily access best-in-class software tools (both newly developed and legacy tools) regardless of geographic location or computer platform.

### Background and Purpose of Prototype

The commercially available structural analysis and sizing tool, HyperSizer, has a built-in object model that exposes much of its functionality through Windows COM / ActiveX. This allows HyperSizer processes to be automated, called as part of a batch process, and integrated into a larger design environment. For example, we have successfully integrated HyperSizer's detail optimization with a global vehicle optimization using the non-linear solver capability of Microsoft Excel. HyperSizer was also integrated into a multi-disciplinary design environment using ModelCenter from Phoenix Integration as part of NASA's HPCCP (High Performance Computing and Communications Program).

The capabilities of the HyperSizer Object Model are described in some detail in the white paper "Using the HyperSizer Object Model for Software Integration", which is downloadable from the HyperSizer.com website.

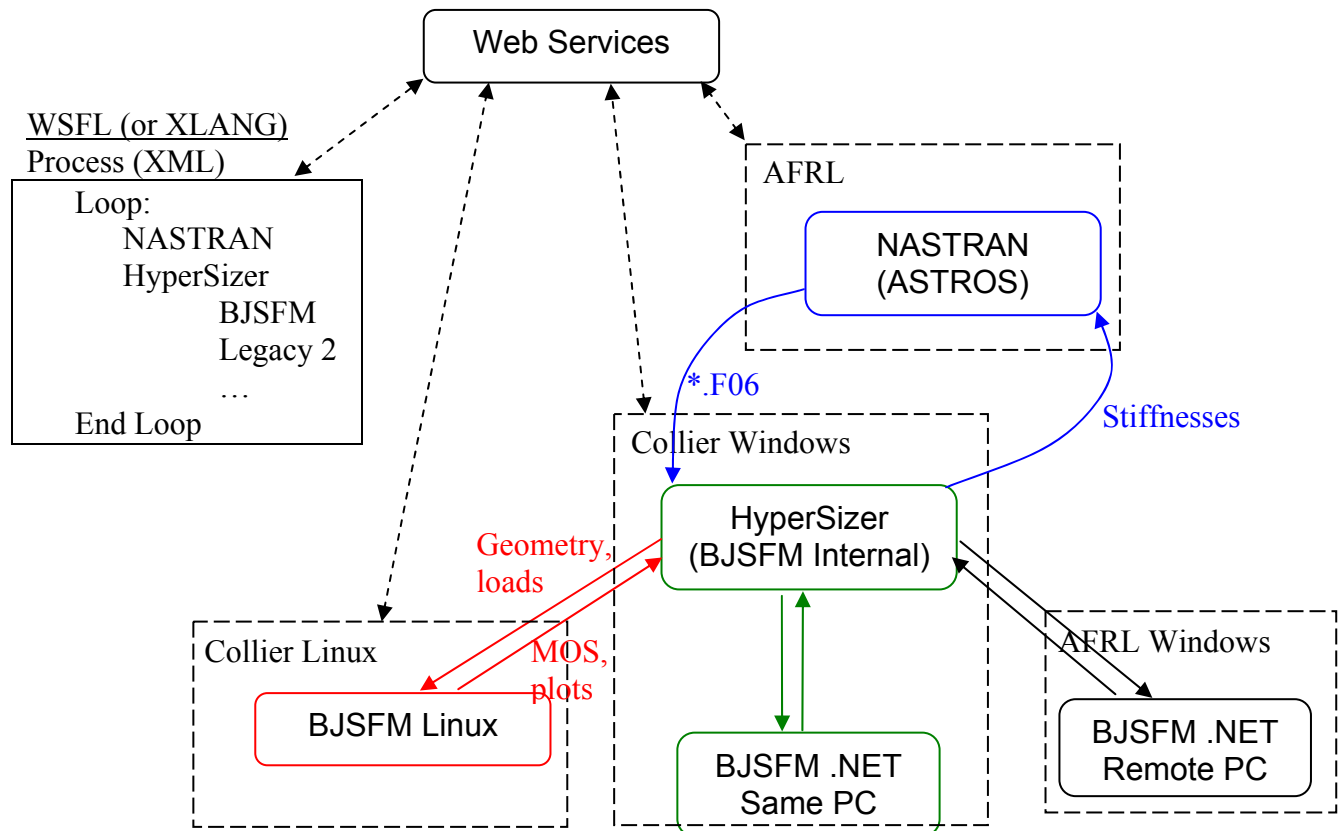
[http://hypersizer.com/pdf/wp01\\_using\\_the\\_hypersizer\\_object\\_model\\_for\\_software\\_integration.pdf](http://hypersizer.com/pdf/wp01_using_the_hypersizer_object_model_for_software_integration.pdf)

In the development of the proposed prototype, we will leverage HyperSizer's automation capability and demonstrate its usefulness to an Enterprise wide aerospace vehicle design environment in two capacities.

1. Establish HyperSizer as a WEB SERVICE that can be called from any platform and included as part of a Web Service Process.
2. Use HyperSizer's structural analysis specific database and infrastructure as a hub that exposes best-in-class structural legacy codes to an industry and government wide user base through web services.

## HyperSizer Specific Proposed Tasks and Data Flow

Our intention is to construct a prototype web-service process that has HyperSizer as a web service and HyperSizer able to call other web services. This entire procedure will be tied together using Web Service technology as shown in the diagram below.



The development of our prototype will follow a series of increasingly complex steps that are outlined in detail in the following section, HyperSizer Web Service.

In general terms the steps are:

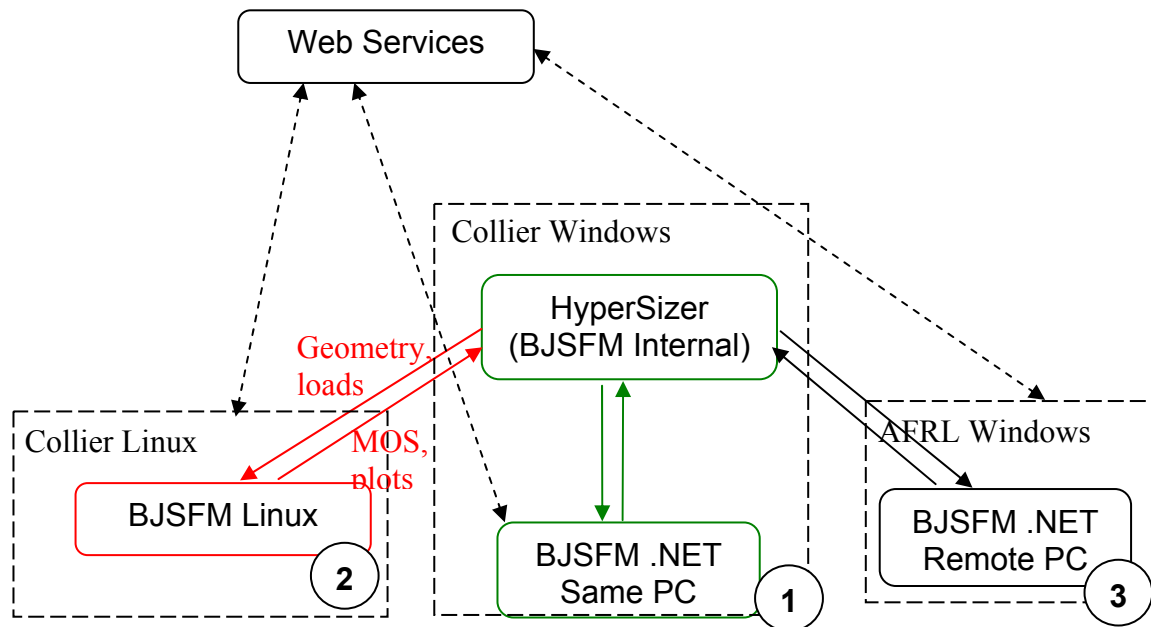
### Scenario Level 1: Demonstrate a web service using simple functions that can be called from a client

The purpose of this step is mainly to allow us to learn about the various technologies involved and how they are implemented on Windows or other platforms. We will be using very simple functions for the demonstration such as the traditional "Hello World" program. We will follow a progression from building the web service and calling from a web page to building a client program on a) the same computer b) the same platform (but different computer) and c) a different platform.

## Scenario Level 2: Demonstrate Peer-to-Peer, WSFL/Scripting file to control the process

Here we will still be using the simple “Hello World” functions but investigating how to publish, request, bind, etc. using the tools provided in the .NET environment, as well as learning about the different web service technologies such as WSDL (Web Services Description Language), WSFL (Web Services Flow Language), and UDDI (Universal Description, Discovery, and Integration).

## Scenario Level 3: BJSFM legacy bolt program web service



Using lessons learned in Levels 1 and 2 we will implement the legacy BJSFM code as a web service and begin the integration of that service into HyperSizer. This will also be done in a progression of steps starting with 1) building the BJSFM web service with the MS .NET fortran compiler and calling it from the same PC in the Collier office or from another local Windows PC in our office. 2) we will demonstrate the heterogeneous capability by installing BJSFM as a web service on a Linux workstation, but still in our office within our firewall. 3) Finally, we may try to implement this web service on a completely remote computer, possibly within AFRL to demonstrate its flexibility. In this step, HyperSizer itself is not yet a web service.

[Refer to Volume 3, Section 17 for more detailed information.](#)

## 9 3<sup>rd</sup> SBIR Thrust: Test Data Driven Reliability Analysis

The first four inconsistencies identified in Ch 5 are resolved with the innovation of this 3<sup>rd</sup> SBIR thrust. The shortcomings of the traditional zero margin-of-safety analyses are resolved by developing a method for *test data driven reliability analysis* as implemented in HyperSizer.

Test data driven reliability analysis is a process of defining reliably consistent allowable loads to be used with reliably consistent design-to loads using on-the-fly statistics. The computation of reliably consistent design-to loads was an existing capability of HyperSizer and is described in the following section 9.1. The bulk of this SBIR innovation addresses the manner in which to define reliably consistent allowable loads and is described in the following section 9.2.

The emphasis of our SBIR innovation is on the allowable load distribution, indicated as the curve on the right hand side of Fig. 9.1, which portrays how a structure of the same shape, size, and material will exhibit a range of allowable load capability. That is, seemingly identical test articles will not fail at a one given load, but instead fail within a range of loads due to natural data scatter/stochastic response. Before presenting the SBIR innovations, the essential existing capabilities in HyperSizer that address the required load, the left maroon circle of Fig. 9.1 are described.

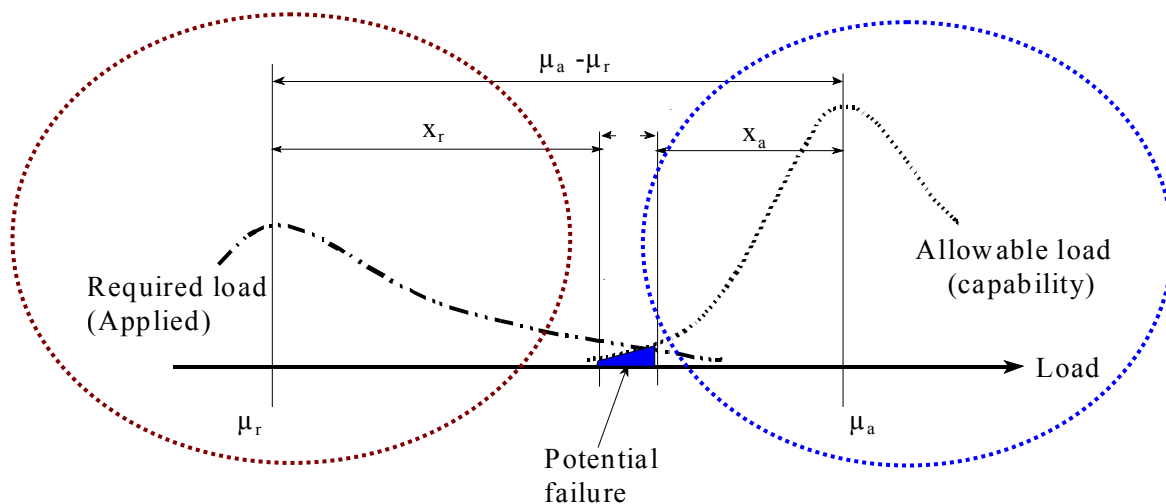


Fig. 9.1, A statistical approach is used for analyzing potential failure. An **allowable loading** is due to a combination of the material's strength and the nature of the structural design such as panel concept, shape, and size. **Required load** is the resulting FEA computed internal loads in the airframe structure. Reliability is defined as probability the allowable load is greater than the required load, or as 1.0 minus the probability of failure:  $R=1-PF$ . The blue circle is an SBIR development. The maroon circle is an existing HyperSizer capability.

## 9.1 HyperSizer as it Existed

Substantial preexisting HyperSizer capabilities were available for implementing a statistical approach for analyzing potential failure. Structural analysis is performed using two primary data: applied loadings and allowable loadings. The ultimate question being what is the appropriate ‘design-to’ loading for performing a deterministic structural component analysis.. Essentially the left side of Fig. 9.1 indicated with the maroon circle quantifies the required load to carry.

### 9.1.1 Statistically processed design-to FEA computed internal loads

A substantial challenge to automating structural analysis/sizing optimization is ‘pulling-loads.’ The problem arises when many finite elements are used to represent a structural component. This is especially true if the panel has varying load from midspan to edge, or from one edge to another edge. Designing to the maximum element load could be far too conservative and result in over weight. Some failures such as buckling are more dependent on integrated compressive load than an element peak load which may be located at the panel's corner. HyperSizer uses statistical methods to determine the appropriate design-to load.

$$\text{“Design-to” loading} = \mu + K\sigma$$

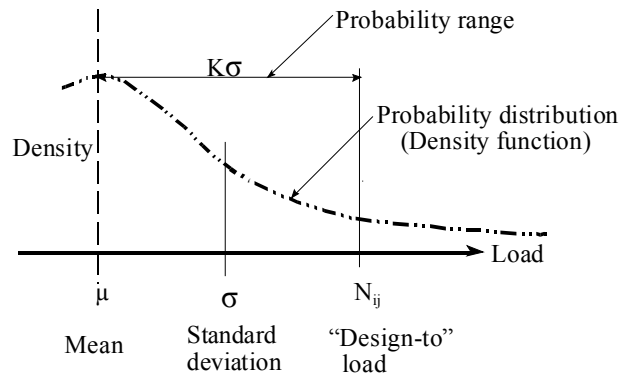


Fig. 9.2, The HyperSizer user can select the  $K$  standard deviation factor for determining the “Design-To” applied loading for strength analysis.

Structural analyses are typically performed using a component’s peak loading without much concern given to the actual load distribution. For components with uniform loadings, i.e. narrowly varying load distributions (in statistical terms a large Kurtosis), this approach is sufficient. However for components with widely varying load distributions, i.e. higher loading gradients, this approach becomes overly conservative. The statistical approach of HyperSizer treats the individual force components ( $N_x$ ,  $N_y$ ,  $N_{xy}$ ,  $M_x$ ,  $M_y$ ,  $M_{xy}$ ,  $Q_x$ ,  $Q_y$ ,) of each element of a structural component, in essence, as if they were a frequency distribution, or a probability histogram. In this sense, the height of the probability histogram represents force magnitude, and the base of the graph represents the number of occurrences of each loading magnitude.

Yet the true histogram of load/stress/strain gradients are continuous variables which are being predicted with discrete points of the FEM mesh. In essence, the FEM computed loads are a sample of the structure’s true loads, the grid and element mesh density being a measure of the sample population. It is this premise which led us to implement element area into the statistical

analysis. Instead of implementing statistical approaches based on the number of data points, i.e. number of elements, implementation is based on each element's area. In this case the probability histogram has the base of the graph represented, not by the number of finite elements, but by the % of area of the component that is experiencing each loading magnitude.

In this way, the *K factor* (referred to as K sigma, such as  $3\sigma$ ) identified in Fig. 9.2 is now used to achieve the desired *confidence limit* of the component's area which is experiencing a level of load. Conventionally used, K represents the level of a component's highest loading. This subtle difference in thought permits the useful analogy of quantifying how much area of a component will confidently withstand the component's loading. As a result, for a one-sided distribution, a K factor equal to 1, 2, or 3 indicates 85.1, 97.72, and 99.86 % of the component's area. The remaining small percentage of structural component area is best designed with a doubler or a small pad up of additional material.

The standard deviation K factor is used for strength analysis. However, for instability, a different statistical approach is used by HyperSizer. A key aspect of which is to statistically determine the percentage of the component's area that is in the compressive, buckling zone and integrate the compressive magnitude over that area. In-plane shear loading is considered as being compressive for shear buckling effects.

Other researchers have applied statistical approaches to stress analysis. Of particular note is the work of Verderaine [10] which is applicable to isotropic, unstiffened structure such as solid-rocket motor thrust mounts, casings, shrouds, main frames, supports, fittings, castings, etc. That approach combines multiaxial applied stresses into one value using the minimum strain energy distortion theory, referred to as Mises failure criterion. Therefore, multiaxial loadings are stated in terms of a single value to perform the statistical analyses. As a result of using a single stress value for the statistical procedures, the method is not applicable to instability failure modes nor stiffened panel structures. The implementation with HyperSizer is to use unit loadings such as  $N_x$ ,  $N_y$ ,  $N_{xy}$ , etc. separately in a statistical manner, so that composite materials, panel buckling, local buckling, crippling, etc. of airframe structure can also be handled.

### **9.1.2 Separate load factors for limit and ultimate**

HyperSizer allows the user to enter in separate factors for limit and ultimate loads. This includes proper use of yield material stress/strain allowables for limit loads, and ultimate material stress/strain allowables for ultimate loads.

## 9.2 SBIR Innovations

As introduced at the beginning of this section, the emphasis of our SBIR innovation is on the allowable load distribution, indicated as the curve on the right hand side of Fig. 9.1, which portrays how a structure of the same shape, size, and material will exhibit a range of allowable load capability. That is, seemingly identical test articles will not fail at a one given load, but instead fail within a range of loads due to natural data scatter/stochastic response. Fig. 9.3 illustrates this as a histogram of occurrences, with the highest frequency of failure centered on the mean value, and the range quantified as a statistical deviation,  $\sigma$ . The test scatter represented as a histogram, can also be statistically characterized as a probability density function (PDF). It seems conceivable to categorize the types of structures and loadings that will have responses fall within tight bands of results, and those that have a large amount of scatter in their behavior. These response PDF distributions can be categorized into what we call **PDF signatures**. By definition, PDF signatures are unique, repeatable, and, as demonstrated next, crucial for reliability based structural certification.

A PDF is also necessary to establish the SBIR principal innovation of **two correlation factors** based on experimental data collection:  $\gamma_{\mu}$  (abbreviated to  $\mu$ ) for analysis uncertainties, and  $\gamma_{\eta}$  (abbreviated to  $\eta$ ) for specific failure mode test data scatter repeatability. The approach is to base the calculation of probability of failure (or said in a positive way, reliability against failure) by use of the two newly defined, test data generated CF's. These CFs are generated from normalizing test data PDFs to specific failure analysis methods. In this way fidelity can be selected by the analyst for an airframe structural reliability analysis and sizing. More importantly, consistent structural integrity can be designed in during the preliminary phase of a project. Though this approach is based on probabilistic methods (PM), it is not the traditional and widely reported PM approach in use today. Industry movement toward implementing formal probabilistic methods has already begun, [15 and 16]. That approach is based on identifying PDFs for input variables (such as variability in material properties or manufacturing thickness variations) and computing the effects of their complex interactions on the combined probability of failure. A Monte Carlo simulation is the most familiar of these but other computationally efficient techniques have been developed over the years. Doing so provides valuable benefits, and though we plan to implement such an approach into HyperSizer in the future, this is completely different from the probabilistic approach developed in this SBIR.

Using HyperSizer's implementation of the test data driven reliability analysis developed in Phase II of this SBIR will not cost the end user more money to deploy for production work, nor will it cause a schedule delay to their analysis process. This is a solution that does not cause either to be increased. It is very practical to apply as demonstrated in Section 10 for the AFRL LRS.

From a design and certification perspective, uncertainties in the material allowables, manufacturing tolerances, boundary conditions, and analysis inaccuracies all come into play into the single set of CFs identified for each different analysis methods.

The purpose of this section is to establish that CFs are:

- Repeatable (this characteristic is necessary)
- Unique (this characteristic is not desirable, but has to be accounted)
- Required (needed for consistent structural integrity)
- Easy to use and very practical

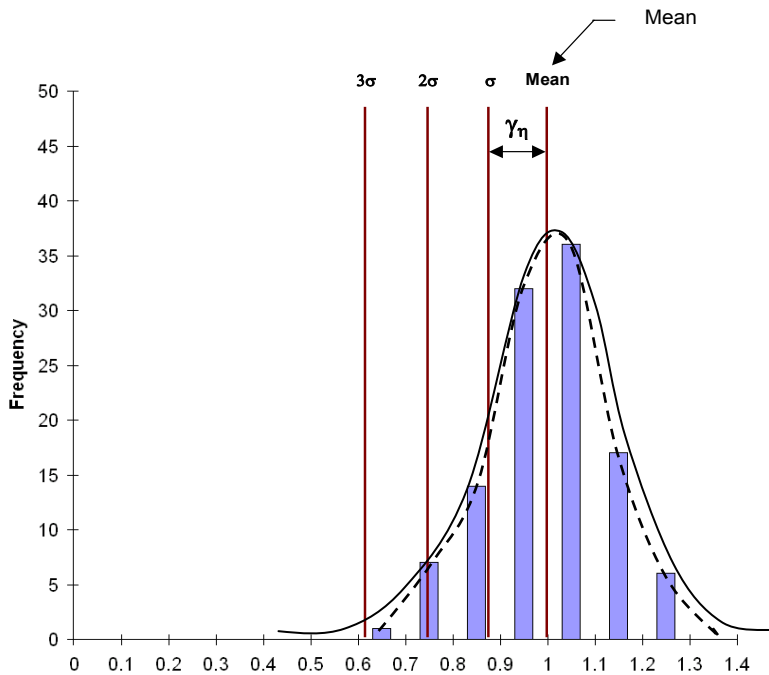
## 9.2.1 PDFs (probability density functions) statistically characterize histograms

Review section 5.1.2. Fig 5.2 is referenced often in this section.

Test data presented in Fig. 9.2 can also be presented in the form of an histogram, Fig. 9.3., where the height of the vertical bars quantify the frequency of occurrence of test scatter. This histogram is normalized by the **mean** of the test data collection. The horizontal distance of a vertical bar from the mean is noted in terms of the statistical standard deviation,  $\sigma$ . Therefore, a normal distribution has the highest frequency near the mean with the left and right halves dropping off into tails forming a “bell shaped curve.” Such a curve is also known statistically as a probability density function (PDF). The equation for the graph of a normal distribution is:

$$f(x) = \frac{e^{-(x-\mu)^2/(2\sigma^2)}}{\sigma\sqrt{2\pi}} \quad (9.1)$$

where the equation is defined with two inputs, the mean ( $\mu$ ) and the standard deviation, ( $\sigma$ ). This equation is used by HyperSizer to generate interactive plots and for making the figures that follow. The value in representing test results as a histogram, or PDF, is that it provides a universal way to compare the relative accuracies of different failure analyses and associated test results that are graphed using various parameters.



The standard deviation of a set of test data,  $\sigma$ , is determined and normalized against the average test failure load ( $\mu$ ). The normalized  $\sigma$  is:

$$\eta = \frac{\sigma}{\mu} \quad (9.2)$$

where the parameter,  $\eta$  is one of the two correlation factors, Also, ( $P_{\text{Mean}} = \mu$ ), where  $P_{\text{pred}}$  is the analysis prediction after being calibrated to the tests.

Fig. 9.3, The frequency of failure from test data, illustrated as a histogram with a statistical normal distribution (dotted curve on top of vertical bars) used to quantify load carrying confidence. The solid curve represents a statistical PDF. The histogram is normalized to the mean (average test result).

## 9.2.2 PDF signatures represent test scatter and analysis inaccuracy

As an example of the utility of a PDF, two examples are presented. The first is for cylindrical panel buckling and the second for bending strength of a composite beam. The following PDF graphs portray to relative scale inaccuracy of theoretical predictions along with test scatter.

### 9.2.2.1 Cylindrical panel buckling

This cylindrical panel buckling test data presented in Fig. 9.4 is not the same data as that from Fig. 5.2, but is indicative of observed test scatter and analysis inaccuracy. This figure is based on 32 beer can buckling failure tests [17]. The beer cans were stainless steel and tested in a special purpose testing machine at the University of Delft in 1987 [18]. Professor Arbocz of the Delft University of Technology presented results to this set of 32 can crush tests at the AIAA SDM 2001 conference. The representation of the data shown in Fig. 9.4 was not presented by Arbocz and is depicted in this report for an alternative purpose. Professor Arbocz's purpose was to predict with probabilistic methods (PM) the outcome using imperfection data and the high fidelity FEA post buckling software called STAGS. The purpose here is to statistically analyze test data scatter for this particular structural type and loading.

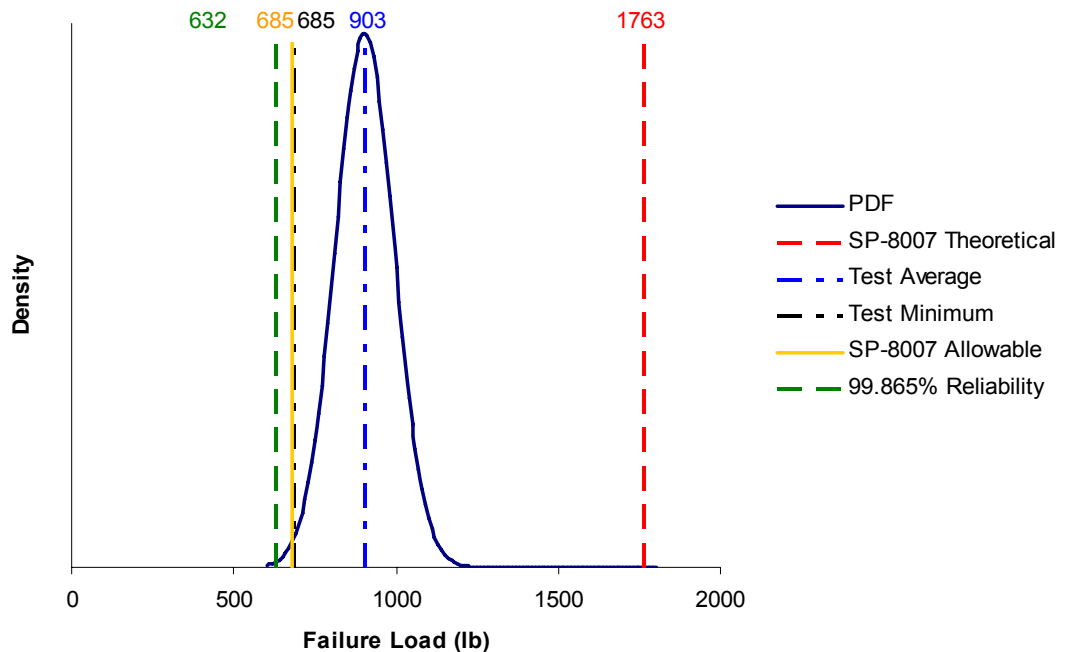


Fig. 9.4, PDF of test data *before normalizing* about the test mean of 903. The data is for 32 beer can buckling failure loads. The NASA SP-8007 theoretical buckling load (as verified with HyperSizer and with FEA) is shown as the vertical red line. The other plotted vertical lines are for the test minimum (685), and the 99.9% reliability buckling allowable load (632).

From the values in Fig. 9.4, the cylindrical buckling test failure load mean is 903, the theoretical is 1763, and the design-to-knockdown allowable based on a 99.9% reliability is 632. Using these numbers, the average analytical inaccuracy is:

$$\frac{\text{test mean}}{\text{theoretical } l} = \frac{903}{1763} = 0.513$$

and the overall design-to knockdown factor is:

$$\frac{99.9\% \text{ reliability}}{\text{theoretical}} = \frac{632}{1763} = 0.359$$

Both of these ratios are a significant reduction to theoretical predictions.

### 9.2.2.2 Four point composite beam bending strength

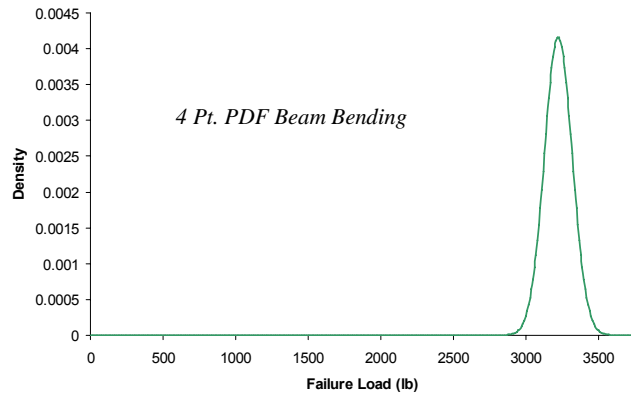


Fig. 9.5, PDF four point composite beam that failed in strength, before normalizing.

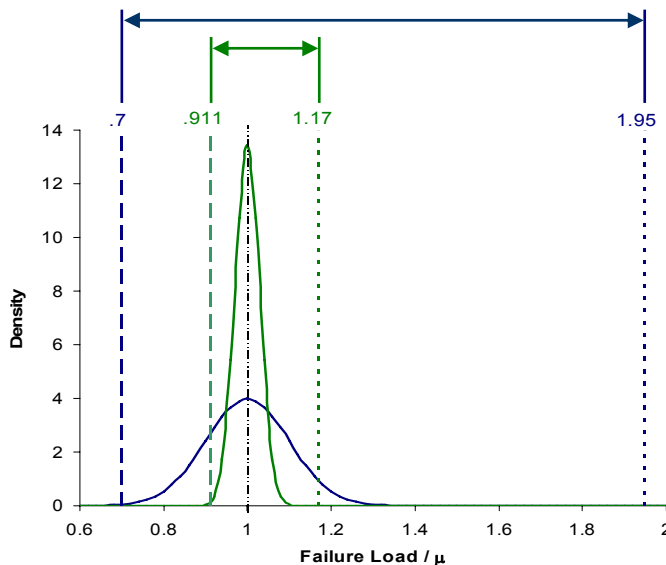


Fig. 9.6, PDFs of test data after normalizing about test mean. Two different failure analyses superimposed. The cylindrical buckling and a four point beam bending failure. The buckling has a flatter PDF where as the beam strength has a narrower and steeper PDF (a larger Kurtosis) representing less scatter (variance) in tests results.

For comparative purposes, a PDF from tests of composite beams is presented, Fig. 9.5. This PDF is then superimposed with the cylindrical buckling PDF, Fig. 9.6. to illustrate how two different PDF signatures indicate the amount of additional safety factor required to meet prescribed structural integrity reliability.

Cylindrical buckling (a flatter PDF) requires a substantial buckling knockdown factor of  $(0.7/1.95 = 0.375)$  for a deterministic analysis that then would include an additional 1.5 ultimate load factor. In contrast, beam strength analyses (a narrow PDF) are not typically knocked down, but if they were in this case it would be by the ratio of  $(0.911/1.17 = .78)$  to achieve the same safety as a 0.375 cylindrical buckling knockdown. Fig. 9.6 illustrates these relative differences as distances that span from the theoretical predictions to the allowables. The numbers in Fig. 9.6 are defined as

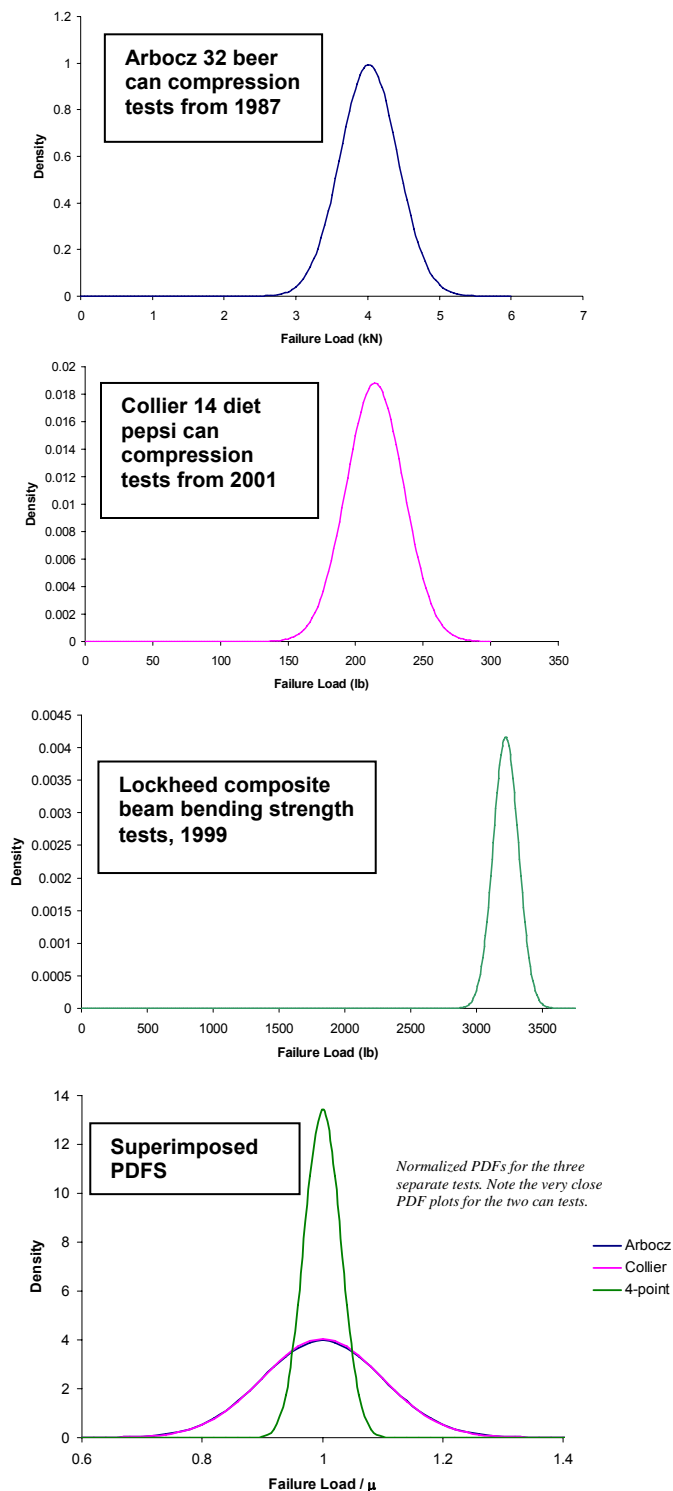
$$\frac{99.9\% \text{ reliability}}{\text{theoretical}} = \frac{632}{1763} = \frac{.7}{1.95} = .359$$

for cylindrical buckling and

$$\frac{99.9\% \text{ reliability}}{\text{theoretical}} = \frac{.911}{1.17} = .779$$

for beam bending strength.

### 9.2.3 PDF signatures are found to be repeatable and unique for each failure analysis mode



PDFs would not be useful unless they are both repeatable and unique. Fortunately, they have been found to be both. Fig. 9.7 shows the PDF for cylindrical panel buckling from section 9.2.2 next to a PDF from another set of cylindrical panel buckling tests. Note how they are repeatable. A third PDF is included for beam bending strength tests, which was also presented in section 9.2.2, for the purpose of showing how it is different from the buckling PDFs.

← **Repeatability in PDFs**

← **Unique PDF**

← **After normalizing**

Fig. 9.7, Repeatability and Uniqueness of PDFs. Three different PDFs from three different sets of tests before normalizing about the test mean. Then all superimposed after normalizing.

The first PDF of Fig. 9.7 of the beer can compression tests is plotted this time in metric units to convey the point that it doesn't matter what units the data is presented. All three PDFs are for tests to ultimate failure: 1) 32 steel beer cans compression tested in 1987, 2) 14 aluminum diet Pepsi cans compression tested in 2001, 3) composite beams flexural strength tested in 1998. These PDFs are then normalized and superimposed as shown in the bottom of Fig. 9.7.

Fig. 9.8 includes these three PDFs along with another PDF generated from a set of composite material, cylindrical panel buckling tests. This set of tests included 74 composite curved laminates compression tested in 1973. Note the very close match in PDF curves for the two metallic can buckling tests, indicating the same PDF signature. As expected, the curved laminate test is slightly more stochastic than the metallic cylinder test, and both PDF signatures are drastically different than the composite beam bending strength PDF.

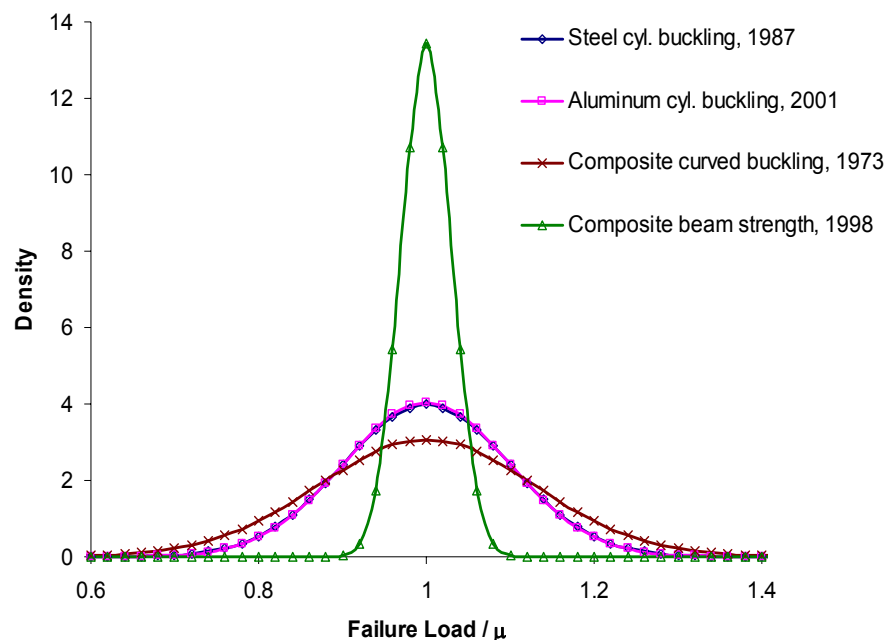


*Fig. 9.8, Four PDFs superimposed, this time including results from composite cylindrical buckling. As expected, by using composite materials, more test scatter is observed and noted with a flatter PDF.*

## 9.2.4 Two correlation factors are defined for each failure analysis mode

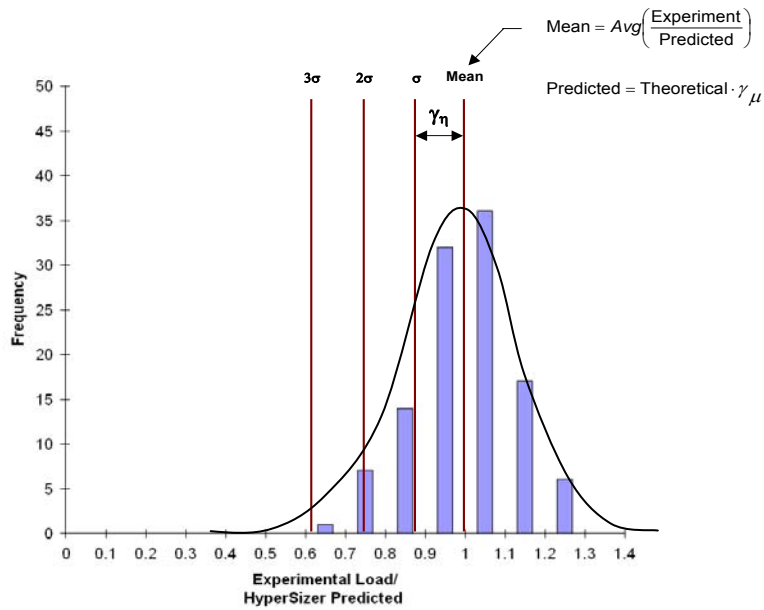


Fig. 9.9, The histogram is normalized to the mean test result, which by definition equals the analysis prediction of expected failure load.

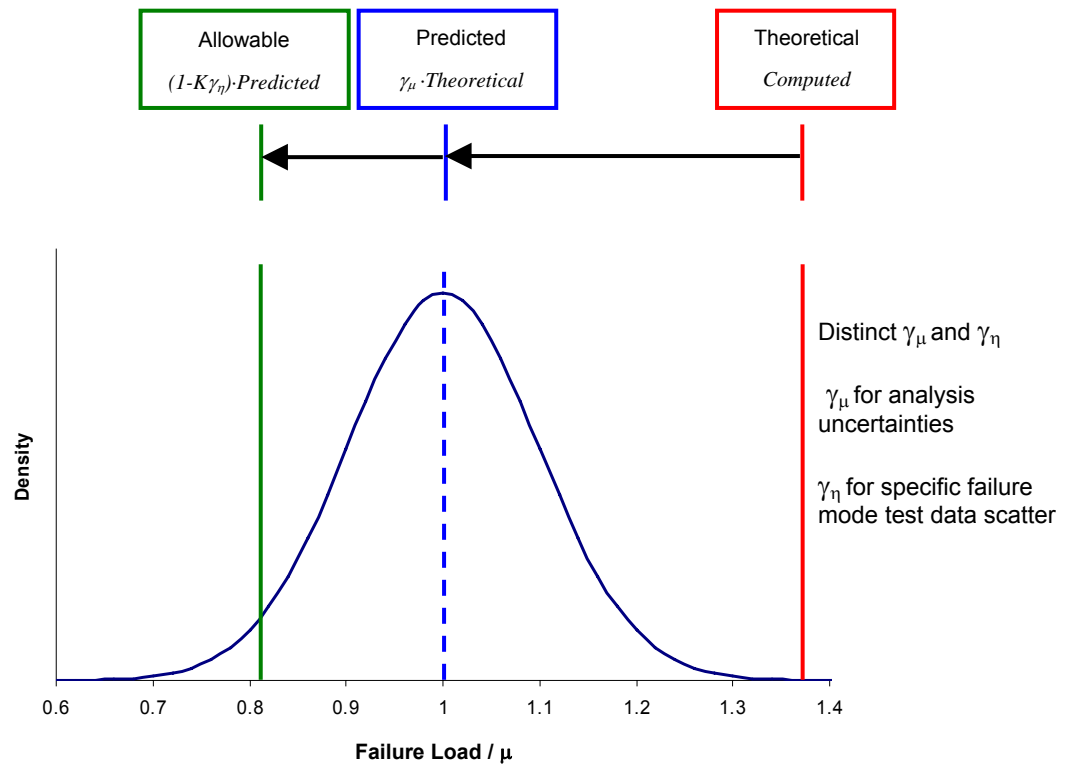


Fig. 9.10, Application of the two correlation factors on a probability density function (PDF) for determining desired reliability (allowable load).

Fig. 9.3 introduced the test data histogram. Fig. 9.9 expands on that introduction by defining a correlation factor,  $\gamma_\mu$ , for calibrating theoretical solutions to typical measured test values.

Fig. 9.10 represents a typical PDF signature derived from test data that can be used for accurate prediction of mean ( $\mu$ ) failure load, and choosing the level of risk. This is accomplished with two factors. The first factor mentioned above,  $\gamma_\mu$  (abbreviated to  $\mu$ ) for analysis uncertainties is used to calibrate theoretical solutions to typical measured test values. The calibration is usually a reduction of the theoretical as indicated by the arrow moving to the left. The second factor, coefficient of experimental failure load variation,  $\gamma_\eta$  (abbreviated to  $\eta$ ) for specific failure mode test data scatter repeatability is a measure of the variance (statistical deviation) of the test results. Recall that the coefficient of variation,  $\eta$ , is defined as

$$\eta = \frac{\sigma}{\mu}$$

As shown in Fig. 9.10, the theoretical value (red line) can be scaled by  $\gamma_\mu$ , to establish a **predicted** failure load (blue dashed line), then the user selects a desired level of reliability. The “K” value, Table 9.1, represents a specific reliability percentage (i.e. 99.9%) and is used to scale  $\gamma_\eta$ , the coefficient of experimental failure load variation to define an appropriate design-to allowable load (green line). Thus, a specific PDF signature for a given structure and loading type permits more reliable prediction of both expected failure load and allowable load.

**Table 9.1 Reliability, standard deviations, and lifetime airframe failures for a one sided normal distribution PDF curve.**

K value - Standard Deviation	Reliability	Lifetime Airframe Failures
1 $\sigma$	85.1%	1 in 34
2 $\sigma$	97.725%	1 in 217
2.33 $\sigma$	99.0%	1 in 500
2.58 $\sigma$	99.5%	1 in 1000
2.81 $\sigma$	99.75%	1 in 2000
3 $\sigma$	99.865%	1 in 3571

Table 9.1 lists some commonly used reliability percentages and their corresponding lifetime airframe failures and backed out standard deviations. The manner to equate these values together is described in Section 11.2. Also contained in Section 11.2 is a method for backing out the reliability from traditionally computed margins-of-safety based on ultimate load factors.

There are specific benefits derived from implementing two correlation factors per failure mode.

- Each failure mode, after individually being correlated to test data, can now be adjusted “on-the-fly” to provide across the board consistent reliability and safety
- Predicted failure load can be distinguished from design allowable load at any given time and made available to the engineering community at large
- The PDF is a universal way to be able to represent all failure mode test correlations
- Comparison to test data is widely available or known by the practicing engineer
- As more data becomes available, there is a readily available means to reevaluate correlations and to assign risk appropriately to meet missions and customers preferences

## 9.2.5 Two correlation factors for composite material strength demonstrated with HyperSizer

The complete listing of our established correlation factors (CFs) for each failure criteria is reported in the next section. This section uses the World Wide Failure Exercises (WWFE) case 1 as an example of HyperSizer implementation of correlation factors.

### 9.2.5.1 WWFE Case 1 with 19 test data

This is an example only. Refer to Section 12 for actual CF definition based all available test data.

A typical failure envelope for a composite material has four quadrants representing the four possibilities of compression-tension biaxial loading. As a way of introduction, however, we start with Case 1 of the WWFE that only shows two quadrants of the failure envelope - meaning no distinction between positive/negative shear. The calculated failure envelopes generated for that material system and loading is illustrated in Fig. 9.11, along with test data shown as blue circles.

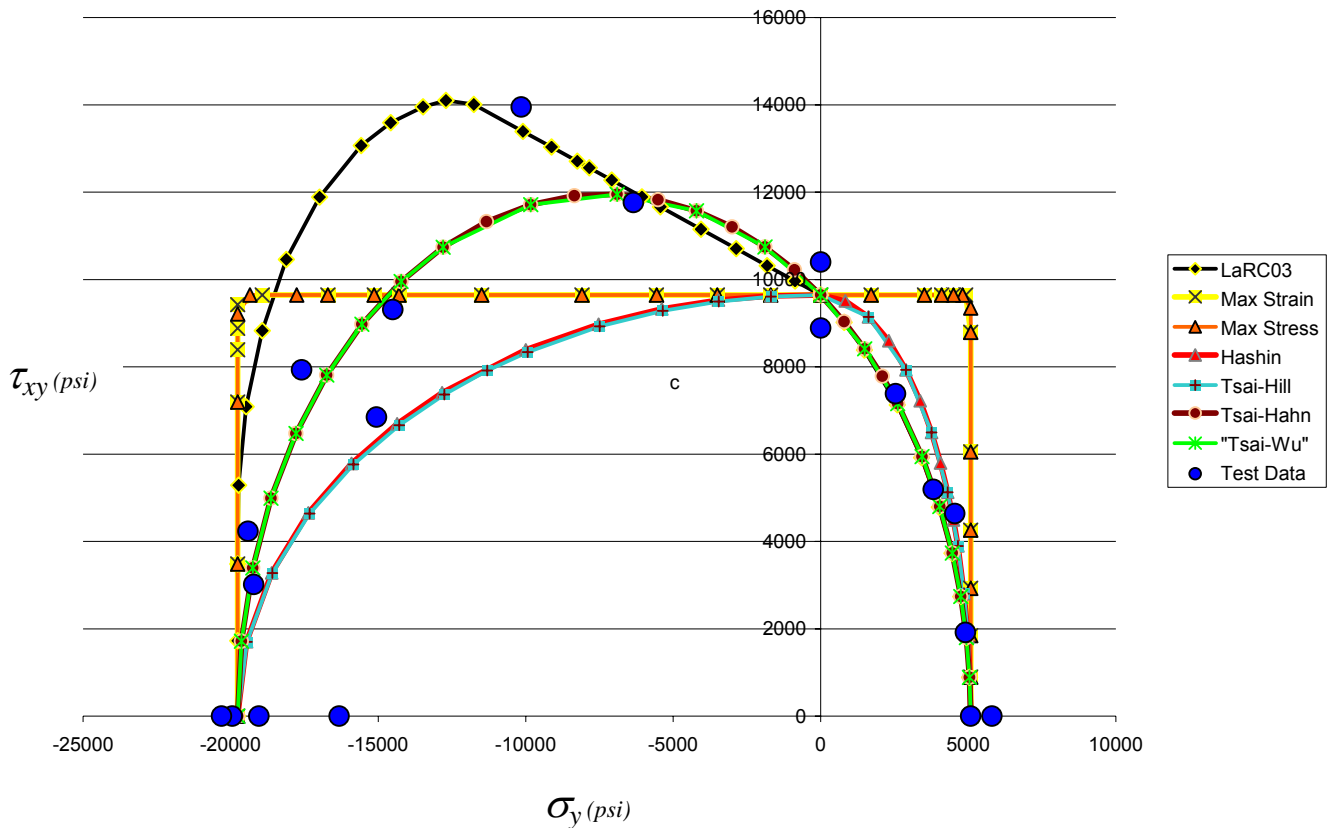


Fig. 9.11, HyperSizer generated failure envelopes for WWFE Case 1, biaxial  $\sigma_y$ - $\tau_{xy}$  of  $0^\circ$  E-glass/LY556 lamina. 19 Test data shown as filled blue circles. These plots use unidirectional strengths based on test results.

The discrepancy between the test data and the failure envelopes shows the analysis inaccuracies of many leading composite failure theories. We see that the Max Strain and Max Stress failure theories do not appear to be capturing the measured biaxial loading strength behavior. Both Tsai-

Hahn and LaRC03 appear to do quite well, particularly in the first quadrant of tension transverse stress combined with in-plane shear stress. LaRC03 failure theory seems to be tracking well an apparent linear relationship in the compressive/in-plane shear quadrant. However, by doing so, it appears to be overshooting failures that are best captured with Tsai-Hahn interaction criteria. However the one data point not being predicted by Tsai-Hahn is captured by LaRC03.

While some criteria match test data better than others, all failure theories exhibit inaccuracies, as illustrated by their calculated failure envelopes. Even if there was a perfect criterion, there always exists natural scatter in observed strengths. Referring back to Fig. 5.1, as indicated with the blue filled circles, there exists large variations in test measured strengths for pristine laminates. All of the reported test cases of WWFE and those collected by the authors show a great amount of test data scatter in measured strengths. It is for this reason that the CF approach provides significant value to establishing consistent structural integrity and the means to move toward more efficient certification with analysis.

### Test data entered, and histograms and PDFs generated

Fig. 9.12 and Fig. 9.13 show histograms for the 19 test values of WWFE Case 1. Three different failure theories are included: Tsai-Hahn, LaRC03, and Max Strain since it is the most frequently used in industry. Tsai-Hahn and LaRC03 show the 19 values in one histogram, where as for Max Strain, two histograms are shown: one for the condition where strain 2 (transverse to the fiber) controls and one for the condition where max strain 12 (in-plane shear) controls. For these combinations of stresses, a matrix cracking criteria controls for LaRC03 in all 19 tests.

### Failure theories compared for case 1

The four histograms, displayed side-by-side, give a statistical indication of the relative accuracy of the different failure theories. In general we see that Tsai-Hahn and LaRC03 do considerably better than Max Strain. Also note that **Tsai-Hahn** does exceptionally well for Case 1, as it also did for the entire collection of test data as presented in later sections. Again, its histogram illustrates the ratio of failure load to failure prediction = **1.012** which is very close to 1.0 and its standard deviation is small ( $1.012 - 0.933 = \mathbf{0.079}$ ) meaning the test data is relatively tight without much scatter. Each dashed vertical bar, starting from left to right represents  $3\sigma$ ,  $2\sigma$ , and  $1\sigma$  standard deviations. In contrast to the accuracy of Tsai-Hahn, Max Strain is less accurate. For instance, **Max Strain 12** shows a ratio of failure load to failure prediction = **1.072** which is not that bad, however more importantly, its standard deviation is quite large ( $1.072 - 0.829 = \mathbf{0.243}$ ). This will cause this failure theory's theoretical prediction to be heavily knocked down to achieve equal reliability as other failure theories. Finally, since the ratio of failure load to failure prediction, and standard deviation are slightly smaller for Tsai-Hahn, the histograms quantify what is observed in the graphical failure envelopes of Fig. 9.11, and that is it matches test data slightly better than LaRC03.

### Two step process for defining correlations factors

After statistically quantifying analysis inaccuracy and scatter in measured tests, the next step is to establish proper CFs for a particular correlation category. The entire process is performed in two steps. The first step is to collect test data and make comparisons directly between theoretical and test data. In-fact, Fig. 9.12 and Fig. 9.13 are histograms of this first step. They are untouched theoretical failure predictions against experimentally measured failure loads.

The second step is to define the CFs and then rerun HyperSizer (using the new reliability analysis) for all the components that comprise the 19 test data points. The CFs are established by using the inaccuracy of the theoretical and standard deviation of the test scatter. Using max strain 2 as an example, from Fig. 9.13 we see that T=P=0.9422. The horizontal axis (failure load/HyperSizer predicted) means that HyperSizer is theoretically over predicting failure. We need to knockdown the theoretical by 0.9422. This value is placed into the user input box for  $\mu$ , Fig. 9.15. The CF  $\eta$  is entered into the user input box as well.  $\eta$  is calculated as:

$$\eta = \frac{\sigma}{\mu} = \frac{(0.9422 - 0.616)}{3} \left( \frac{1}{0.9422} \right) = 0.115$$

Fig. 9.14 and Fig. 9.15 are histograms made after the second step. They show us how well HyperSizer is now predicting average failure. After running HyperSizer with the CFs for the 19 tests, the histograms of Figs. 9.14 and 9.15 should show P=1.0, or very close due to round off. A P=1.0 means that we can now predict average failure load. Fig. 9.15 for Max Strain 2 now shows theoretical to be 1.061 higher than the calibrated predicted failure load (T=1.061=1/0.942). Section 9.2.7 shows how HyperSizer makes use of the  $\mu$  and  $\eta$  CFs.

Since this is one material system, the material characterization and calibration of correlation factors is based on in-situ properties from the tests. One of the more important in-situ data is for the shear allowable, Fsu. These issues are covered in detail in Volume III.

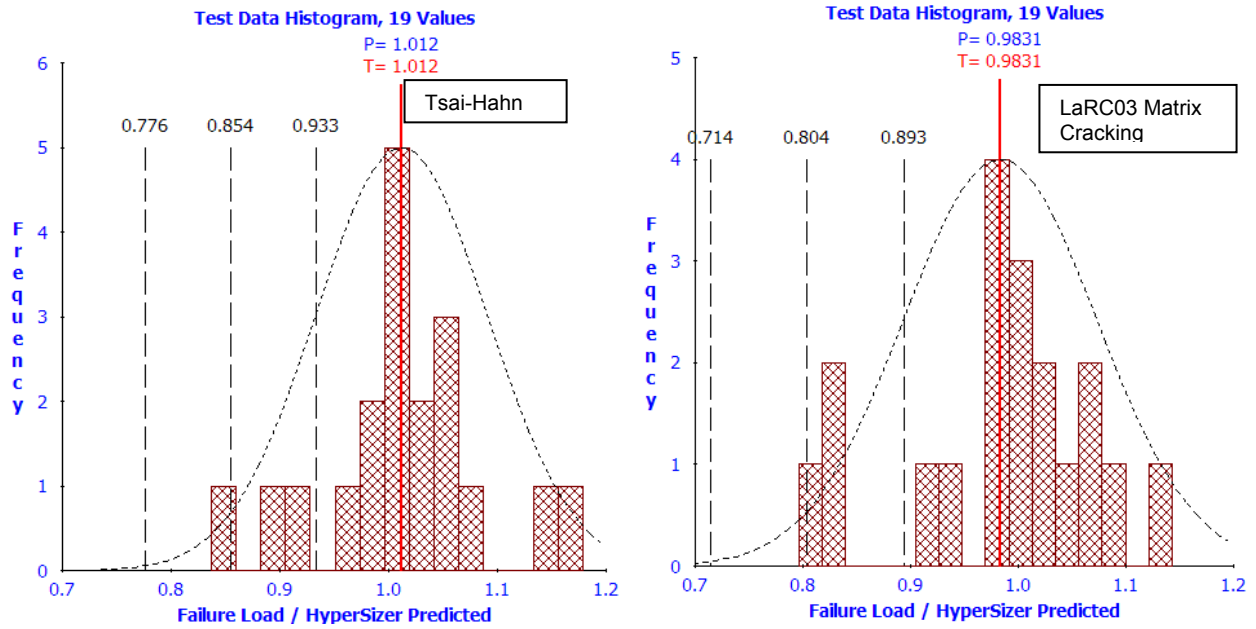


Fig. 9.12, For WWFE Case 1, biaxial  $\sigma_y$ - $\tau_{xy}$  failure envelopes of  $0^\circ$  E-glass/LY556 lamina. Composite Failure Theories: Tsai-Hahn on the left, LaRC03 Matrix Cracking on the right.

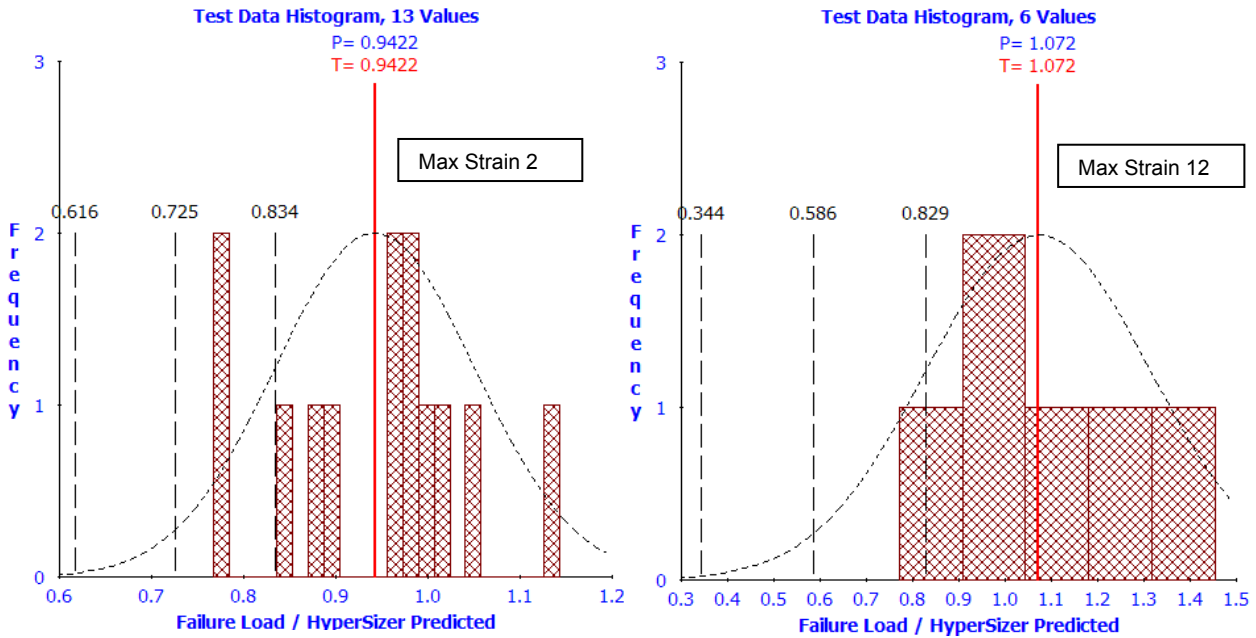


Fig. 9.13, For WWFE Case 1, biaxial  $\sigma_y$ - $\tau_{xy}$  failure envelopes. Max Strain Failure Theory: Max strain 2 direction on the left, Max strain 12 direction on the right.

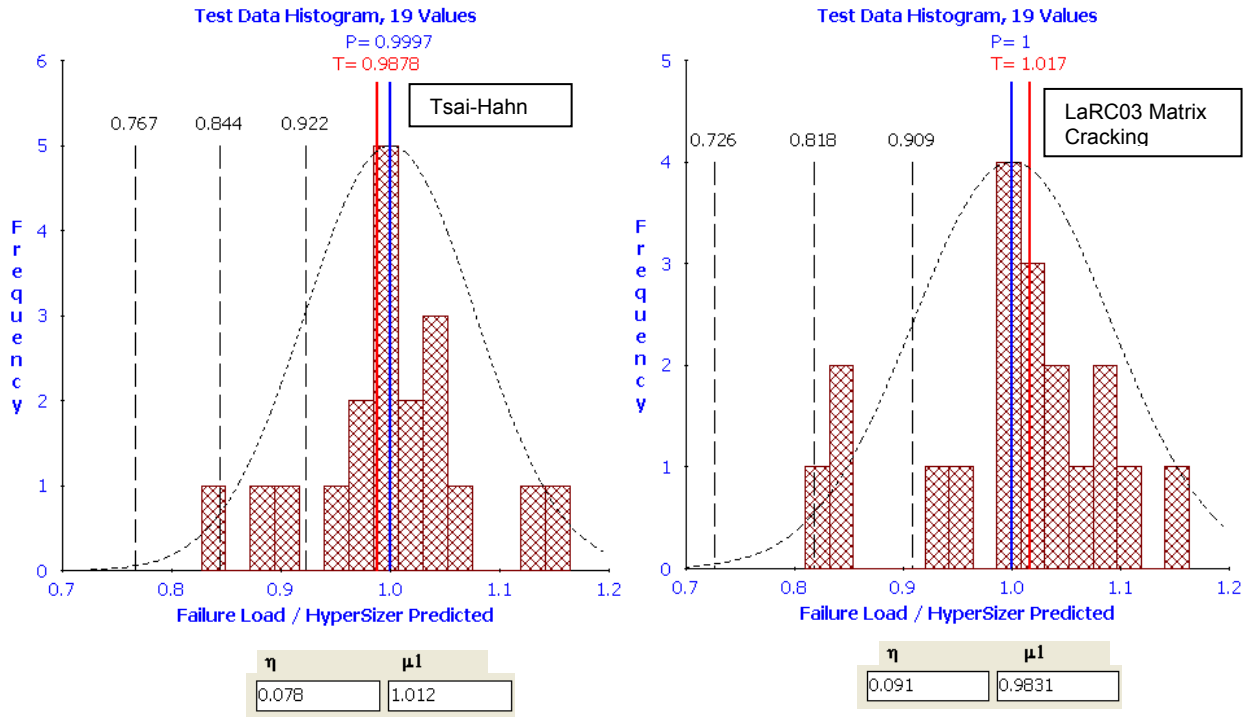


Fig. 9.14, After applying correlation factors for WWFE Case 1, biaxial  $\sigma_y$ - $\tau_{xy}$  failure envelopes of  $0^\circ$  E-glass/LY556 lamina. Tsai-Hahn on the left, LaRC03 Matrix Cracking on the right.

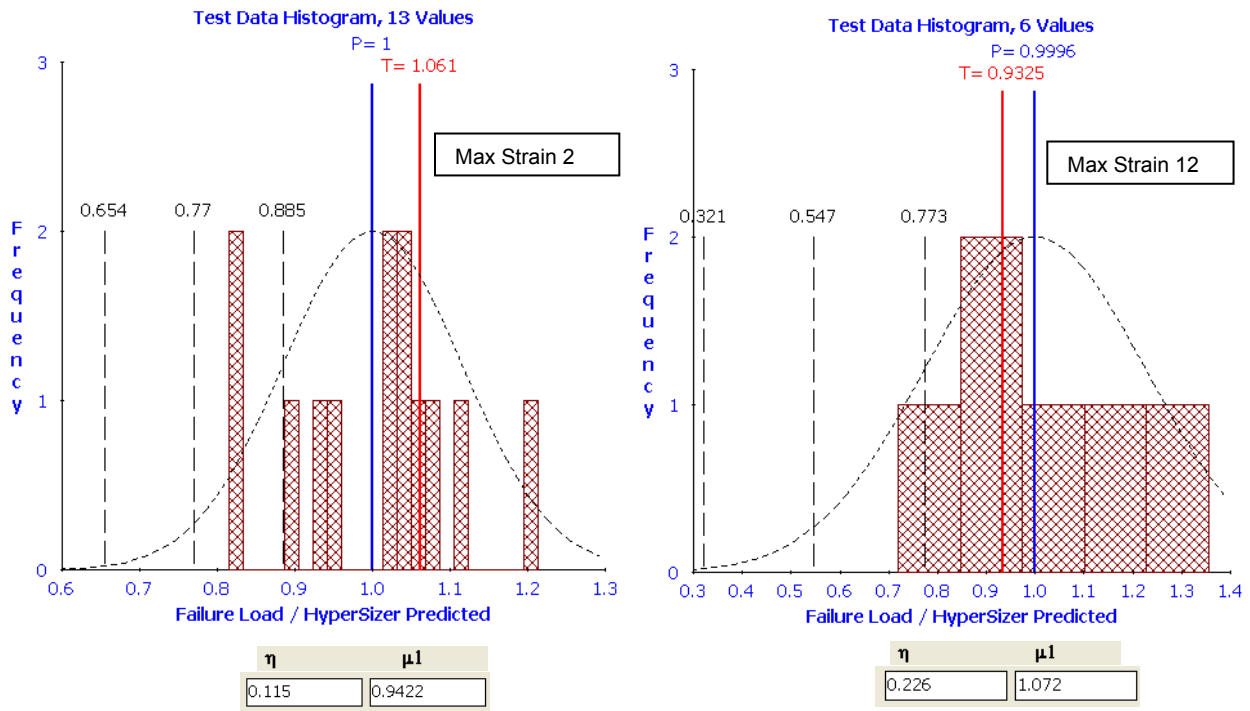


Fig. 9.15, After applying correlation factors for WWFE Case 1, biaxial  $\sigma_y$ - $\tau_{xy}$  failure envelopes. Max Strain Failure Theory: Max strain 2 direction on the left, Max strain 12 direction on the right.

### 9.2.5.2 As an example, actual Tsai-Hahn correlations to 130 tests

In Section 8.2 we described the process for inputting test data and displaying it as a histogram using the Tsai-Hahn failure analysis. Here we continue discussion of that process by giving more detail into the source of the data and by showing the final histogram generated after running HyperSizer on all 130 applicable tests with the Tsai-Hahn specific CFs.

Included in the 130 test correlations for composite laminate strength are all of the unidirectional and  $[\pm\theta]$  failure envelope test cases (cases 1, 2, and 3) from the World Wide Failure Exercises (WWFE), two additional failure envelope unidirectional cases (cases 8 and 9) from other publications, and case 10, a  $\pm\theta$  layup case of AS4/3502 material reported by [19 and 12]. Failure of a laminate comprised of unidirectional or  $[\pm\theta]$  layups occurs at first ply failure. Strength allowables presented here are based on damage initiation and not ultimate laminate strength which can be predicted using progressive failure techniques. The cases not included from WWFE involve progressive failure. Correlations to these progressive failure test data will come later. As a final point, the composite strengths are for pristine laminates, that is without damage. For an airframe design, damage tolerance and survivability allowables would be established and used as additional limiting strength requirements.

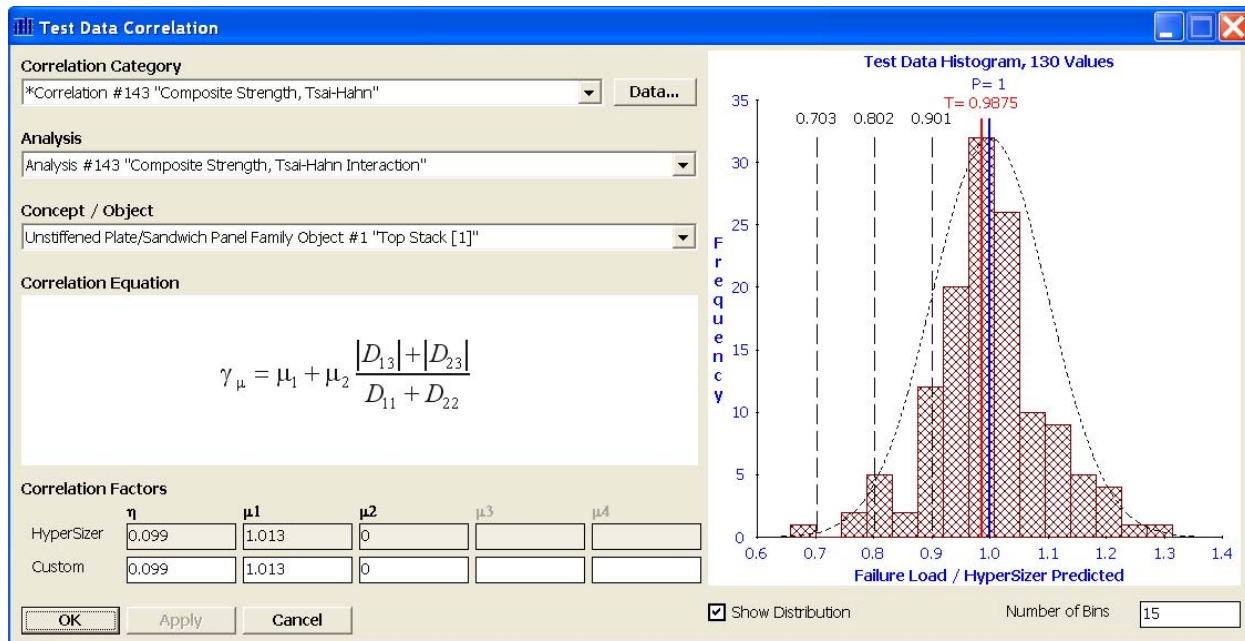


Fig. 9.16, A HyperSizer representative histogram plot of 130 test data points, before correlation. These are untouched, theoretical comparisons to tests. Tsai-Hahn theory matches test very well.

Shown in Fig. 9.16 is a histogram generated by HyperSizer that plots the statistical distribution of the 130 test failures normalized by predicted failures. The histogram is used to determine the proper correlation factors (CFs) for a given correlation category: in this case “Composite Strength, Tsai-Hahn.” The height of the vertical bars indicates frequency of occurrence and to some degree a normal distribution. More importantly, the histogram illustrates the ratio of failure load to failure prediction is very close to 1.0 for the Tsai-Hahn failure theory and the standard deviation is small meaning the data is relatively tight without much scatter.

Section 12 contains more insightful and detail information for four different failure analysis correlations.

### 9.2.6 Two correlation factor values have been established from test data for each failure analysis mode

The previous sections introduced concepts that form the basis of our test data driven reliability. This section defines the actual PDF's and CF's defined from all available test data for the following general failure modes: composite material strength, panel buckling, composite bonded joint, and honeycomb sandwich wrinkling. The complete listing of our established correlation factors (CFs) for each failure criteria is reported at the end of this section in Table 9.2

Hundreds of test data were collected for nine specific different failure modes and correlated to theoretical analysis predictions. They are:

- Panel buckling
- Honeycomb wrinkling
- Bonded Joint Delamination, Linear
- Bonded Joint Delamination, Non-Linear
- Bonded Joint Fracture, Linear
- Bonded Joint Fracture, Non-Linear
- Composite Strength: Tsai-Hahn
- Composite Strength: LaRC03 Matrix Cracking
- Composite Strength: LaRC03 Fiber Failure

Shown in Figs. 9.17 to 9.19 are these test results plotted as PDFs, normalized by the ratio of experimental test failure load to theoretical failure load prediction which is depicted as a dashed (experimental/theoretical) line. Analysis PDFs that fall left of the dashed line unconservatively predict failure loads higher than experiments. These methods include panel buckling (blue curve) and honeycomb wrinkling (green curve). These theoretical analysis predictions need to be knocked down before using as design allowables.

**Table 9.2, Summary Correlation Factors**

<b>Failure mode</b>	<b><math>\eta</math></b>	<b><math>\mu_1</math></b>	<b><math>\mu_2</math></b>	<b><math>\mu_3</math></b>	<b><math>\mu</math></b>
<b><i>Cylindrical Panel Buckling</i></b>	<b>.136</b>	<b>.3956</b>	<b>-.1144</b>	<b>.8751</b>	<b>.768*</b>
<b><i>Wrinkling</i></b>	<b>.102</b>	<b>.59</b>		<b>1,000,000</b>	
<b><i>Tsai-Hahn</i></b>	<b>.099</b>	<b>1.013</b>			
<b><i>LaRC03 Fiber Failure</i></b>	<b>.1107</b>	<b>.9388</b>			
<b><i>LaRC03 Matrix Cracking</i></b>	<b>.157</b>	<b>1.001</b>			
<b><i>Bonded Joint Delamination, Linear</i></b>	<b>0.0819</b>	<b>1.32</b>			
<b><i>Bonded Joint Fracture, Linear</i></b>	<b>0.132</b>	<b>1.28</b>			

\* an average value from Table 9.3, also this table is contained in Section 1 of Vol 3.

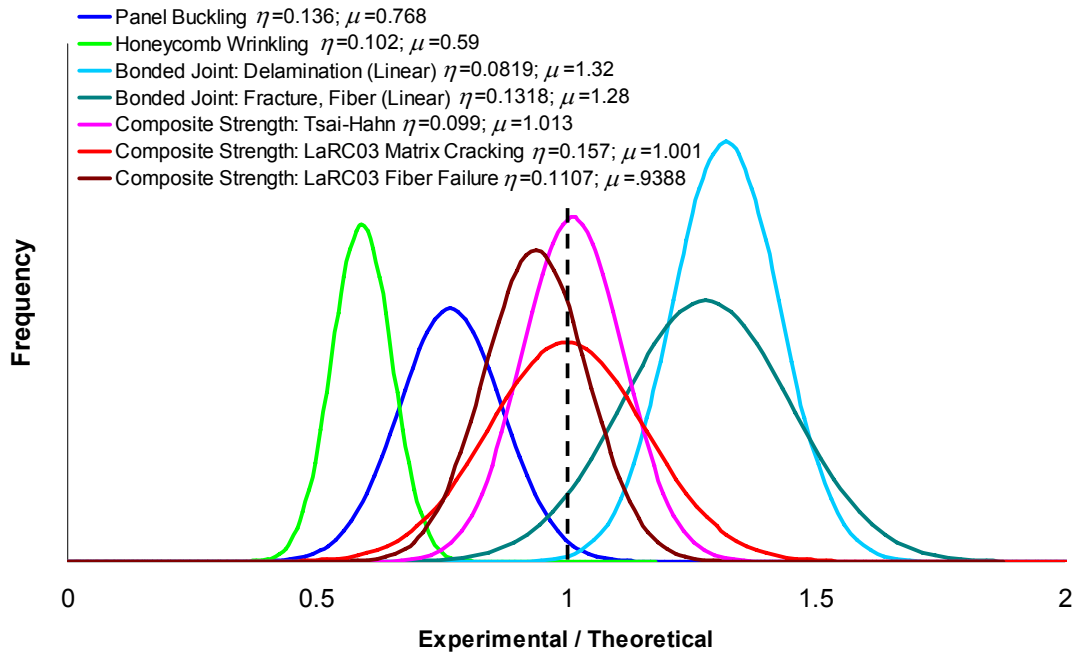


Fig. 9.17, *Normalizing to theoretical. The relative inaccuracies of the theoretical analysis and their relative scatter from experimental measurements. Wrinkling has the worst inaccuracy and Tsai-Hahn the best accuracy. Though both Tsai-Hahn and LaRC03 matrix cracking failures have the same average accuracy, Tsai-Hahn can be more confidently used due to its narrower PDF and therefore will have less knockdown for a given reliability.*

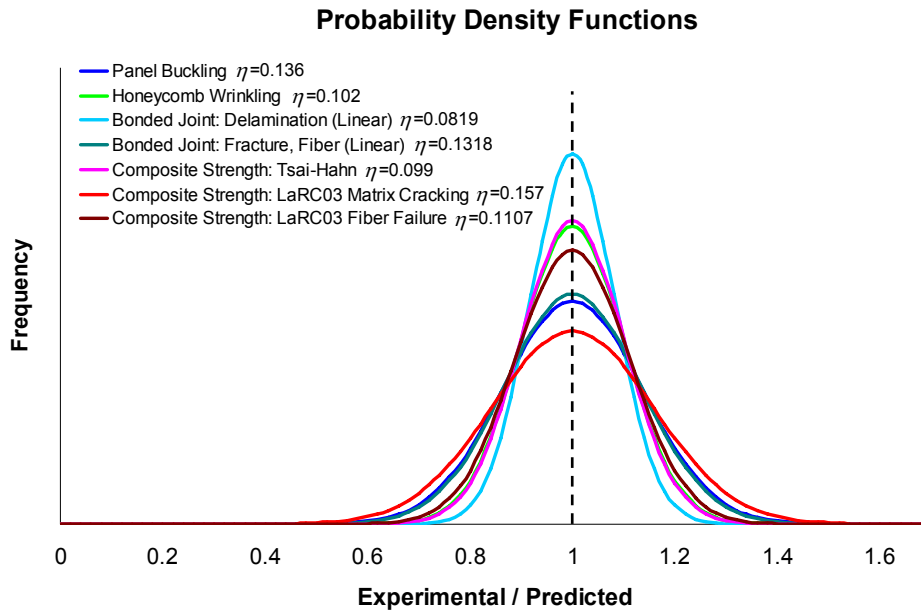


Fig. 9.18, *Normalization to predicted. The PDF signatures of the five different specific failure modes. It is coincidental that panel buckling and LaRC03 have the same PDF shape once normalized by  $\mu$ . Only the relative shape (flatter versus narrower) of the PDF curve will effect a change in results when using different % reliabilities.*

Fig. 9.17 graphically depicts the PDF curves for the values in Table 9.2 and their relative inaccuracies and test data scatter normalized by (experiment data/theoretical calculation). Wrinkling, shown in green has the worst inaccuracy (noted with the smallest  $\mu$  value) as it is the

farthest away from the vertical dashed line. Since the wrinkling PDF is left of the vertical dashed line, it over predicts strength by a ratio of  $1/.59 = 1.695$ .

Fig. 9.19 graphically depicts the same PDF curves but normalized this time by (experiment data/predicted) by use of the analysis inaccuracy correlation factor,  $\mu$ . Once the analysis inaccuracy is accounted, then the natural scatter in failure load is quantified with the correlation factor,  $\eta$ . Failure modes that fall within a tighter, narrower band can be more confidently used with a smaller knockdown to obtain the same given reliability.

### 9.2.6.1 Bonded Composite Joints

The SBIR developed stress analysis and strength prediction of bonded doubler joints as described in Ch 7.2 has also been calibrated to test results. A bonded doubler is the joint between a flange and facesheet of a stiffened panel.

There are two primary strength failures: delamination and fracture. For both of these failures, two types of analyses are performed: linear and non-linear.

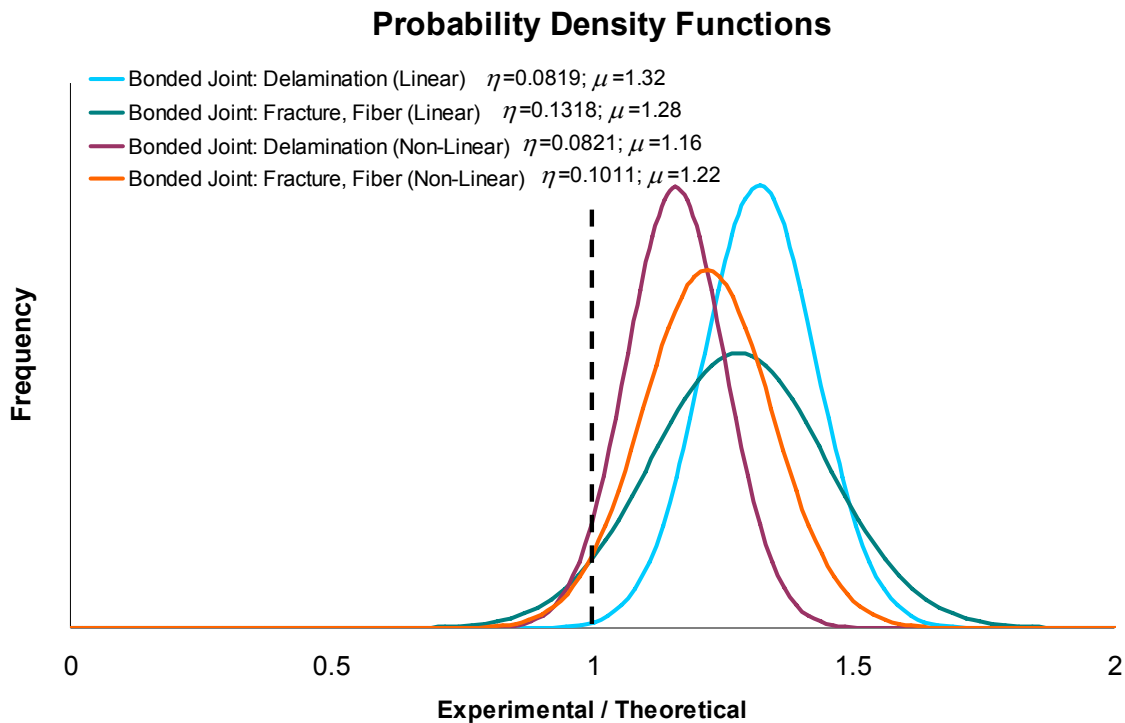


Fig. 9.19, Application of the (PDF) for determining desired reliability (allowable load). As expected, the theoretical predictions are more accurate when non-linear analyses are used, as indicated by the PDF's being closer centered to the test mean.

**Table 9.3, All Currently Defined Correlation Factors**  
(Eqn# refers to Volume 3, Table 1.1)

<i>Correlation Description</i>	<i>Eqn#**</i>	$\eta$	$\mu_1$	$\mu_2$	$\mu_3$	$\mu_4$	$3\sigma^*$
<i>Panel Buckling, Curved, Simple, Fixed or Free, Biaxial</i>	1.1.1	0.136	0.3956	-0.1144	0.8751		0.36
<i>Panel Buckling, Curved, Simple, Fixed or Free, Uniaxial</i>	1.1.1	0.136	0.3956		0.8751		0.36
<i>Panel Buckling, Flat, Simple BC, Biaxial</i>	1.1.2	0.06	0.4411	-0.2615		0.6	0.75
<i>Panel Buckling, Flat, Simple BC, Uniaxial</i>	1.1.2	0.06	0.4411			0.6	0.75
<i>Beam Buckling</i>	1.1.2	0.04	0.4711			0.6	0.84
<i>Local Buckling</i>	1.1.2	0.03	1				0.91
<i>Crippling</i>	1.1.4	0.1	1	-0.2615			0.7
<i>Deformation Limit</i>	1.1.4	0	1	0			1.0
<i>Stiffness Requirement</i>	1.1.4	0	1	0			1.0
<i>Frequency Limit</i>	1.1.4	0	1	0			1.0
<i>Sandwich Wrinkling, Isotropic or Honeycomb Core</i>	1.1.3	0.08	0.88	0	1.0E6		0.64
<i>Sandwich Wrinkling, Wrinkling, Honeycomb Core</i>	1.1.3	0.102	0.59	0	1.0E6		0.29
<i>Sandwich Intracell Dimpling</i>	1.1.3	0	1	0	1.0E6		1.0
<i>Sandwich Core Shear Crimping</i>	1.1.3	0	1	0	1.0E6		1.0
<i>Micromechanics, Max Stress</i>	1.1.4	0	1	0			1.0
<i>Micromechanics, Max Strain</i>	1.1.4	0	1	0			1.0
<i>Micromechanics, Tsai-Hill</i>	1.1.4	0	1	0			1.0
<i>Micromechanics, Strain Invariant Failure Theory</i>	1.1.4	0	1	0			1.0
<i>Composite Strength, Max Strain 1 Direction</i>	1.1.4	0.092	0.9184	0			0.66
<i>Composite Strength, Max Strain 2 Direction</i>	1.1.4	0.167	0.9772	0			0.49
<i>Composite Strength, Max Strain 12 Direction</i>	1.1.4	0.210	1.104	0			0.41
<i>Composite Strength, Max Stress 1 Direction</i>	1.1.4	0.1067	0.8922	0			0.57
<i>Composite Strength, Max Stress 2 Direction</i>	1.1.4	0.1427	0.9305	0			0.53
<i>Composite Strength, Max Stress 12 Direction</i>	1.1.4	0.218	1.034	0			0.36
<i>Composite Strength, Tsai-Hill</i>	1.1.4	0.165	1.051	0			0.53
<i>Composite Strength, Tsai-Wu</i>	1.1.4	0.125	1.012	0			0.63
<i>Composite Strength, Tsai-Hahn</i>	1.1.4	0.099	1.013	0			0.71
<i>Composite Strength, Hoffman</i>	1.1.4	0.121	1.012	0			0.64
<i>Composite Strength, Hashin Matrix Cracking</i>	1.1.4	0.191	1.034	0			0.44
<i>Composite Strength, Hashin Fiber Failure</i>	1.1.4	0.143	0.9328	0			0.53
<i>Composite Strength, LaRC03 Matrix Cracking</i>	1.1.4	0.157	1.001	0			0.53
<i>Composite Strength, LaRC03 Fiber Failure</i>	1.1.4	0.1107	0.9388	0			0.61
<i>Joint, Bonded, Adherend Fracture</i>	1.1.4	0.1318	1.28	0			0.61
<i>Joint, Bonded, Adherend Delamination</i>	1.1.4	0.0819	1.32	0			0.75
<i>Joint, Bonded, Adhesive</i>	1.1.4	0	1	0			1.0

\*  $3\sigma$  is a useful value for comparing the relative effective knockdown required

\*\* Eqn# is provided in Vol 3, Section 1

### 9.2.7 HyperSizer implementation of test data driven reliability analysis and sizing optimization

In this section, using the LRS airframe, we show how easy it is to use the HyperSizer newly developed test data driven reliability analysis and sizing optimization. This new capability will allow us to size the airframe structure using all analyses to the same level of reliability.

Referring to Fig. 9.1, we will use the existing capabilities of HyperSizer which provide statistically derived FEA computed “design-to” loads at prescribed reliability (the maroon circle), and the new capabilities of HyperSizer which provide statistically derived allowable loads at prescribed reliability, (the blue circle).

The prescribed reliability that can now be consistently applied, is selected as an example for the following figures to be 2 standard deviations which corresponds to a 97.7% reliability or a 1 in 217 lifetime airframe failures. Table 9.1 lists some commonly used reliability percentages and their corresponding lifetime airframe failures and backed out standard deviations.

There are three simple steps for using the new reliability analysis:

**1<sup>st</sup> step:** Turn on the reliability analysis by placing a checkmark in the box on the failure tab next to your selected failure analyses, as illustrated in Fig. 9.18.

**2<sup>nd</sup> step:** Select the percent reliability, set the limit and ultimate load factors to 1.0, and select a standard deviation for the *FEA statistical loading method* to be consistent with the standard deviation of the selected percent reliability, as illustrated in Fig. 9.19. The ultimate load factor should be set to 1.0 instead of the typical 1.5 because the necessary conservatism is already included in the reliability analysis.

**3<sup>rd</sup> step:** Select the buckling knockdown factor to 1.0, as illustrated in Fig. 9.20, since the reliability will automatically compute on the fly an appropriate knockdown.

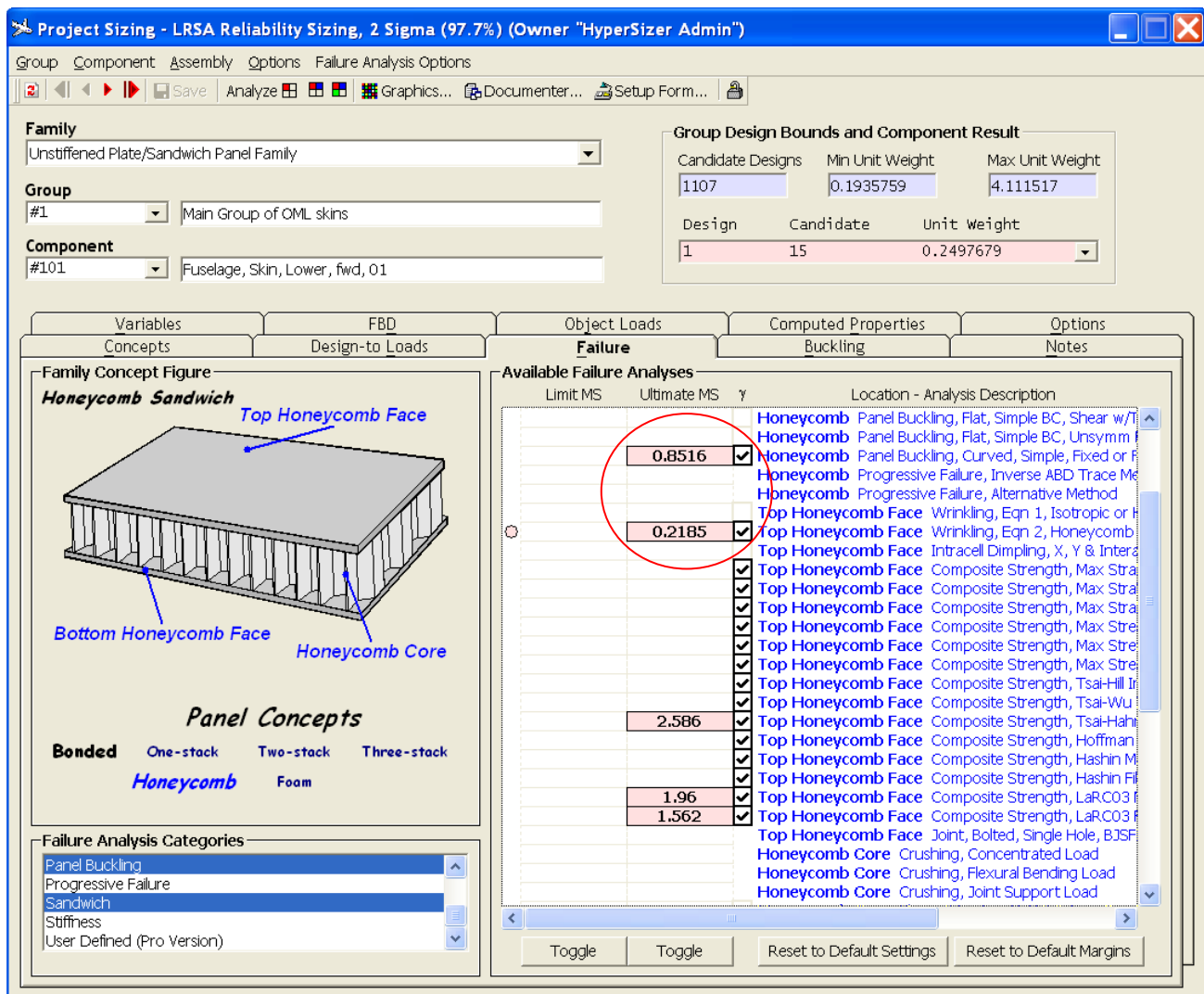


Fig. 9.18, 1<sup>st</sup> step; HyperSizer failure tab provides the user an option to select which failure analyses to perform reliability analysis. As shown above, the cylindrical panel buckling, facesheet wrinkling, Tsai-Hahn, LaRC03 fiber, and LaRC03 matrix cracking failure analyses have been selected. Margins for these toggled on analyses are displayed. The other composite failure analyses such as Max Strain have checks next to them, but neither the limit nor ultimate box has been activated and therefore no MS is provided for them.

For the LRS airframe application of Sections 10 and 11, as shown in Fig. 9.18, the cylindrical panel buckling, facesheet wrinkling, Tsai-Hahn, LaRC03 fiber, and LaRC03 matrix cracking failure analyses have been selected for reliability analysis. All other failure analysis modes have been turned off.

Note in Fig. 9.19 that a 97.7% reliability has been selected. This corresponds to a 2 sigma standard deviation as reported in Table 9.1. This same level of conservatism has been selected for the FEA Statistical Loading Method.

Factors	
Reliability (%)	97.7
Mechanical Limit	1
Mechanical Ultimate	1
Thermal Hurt	1
Thermal Help	0.8
Biaxial Buckling Tension	
Field Stiffening	
Tensile	1
Compressive	1
FEA Statistical Loading Method	2-Sigma

Fig. 9.19, 2<sup>nd</sup> Step. Select reliability %, 1.0 for mechanical load factor, and a consistent FEA Statistical Loading Method.

Buckling		Notes
Setup		
X Span	33.06048	
Y Span	19.81871	
Knockdown Factor	1	
Initial Imperfection	0	
Panel is Curved	<input type="checkbox"/>	

Fig. 9.20, 3<sup>rd</sup> Step. Select 1.0 for a buckling knockdown factor.

## **Part D: SBIR Solution Demonstrated with New HyperSizer Software**

In this part of the report, the newly developed capabilities of this Phase II SBIR as implemented in HyperSizer are demonstrated. Section 10 first demonstrates the ability to include probabilistic methods based on test data for an air platform preliminary design and its weight savings. Section 11 compares the traditional zero-margin-of-safety method used in the aerospace industry today to the newly developed reliability analysis and quantifies its affect and significance. Vol 2, Ch's 2-5 provide a summary of test data and the associated CF's for the four different failure analyses.

## 10 Reliability Trades during Preliminary Design for Entire Airframe: AFRL Long Range Strike (LRS)

Presented in Fig. 10.1 is the weight increase of the example Long Range Strike aircraft as a function of the chosen reliability. Program Managers need to know this extremely valuable information for their decision of determining acceptable levels of risk. This type of data is useful for selecting structural certification tests and can also feed into important weight versus life cycle cost trades.

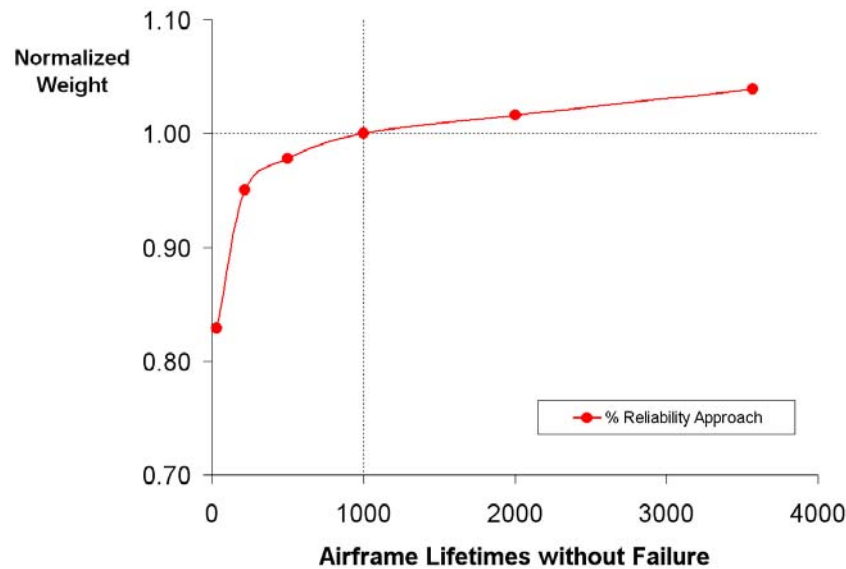


Fig. 10.1, Airframe structural weight versus lifetime failures. Note that significant reliability can be achieved with moderate weight growth. Data for this graph is tabulated in Table 10.1, and normalized arbitrarily to 1 in 1000 lifetime airframe failures.

**Table 10.1, Airframe Weight Increases with Increasing Structural Integrity  
normalized arbitrarily to 1 in 1000 lifetime airframe failures**

PDF Standard Deviation	Reliability	Lifetime Airframe Failures	Normalized Weight	Weight Savings
1 $\sigma$	85.1%	1 in 34	.829	17.1%
2 $\sigma$	97.7%	1 in 217	.950	5.0%
2.33 $\sigma$	99.0%	1 in 500	.978	2.2%
<b>2.58 <math>\sigma</math></b>	<b>99.5%</b>	<b>1 in 1000</b>	<b>1.0</b>	<b>0%</b>
2.81 $\sigma$	99.75%	1 in 2000	1.016	-1.6%
3 $\sigma$	99.86%	1 in 3571	1.039	-3.9%

## 10.1 Specific Airframe Application

The vehicle chosen as an example application is a Mach 3.5 long range strike aircraft designed by LM Aero in Fort Worth and sponsored by Air Force Research Lab (AFRL) Air Vehicles Directorate. See Section 6.6 for introduction to HyperSizer application to the LRS. The analysis and sizing documented in that section is for the entire FEM. For the following examples, a subset of the FEM, defined as an assembly, consisting of external surface panels is analyzed. This assembly includes 3 groups and 84 components. For these groups, honeycomb sandwich panels and thick laminate skins are used. Stiffened panels are not included and as such, neither was bonded composite joint analysis. All of the seven load cases are included in the trades.

Table 10.2, Vehicle Load Cases

Load Set	Description
#1	3G Begin Cruise
#2	3G Before Weapon Drop
#3	3G End Cruise
#4	2G Begin Cruise
#5	-1G TOGW
#6	Taxi Bump
#7	Vertical Tail Loads

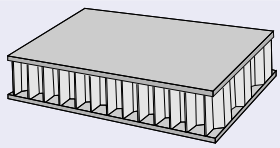
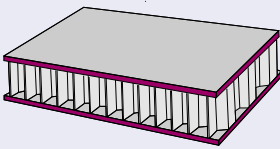
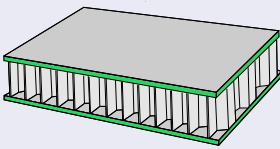
## 10.2 Materials and Panel Concepts

Honeycomb sandwich panels and solid “plank” laminates are used in the airframe, see Fig. 10.2.

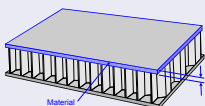
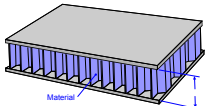
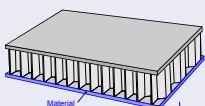
***Honeycomb Sandwich (as an example, Group 1 which is the largest group of the assembly)***

The top and bottom facesheets have their sizing variables linked.

### Group Options

Honeycomb sandwich	
Link facesheet top and bottom stack materials	
Link layups/thicknesses (requires material linking)	

The AS4/3502 graphite epoxy facesheets have 42 different layups to choose from and the Nomex honeycomb core considers 27 different thicknesses ranging from .05” to 2”.

Group Variables					
Var		Min Bnd.	Max Bnd.	#	Materials
Top Face - Thickness		NA	NA	NA	<ol style="list-style-type: none"> <li>1. <a href="#">Layup Templates Primitive "2 [0/0]"</a></li> <li>2. <a href="#">Layup Templates Primitive "2 [0/90]"</a></li> <li>3. <a href="#">Layup Templates Primitive "2 [45/-45]"</a></li> <li>4. <a href="#">Layup Templates Primitive "2 [90/90]"</a></li> <li>5. <a href="#">3-6 plies; Symm; 0/30/45/60/90 "4 [45/-45]s"</a></li> <li>6. <a href="#">3-6 plies; Symm; 0/30/45/60/90 "5 [45/-45/ 0 ]s"</a></li> <li>7. <a href="#">3-6 plies; Symm; 0/30/45/60/90 "5 [45/-45/ 90 ]s"</a></li> <li>8. <a href="#">3-6 plies; Symm; 0/30/45/60/90 "6 [0/45/-45]s"</a></li> <li>9. <a href="#">3-6 plies; Symm; 0/30/45/60/90 "6 [45/90/-45]s"</a></li> <li>10. <a href="#">3-6 plies; Symm; 0/30/45/60/90 "6 [60/90/-60]s"</a></li> <li>11. <a href="#">3-5 plies; Unsymm; 0/30/45/60/90 "3 [90/30/-30]"</a></li> <li>12. <a href="#">3-5 plies; Unsymm; 0/30/45/60/90 "3 [0/45/-45]"</a></li> <li>13. <a href="#">3-5 plies; Unsymm; 0/30/45/60/90 "3 [60/0/-60]"</a></li> <li>14. <a href="#">3-5 plies; Unsymm; 0/30/45/60/90 "3 [60/90/-60]"</a></li> <li>15. <a href="#">3-5 plies; Unsymm; 0/30/45/60/90 "3 [30/-30/90]"</a></li> <li>16. <a href="#">3-5 plies; Unsymm; 0/30/45/60/90 "3 [45/-45/90]"</a></li> <li>17. <a href="#">3-5 plies; Unsymm; 0/30/45/60/90 "4 [0/45/0/-45]"</a></li> <li>18. <a href="#">3-5 plies; Unsymm; 0/30/45/60/90 "4 [45/30/-30/-45]"</a></li> <li>19. <a href="#">3-5 plies; Unsymm; 0/30/45/60/90 "4 [90/45/90/-45]"</a></li> <li>20. <a href="#">3-5 plies; Unsymm; 0/30/45/60/90 "4 [0/60/0/-60]"</a></li> <li>21. <a href="#">3-5 plies; Unsymm; 0/30/45/60/90 "4 [60/45/-45/-60]"</a></li> <li>22. <a href="#">3-5 plies; Unsymm; 0/30/45/60/90 "4 [0/60/90/-60]"</a></li> <li>23. <a href="#">3-5 plies; Unsymm; 0/30/45/60/90 "4 [0/45/-45/90]"</a></li> <li>24. <a href="#">3-5 plies; Unsymm; 0/30/45/60/90 "4 [60/0/-60/90]"</a></li> <li>25. <a href="#">7-9 plies; Symm; 0/45/90 "7 [0/45/-45/ 0 ]s"</a></li> <li>26. <a href="#">7-9 plies; Symm; 0/45/90 "7 [0/45/-45/ 90 ]s"</a></li> <li>27. <a href="#">7-9 plies; Symm; 0/45/90 "7 [90/45/-45/ 90 ]s"</a></li> <li>28. <a href="#">7-9 plies; Symm; 0/45/90 "8 [0/45/0/-45]s"</a></li> <li>29. <a href="#">7-9 plies; Symm; 0/45/90 "8 [0/45/90/-45]s"</a></li> <li>30. <a href="#">7-9 plies; Symm; 0/45/90 "8 [90/45/90/-45]s"</a></li> <li>31. <a href="#">7-9 plies; Symm; 0/45/90 "9 [45/0/0/-45/ 0 ]s"</a></li> <li>32. <a href="#">7-9 plies; Symm; 0/45/90 "9 [45/90/-45/0/ 0 ]s"</a></li> <li>33. <a href="#">7-9 plies; Symm; 0/45/90 "9 [90/45/90/-45/ 0 ]s"</a></li> <li>34. <a href="#">10&amp;12 plies; Symm; 0/45/90; 45/-45 outside "10 [45/-45/0/45/-45]s"</a></li> <li>35. <a href="#">10&amp;12 plies; Symm; 0/45/90; 45/-45 outside "12 [45/-45/0/45/90/-45]s"</a></li> <li>36. <a href="#">14&amp;16 plies; Symm; 0/45/90; 10% rule; 45/-45 outside "14 [45/-45/0/0/45/90/-45]s"</a></li> <li>37. <a href="#">14&amp;16 plies; Symm; 0/45/90; 10% rule; 45/-45 outside "16 [45/-45/0/45/90/-45/45/-45]s"</a></li> <li>38. <a href="#">18&amp;20 plies; Symm; 0/45/90; 10% rule; 45/-45 outside "18 [45/-45/0/0/45/-45/90/45/-45]s"</a></li> <li>39. <a href="#">18&amp;20 plies; Symm; 0/45/90; 10% rule; 45/-45 outside "20 [45/-45/0/0/0/45/90/-45/0/0]s"</a></li> <li>40. <a href="#">18&amp;20 plies; Symm; 0/45/90; 10% rule; 45/-45 "20 [45/-45/0/45/90/-45/90/45/90/-45]s"</a></li> <li>41. <a href="#">User Layups "40 [45/-45/0/45/90/-45/90/45/90/-45]2s"</a></li> <li>42. <a href="#">Graphite/Epoxy "AS4/3502 Typical properties"</a></li> </ol>
Core - Thickness		0.052 (in)	2 (in)	27	1. <a href="#">Honeycomb "Nomex 3.0 lb Scaled-Ruddy Test"</a>
Bottom Face - Thickness		NA)	NA	NA	Linked

## Solid laminates (Group 5)

The optimization used AS4/3502 graphite epoxy (typical properties) with 29 different layups.

### Materials

1. User Layups "28 [45/-45/0/90/0/-45/45/45/-45/0/90/0/-45/45/45/-45/0/90/0/-45/45/45/-45/0/90/0/-45/45]"
2. User Layups "32 [45/-45/45/-45/0/90/0/-45/45/45/-45/0/90/0/-45/45/45/-45/0/90/0/-45/45/45/-45/45/45]"
3. User Layups "36 [45/-45/45/45/-45/0/90/0/-45/45/45/-45/0/90/0/-45/45/45/-45/0/90/0/-45/45/45/-45/45/45]"
4. User Layups "40 [0/90/45/-45/45/-45/45/-45/0/90/0/-45/45/45/-45/0/90/0/-45/45/45/-45/0/90/0/-45/45/45/-45/45/45/0/90]"
5. User Layups "44 [0/90/0/90/45/-45/45/-45/45/-45/0/90/0/-45/45/45/-45/0/90/0/-45/45/45/-45/0/90/0/-45/45/45/-45/45/45/0/90/0]"
6. User Layups "48 [45/-45/0/90/0/90/45/-45/45/-45/45/-45/0/90/0/-45/45/45/-45/0/90/0/-45/45/45/-45/0/90/0/-45/45/45/-45/45/45/0/90/45/-45]"
7. User Layups "52 [45/-45/0/90/0/90/0/45/-45/45/-45/45/-45/0/90/0/-45/45/45/-45/0/90/0/-45/45/45/-45/0/90/0/-45/45/45/-45/45/45/0/90/45/-45/45/-45]"
8. User Layups "56 [0/90/45/-45/45/-45/0/90/0/90/45/-45/45/-45/45/-45/0/90/0/-45/45/45/-45/0/90/0/-45/45/45/-45/0/90/0/-45/45/45/-45/45/45/0/90/45/-45/45/-45/0/90]"
9. User Layups "60 [0/90/0/90/45/-45/45/-45/0/90/0/90/45/-45/45/-45/45/-45/0/90/0/-45/45/45/-45/0/90/0/-45/45/45/-45/0/90/0/-45/45/45/-45/45/45/0/90/45/-45/45/-45/0/90/0]"
10. User Layups "30 [45/-45/45/-45/0/90/0/-45/45/45/-45/0/90/0/-45/45/45/-45/0/90/0/-45/45/45/-45/0/90/0/-45/45/45/-45]"
11. User Layups "34 [45/-45/45/-45/45/-45/0/90/0/-45/45/45/-45/0/90/0/-45/45/45/-45/0/90/0/-45/45/45/-45/45/45/-45/45/-45]"
12. User Layups "38 [0/45/-45/45/-45/45/-45/0/90/0/-45/45/45/-45/0/90/0/-45/45/45/-45/0/90/0/-45/45/45/-45/0/90/0/-45/45/45/-45/45/45/0]"
13. User Layups "42 [0/90/90/45/-45/45/-45/45/-45/0/90/0/-45/45/45/-45/0/90/0/-45/45/45/-45/0/90/0/-45/45/45/-45/45/45/-45/45/-45/0/90/0]"
14. User Layups "46 [45/-45/0/90/0/90/45/-45/45/-45/45/-45/0/90/0/-45/45/45/-45/0/90/0/-45/45/45/-45/0/90/0/-45/45/45/-45/45/45/-45/45/45/0/90/45/-45]"
15. User Layups "54 [0/90/45/-45/45/-45/0/90/0/45/-45/45/-45/45/-45/0/90/0/-45/45/45/-45/0/90/0/-45/45/45/-45/0/90/0/-45/45/45/-45/45/45/-45/45/45/0/90/45/-45/45/-45/0/90]"
16. User Layups "58 [0/90/0/45/-45/45/-45/0/90/0/90/45/-45/45/-45/45/-45/0/90/0/-45/45/45/-45/0/90/0/-45/45/45/-45/0/90/0/-45/45/45/-45/45/45/0/90/45/-45/45/-45/0/90/0]"
17. User Layups "26 [45/-45/0/90/-45/45/45/-45/0/90/0/-45/45/45/-45/0/90/0/-45/45/45/-45/0/90/0/-45/45/45/-45/45]"
18. User Layups "38 [0/90/0/45/-45/45/-45/0/90/0/-45/45/45/-45/0/90/0/-45/45/45/-45/0/90/0/-45/45/45/-45/0/90/0/-45/45/45/-45/45/45/-45/0/90/0]"
19. User Layups "39 [0/90/0/45/-45/45/-45/45/-45/0/90/0/-45/45/45/-45/0/90/0/-45/45/45/-45/0/90/0/-45/45/45/-45/0/90/0/-45/45/45/-45/45/45/-45/0/90/0]"
20. User Layups "47 [45/-45/0/90/0/90/45/-45/45/-45/45/-45/0/90/0/-45/45/45/-45/0/90/0/-45/45/45/-45/0/90/0/-45/45/45/-45/45/45/-45/45/45/0/90/45/-45]"
21. User Layups "57 [0/90/0/45/-45/45/-45/0/90/0/90/45/-45/45/-45/45/-45/0/90/0/-45/45/45/-45/0/90/0/-45/45/45/-45/0/90/0/-45/45/45/-45/45/45/-45/45/45/0/90/45/-45/45/-45/0/90/0]"
22. User Layups "28 [0/90/0/90/0/-45/45/45/-45/0/90/0/-45/45/45/-45/0/90/0/-45/45/45/-45/0/90/0/0/0/0]"
23. User Layups "29 [45/-45/45/-45/0/90/0/-45/45/45/-45/0/90/0/-45/45/45/-45/0/90/0/-45/45/45/-45/0/90/0/-45/45/45/-45/45/45/-45/45/45/0/90/45/-45/45/-45/0/90/0/90/45/-45]"
24. User Layups "64 [45/-45/0/90/0/90/45/-45/45/-45/45/-45/0/90/0/-45/45/45/-45/0/90/0/-45/45/45/-45/0/90/0/-45/45/45/-45/45/45/-45/45/45/0/90/45/-45/45/-45/0/90/0/90/45/-45]"
25. User Layups "62 [45/-45/0/90/0/45/-45/45/-45/0/90/0/90/45/-45/45/-45/45/-45/0/90/0/-45/45/45/-45/0/90/0/-45/45/45/-45/0/90/0/-45/45/45/-45/45/45/-45/45/45/0/90/45/-45/45/-45/0/90/0/45/-45]"
26. User Layups "27 [0/90/0/90/0/-45/45/45/-45/0/90/0/-45/45/45/-45/0/90/0/-45/45/45/-45/0/90/0/-45/45/45/-45/45/45/-45/45/45/0/90/45/-45/45/-45/0/90/0/0/0/0]"
27. User Layups "25 [0/90/0/90/0/-45/45/45/-45/0/90/0/45/0/90/0/-45/45/45/-45/0/90/0/0/0/0]"
28. User Layups "50 [0/45/-45/0/90/0/90/45/-45/45/-45/45/-45/0/90/0/-45/45/45/-45/0/90/0/-45/45/45/-45/0/90/0/-45/45/45/-45/45/45/-45/45/45/0/90/45/-45/45/-45/0/90/0/45/0/0]"
29. User Layups "51 [45/-45/45/-45/0/90/0/90/45/-45/45/-45/45/-45/0/90/0/-45/45/45/-45/0/90/0/-45/45/45/-45/0/90/0/-45/45/45/-45/45/45/-45/45/45/0/90/45/-45/45/-45/0/90/0/90/45/-45/45/-45]"
30. Graphite/Epoxy "AS4/3502 Typical properties"

## Material properties (typical values used for the reliability based analyses)

### Material Summary (name and \* fields determine unique material)

Description Data entered from MIL-HDBK-17-2E using the \*\* Mean values \*\* TYPICAL average data

### Temperature Dependent Stiffness Properties

Temperature	Tension 0 degrees, Et1	Tension 90 degrees, Et2	Tension Poisson's Ratio, vt12	Compression 0 degrees, Ec1	Compression 90 degrees, Ec2	Compression Poisson's Ratio, vc12
-------------	---------------------------	----------------------------	----------------------------------	-------------------------------	--------------------------------	--------------------------------------

	(Msi)	(Msi)		(Msi)	(Msi)	
72	19.3	1.35	0.3	18	1.41	0.3

Temperature	Tension 0 degrees, Ftu1	Tension 90 degrees, Ftu2	Compression 0 degrees, Fcu1	Compression 90 degrees, Fcu2
-------------	----------------------------	-----------------------------	--------------------------------	---------------------------------

	(ksi)	(ksi)	(ksi)	(ksi)
72	258	7.76	-204	-34.6

### Temperature Dependent Strain Allowable Properties

Temperature	Tension 0 degrees, etu1	Tension 90 degrees, etu2	Compression 0 degrees, ecu1	Compression 90 degrees, ecu2	Miscellaneous ecuoh	Miscellaneous ecuai
-------------	----------------------------	-----------------------------	--------------------------------	---------------------------------	------------------------	------------------------

	(uin/in)	(uin/in)	(uin/in)	(uin/in)	(uin/in)	(uin/in)
72	13367.88	5748.148	-11333.33	-24539.01	-	-

### Temperature Dependent Shear Properties

Temperature	Stiffness In-Plane, G12	Stiffness Interlaminar, G13	Stiffness Interlaminar, G23	Strain Allowable In-Plane, esu12
-------------	----------------------------	--------------------------------	--------------------------------	-------------------------------------

	(Msi)	(Msi)	(Msi)	(uin/in)
72	0.543	0.543	0.543	27255.99

Temperature	Shear In-Plane, Fsu12	Shear Interlaminar, Fsu13	Shear Interlaminar, Fsu23
-------------	--------------------------	------------------------------	------------------------------

	(ksi)	(ksi)	(ksi)
72	14.8	14.8	14.8

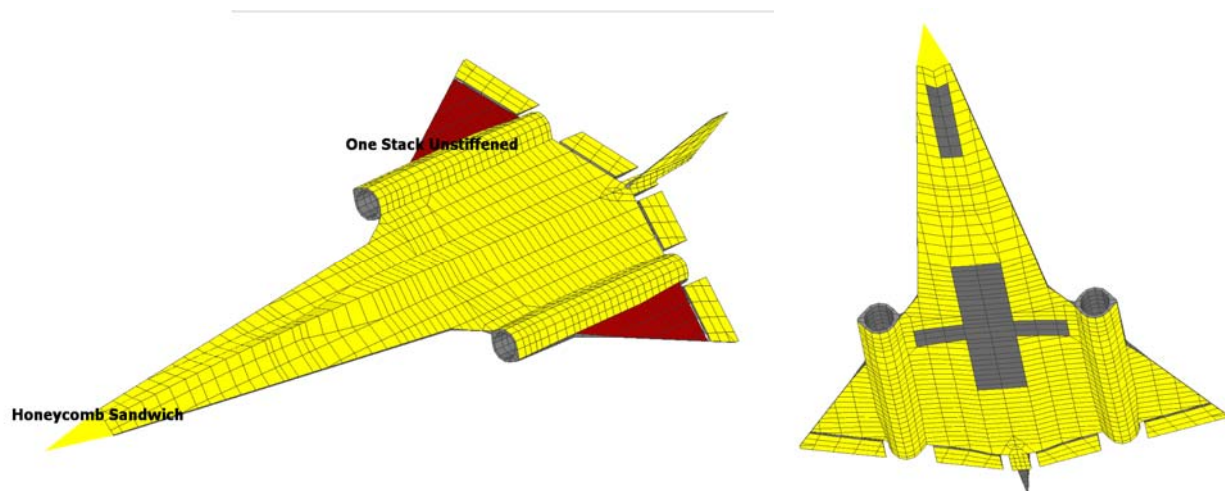


Fig. 10.2, Panel concept for LRSA vehicle analyses. The top surface of the wing (brown color) is unstiffened laminate, with the rest of the airframe honeycomb sandwich (yellow color). Gray represents the weapons and landing gear doors which are not part of the sized assembly.

### 10.3 Failure Analyses Performed

Three failure modes are used in this example: 1) panel buckling, 2) honeycomb sandwich wrinkling, and 3) composite laminate strength (refer to Volume 2, Section 2, 3, 4, and 5 for detailed information on these failure criteria). For composite strength, three failure criteria are turned on: Tsai-Hahn, LaRC03 fiber failure, and LaRC03 matrix cracking. Two CFs per each of these failure analyses documented in Section 9.2 are used. As a summary, they are repeated here, Table 10.3. Refer to Figs. 9.18 and 9.19 for a graphical representation of their PDFs.

Table 10.3, Summary Correlation Factors

Failure mode	$\eta$	$\mu_1$	$\mu_2$	$\mu_3$	$\mu$
<b>Cylindrical Panel Buckling</b>	.136	.3956	-.1144	.8751	.768*
<b>Wrinkling</b>	.102	.59		1,000,000	
<b>Tsai-Hahn</b>	.099	1.013			
<b>LaRC03 Fiber Failure</b>	.1107	.9388			
<b>LaRC03 Matrix Cracking</b>	.157	1.001			

\* an average value from Table 5.7 of Vol 3

If all of the composite strength failure criteria are turned on, now with the CF we can achieve the same % reliability. However we penalize ourselves if we leave on the failure methods that have more uncertainty. So therefore, we recommend using just Tsai-Hahn or perhaps using the Tsai-Hahn interaction criteria together with a phenomenologically based criterion such as LaRC03 that distinguishes between fiber and matrix failure mechanisms. For ply level failure predictions (including unidirectional laminates and  $\pm\theta$  laminates that do not exhibit progressive failure) we suggest to not use Max Strain or Max Stress, Tsai-Hill, etc.

## **10.4 Comparison to 85.1%, 97.7% and 99.86% Reliability Sizing**

Fig. 10.3 illustrates an interesting result. As the reliability criteria is increased, the controlling failure modes change. Failure modes which have the highest observed scatter in test results (a higher statistical standard deviation) will control more as reliability is increased. Therefore the relative width of the PDF as shown in Fig. 9.18, and quantified with the CF  $\gamma_\eta$  (also noted simply as  $\eta$ ), has a larger affect for higher reliabilities because of their greater uncertainty (less confidence). As shown in Table 10.3, wrinkling, Tsai-Hahn, and LaRC03 fiber failure criteria all have  $\eta$  values close to 0.1. Panel buckling has a  $\eta = 0.136$  and LaRC03 matrix cracking composite strength has a  $\eta = 0.157$ . Therefore, as depicted in Fig. 10.3, as the reliability increases, the controlling failure mode goes toward panel buckling (blue) and LaRC03 matrix cracking (red) which have higher  $\eta$  factors and away from honeycomb facesheet wrinkling (green), Tsai-Hahn interaction (yellow), and LaRC03 fiber breakage (brown) failures.

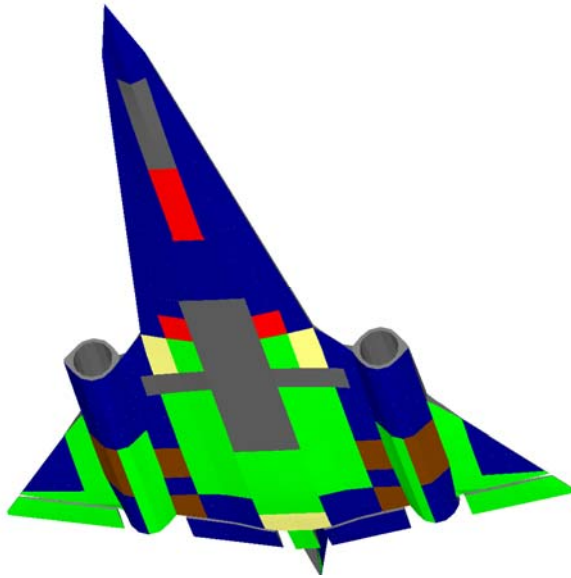
## **10.5 Effect of FEA Statistically Processed Loads**

A  $1\sigma$  FEA loads selection was made to be consistent with the  $1\sigma$  sizing, Fig. 10.3 (a). For illustrative purposes, a  $2\sigma$  FEA selection was used for both the  $2\sigma$  and  $3\sigma$  sizings, Fig. 10.3 (b) and (c). The purpose is to isolate the change in failure mode due to the reliability analysis. In contrast, Fig. 10.4 purpose is to isolate a change in failure mode due to a change in FEA statistical processing.

Referring to the next figure, 10.4(a), even though panel buckling analysis has high uncertainty, (high  $\eta$ ), this failure mode becomes less controlling than in Fig. 10.4(b) where a 3 sigma statistical choice has been made for processing the FEA design-to loads. Panel buckling design-to loads are not influenced as much as strength design-to loads are to concentrated peak forces. Buckling is based on a panel's average loading, whereas material strength and facesheet wrinkling for a panel are controlled by peak loads in the panel. FEA computed peak loads (perhaps at corners) are highly dependent on mesh fineness, load concentrations, etc and therefore have more uncertainty than the average surface area running load. In HyperSizer, not only do the allowables of the failure modes get assigned by the chosen reliability, but so do the processed FEA computed design-to loads. Refer to Section 9.1.1 for more detail about FEA statistical loads.

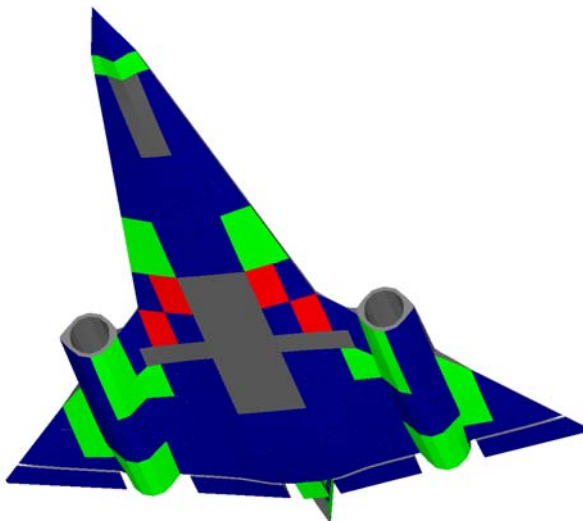
Note the other defined correlation factor,  $\gamma_\mu(\mu)$ , for analysis inaccuracy is constant regardless of a change in reliability. It provides the knockdown to bring the theoretical prediction to the test failure mean, and as such is not affected by the relative width of its PDF which indicates test scatter.

**a)  $1\sigma$  (85.1%) Sizing**  
 **$1\sigma$  FEA loads**



Green = Honeycomb facesheet wrinkling  
Blue = Cylindrical panel buckling  
Red = LaRC03 matrix cracking  
Brown = LaRC03 fiber breakage  
Yellow = Tsai-Hahn

**b)  $2\sigma$  (97.7%) Sizing**  
 **$2\sigma$  FEA loads**



**c)  $3\sigma$  (99.86%) Sizing**  
 **$2\sigma$  FEA loads**

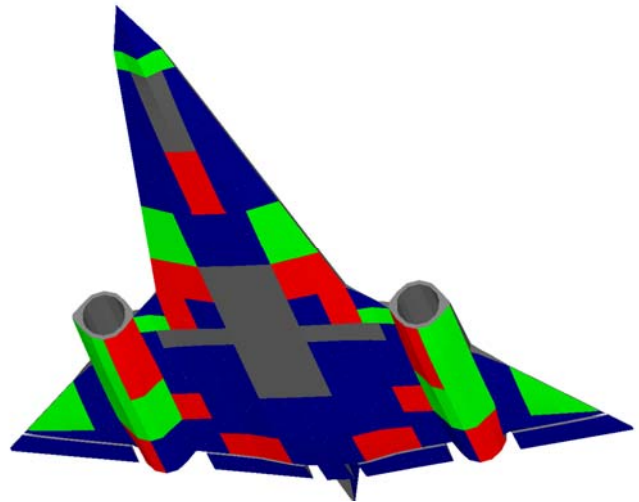
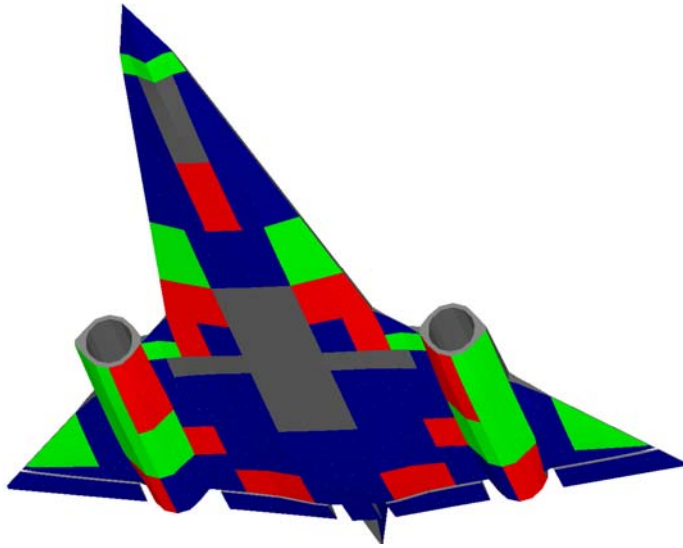


*Fig. 10.3, Effect of varying reliability on controlling failure mode. As the specified reliability increases, the controlling failure modes change. At the lowest reliability ( $1\sigma$  or 85.1%), all activated failure modes are controlling some location of the vehicle, with most of the bottom surface controlled by honeycomb wrinkling. Wrinkling, Tsai-Hahn, and LaRC03 fiber failure criteria all have CFs for test scatter,  $\gamma_\eta$ , close to 0.1. As the reliability increases, the controlling failure mode goes toward panel buckling (blue) at 97.7% reliability and LaRC03 matrix cracking (red) at 98.86% reliability which have increasing test scatter,  $\gamma_\eta$  factors respectively. The gray areas represent structure not sized in this study such as the doors for the main landing gear and the nose gear.*

a)  $3\sigma$  (99.86%) Sizing  
 $2\sigma$  FEA loads



Green = Honeycomb facesheet wrinkling  
 Blue = Cylindrical panel buckling  
 Red = LaRC03 matrix cracking  
 Brown = LaRC03 fiber breakage  
 Yellow = Tsai-Hahn

b)  $3\sigma$  (99.86%) Sizing  
 $3\sigma$  FEA loads

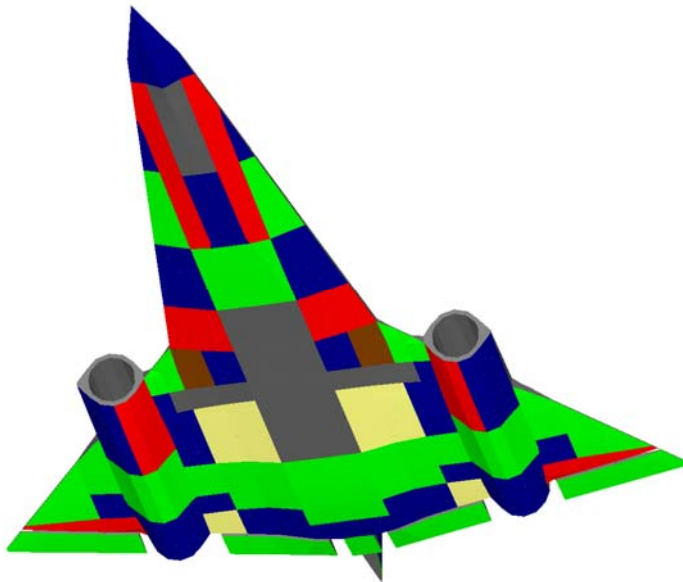


Fig. 10.4, Effect of varying reliability of the FEA loads processing. As the specified reliability of the FEA internal loads increases, the controlling failure modes change. For the  $2\sigma$  FEA loads selection there is a large surface area controlled by panel buckling. At the  $3\sigma$  FEA loads selection the majority of the surfaces are no longer controlled by panel buckling but rather by wrinkling and composite strength. The controlling failure modes are being affected by the higher stress concentrations being statistically determined at the higher reliability ( $k\sigma$  factor). While localized failure modes like wrinkling and composite strength are driven by peak concentrated loads, panel buckling is driven by an average compression load which is less sensitive to peak stresses.

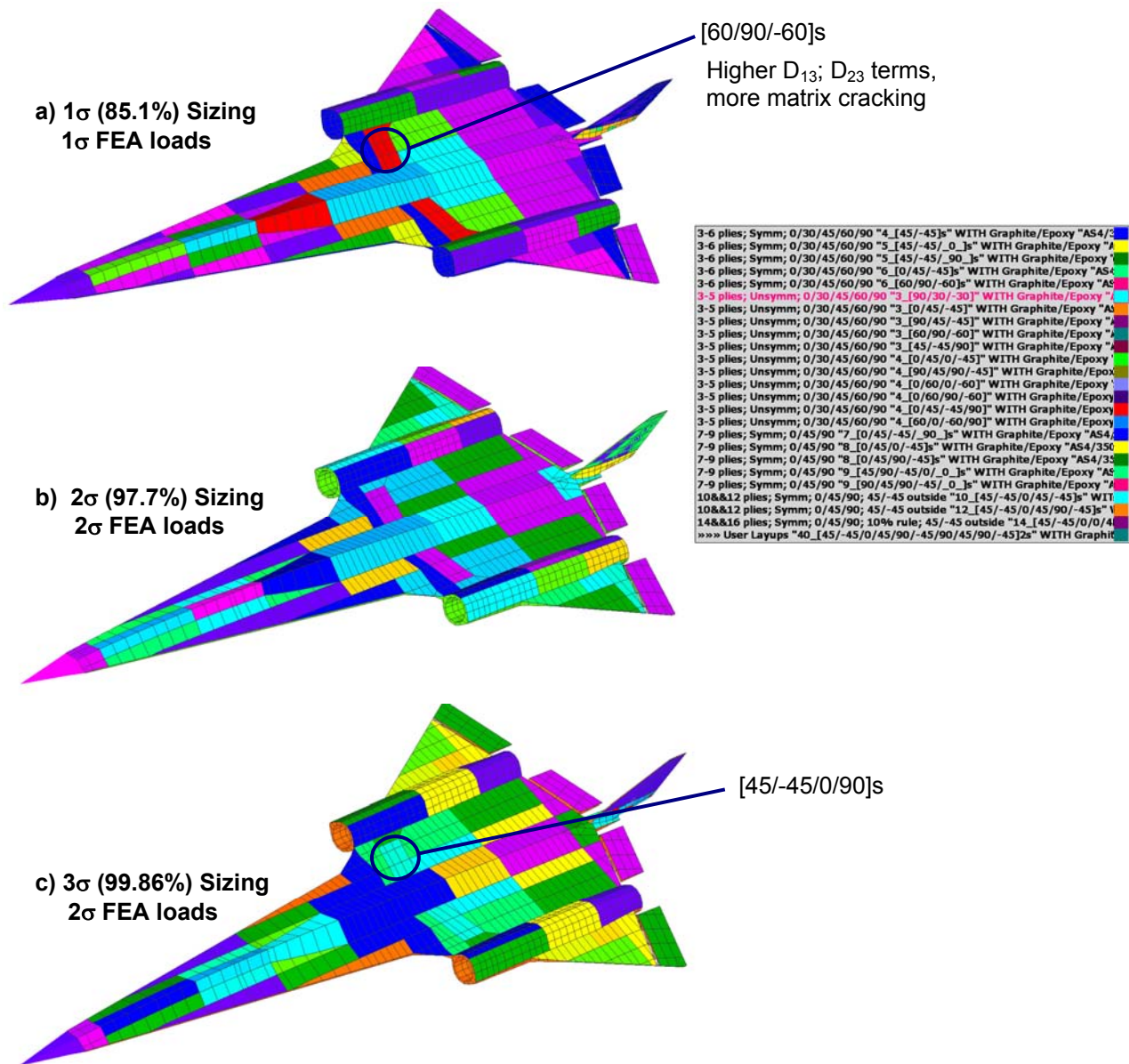


Fig. 10.5, Effect of varying reliability on controlling optimum layup. As the specified reliability increases, the best suited layup varies as indicated by the change in color pattern. Certain layups for a given load of a vehicle location are more efficient and selected by HyperSizer as optimum. However some of those layups may be less confidently used because of their measured variability in strength and as a result not optimum at higher reliabilities.

The test data driven reliability is integrated into the fundamental HyperSizer strength analysis, and as such is automatically influencing the sizing optimizations. Results for several different reliability percentages show not only the weight going up, but also another interesting transition in the optimum layup design, Fig. 10.5. As the optimization attempts to use layups that are dominated by failure modes that exhibit more test data scatter, say for material matrix cracking strength, they will effectively be penalized more and not chosen at higher reliabilities. Therefore, for different required reliabilities the optimization finds different materials and design variables. Each unique combination of variables provides different levels of reliability. Fig. 10.5a shows a [60/90/-60]s is suitable for 85% reliability, but a [45/-45/0/90]s is selected for 99.9% reliability.

## **11 Comparing Analysis Approaches: Traditional Zero Margin-of-Safety versus New Test Data Driven Reliability**

In this section two different examples are presented. The first exemplifies the affect and significance of performing reliability analysis in contrast to the traditional zero-margin-of-safety method used in aerospace industry today. The second example provides a detailed study of the two approaches using a single vehicle component.

### **11.1 Example: Entire Airframe - AFRL Long Range Strike (LRS)**

This example, which uses the Long Range Strike airframe introduced in Section 6, quantifies the relative difference in predicted weights and controlling failure modes between the traditional zero-margin approach and the reliability approach. Refer to Sections 6.6 and 10 for background into this vehicle application.

#### **11.1.1 Significance of Weight Reduction and Increased Airframe Lifetimes without Failure**

In this preliminary design example, it is shown that the traditional zero-margin approach sizes the vehicle weight to be about 9% heavier than the reliability approach if the lifetime airframe failures are the same. By allowing airframe weight to increase, but still be less than the traditional approach, 10 times more airframe lifetimes is achievable. This relationship is depicted in Fig. 11.1. Fig. 11.1 is repeated from Fig. 10.1, but this time with one piece of additional data generated from a traditional zero margin sizing optimization. The blue diamond is the lowest weight achievable using the current aerospace industry structural analysis approach of attempting to bring all failure modes to a zero margin-of-safety and by obtaining conservatism with use of a uniformly applied 1.5 ultimate load factor to all potential failure modes.

For traditional zero-margin analysis, the reliability of material strength (metallic and composite damage initiation) is very high. The use of 'A' or 'B' Basis allowables from MIL-HDBK- 5 and 17 provide substantial conservatism, especially when combined with the 1.5 ultimate load factor. So a material strength failure is not likely to occur in-service, at least not for pristine (undamaged) material. Other failures, such as instability (panel buckling, local buckling, crippling) or honeycomb wrinkling, are more likely to occur in traditional zero margin designs. This is because the same level of conservatism is not built-in to the analysis process for all failure modes.

Table 10.1 is repeated here as Table 11.1 while also including the additional data generated from a traditional zero-margin sizing optimization on the bottom row. Both Table 11.1 and Fig. 11.1 are normalized against the traditional zero-margin result.

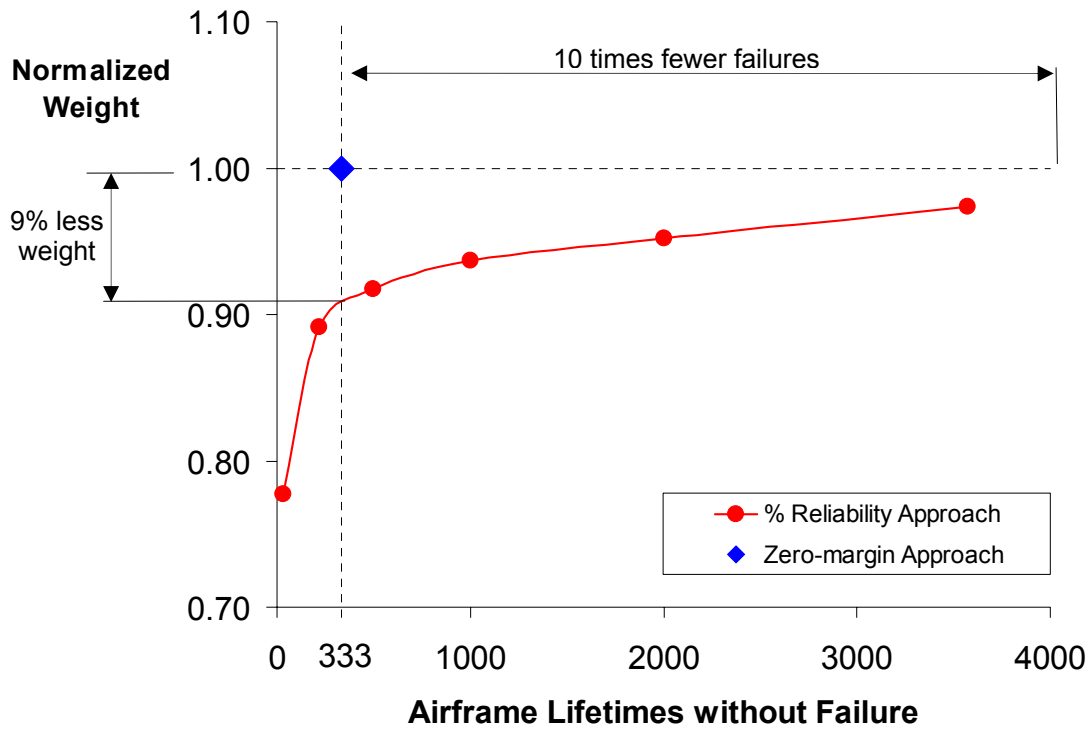


Fig. 11.1, Airframe structural weight versus lifetime failures. Note that the traditional zero-margin analysis (blue diamond) currently practiced in aerospace provides neither acceptable structural integrity nor minimum weight. This data is normalized to the traditional analysis.

**Table 11.1, The New Test Data Driven Reliability Provides Less Airframe Weight and More Structural Integrity**

PDF Standard Deviation	Reliability	Lifetime Airframe Failures	Normalized Weight	Weight Savings
1 $\sigma$	85.1%	1 in 34	.773	22.7%
2 $\sigma$	97.7%	1 in 217	.887	11.3%
2.33 $\sigma$	99.0%	1 in 500	.912	8.8%
2.58 $\sigma$	99.5%	1 in 1000	.932	6.8%
2.81 $\sigma$	99.75%	1 in 2000	.947	5.3%
3 $\sigma$	99.86%	1 in 3571	.969	3.1%
<b>Traditional</b>	<b>98.5%</b>	<b>1 in 333</b>	<b>1</b>	<b>0%</b>

### 11.1.2 Comparison of load factors and material allowables.

The traditional zero-margin sizing is based on the author's experience of current industry practice with structural analysis margin-of-safety reporting. Essentially, the key aspects in contrast to the new reliability approach are summarized in Table 11.2.

**Table 11.2, Contrasting Approaches for the LRS Airframe Analysis.**

Issue	Traditional Zero-Margin Analysis	New Reliability Analysis
<b>Load Factor</b>	1.0 limit* 1.5 ultimate**	1.0 limit* only
<b>FEA Computed Design-to Loads</b>	2 Sigma statistical loading method	2 Sigma statistical loading method
<b>Material Allowable</b>	A or B basis "Design-to" from Mil Handbook 5 or 17	"Typical test" properties (average) from Mil Handbook 5 or 17. Two Correlation Factors that dynamically change with layup optimization.
<b>Panel Buckling</b>	Constant knockdown of 0.85 for all panels and laminates	All panels and laminates have two Correlation Factors that dynamically change with panel spans, radius of curvature, and with thickness and layup sequence.
<b>Sandwich Wrinkling</b>	A required MS of 0.695 was used that is equivalent to the test average knockdown of .59 as described in section 4.	All panels and laminates have two Correlation Factors that dynamically change with core thickness and facesheet layup sequence.

*\* Limit loads are load values that are estimated to occur only once in five vehicle lifetimes.*

*\*\* 1.5 ultimate loads are limit loads increased by 50%. They have no physical basis.*

#### 11.1.2.1 Panel Buckling

Both sandwich panels and solid "plank" laminates are used in the airframe. The vast majority of the sized assembly is honeycomb sandwich. For the 'stiffened' sandwich panels, the industry practice is to use a constant knockdown factor of anywhere between 0.75 and 0.9 as is recommended in [2]. The authors experience is that a 0.85 knockdown is more frequently used during Preliminary Design. So for the traditional zero MS analysis of the sandwich panels, a constant 0.85 is used, and for the reliability analysis, the knockdown of the sandwich is a dynamic function of the panels core thickness, facesheet layups, panel span lengths, and radius of curvature.

#### 11.1.2.2 Sandwich Wrinkling

The traditional analysis is not based on theoretically wrinkling allowables, but instead on the same knocked-down allowable (predicted failure loads) as used in the reliability analysis. This provides a more realistic and fair comparison. An average knockdown of 0.59 equals an equivalent required MS = 0.695, refer to equation (11.17). Refer to Volume 2, Section 2 that summarizes the test data collected and derivation for the relevant CFs.

### 11.1.2.3 Material Strength

#### *Material properties (“B” basis design-to allowables)*

For the traditional analysis, Mil Handbook 17 data was used for the “B” basis design-to allowables. The *design-to* allowables were used for the traditional zero margin analysis and the *typical* material properties used with the reliability analysis. Refer to section 10.2 which lists the typical material properties for AS4/3502. Below is the HyperSizer generated HTML data for the AS4/3502 design-to allowables.

Description	Data entered from MIL-HDBK-17-2E using the ** B Basis** design allowable data					
Temperature Dependent Stiffness Properties						
Temperature	Tension 0 degrees, Et1	Tension 90 degrees, Et2	Tension Poisson's Ratio, vt12	Compression 0 degrees, Ec1	Compression 90 degrees, Ec2	Compression Poisson's Ratio, vc12
	(Msi)	(Msi)		(Msi)	(Msi)	
72	19.3	1.35	0.3	18	1.41	0.3
Temperature	Tension 0 degrees, Ftu1	Tension 90 degrees, Ftu2	Compression 0 degrees, Fcu1	Compression 90 degrees, Fcu2		
	(ksi)	(ksi)	(ksi)	(ksi)		
72	205	6.28	-171	-26.6		
Temperature Dependent Strain Allowable Properties						
Temperature	Tension 0 degrees, etu1	Tension 90 degrees, etu2	Compression 0 degrees, ecu1	Compression 90 degrees, ecu2		
	(uin/in)	(uin/in)	(uin/in)	(uin/in)		
72	10621.76	4651.852	-9500	-18865.25		
Temperature Dependent Shear Properties						
Temperature	Stiffness In-Plane, G12	Stiffness Interlaminar, G13	Stiffness Interlaminar, G23	Strain Allowable In-Plane, esu12		
	(Msi)	(Msi)	(Msi)	(uin/in)		
72	0.543	0.543	0.543	24677.72		

### 11.1.3 Process for calculating reliability for traditional analysis

The process used to reveal the reliability of the traditional zero-margin design was the following.

1) Perform traditional sizing optimization, 2) send that design (optimum variables) to the reliability project, 3) perform a reliability analysis with those optimization variables frozen. This process is defined in five steps.

### 11.1.4 1<sup>st</sup> step, size airframe to zero margins

The Long Range Strike preliminary design is based on achieving positive near zero MS for each structural component of the external surface assembly. This was accomplished by finely adjusting each sizing variable's bounds. Using this resulting design as a basis of comparison, this design was 'frozen' and passed to the new reliability analysis.

HyperSizer was used to perform both the automated failure analyses and sizing optimization. The sizing process generates candidate designs and computes MS for the many potential failures.

If a particular MS analysis was negative, then another candidate design is attempted. This process continues until all vehicle components have positive MS. A goal is to achieve only the amount of margin required. The assumption is that the lightest possible design will have close to zero MS for all failure modes. Therefore, the 1<sup>st</sup> step is to achieve the lowest obtainable weight (as the comparative benchmark) using the traditional zero-margin approach. In reporting the traditional MS, the required MS as entered on the HyperSizer failure tab needs to be accounted. Unlike the panel buckling knockdown factor which has a separate input method; the knockdown for sandwich wrinkling is taken into account by specifying a required MS. For this case, the proper MS to graphically plot is the delta MS, using equation (11.11).

Fig. 11.2 illustrates each airframe component's MS delta. Note that most of the sized assembly, i.e. 73 components out of 83 with margins < 0.25, and the remaining 10 components have margins < 0.5. Therefore this represents a fairly optimum PD.

*User note:* Plotting the delta MS is not yet automated in HyperSizer. The task was accomplished with a separate VB utility called: **Computing Reliability for Traditional Sizing.exe**. A file was generated for import into HyperSizer graphics. The file was saved with the name: *project\_name delta MS.txt* and placed into the project input folder.

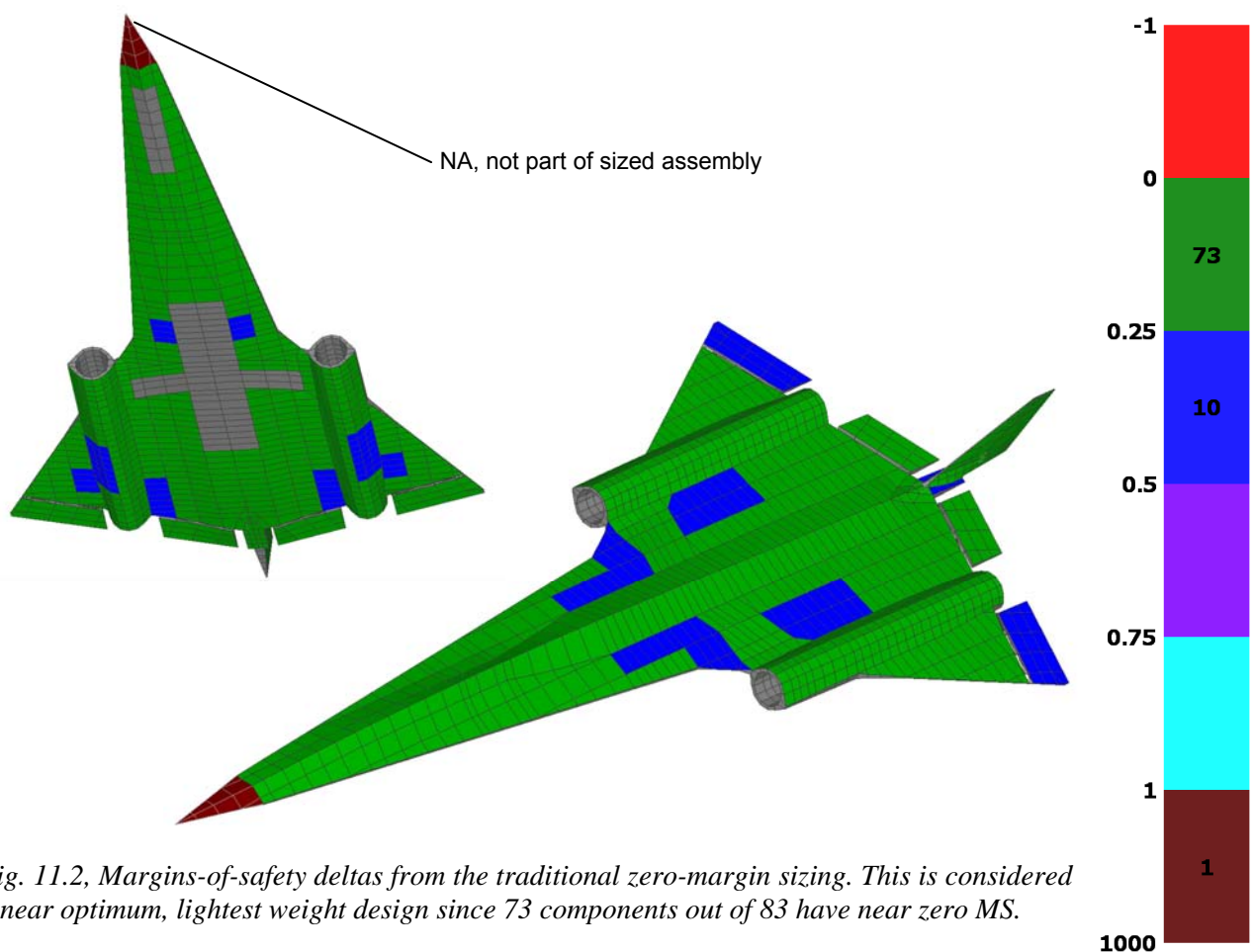


Fig. 11.2, Margins-of-safety deltas from the traditional zero-margin sizing. This is considered a near optimum, lightest weight design since 73 components out of 83 have near zero MS.

### 11.1.5 2<sup>nd</sup> step, pass the traditional optimum variables to the reliability analysis

Once the optimum LRS preliminary design has been established, the next step is to pass the state of the design to the reliability analysis. In essence, the sizing variable optimum values are sent to the reliability analysis and the reliability analyses treats them as “frozen”, where no further sizing optimization is performed. Fig. 11.3 illustrates the optimum layups that are frozen.

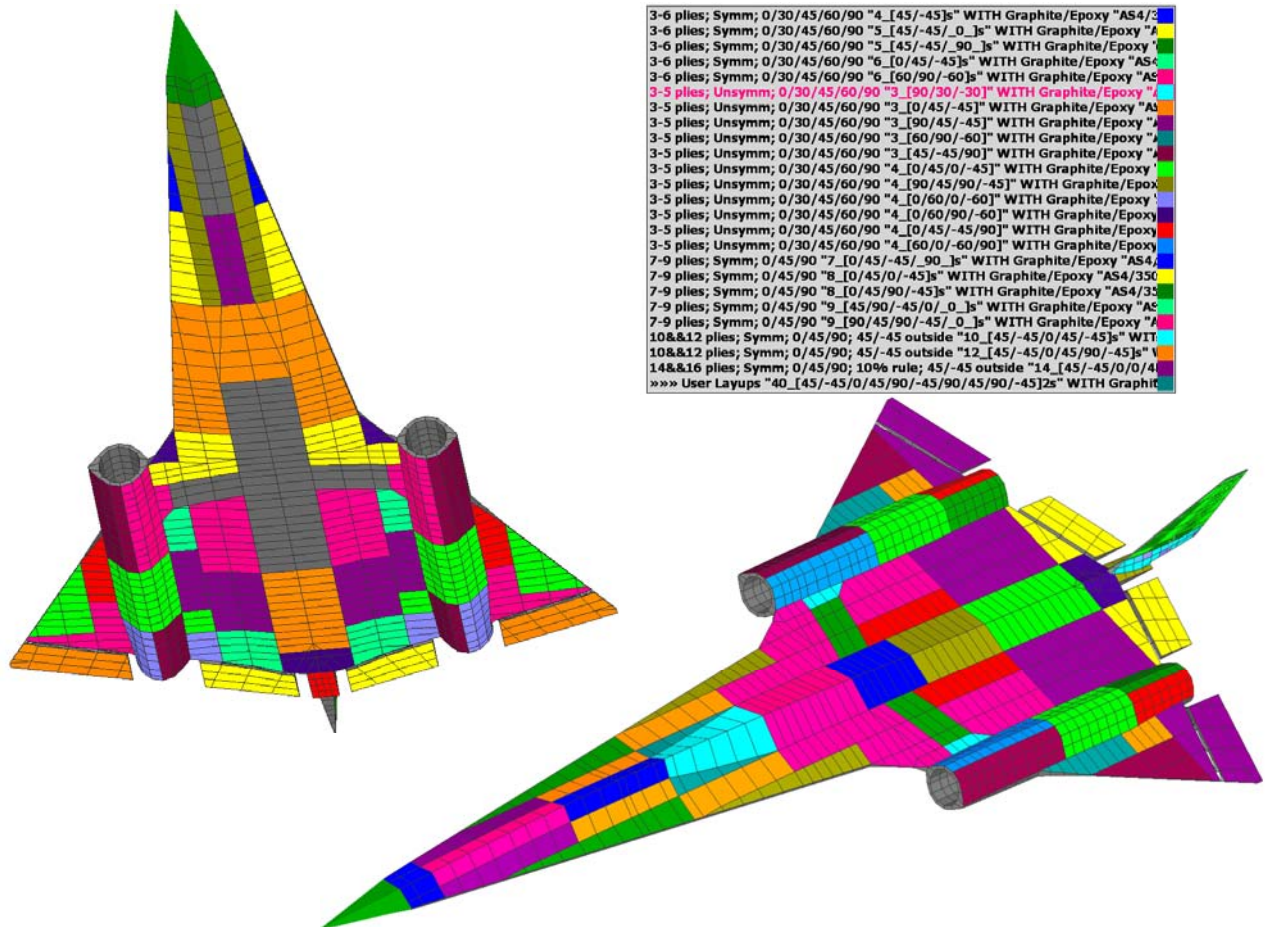


Fig. 11.3, Optimum layup from the traditional zero-margin sizing. This design is sent to the reliability analysis.

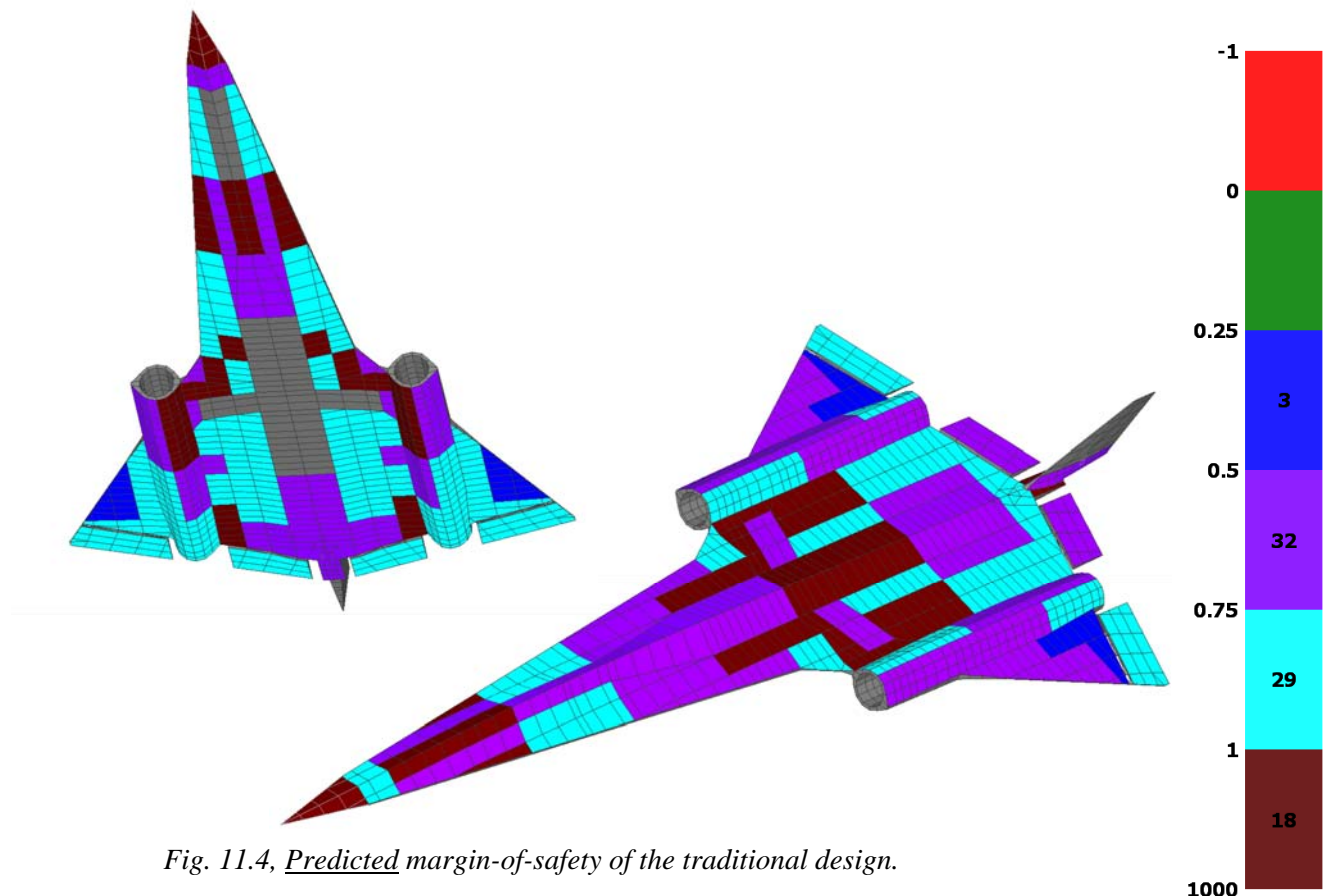
**User note:** Passing in the traditional optimum variables (frozen design) to the reliability analysis for each airframe component is a non-standard capability, infrequently performed and therefore not chosen to be automated in HyperSizer. The task was accomplished with a separate VB utility and spreadsheet called: **Component Optimum Design Candidate Number.xls**. A file was generated with the VB utility for import into HyperSizer analysis software as a back door file. This file needs to be set as read only. The file was saved with the name: **project\_name.HBD** and placed into the project input folder.

### 11.1.6 3<sup>rd</sup> step, perform reliability analysis on the traditional design and compute true margins

As introduced in several pages of Section 2.4.2, of this Volume I, the newly defined CFs for the failure modes of composite laminate strength, panel buckling, and honeycomb sandwich wrinkling were used for a reliability analysis of the AFRL Long range Strike airframe. After the traditional design is passed into the reliability analysis, the next step is to compute true MS. In this definition, true MS are those that are based on specific test data derived CF's. Even though the same variables from the traditional design were used in the reliability analysis, including the same FEA computed internal loads, different MS are established.

Fig. 11.4 quantifies the MS based on *predicted* failure loads. Predicted failure loads are the statistically determined average failure load = ( $\mu$  \* theoretical failure). Refer to Fig. 2.5. Therefore predicted MS are those without considering test scatter and as such without any conservatism. Most of these MS range from 0.5 to 1.0.

Fig. 11.5 quantifies the MS based on *allowable* failure loads. Again referring to Fig. 2.5, these include a level of safety based on the user's choice of reliability. The choice for this LRS preliminary design was to use a 99.5% reliability which translates into 1 in 1000 lifetime airframe failures. Refer to Table 10.1. At this required reliability, Fig. 11.5 identifies nine structural components on the airframe which the traditional zero margin design fail this criterion, as indicated in red color for a negative MS.



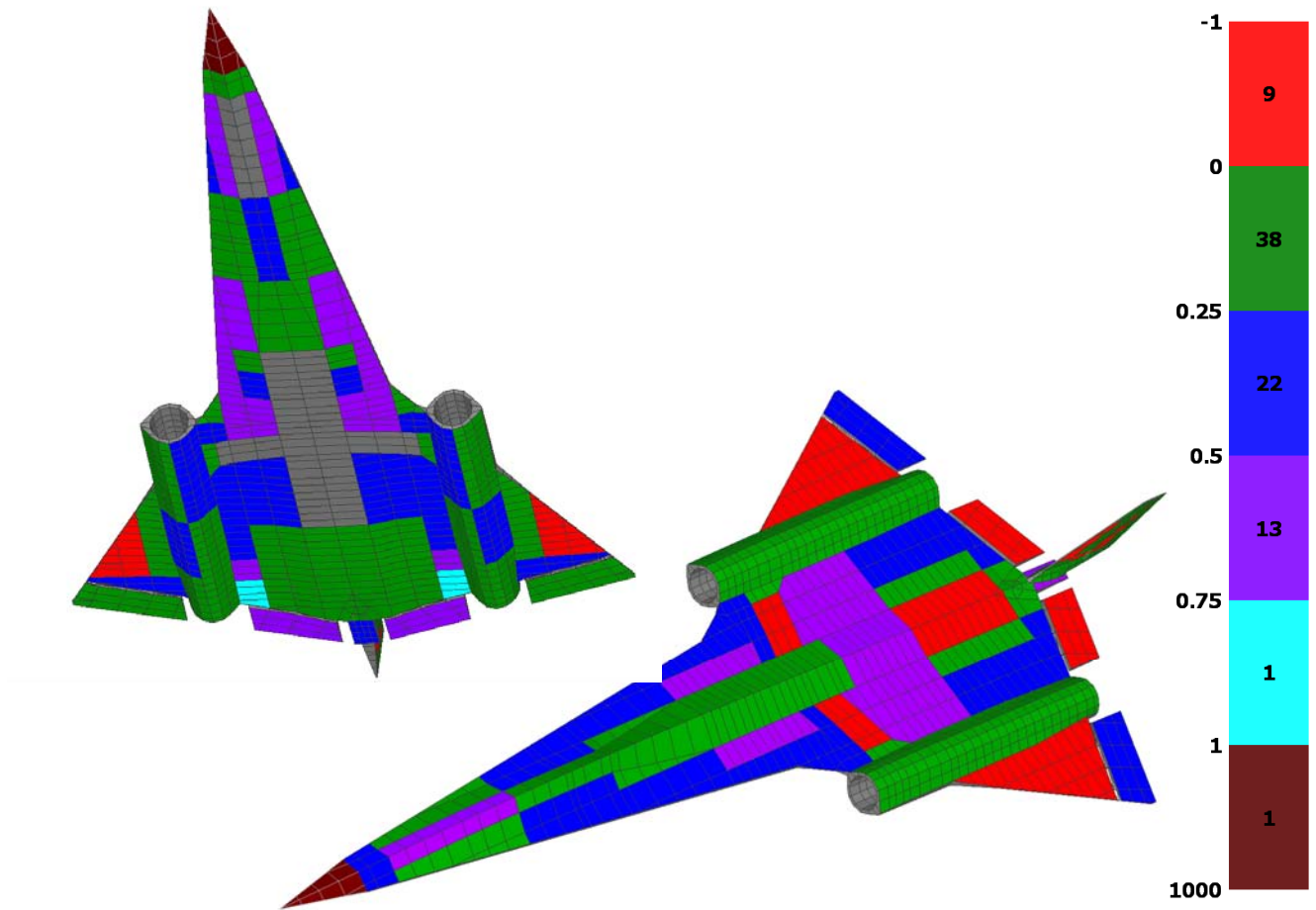


Fig. 11.5, 99.5% Reliability margin-of-safety of the traditional design.

#### 11.1.7 4<sup>th</sup> step, back out reliability for each airframe component

Note: Refer to section 11.2 for a derivation of the equations and a detailed example of the process for backing out the reliability from a traditional analysis. Highlighted here is the significance of doing so as demonstrated on the LRS airframe. As a quick summary, section 11.1.6 quantifies the true MS of the Long Range Strike preliminary design. This section presents the reliability of each structural component. Identified are areas of the vehicle sized the traditional way that result in an unexpected and unacceptable low reliability.

The margins of the traditional design are shown to be consistently near the desired value of zero in Fig. 11.2, but were determined by the developed reliability analysis to be inconsistent as depicted in Fig. 11.5. Though most were significantly greater than zero (i.e. 35 components out of 82 > 0.25 MS), nine were negative. Fig. 11.6 identifies the reliability of each structural component to the seven loadcases. Again the inconsistency of the traditional design is obvious. 65 out of 82 structural components have a reliability > 99.9% causing the weight of the airframe to be heavier than necessary.

Using the lowest margin of any failure mode, for any component, the airframe reliability was backed out of the HyperSizer analysis to equal **98.5%**. This equates to  $(1 / (1 - .985)) = 66.6$ ,

which implies 1 in 66.6 vehicles will fail due to the design limit loading. However, DLL is statistically predicted to occur once in five (1 in 5) vehicle lifetimes. Therefore, the probability of failure for this approach is 1 in 333,  $(5 \times 66.6) = 333$ . Based on the few known actual in-service structural failures, this appears to be low. We postulate that the magnitudes of the limit loads are also likely conservative, meaning airframes likely experience limit loads less than predicted by the loads group. Therefore, in-service operation loads using the traditional zero-margin approach likely provides more than 1 in 333 lifetime airframe failures.

*User note: Backing out reliability of traditional zero-margin sizing for each airframe component is a non-standard capability, infrequently performed and therefore chosen not to be automated in HyperSizer. The task was accomplished with a separate VB utility called: **Computing Reliability for Traditional Sizing.exe**. A file was generated for import into HyperSizer graphics. The file was saved with the name: `project_name_traditional_reliability.txt` and placed into the project input folder.*

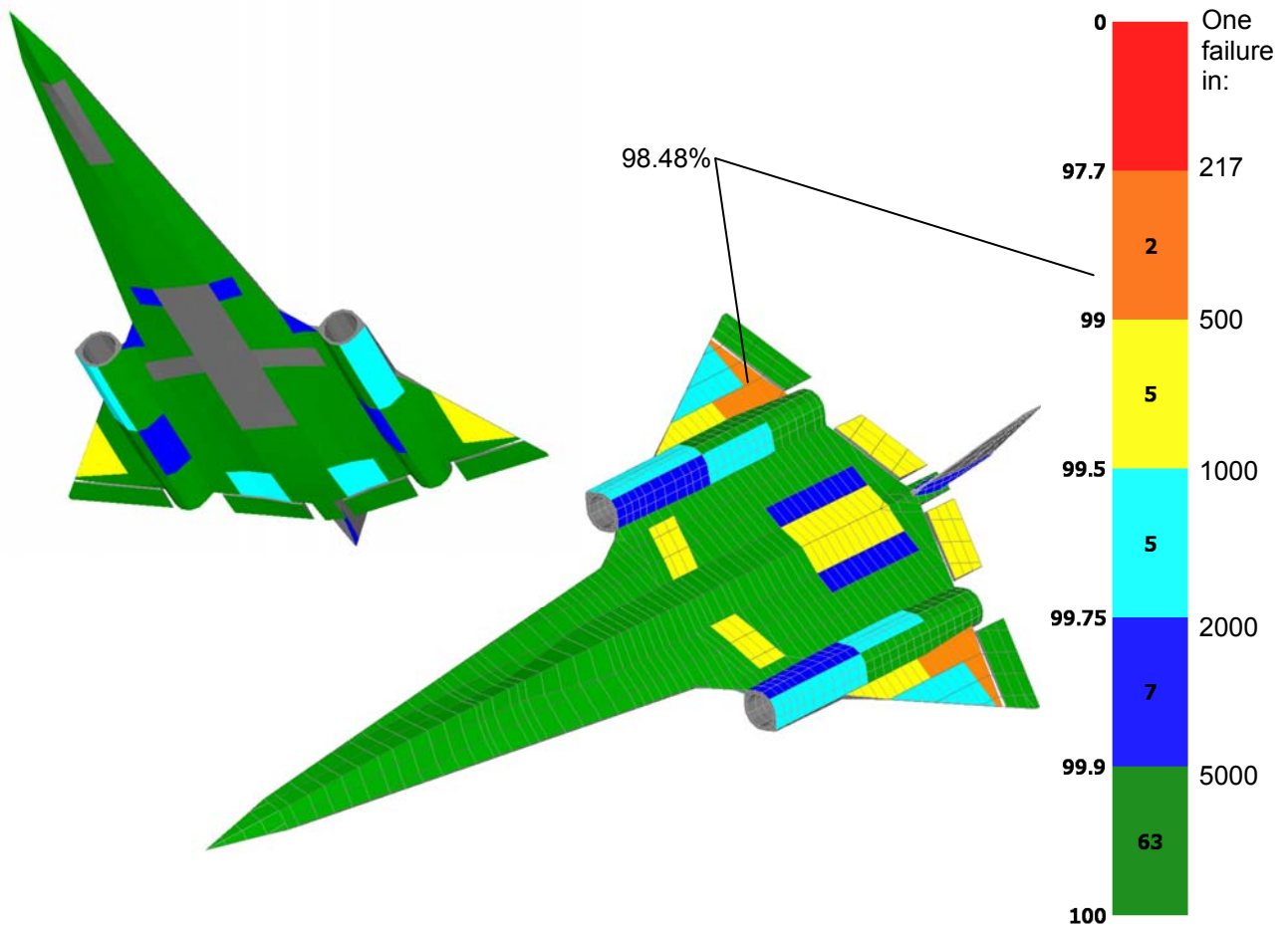


*Fig. 11.6, The traditional zero-margin sizing approach cannot produce consistent structural integrity. The major concern is the areas of the vehicle identified in orange. These two structural components have less than 99% reliability.*

As a summary, shown in Fig. 11.7 are four LRS images where red color identifies areas of the airframe that have unacceptable safety based on two different lifetime criteria. As the criteria goes from 1 in 1000 failures to 1 in 2000 failures, as expected, more area shows up red.

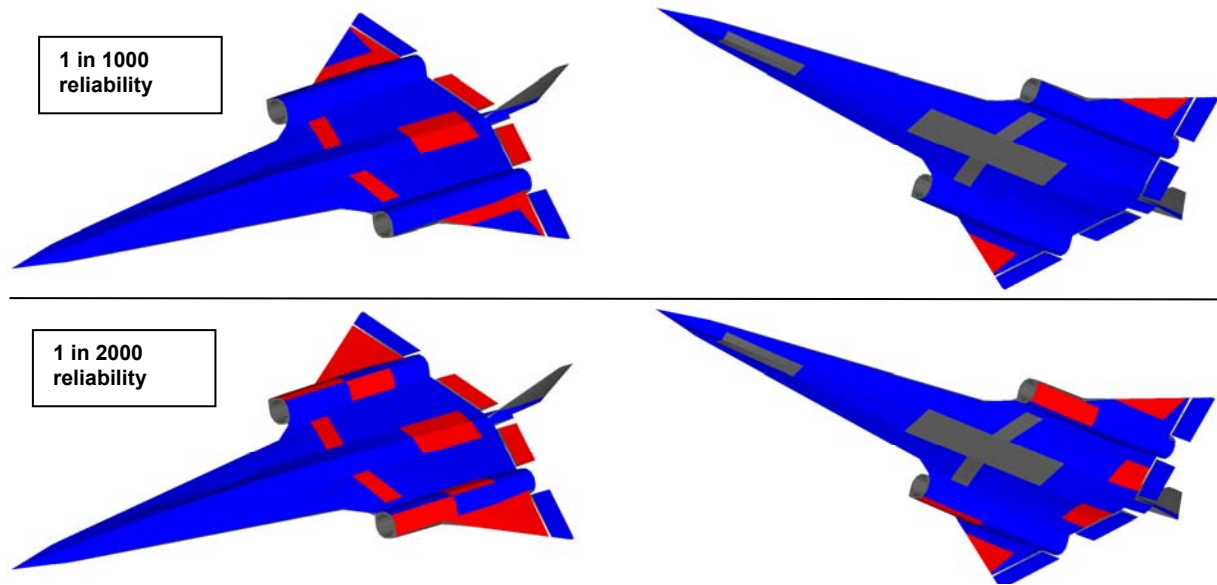


*Fig. 11.7, The traditional zero-margin sizing approach cannot produce consistent structural integrity. The major concern is the areas of the vehicle identified in red. These are panel components that have less than 99.5% (1 in 1000) reliability top images and 99.75% (1 in 2000) reliability bottom images. The left images are the top of the LRS aircraft and the right images are the bottom. Gray color are unsized areas.*

#### 11.1.8 5<sup>th</sup> step, compare controlling failure analyses and load cases

The last step is informational and useful for a more in-depth understanding. Fig. 11.8 shows how the controlling failure analyses differ between the traditional and reliability analyses. Even though the same variables from the traditional design were used in the reliability analysis, including the same FEA computed internal loads, a different set of controlling failure modes are identified. Note primarily how the composite strength criteria for matrix cracking (an analysis with relatively high uncertainty) controls for the reliability analysis while Tsia-Hahn and fiber breakage (analyses with relatively high confidence) controls for the traditional.

Though using the same design and loads, the reliability analysis also identified (per each structural component) different controlling load cases, Fig. 11.9. The traditional analysis indicates the “3g begin cruise” load condition as more controlling while the reliability analysis indicates a larger influence by the taxi bump load condition.

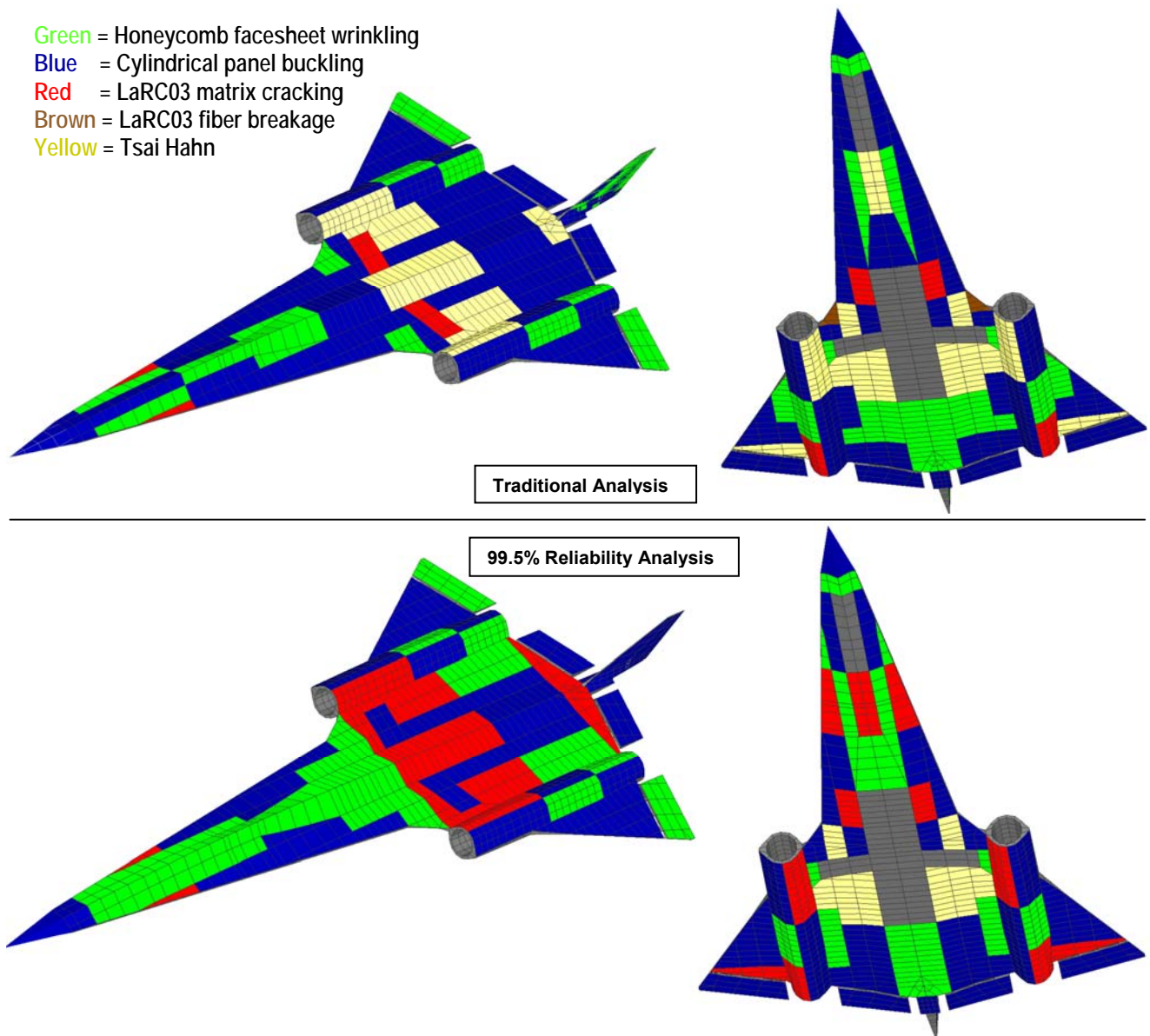
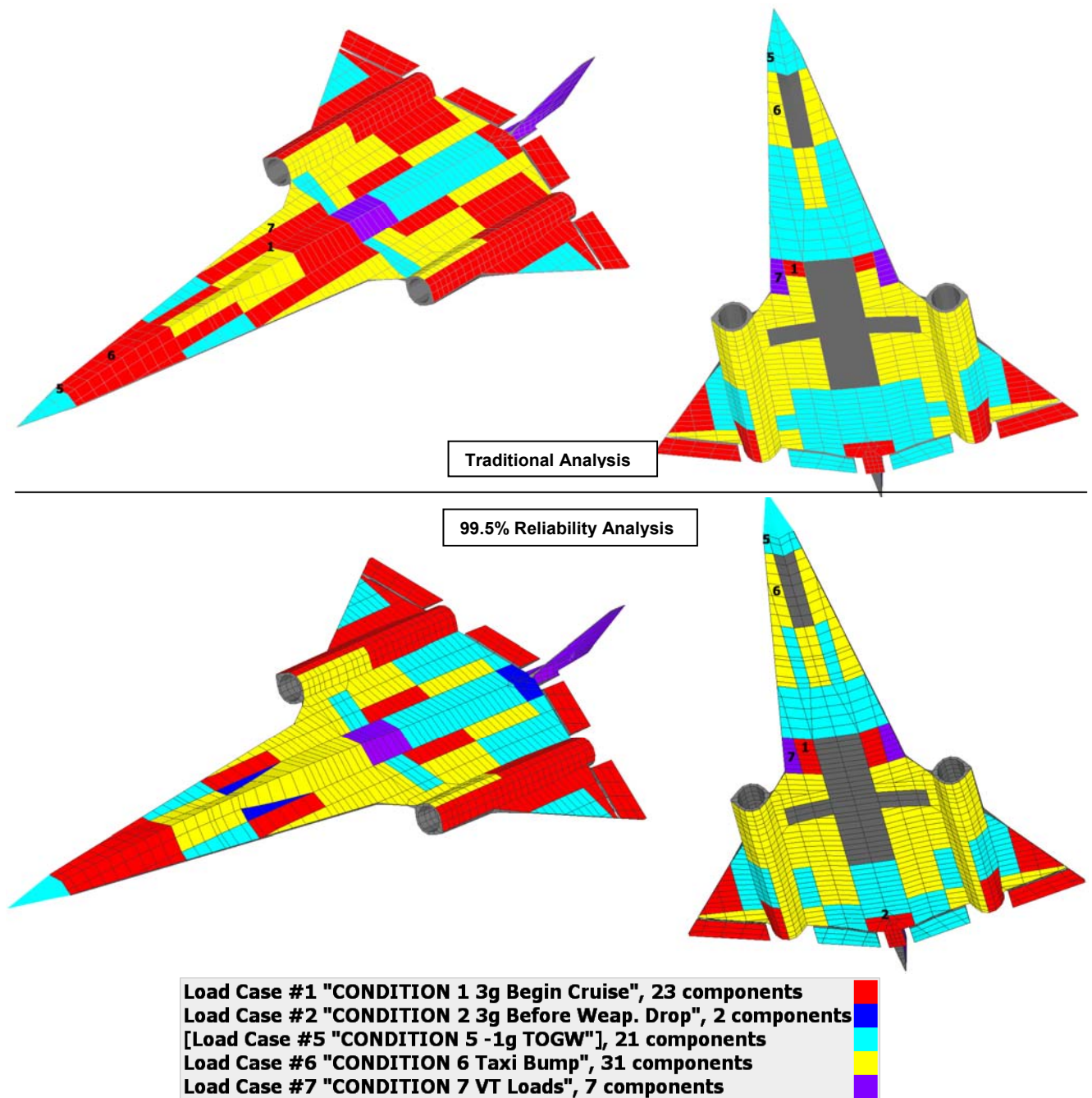


Fig. 11.8, Compared are the controlling failure modes between the traditional zero-margin approach versus a 99.5% reliability analysis using the same design. Traditional design on top, reliability on bottom.



*Fig. 11.9, Compared are the controlling load cases between the traditional zero-margin approach versus a 99.5% reliability approach. Traditional design on top, reliability on bottom. The traditional analysis indicates the 3g begin cruise load condition as more controlling while the reliability analysis indicates a larger influence by the taxi bump load condition.*

## 11.2 How to Back Out Reliability of Traditional Zero-Margin Analysis

In this section a standalone example is presented to bridge the traditional approach to the new test data driven reliability. The traditional approach is based on a limit load factor of 1.0, an ultimate load factor of 1.5, and with all of the failure modes being analyzed deterministically to the same 0.0 margin-of-safety. The new approach assigns, in effect, a different required margin-of-safety for each failure mode. Each failure mode's required margin is based on achieving the same % reliability against failure. In this way, consistency is achieved in that all failure modes are targeted to the same chosen level of structural integrity.

To quickly grasp the comparison between the traditional margin of safety and the reliability margin of safety, visualize the possible “load” for a particular structure on a continuous line as shown in Fig. 11.10. The load shown on the top corresponds to the traditional margin of safety analysis, while the load shown on the bottom corresponds to the new reliability analysis.

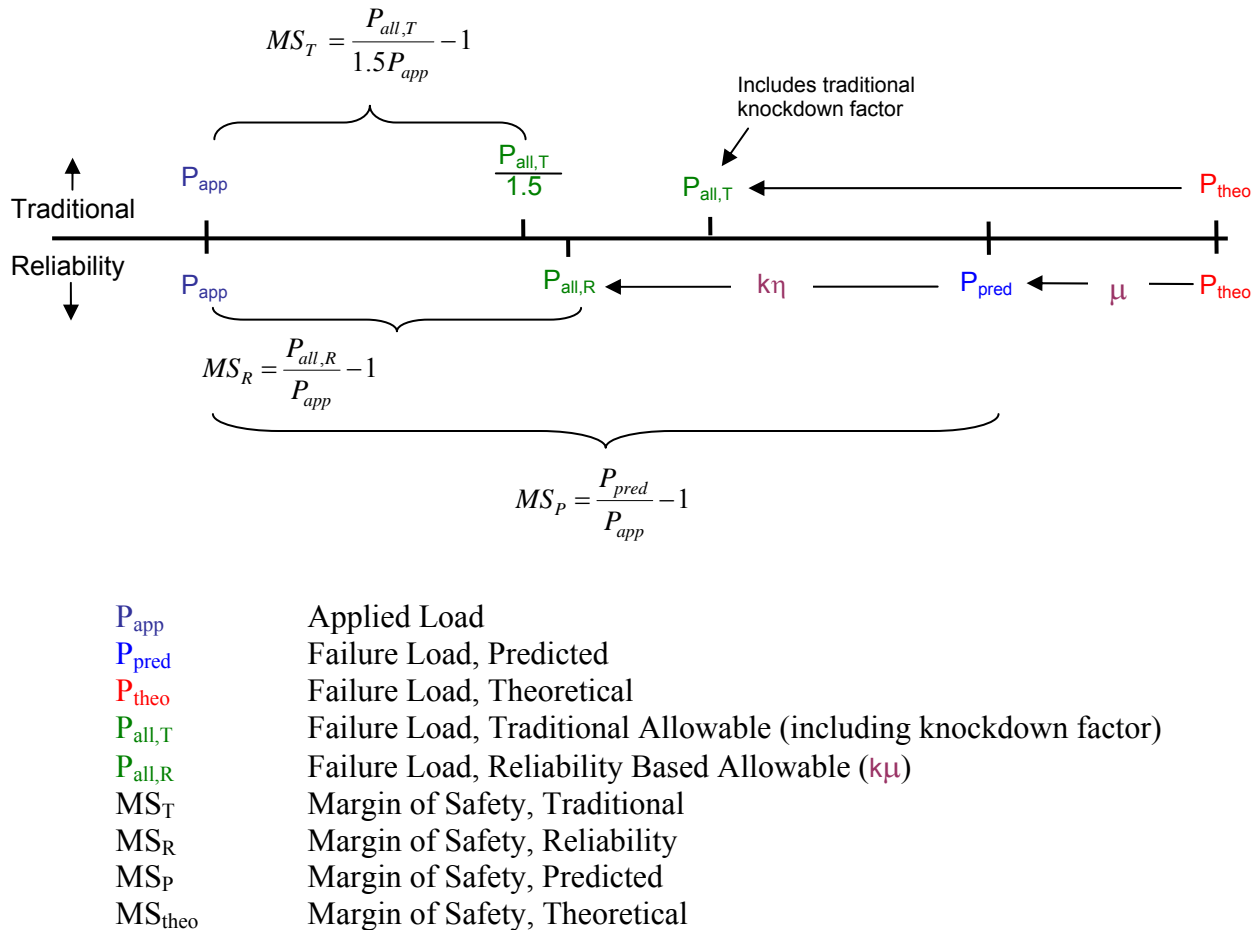


Fig. 11.10, The way allowable loads are determined for the two approaches. Top is traditional zero-margin approach. Bottom is reliability approach. Relative distances on horizontal load line are meaningful. Theoretical shown on right is highest value. Applied load is on left.

The applied load,  $P_{app}$ , is the same for both traditional sizing and reliability sizing as is the theoretical load,  $P_{theo}$ . The predicted load,  $P_{pred}$ , is that load that results from a knockdown on the theoretical load that comes from a statistical analysis of test data. In other words, it is the average of the test failure loads. Relative distances on the horizontal load line are meaningful, i.e. somewhat to scale. We expect that most structural components will have a  $P_{all,R}$  greater than  $P_{all,T}/1.5$  which is the traditional allowable load divided by the ultimate load factor of 1.5. That is the traditional analysis will produce more conservatism than necessary for most components (with a few components dangerously unconservative). Likewise, we expect for most cases that  $MS_R > MS_T$ , as depicted in Fig. 11.10.

On the traditional side, the traditional, allowable load,  $P_{all,T}$  is the load obtained by multiplying the theoretical load by a traditional knockdown factor, such as 0.85 for flat sandwich panel buckling. To determine the traditional margin of safety, the applied load is multiplied by some load factor (typically 1.5 for ultimate loads) and compared to the traditional allowable load. Another way of looking at this is that the traditional allowable load is divided by 1.5 and compared to the applied load. Either way, this gives,

$$MS_T = \frac{P_{all,T}}{1.5P_{app}} - 1 \quad (11.1)$$

On the reliability side, the standard deviation of a set of test data,  $\sigma$ , is determined and normalized against the average test failure load ( $P_{pred}$ ). The normalized standard deviation of the test data is denoted as  $\eta = \sigma / P_{pred}$ . This parameter,  $\eta$ , is one of the two correlation factors identified earlier for the reliability analysis. The allowable load for a given reliability is then,

$$P_{all,R} = P_{pred}(1 - K_R\eta) \quad (11.2)$$

where  $K_R$  is the user-specified number of standard deviations corresponding to a particular reliability. The predicted and reliability margins of safety are

$$MS_P = \frac{P_{pred}}{P_{app}} - 1 \quad MS_R = \frac{P_{all,R}}{P_{app}} - 1 \quad (11.3)$$

We can determine the reliability of the traditional allowable load by comparing it to the predicted load, just as the reliability allowable was compared to the predicted load in Equation (11.2). We can then solve for a new factor,  $K_T$  which will give the reliability of the traditional allowable. Fig. 11.11 portrays this process graphically.

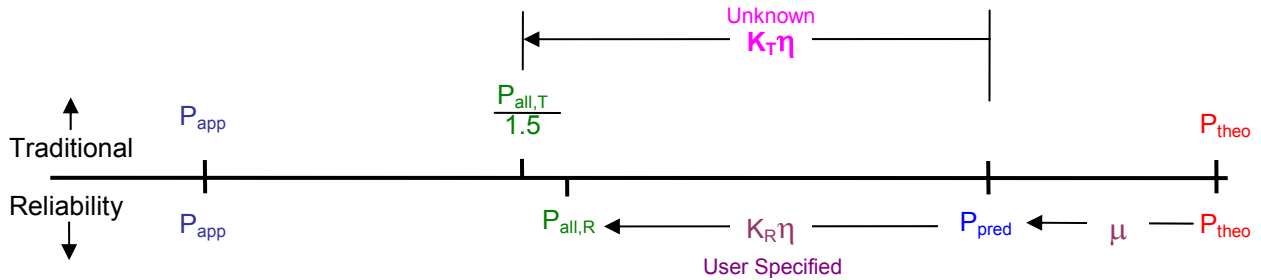


Fig. 11.11, A graphical representation of how the reliability of the traditional allowable is backed out.

Repeating equation (11.2), but replacing  $P_{all,R}$  with  $P_{all,T}/1.5$  and replacing  $K_R$  with  $K_T$ ,

$$\frac{P_{all,T}}{1.5} = P_{pred}(1 - K_T\eta) \quad (11.4)$$

$$K_T = \frac{P_{pred} - P_{all,T}/1.5}{P_{pred}\eta} \quad (11.5)$$

The “load” of a given structure is the combination of biaxial, bending and shear loads, and not a single load value. The margin of safety, however, is a single quantifiable value, which is also a primary HyperSizer output. Therefore using Equations (11.1) and (11.3), we can rearrange (11.5) to solve for  $K_T$  in terms of margins of safety.

$$K_T = \frac{P_{app}((MS_P + 1) - (MS_T + 1))}{P_{app}(MS_P + 1)\eta} \quad (11.6)$$

$$K_T = \frac{MS_P - MS_T}{(MS_P + 1)\eta} \quad (11.7)$$

Next we solve for  $\eta$  by combining equations 11.2 and 11.3,

$$MS_R + 1 = (MS_P + 1)(1 - K_R\eta) \quad (11.8)$$

$$\eta = \frac{MS_P - MS_R}{K_R(MS_P + 1)} \quad (11.9)$$

substituting  $\eta$  back into (11.7) gives

$$K_T = \frac{K_R(MS_P - MS_T)}{MS_P - MS_R} \quad (11.10)$$

The traditional sizing margin-of-safety can further be changed by using a non-zero “required margin-of-safety”. For example, it is customary for aircraft programs to specify a required  $MS=0.25$  for joint strength analysis, especially when the joint is bonded composite [4 and 5]. If this is the case, any margin of safety less than this required margin is considered to be failure. If a required margin of safety is used, then any comparisons done should not use the margin of safety calculated from the allowable load, but should rather use the delta between the calculated margin of safety and the required margin.

$$MS_T\Delta = \frac{(MS_T + 1)}{(MS_{required} + 1)} - 1 \quad (11.11)$$

To determine the actual reliability of a particular structure that is sized by the traditional method is fairly straightforward. First, the variables, concepts and materials from the traditionally sized

structure are “frozen” and passed to a HyperSizer reliability analysis, without performing a sizing. Next, a reliability is chosen, such as 97.7% ( $K_R=2$ ) and the HyperSizer analysis is performed for this structure. The comparative  $K_T$  value is then calculated from Equation (11.10), where  $MS_T$  is replaced by  $MS_T\Delta$

$$K_T = \frac{K_R(MS_P - MS_T\Delta)}{MS_P - MS_R} \quad (11.12)$$

Once  $K_T$  is calculated, the reliability can be solved using the cumulative probability density function,  $\Phi$ , of a normal distribution. This function is from [20]

$$\Phi(K) = \frac{1}{\sqrt{2\pi}} \int_{-\infty}^K e^{-\frac{t^2}{2}} dt \quad (11.13)$$

or

$$\Phi(K) = \frac{1}{2} \left[ \text{erf}\left(\frac{K}{\sqrt{2}}\right) + 1 \right] \quad (11.14)$$

where  $\text{erf}$  is the so-called “error function” which can be found in any mathematical handbook to be defined as

$$\text{erf}(x) = \frac{2}{\sqrt{\pi}} \int_{-\infty}^x e^{-t^2} dt \quad (11.15)$$

Finally, the reliability,  $R$ , which is defined as  $R = 1 - \Phi$ ,

$$R = \frac{1}{2} \left[ 1 - \text{erf}\left(\frac{K}{\sqrt{2}}\right) \right] \quad (11.16)$$

can be solved using built-in functions for  $\text{erf}$  in Microsoft Excel or MATLAB or using math libraries available for Fortran or C. A graphical representation is provided in Fig. 11.12.

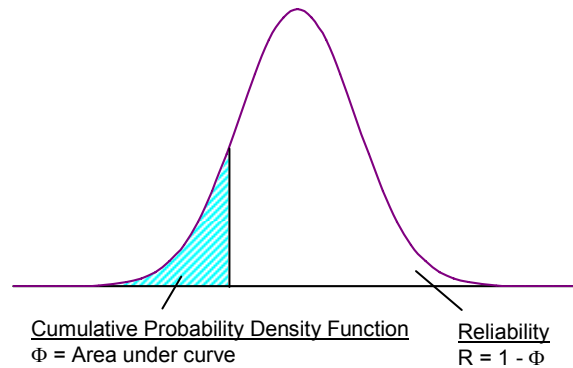
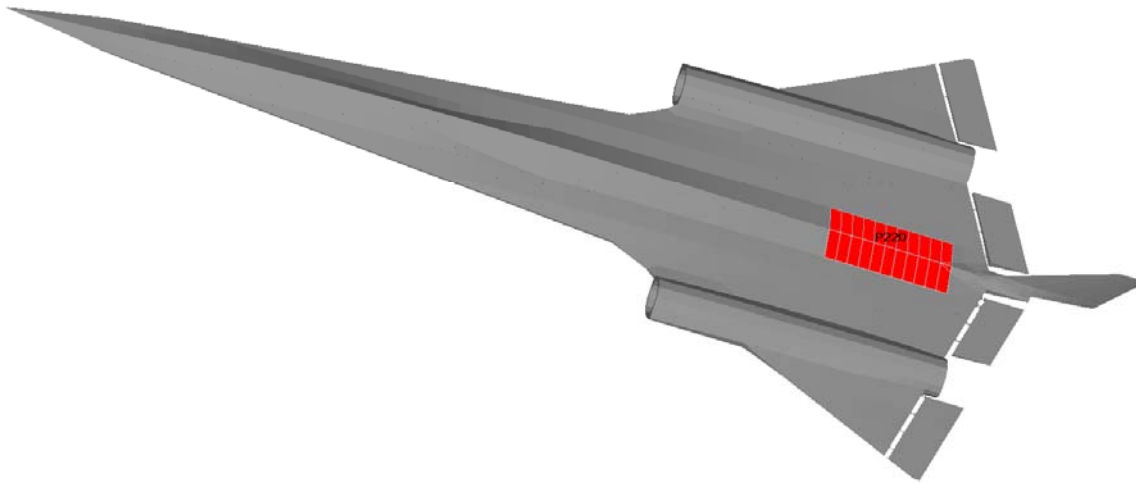


Fig. 11.12, A one sided depiction of reliability of a normal distribution.

### 11.3 Example: Single Airframe Location - A Detailed Comparison

This example compares in detail the two analysis approaches, and shows how to back out the traditional sizing reliability, calculate an effective knockdown, and how to calculate an effective required MS.



*Fig. 11.13, A single airframe location - component 220, used for the detailed example.*

#### 11.3.1 Comparing the two analysis methods

Comparing the two analysis methods is a bridge for understanding from the old to the new approach. The demonstration failure analysis chosen is honeycomb sandwich facesheet wrinkling. An introduction to the test data and process followed to quantify proper correlation factors for facesheet wrinkling analysis is provided in **Volume 2, Section 2**.

Volume 2, Section 5 provides much more detail in comparing traditional and the new test data driven reliability analysis. The selected failure analysis documented in Section 5 is panel buckling. Including are detail discussions on the panel buckling knockdown equation from NASA technical report SP8007.

First, results for the traditional analysis are shown, and then for the same design, the reliability analysis is shown.

Note: The detailed example shown here considers a single failure mode, wrinkling, only. Because wrinkling was not the controlling failure mode for component 220, the backed out reliability does not match that shown in Fig. 11.6, which considers all failure modes. For the controlling failure mode of panel buckling, the backed out reliability was approximately 99.5%.

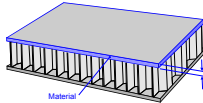
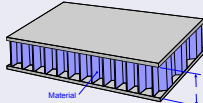
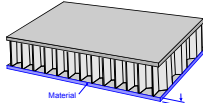
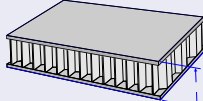
### 11.3.1.1 Traditional sizing with ultimate load factor = 1.5.

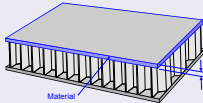
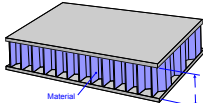
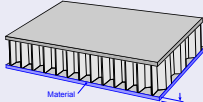
Project = LRS Traditional Sizing

Component = 220

A typical HyperSizer sizing optimization was performed for component 220 to all seven loadcases. The optimum unit weight = 0.3588 psf. The optimum design follows as a HyperSizer generated HTML.

Component Summary	
Unit Weight (lb / ft^2)	0.3587865
Area (ft^2)	77.93096
Weight (lb)	27.96058
Controlling Load Case	5
Controlling Limit or Ultimate	Ultimate
Controlling Failure Mode Type	Strength
Controlling Analysis Description	Panel Buckling, Curved, Simple, Fixed or Free BC
Margin of Safety	0.0226277
Component Loading Factors, Loading Methods, and Buckling Conditions	
User Defined Loading	NO
FEA Statistical Loading Method	2-Sigma
Load Factor Ultimate Mechanical	1.5
Load Factor Limit Mechanical	1
Buckling X-Span (in)	20
Buckling Y-Span (in)	46.34976
Buckling Knockdown Factor	0.85
Buckling Panel is Curved	YES
Buckling Shape	External, Y Curvature
Buckling Curvature (in)	241.0573
Buckling Panel is Full Cylinder	NO
Buckling Side X (+)	SIMPLE
Buckling Side X (-)	SIMPLE
Buckling Side Y (+)	SIMPLE
Buckling Side Y (-)	SIMPLE
Superimpose Local Effects onto Facesheet Spans	YES
Superimpose Panel Effects	YES
Superimpose Boundary Conditions	FIXED
Zero Out FEA Computed Panel Moments	YES

Variable Designs									
	Design	1	2	3	4	5	6	7	8
Unit Weight (lb / ft^2)		0.3588							
Top Face - Thickness (in)		0.0165							
Core - Thickness (in)		0.3517							
Bottom Face - Thickness (in)		0							
Panel - Height (in)		0.3847							

Variable Design Materials		
Variable		Materials
Top Face - Thickness		1 - <a href="#">3-5 plies; Unsymm: 0/30/45/60/90 "3_ [45/-45/90]"</a>
Core - Thickness		1 - <a href="#">Honeycomb "Nomex 3.0 lb Scaled-Ruddy Test"</a>
Bottom Face - Thickness		

### Load Set Controlling Unfactored

	Nx (lb / in)	Ny (lb / in)	Nxy (lb / in)	Mx (lb-in / in)	My (lb-in / in)	Mxy (lb-in / in)	Qx (lb / in)	Qy (lb / in)
Strength	-310.399	331.501	-22.523	-56.6248	63.8943	-3.65318	0	0
Buckling	-265.514	331.501	-9.17562	-48.4709	63.6448	-1.30266	0	0

### Load Set Controlling Factored

	Nx (lb / in)	Ny (lb / in)	Nxy (lb / in)	Mx (lb-in / in)	My (lb-in / in)	Mxy (lb-in / in)	Qx (lb / in)	Qy (lb / in)
Strength	-465.599	497.251	-33.7845	-84.9372	95.8415	-5.47977	0	0
Buckling	-398.271	497.251	-13.7634	-72.7064	95.4672	-1.95399	0	0

### MOS, Concept "Honeycomb Sandwich"

	MOS Limit	MOS Ultimate	Lowest MOS (Lim/Ult)	Load Case for Lowest MOS
<a href="#">Panel Buckling, Curved, Simple, Fixed or Free BC</a>		0.022627	0.0226277	5

### MOS, Object "Top Honeycomb Face"

	MOS Limit	MOS Ultimate	Lowest MOS (Lim/Ult)	Load Case for Lowest MOS
Category "Composite Material Strength"				
<a href="#">Composite Strength, Tsai-Hahn Interaction</a>		1.304116	0.1162633	6
<a href="#">Composite Strength, LaRC03 Matrix Cracking</a>		1.457527	0.3512397	6
<a href="#">Composite Strength, LaRC03 Fiber Failure</a>		1.429399	0.3046516	6
Category "Sandwich"				
<a href="#">Wrinkling, Eqn 2, Honeycomb Core, X, Y &amp; Interaction</a>		1.335795	1.335795	5

On the failure tab the following traditional margins-of-safety is reported.

Traditional  $MS_T = 1.336$

#### 11.3.1.2 Reliability sizing without ultimate load factor = 1.5

*Project = LRSA Reliability Analysis, 2 Sigma, frozen design from traditional*

*Component = 220*

This analysis is performed by freezing the optimum design from the traditional sizing and passing it to the reliability project to be analyzed with an arbitrary selection of 2 sigma, 97.7%.

An important distinction is the traditional analysis uses a 1.5 ultimate load factor, whereas the reliability analysis does not.

*Though the same composite material is used, a different set of material properties are used. The design-to allowables are used for the traditional zero margin analysis, and the typical material properties are used with the reliability analysis. Mil Handbook 17 data was used both for the typical and "B" basis design-to allowables. Since the failure analysis being compared is facesheet wrinkling which only uses composite material stiffness, these material differences do not come in to play where only the design-to versus typical property differences are for stress/strain allowables.*

On the failure tab the following margins-of-safety are reported.

Predicted  $MS_P = 1.067$

Reliability  $MS_R = 0.6464$

Theoretical  $MS_{Theo} = 2.504$  {As a check:  $((1.336+1)1.5)-1 = 2.504$ }

Effective Knockdown = **0.4699**

Effective Required MS = **1.128**

### 11.3.2 Backing out the traditional sizing reliability

For a fair comparison between the traditional and reliability approach for wrinkling, the required MS in the traditional approach is set to equal to 0.695. Wrinkling test data presented in Volume 2, Section 2 summarizes the average ratio of test failure load divided by theoretical failure load to equal approximately 0.59. This ratio is a knockdown factor, which can be used to multiply the theoretical failure load by to obtain a predicted failure load. This knockdown is used to derive the required MS using the following equation.

$$MS_{Reqd} = \frac{P_{Theoretical\ allowable}}{P_{predicted\ allowable}} - 1 \quad (11.17)$$

$$MS_{Reqd} = \frac{1}{.59} - 1 = 0.695$$

From Equation (11.12)

$$K_T = \frac{K_R (MS_P - MS_T \Delta)}{(MS_P - MS_R)} = \frac{2(1.067 - 0.3782)}{(1.067 - 0.6464)} = 3.275$$

where

$$MS_T \Delta = \frac{MS_T + 1}{MS_{required} + 1} - 1 = \frac{1.336 + 1}{0.695 + 1} - 1 = 0.3782$$

Once  $K_T$  is calculated to be 3.275, it can be put into equation (11.16) to back out a reliability = 99.95%.

### 11.3.3 Calculating an effective knockdown

As shown above in section 11.3.1.2, HyperSizer reports an *effective knockdown* = 0.4699. This value indicates the relative amount the theoretical failure load has to be reduced in order to arrive at a 2 sigma (97.7%) reliability. As a check:

$$effective\ knockdown = \frac{MS_R + 1}{MS_{Theo} + 1} = \frac{.6464 + 1}{2.504 + 1} = 0.4699$$

### 11.3.4 Calculating an effective required MS

The meaning of *effective required MS* is not so straight forward. However, it is an important quantity because it is a convenient way to input specified % reliability in terms of an equivalent

required MS. In this way it serves as a bridge between the new reliability approach and the traditional Zero MS approach.

As shown above in section 11.3.1.2, HyperSizer reports an *effective required MS* = **1.128**. This value indicates the relative amount the theoretical failure load has to be reduced in order to arrive at a 2 sigma (97.7%) reliability. As a check:

$$\text{effective required MS} = \frac{MS_{Theo} + 1}{MS_R + 1} - 1 = \frac{2.504 + 1}{0.6464 + 1} - 1 = 1.128$$

Using the effective required MS is an alternative way that each unique failure analysis can obtain the same consistent reliability using traditional methods for the same combination of loads.

## 12 Conclusions

Described in this report is a design sizing and analysis process, based on building-block test data that brings all applied failure mode analyses to the same reliability. Incorporating this recommended approach, as implemented in HyperSizer, will lead to more consistent structural integrity in airframes and thus contribute to more successful test programs in the future. This capability resolves the most important reason test failures occur which is one constant load factor, applied to all potential failure modes, is not possible to raise all deterministic failure analyses to the same level of safety. Some failures, under certain load combinations are not predictable to within 50%. Meaning that aerospace industry's use of designing to 150% Design Limit Load, DLL, (a 1.5 load safety factor) is not sufficient for some failure modes, and far too conservative for others.

The goal of designing for reliability is consistency for all analyses. The reliability of material strength (both metallic and composite damage initiation) is very high. The use of 'A' or 'B' Basis allowables from MIL-HDBK- 5 and 17 provide substantial conservatism, especially when combined with the 1.5 ultimate load factor. So a material strength failure is not likely to occur in-service, at least not for pristine (undamaged) material. In contrast, other failures such as buckling, cross section crippling, and honeycomb sandwich wrinkling are more likely to occur. The same level of conservatism is not built-in to the analysis process for all failure modes.

To resolve this inconsistency, two correlation factors (CF) are recommended for all failure analyses used by the aerospace industry. [21 and 5], The first CF,  $\gamma_{\mu}$ , should be established to correlate theoretical calculations to typical (average) test results. The second CF,  $\gamma_{\eta}$  quantifies the variance (or standard deviation) and accounts for natural scatter of test results, represented as a probability density function (PDF).

The presented approach implemented in the HyperSizer® commercial automated analysis and design tool results in significant design cycle time reduction with the ability to analyze orders of magnitude more design configurations than current industry practices. Substantial risk reduction in final design is achieved from the integration and use of correlated, higher fidelity tools earlier in the design process. This makes it practical to bring into Preliminary Design (PD) many higher fidelity analyses that are performed for all identified external load cases and for all airframe locations (no spot checking of parts). All potential failure modes can be accurately assessed at the same level of confidence in a rapid manner that will not delay schedule nor require increase project funding.

As a PD tool that specializes in composite stiffened panels, a capability to accurately and rapidly perform bonded joint analysis and optimization of the bond between the stiffener flange and skin was required. Developed is a capability to perform accurate and rapid 3D through-the-depth stress/strain predictions for input into 19 specific bonded joint failure criteria. Provided are over 300 pages documenting theoretical development along with verification and validation examples.

Another primary analysis method developed is for composite laminate strength. Physics based failure criteria that identify failures between fiber and matrix were implemented and validated. Of particularly note is the LaRC03 (2004) failure criterion integrated into HyperSizer which provides similar accuracy to Puck while being far more practical to implement robustly. For all

composite failure criteria, CFs have been identified based on 130 different tests data points, including composite laminate failure from the World Wide Failure Exercises (WWFE).

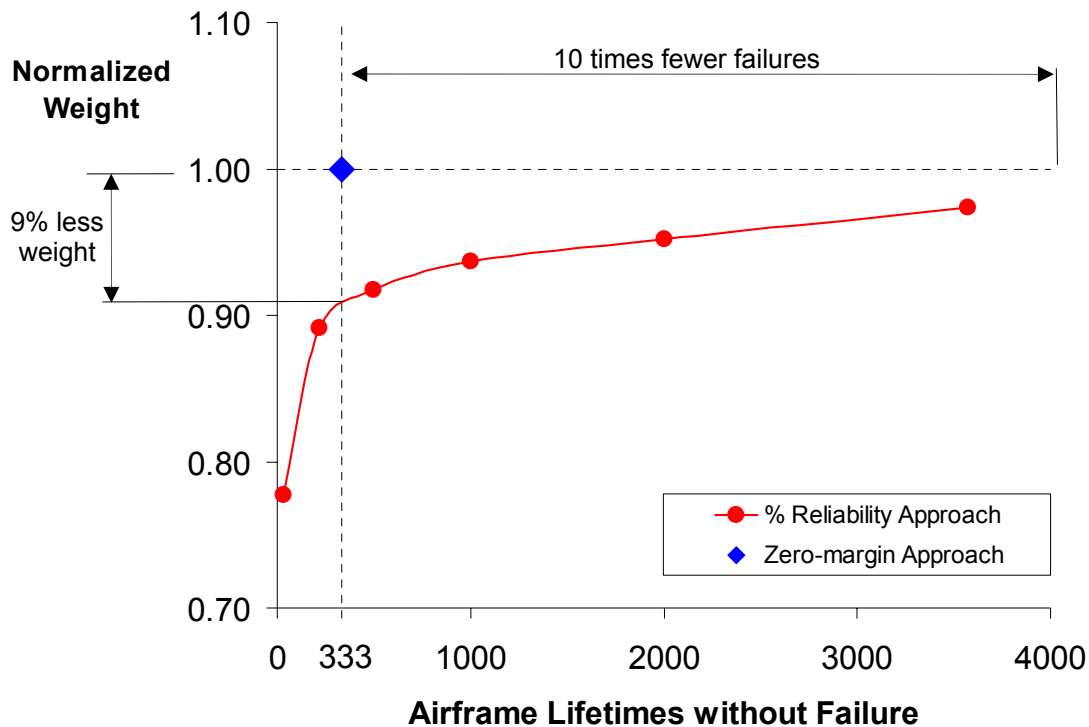


*Fig. 12.1, An example airframe structural weight versus lifetime failures. Note that significant reliability can be achieved with moderate weight growth. Note also that the traditional zero-margin analysis currently practiced in aerospace provides neither acceptable structural integrity nor minimum weight.*

Achieving consistent structural integrity was demonstrated in a practical way on a complete airframe PD of a recent AFRL Long Range Strike aircraft. Presented are summary results that compare the traditional, zero margin-of-safety for all failure modes approach, versus the presented approach that achieves consistent reliability for all potential failure modes. Included are identified areas of the vehicle sized using the traditional zero-margin method that results in an unexpected and unacceptable low reliability, even though it is 9% heavier than ‘test data driven’ reliability analysis and design. Alternatively, for the same weight as that provided by the traditional sizing, the vehicle can be sized to provide 10 additional lifetimes of reliability, Fig. 12.1. **This SBIR innovation conclusively provides: 1) substantial weight savings, 2) consistent structural integrity, and 3) convincing rationale to certification authorities of airframe structural airworthiness.**

This SBIR directly addresses the “**Issues that Hinder Reliance on Analysis Methods**” identified in [14], and its primary recommendations.

- Improve verification of External Loads and FEM Internal Loads (Referring to Fig. 9.1, the left side curve)

- Reduce risk in fastened/bonded joint, thermal stress, and stability analyses (Referring to Fig. 9.1, right side curve)
- Develop integration software for stress analysis tasks speedup and quantification of reliability/risk (putting the two together)

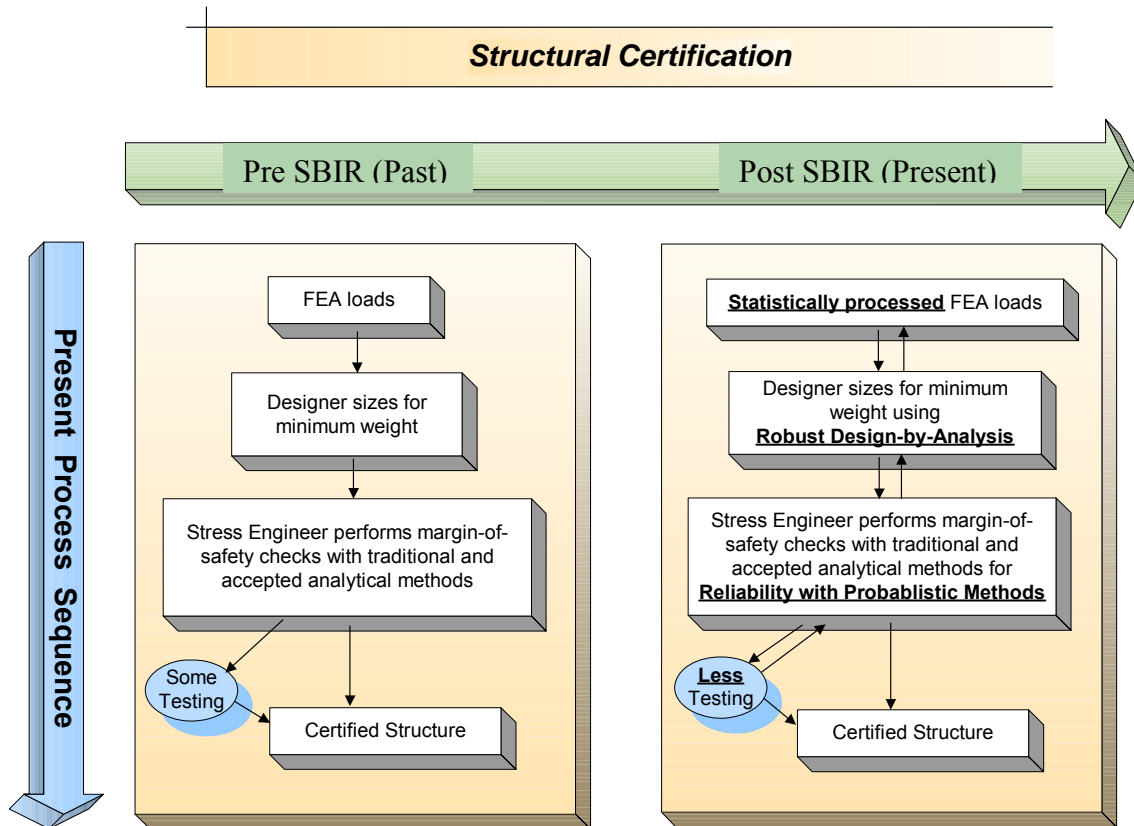


Fig. 12.2, The overall process for structural certification by analysis. The “past” process shown in the left box is one-way and loosely connected. The capability developed under this SBIR is a two-way, highly integrated process with tight I/O communication.

Specifically as depicted in Fig. 12.2, the developed and demonstrated test data driven reliability includes statistically processed FEA loads, the ability to design for minimum weight using a robust design-by-analysis tool in which the stress analyst, using the same tool, can perform final margin-of-safety reporting that includes “test-data-driven” reliability. Together a structure may be certified with less testing.

## 13 References

- 1 Jennewine, Tim, (Air Force ASC/ENFS, Dayton, OH) "Uninhabited Air Vehicle (UAV) Certification," ASIP 2002, Special Session on Certification, Savannah GA, 11 Dec 2002
- 2 NASA SP-8007, Buckling of Thin-Walled Circular Cylinders, NASA Space Vehicle Design Criteria (Structures), August 1968
- 2 Soden, P.D., Hinton, M.J., and Kaddour, A.S., "A Comparison of the Predictive Capabilities of Current Failure Theories for Composite Laminates," Composites Science and Technology, Vol. 58, No. 7, 1998, pp.1225-1254.
- 3 NASA SP-8108, Advanced Composite Structures, NASA Space Vehicle Design Criteria (Structures), December 1974 (of particular interest pp 74-81))
- 4 Niu, M. C. Y., Airframe stress analysis and sizing, 1997, Hong Kong Conmilit Press Limited.
- 5 Collier, Craig, Vele, Duane, and Owens, Steve, "Virtual Testing with Validated Analysis Tools," NATO AVT symposium in Paris, France, April 2002
- 6 Yarrington, P., Zhang, J., Collier, C., and Bednarczyk, B., "Failure Analysis of Adhesively Bonded Composite Joints," accepted by 46th AIAA/ASME/ASCE SDM Conference, Texas, 2005.
- 7 Mortensen, F., "Development of Tools for Engineering Analysis and Design of High Performance FRP-Composite Structural Elements," Ph.D. Thesis, Institute of Mechanical Engineering, Aalborg University (Denmark), Special Report no. 37, 1998.
- 8 Smeltzer, S. "Analysis Method for Inelastic, Adhesively Bonded Joints with Anisotropic Adherends" NASA Langley Research Center, 18th ASC conference, 2003.
- 9 Verderaiame, V., "First-Order Reliability Application and Verification Methods for Semistatic Structures", Journal of Spacecraft and Rockets, Vol 31, No. 6, Dec. 1994, pages 1050-1053.
- 10 Puck, A., Kopp J., and Knops M., "Guidelines for the determination of the parameters in Puck's action plane strength criterion," Compos. Sci. Tech, Vol.62, 2002, pp.371-378.
- 11 Davila, C. G. and Camanho, P. P., "Failure criteria for FRP laminates in plane stress," NASA/TM-2003-212663.
- 12 Harris, C. E.; Starnes, J. H., Jr.; Shuart, M. J., "Advanced Durability and Damage Tolerance Design and Analysis Methods for Composite Structures: Lessons Learned from NASA Technology Development Programs", June 2003.
- 13 Engelstad, S. "US View of Fighter/Attack", Structural Certification, ASIP 2002, Special Session on Challenges to Lean Certification, Savannah GA, 2002.
- 14 B.H. Thacker and D.S. Riha, "Workshop on Non-Deterministic Approaches - Emerging Computer Codes", 43rd Structural Dynamics and Materials Conference, Denver, Colorado, 21 April 2002
- 15 Thacker, Ben "Verification and Validation for Computational Solid Mechanics," Presented to AIAA Structures Technical Committee, Santa Fe, NM, 6 September 2002
- 16 Arbocz, Johann, Delft University of Technology, The Netherlands, James Starnes, and Michael Nemeth, NASA Langley, "On the Accuracy of Probabilistic Buckling Load Predictions" AIAA-2001-1236
- 17 Verduyn, W. D. "A Testing Machine for Statistical Analysis of Small Imperfect Shells" Report LR-357, Delft University of Technology, Sept 1982.
- 18 Shuart, M.J., "Failure of Compression-Loaded Multidirectional Composite Laminates," AIAA Journal, Vol.27, No. 9, 1989, pp. 1274-1279.

- 19 Ayyub & McCuen, "Probability, Statistics, and Reliability for Engineers and Scientists", 2<sup>nd</sup> ed, 2003 ISBN 1-58488-286-7, p135, equation. 5-10.
- 20 Phase I Final Report for Air Force Research Lab (AFRL) SBIR AF01-239, Certification of Aerospace Structures by Analysis, Collier Research Corporation December 2001

## 14 List of Acronyms and Abbreviations

### ACRONYM DESCRIPTION

A <sup>3</sup> I	Advanced Aluminum Aerostructures Initiative
ADP	Advanced Development Program
AFRL	Air Force Research Laboratory
AIAA	American Institute of Aeronautics and Astronautics
ASCE	American Society of Civil Engineering
B/L	Baseline
BJSFM	Bolted Joint Stress Field Method
CAD	Computer Aided Design
CBAR	Beam Finite Element
CFs	Correlation Factors
CLT	Classical Lamination Theory
COM	Component Object Model
COTS	Commercial off the Shelf
CQUAD	Shell Finite Element
CRAD	Company Research and Development
DLL	Design Limit Load (Loading)
FEA	Finite Element Analysis
FEM	Finite Element Model (Modeling)
FEMAP	Commercial Finite Element modeler
FSW	Friction Stir Weld (Welded)
GLD	Global-Local-Detail
GMC	Generalized Method of Cells
Gr/ep	Graphite/Epoxy
GUI	Graphical User Interface
HDB	HyperSizer Database
HME	HyperSizer Methods and Equations
HOT	Higher Order Theory
HPCCP	High Performance Computing and Communications Program
HS	HyperSizer
HTD	HyperSizer Test Data
HVE	HyperSizer Verification Examples
I/O	Input/Output
I-DEAS	Commercial Finite Element modeler
IS	Information System
J-UCAS	Joint Unmanned Combat Aircraft
LM Aero	Lockheed Martin Aeronautics Company
LRS	Long Range Strike Aircraft
M&P	Materials and Processing
MOS	Margin of Safety
MS	Margin of Safety
MSC/NASTRAN	Commercial Finite Element solver
NASA	National Aeronautics and Space Administration

NATO	North American Treaty Organization
NL	Non-linear
NLG	Nose Landing Gear
OML	Outer Mold Line
OS	Operation System
PD	Preliminary Design
PDF	Probabilistic Density Function
PIP	Process Improvement Program
PM	Probabilistic Method
R/T	Radius/Shell Thickness
SAMPE	Society for the Advancement of Material and Process Engineering
SAWE	Society of Allied Weight Engineers
SBIR	Small Business Innovation Research
SDM	Structural Dynamics and Materials
SIFT	Strain Invariant Failure Theory
SOW	Statement of Work
TPS	Thermal Protection System
TSF	Transverse Shear Flexibility
UCAVs	Unmanned Combat Aerial Vehicles
UDDI	Universal Description, Discover, and Integration
USC	The University of Southern California
V&V	Verification and Validation
WSDL	Web Service Description Language
WWFE	World Wide Failure Exercises